A Theoretical Study of Optical Constants of Two Dimensional Carbon Based Materials

Meera V

A thesis
submitted for the degree of
Doctor of Philosophy

Department of Physics
Indian Institute of Technology Guwahati
Guwahati 781039, India

December 2010

A Theoretical Study of Optical Constants of Two Dimensional Carbon Based Materials

Meera V

A thesis
submitted for the degree of
Doctor of Philosophy

Supervisor:
Dr. Girish Sampath Setlur

Department of Physics
Indian Institute of Technology Guwahati
Guwahati 781039, India

December 2010

Certificate

It is certified that the work contained in the thesis entitled "*A Theoretical Study of Optical Constants of Two Dimensional Carbon Based Materials*" by Ms. Meera V, a student of the Department of Physics, IIT Guwahati was carried out under my supervision and has not been submitted elsewhere for award of any degree.

Dr. Girish Sampath Setlur

Dedicated to my parents

Acknowledgements

First I wish to thank my supervisor Dr. Girish Setlur. It has been a wonderful experience to work under his guidance. I still remember the initial days of my PhD during which I was very confused due to many reasons. I appreciate his patience during that time and also the way he handled me. His support and encouragement has been truly a motivation even during the tough times of my PhD. He never gave me any kind of pressure in my work for which I am extremely thankful to him. More than a guide, he is a wonderful human being from whom I have learned a lot of things about research as well as life. The freedom he has given in my PhD work helped me to improve my self confidence and develop many qualities/skills which I am sure will be a great help for my future research career also. His unbiased attitude, frankness, sincerity and ego-less nature influenced me to a great deal. Being his first PhD student I would like to thank him whole heartedly for all the support, assistance, valuable suggestions and the opportunities to develop my character as well as research skills. I feel blessed to have him as my supervisor.

I am thankful to my doctoral committee members, Dr. C. Y. Kadolkar, Dr. P. Poulose and Dr. R. Alam for their support, valuable comments and suggestions during my review seminars and presentations. I am thankful to Dr. C. Y. Kadolkar for the help he has provided whenever I have approached him with my doubts and queries.

I am thankful to the present and past Physics Department Heads for supplying the full support and facilities at their best. I extend my whole hearted thanks to all the faculty members in the Physics Department who supported me in several ways during my research period. Many of them helped me to improve my management skills by allowing me to involve in various scientific events they have organized. I am thankful to IIT Guwahati for providing me with the financial assistantship during the research period.

I express my gratitude towards the organizers of the workshops and schools which I participated during this period and has been very useful to me. Especially I would like to thank the organizers of K S Krishnan meeting 2006 and 2007 which really opened a new way in my research.

I am grateful to Dr. Uma Dutta Setlur for her moral support, valuable suggestions, timely advice and prayer during this period.

I am thankful to all my juniors who were always supportive. I extend my sincere thanks towards all my lab-mates for the great time we have shared, the small jokes, complaints and healthy arguments. I extend my thanks to all my seniors, especially Amal Medhi who has provided valuable suggestions to me from his personal experiences in research. I would like to thank Basab Purakayasthya along with all other technical assistants of our department for the technical supports which they have provided whenever I needed.

I am fortunate enough to have such a kind and supportive hostel-mates Sangeetha and Shyni with whom I felt like home. The lunch and dinner time we spent together are some of the unforgettable moments in my life. During this period their company was a great relief for me and I got to learn many things through those discussions. They were always very understanding, co-operative and moreover a great help for me during the difficult times of my PhD.

I would like to express my gratitude to my friends Aneesh, Suresh, Neethu, Ribu, Shinoj, Soni, Vijutha, Narayanan, Prabhath, Resmi and many other friends for their moral support and company. I am thankful to my friends Veena, Sunish and Sabitha for their company during the initial times of my PhD and the way they have handled their tough times from which I had learned a lot.

I am grateful to my friends Poulumi Dey and Biswanath Dutta. I would like to thank Poulumi for the immense support she has provided me. She has been a great friend who is unbelievably understanding and co-operative. Especially for a person like me who was for the first time in life coming out from home town. She helped me to adjust with the entirely new environment here and even in developing my communication skills by patiently listening to me and correcting. I am always grateful to her for being supportive during the tough times of my research: the support and care she had extended helped me to emerge with enhanced courage. Her friendship is one of the precious gifts I got in my life. It is my pleasure to thank Biswanath for being a good friend who has been always caring, supportive and suggestive whenever I was disturbed with many of the technical issues related to my research.

I am extremely indebted to my most favorite teacher and one of the best teachers I have ever had in my life, Dr. Rajan K John for his kindness and support. Without him I would not be able to qualify any of the national level tests and reach this position. I can never forget the strength and motivation I received from him during my MSc times which inspired me

to achieve this goal. I always remain thankful to him and he is one of the persons who has influenced me the most and helped me to develop myself and go ahead.

I am not sure how would I thank my parents without whom this PhD thesis would not have been possible. I am thankful for the support and care they have extended from the time I started my life. The depth of each of the words they have said to me whenever I was in need and the inspiration I got from it is unforgettable. I still remember the times when I am down with low confidence and excess stress during which their constant counseling made me cross all those adverse situations. I am fortunate enough to have them. During the writing and submission of this thesis they were a great inspiration for me. I appreciate my father's patience during these five years especially in nullifying my difficulties and he was always there by my side when I was extremely in need of him. I am grateful to my sisters whose support was a great relief for me during my whole life.

Finally and foremost I thank God for giving me the good times which I enjoyed and the bad times from which I learned many things. I remain thankful for the mental strength given to face the adverse situations.

Abstract

The electromagnetic response of two dimensional carbon based systems is studied using basic classical tools. The most interesting and important carbon based system known till today is the by now well-known two-dimensional material "Graphene". This material is special in several ways, indeed, its very existence is an enigma. Graphene and a few of graphene based systems are studied using theoretical techniques. The key point of this work is the theoretical formulation of monolayer free-standing graphene. This formulation acts as the reference for the subsequent studies done in various graphene based systems. In this formulation monolayer free standing graphene is modelled as a conducting medium of one atom thickness such that the media is non-refracting. The emergent electric field of the system has been calculated by solving the fundamental equations of electromagnetism, "Maxwell's Equations" which consists of reflected and transmitted fields. Three physically important and experimentally measurable quantities are derived analytically, viz. coefficient of reflection, coefficient of transmission and polarization of reflection. The energy conservation theorem has been derived for the system using which the loss also has been calculated to make sure of the correctness of the formalism. The results obtained for some of these quantities with fixed values of various parameters show an excellent agreement with the experimental observations available in this field. For most of the device and technological applications, graphene has to be deposited on a substrate. For this reason, we next study a related system - substrate graphene. Theoretical modelling of this system has been done by regarding graphene as a conducting medium deposited on top of a purely dielectric material characterized by a dielectric constant. Maxwell's equations for this combined system has been solved using the boundary conditions and derived equations for the two parts of emergent field, reflection and transmission which has been made use to study the optical properties of this system. The linearly polarized limit of incident light in this system is important because of a well-known phenomenon in optics, "Brewster's phenomenon". The most interesting feature of Brewster's phenomenon related to substrate graphene is the azimuthal angle dependence of the Brewsters minimum. The next immediate system related to graphene is the combination of two single graphene sheets separated by a distance of a few Angstroms. With the monolayer results as reference, the optical constants of the bilayer system has been solved using series summation methods used in many fundamental optics books (such as [142]). Presence of an extra layer leads to multiple reflection phenomena. Amplitude changes occur upon each reflection which

have to be taken into account. In addition, for shorter wavelengths (soft X-ray), there are also phase changes brought about by fact that the path length traversed within the two layers is of the same order as the wavelength. More importantly, the presence of more than one layer is known to change the band structure of graphene completely. Thus a first principles calculation of the optical constants of multi-layer graphene would involve details of this modified band structure and other effects such as trigonal warping, next nearest inter-layer hopping, finite energy effects due to nonlinearity in the energy spectrum and so on. It is not our intention in this thesis to present such a calculation. Ours is a phenomenological approach wherein we treat the multilayer system as being composed of effectively independent monolayers, but each with an effective or renormalized conductivity. This effective conductivity depends on the total number of layers present in the system. An interpolation formula is proposed for this quantity that interpolates between bilayer on the one hand and infinitely many layers - bulk graphite on the other. We determine the parameters in the interpolation by making contact with these two extremes. We find that for few layers in the optical regime, the nearly independent layer approximation is quite good. The bilayer calculations act as a fundamental step towards deriving the general theoretical model for a multi-layer system. A general recurrence relation for a multi-layer system is derived for reflection and transmission that are exactly solved in the isotropic limit to obtain a general equation for reflection and transmission as a function of number of layers. This result is one of the most important outcomes of the work. The formalism developed for the multi-layer system enables us to count the number of layers in a few-layer graphene system and compute its transmission coefficient up to five layers (which is an experimental limit). This exercise shows perfect agreement with one of the experimental results available in the literature. The well-known Beer's law is studied using the result obtained for multi-layer graphene which shows a deviation for small number of layers. In addition to these results, many other studies related to the different types of anisotropy present in the system due to various external sources are done in several limiting cases. As a whole this is a study of graphene focused on less well-studied aspects of graphene and its related systems such as a detailed theoretical modelling of its optical properties from a physical optics point of view rather than on the more well studied Dirac fermion aspects.

Contents

List of Figures

Chapter 1

Introduction

Carbon is the element that is intimately related to living things. It is one of the more abundant elements found in the universe, in the sun, stars, comets, atmospheres of most planets, earth's crust and so on. Carbon deserves such a special role because of its ability to be found in various allotropic forms and also because of a wide variety of its properties. For example, graphite is one of the softest known materials while diamond is one of the hardest; diamond is transparent to the visible spectrum, while graphite is opaque; diamond is an electrical insulator while graphite is a conductor, and the fullerenes are different from both of them. Another important property of this element is the ability to form bonds with itself as well as with other elements which lead to the formation of one of the largest sub-branch of chemistry known as organic chemistry. Even though the carbon atom is divalent in its original state, its allotropic forms such as graphite, diamond, fullerenes etc. shows tetra-valency, that is, a single carbon atom in these materials can form bond with four other elements. The significance of carbon can be understood by reminding ourselves that many of the important discoveries in the field of materials in the last few years are related to carbon: carbon fibers, low pressure diamond synthesis, fullerene for example buckyballs (spherical hollow carbon molecules) [1], carbon nanotubes (cylindrical carbon molecules) [2] and very recently graphene [3]. The well known allotropes of carbon are diamond, graphite, Buckminster fullerenes, and carbon nanotubes. If we observe the above mentioned forms, diamond is a three dimensional material made of sp^3 hybridized carbon atoms, whereas graphite is also a three dimensional solid but made of sp^2 hybridized carbon atoms. Whereas carbon nanotubes in which the carbon atoms are sp^2 hybridized, is a material showing transport in one dimension and Buckminster' fullerene is a

zero dimensional material, being compact rather than extended. The dimensionality missing from the above list is a material in two dimensions. If we go deeply behind the non-occurrence of the 2D form, we can find a well known theorem which states that it is impossible to have a long range crystalline order in 2D because of the large thermodynamic fluctuations, which makes the strictly 2D crystal impossible to exist [4]. Even though it was a hypothetical object, 2D carbon was the theoretical basis to study the carbon allotropes in other dimensions. Experimental trials were going on using various methods to produce 2D carbon. This is not only because of the importance of carbon but also the speciality of its two dimensional nature. Low dimensional materials are special because when we restrict the size to one or more dimensions it brings about changes in the material's properties. They are expected to show some exotic behavior as compared to its bulk materials. This may be because of localization effects, geometry effects, high surface to bulk ratio, absence of inter-layer interactions etc [5]. Earlier attempts to produce 2D carbon was through intercalation compounds - by inserting atoms in between the layers of graphite. This was successful to some extent, but obtaining a two dimensional single layer seemed impossible through this procedure. There were various other methods used with the same motivation but with different deposition techniques. Researchers were successful in producing multi-layer graphite or few layer graphite leaving the production of one atom thick one layer of carbon atoms unaccomplished. The dream of producing a 2D material came true in 2004 made possible by two researchers of Manchester university - A. K. Geim and K. S. Novoselov [3] for which they received the 2010 Nobel prize in physics. The 2D carbon material produced in 2004 is called Graphene. The Royal Academy made a statement about this invention, "Carbon - the basis of all known life on earth, has surprised us once again".

1.1 How Is Graphene Different ?

Mono-layer free standing graphene is a densely packed collection of carbon atoms arranged in a honeycomb lattice. As we all know, graphite which is a 3D material has a layered structure with its constituents as the two dimensional one atom thick material called graphene [3, 6]. The relatively recent appearance of this two dimensional material has been attributed by Geim [7] to the infeasibility of traditional methods of crystal growth to produce a two dimensional crystal due to thermal fluctuations. Hence it took a relatively unusual and simple technique

such as scotch tape method to produce such a crystal. Novoselov, Geim and co-workers placed a flake of graphite on some tape and then by folding the tape over it again and again, gradually cleaved it thinner and thinner until it was only one atom thick. The large amount of literature, recent developments in technological and industrial fields and most importantly, the recent announcement of the Nobel Prize for such a young field reflects the expectations from this material and its applications. The peculiarity of graphene starts with its two dimensional nature followed by its high crystal quality, mechanical stiffness and stability, high electrical conductivity and optical transparency [8, 9]. All these properties observed together in one material is really a matter of surprise which really makes it a wonder material [10]. Also graphene may be considered as the basic building block for all of the sp^2 hybridized well known carbon allotropes like carbon nanotubes, buckyballs, graphite etc. In addition to these, the material shows ballistic transport which makes its carriers travel a distance of the order of micrometer without a collision. Due to the hexagonal structure, the band structure of this material shows a peculiarity, that is, it shows a linear dispersion at low energies near the high symmetric points of the first Brillouin zone (K points) where the valence and conduction bands touches each other and these points are termed as Dirac points [11]. This observation and the knowledge that electrons in graphene do not act in a classical way, but behaves more like a massless wave which obeys rules similar to relativistic Dirac mechanics rather than the Schrodinger wave mechanics is an exciting proposition. This observation enables a description of graphene using a $2 + 1$ dimensional theory of massless Dirac fermions. Therefore this material has been considered as a bridge between condensed matter physics and quantum electrodynamics [12]. Many of the exotic properties shown by this material can be explained in terms of the relativistic effects like zitterbewegung [13, 14], Klein paradox etc. [15, 16]. Another major point related to this material is the electric field effects shown by it which helps to tune the type and concentration of charge carriers present in the material [3, 17]. Also graphene shows many exotic properties such as half integer hall effect [18, 19, 20, 21, 22, 23], Aharonov Bohm effect [24, 25], universal conductivity [26, 27], minimum conductivity [28, 29] etc. Although it is a simple technique of scotch tape which produced graphene for the first time, there are several other methods developed for synthesizing high quality as well as large area samples. They are discussed in detail in a later section. There are several experimental techniques to visualize and hence to characterize graphene, for example visual contrast, white light optical microscopy, atomic force microscopy (AFM), scanning tunneling microscopy (STM), near-field scanning microwave microscopy [30], scanning electron microscopy (SEM), Transmission electron microscopy (TEM), electrostatic force microscopy, scanning probe microscopy

(SPM), Raman spectroscopy etc. For graphene to be used in technological applications or device engineering, it is important for it to be supported, hence the most usual technique is to deposit the material on a dielectric substrate. As graphene is a one atom thick 2D material, most of the atoms are in surface and they may interact with the substrate material leading to disorder effects [31, 32, 33, 34, 35]. Sometimes, properties of graphene depends upon the way in which it is prepared [33, 36]. Graphene as such being a semi metal shows edge effects which means that depending upon the shape of edges, the band structure and electronic properties of graphene changes [37, 38, 39, 40]. There are a number of reviews available in the literature dealing with different areas of graphene study such as optical [9, 41, 42, 43], transport [44], electronic [11, 45, 46, 47] studies and in general [7, 8, 10, 48, 49, 50, 51, 52, 53, 54] also which helps one to update the recent trends in this field.

1.2 Crystal Structure

Graphene as mentioned earlier, is a material made entirely of carbon atoms arranged in a hexagonal lattice structure. This hexagonal structure can be considered as a combination of two planar triangular sub-lattices normally labeled as A and B formed by the sp^2 hybridized carbon atoms in graphene. Each of the carbon atoms have four electrons in its valence shell three of which is used to form σ bonds with the neighboring carbon atoms and the left over electron in each carbon atom remaining in the p_z orbital is aligned perpendicular to the plane containing graphene sheet forming the π bonded electron cloud which is responsible for the high conductivity of graphene. Therefore each of the carbon atoms in graphene sheet has three nearest neighbors from the other sub-lattice which has two atoms per unit cell [11].

Fig. 1.1 shows graphene crystal structure with its nearest neighbor vectors and lattice vectors. The nearest neighbor vectors denoted by δ_i can be written as $\delta_1 = -a_{cc}\hat{e}_x$, $\delta_2 = \frac{a_{cc}}{2}\hat{e}_x + \frac{\sqrt{3}}{2}a_{cc}\hat{e}_y$ and $\delta_3 = \frac{a_{cc}}{2}\hat{e}_x - \frac{\sqrt{3}}{2}a_{cc}\hat{e}_y$. Now the lattice vectors in graphene can be expressed as given below:

$$\mathbf{a}_1 = \frac{3}{2}a_{cc}\hat{e}_x + \frac{\sqrt{3}}{2}a_{cc}\hat{e}_y \quad ; \quad \mathbf{a}_2 = \frac{3}{2}a_{cc}\hat{e}_x - \frac{\sqrt{3}}{2}a_{cc}\hat{e}_y \tag{1.1}$$

where a_{cc} is carbon-carbon distance which is 1.42Å.

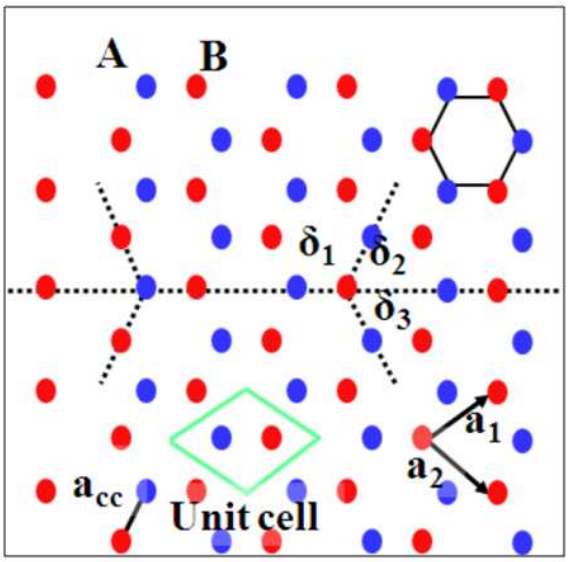

FIGURE 1.1: Crystal structure of graphene. Carbon atoms in two sub-lattices are denoted by red and blue dots. Nearest neighbor distances are denoted by δ_1, δ_2 and δ_3. Lattice vectors are denoted by $\mathbf{a}_1$ and $\mathbf{a}_2$. The carbon-carbon distance denoted by a_{cc} whose value is 1.42Å is also shown in the figure. Two atoms per unit cell is also shown.

Corresponding reciprocal lattice can be constructed as shown in Fig. 1.2 making a 90^0 tilted hexagon as the graphene reciprocal lattice. Constructing the Wigner Seitz cell of the reciprocal lattice cells gives the Brillouin zone as shown in Fig. 1.2.

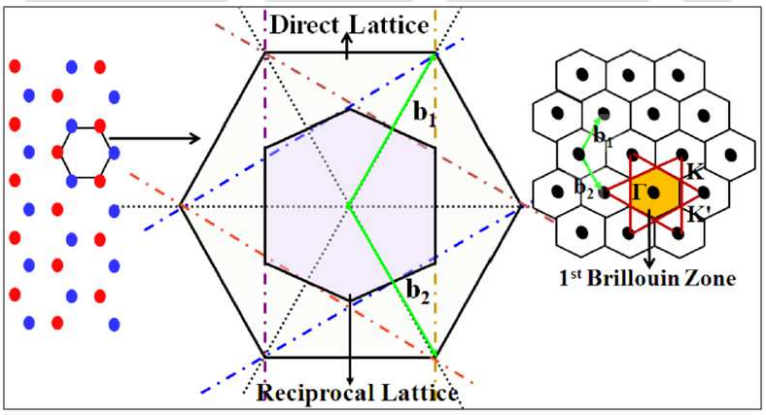

FIGURE 1.2: Reciprocal lattice of graphene. This figure shows the construction of reciprocal lattice and the first Brillouin zone from graphene direct lattice. The left most part with blue and red dots shows the direct lattice of graphene crystal structure, the middle portion shows the reciprocal lattice cell of direct lattice and the right most part shows the reciprocal lattice of graphene with the first Brillouin zone highlighted by orange color. The green arrows shown in the middle and right part is the reciprocal lattice vectors.

Three points in the first Brillouin zone are of special interest denoted by Γ (centre of Brillouin zone), K and $K^{'}$ (corners of the Brillouin zone). K and $K^{'}$ are those highly symmetric points in the reciprocal lattice where the valence and conduction bands of graphene touches and are called the Dirac points which is explained in detail in next section. The reciprocal lattice vectors denoted by b_i is given below:

$$b_1 = \frac{2\pi}{a_{cc}}\left(\frac{1}{3}\hat{e}_x + \frac{1}{\sqrt{3}}\hat{e}_y\right) \;\; ; \;\; b_2 = \frac{2\pi}{a_{cc}}\left(\frac{1}{3}\hat{e}_x - \frac{1}{\sqrt{3}}\hat{e}_y\right) \tag{1.2}$$

The first Brillouin zone can be constructed from the reciprocal lattice, taken as bounded by the planes bisecting the vectors to the nearest reciprocal lattice points. This is shown in figure. We can see that the first Brillouin zone has the same shape as the reciprocal lattice cell (that is 90^0 rotated by the direct lattice cell). The six corners of the first Brillouin zone can be considered as points in two groups of three that are equivalent [55]. This makes us consider only two equivalent points denoted by K and $K^{'}$ with positions,

$$\mathbf{K} = \frac{2\pi}{a_{cc}}\left(\frac{1}{3}\hat{e}_x + \frac{1}{3\sqrt{3}}\hat{e}_y\right) \;\; \mathbf{K}^{'} = \frac{2\pi}{a_{cc}}\left(\frac{1}{3}\hat{e}_x - \frac{1}{3\sqrt{3}}\hat{e}_y\right) \tag{1.3}$$

1.3 Band Structure

Electronic band structure of graphene can be calculated and explained using several methods, for example, Tight Binding Method, 2 + 1 dimensional effective theory of Dirac fermions etc. Below each of these methods are discussed one by one.

1.3.1 Tight Binding Calculation

The tight binding approach is a traditional method to calculate electronic band structure of a condensed matter system. This is explained in any of the condensed matter physics texts [56, 57]. It starts with a basis set of localized orbitals on each site of an atomic structure and the wave function of the system is assumed to be a linear combination of these localized atomic orbitals. Solving the energy eigenvalue equation we obtain the energy dispersion relation which describes the band structure for the system.

The first tight binding description of graphene was given by Wallace in 1947 [58] which takes into account nearest and next nearest neighbor interaction for the unbonded p_z orbitals directed normal to the graphene plane and neglected the overlap between the wave functions centered at different atoms. There is another effort done by Saito et. al. [59] which included only the nearest neighbor interaction within the graphene sheet along with the non-zero overlap between the basis functions. There are a number of references in the literature which is fully dedicated to the tight binding study of graphene [60, 61, 62].

Consider the graphene system which has a planar structure due to the sp^2 hybridized atomic orbitals. As mentioned in the earlier section, the left over p orbital remains unbonded, so only this orbital in each site is included in the calculation for band structure which can accommodate two electrons [55]. This is a valid assumption since the bonded orbitals have very low energy. For simplicity, we can consider the Hamiltonian with nearest neighbor hopping as given below:

$$H = -t \sum_{<i,j>,\sigma} \left(a^{\dagger}_{i\sigma} b_{j\sigma} + h.c. \right) \tag{1.4}$$

where i, j are the indices denoting atoms with spin σ, $a^{\dagger}_{i\sigma}$ is the creation operator for an atom in the A sub-lattice. Similarly the case with atoms on B sub-lattice. The $< i, j >$ in the summation simply means the inclusion of only nearest neighbor cases and t is the nearest neighbor hopping amplitude which has the magnitude of the order of $2.8eV$. Consider the eigenfunctions in a spinor form denoted by $\begin{pmatrix} \alpha_{\mathbf{k}} \\ \beta_{\mathbf{k}} \end{pmatrix}$. Components of the spinor represents the amplitudes on the A and B atoms respectively within the unit cell labeled by a reference point $\mathbf{R}^0_i$. Assume that for a particular pair of A and B, the latter is at distance δ_1 from the former with the reference point chosen as an A sub-lattice point. At this stage the spinor has the form

$$\begin{pmatrix} \alpha_{\mathbf{k}} \\ \beta_{\mathbf{k}} \end{pmatrix} = \sum_i e^{i\mathbf{k}\cdot\mathbf{R}^0_i} \begin{pmatrix} a^{\dagger}_i e^{-i\mathbf{k}\cdot\delta_1/2} \\ b^{\dagger}_i e^{i\mathbf{k}\cdot\delta_1/2} \end{pmatrix} \tag{1.5}$$

Therefore the $\mathbf{k}$ space Hamiltonian is as given below:

$$H_{\mathbf{k}} = \begin{pmatrix} 0 & \Delta_{\mathbf{k}} \\ \Delta_{\mathbf{k}} & 0 \end{pmatrix} \tag{1.6}$$

where $\Delta_{\mathbf{k}} = -t\sum_{l=1}^{3} e^{i\mathbf{k}\cdot\delta_l}$. Substituting for the nearest neighbor vectors we obtain

$$\Delta_{\mathbf{k}} = -te^{-ik_x a_{cc}}\left(1 + 2e^{i\frac{3}{2}k_x a_{cc}}\cos[\frac{\sqrt{3}}{2}k_y a_{cc}]\right) \tag{1.7}$$

We can obtain the eigenvalues of the Hamiltonian as

$$E_{\mathbf{k}} = \pm|\Delta_{\mathbf{k}}| = \pm t\sqrt{3 + 2\cos[\sqrt{3}k_y a_{cc}] + 4\cos[\frac{\sqrt{3}}{2}k_y a_{cc}]\cos[\frac{3}{2}k_x a_{cc}]} \tag{1.8}$$

There are two zeroes of the energy eigenvalue which an be found out from equation (1.7) which are listed below:

$$\frac{3}{2}k_x a_{cc} = 2n\pi \quad \& \quad \cos[\frac{\sqrt{3}}{2}k_y a_{cc}] = -\frac{1}{2}$$
$$\frac{3}{2}k_x a_{cc} = (2n+1)\pi \quad \& \quad \cos[\frac{\sqrt{3}}{2}k_y a_{cc}] = \frac{1}{2}$$

Here n is an integer. For the first case mentioned above, the y - component of the wave vector $\mathbf{k}$ goes outside the first Brillouin zone and the second point lies in the corners of the first Brillouin zone as shown in equation (1.3). These points denoted by $\mathbf{K}$ and $\mathbf{K}'$ are called "Dirac Points". The graphical representation of equation (1.8) is given in Fig. 1.3. We can see

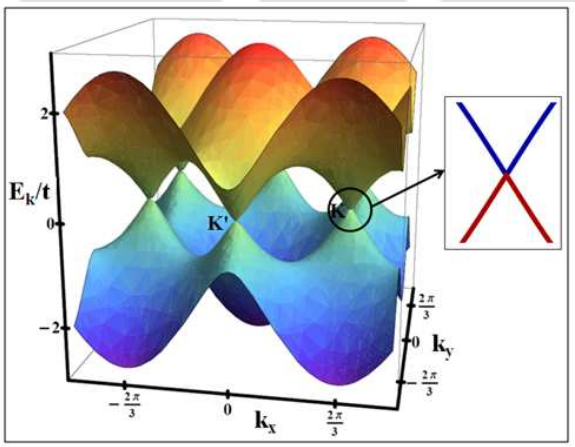

FIGURE 1.3: Band structure of graphene. Three dimensional plot of the tight binding formula given by equation (1.8). The top band is for positive energy and the bottom band is for the negative energy. The two bands touch at several points which are labeled as $\mathbf{K}$ and $\mathbf{K}'$, they are the corners of first Brillouin zone of graphene reciprocal lattice which are called Dirac points. The dispersion relation is enlarged near one of the Dirac points shown as inset where the blue lines are for E_+ and red curves are for E_-.

that the energy dispersion is linear near the corners of the first Brillouin zone. We can see that the energy band is exactly symmetric about Dirac points and the density of state at the Fermi level is exactly zero for half filling of the band. When the graphene is not doped, it has one electron per spin per atom, therefore the bond can be considered as half filled and therefore the undoped graphene is considered as a perfect semi-metal [55]. An elaborate description of the tight binding calculations for graphene can be obtained from the lecture notes by A. J. Leggett [55].

1.3.2 QED_{2+1} Theory

One of the important aspects of graphene is that it can be studied using the 2 + 1 dimensional quantum theory of electrodynamics (QED_{2+1}) namely Dirac fermions, with one important change namely that the electromagnetic field lives in three dimensions but the graphene sheet is two dimensional. It is surprising to note that the field theoretical view of graphene started almost 20 years before its discovery [63]. This means that the low energy excitations of graphene can be considered as massless Dirac fermions. Existence of Dirac fermions in graphene is proved experimentally by the observation of unconventional Quantum Hall Effect [18, 20, 21, 22, 23]. This fact made us study the properties of QED_{2+1} in a condensed matter system for example, Klein paradox, Zitterbewegung etc. The theoretical link between the condensed matter lattice description of graphene and the continuum QED_{2+1} formulation acts as a bridge between Condensed Matter and Quantum Electro Dynamics [12]. The non interacting Dirac Hamiltonian which explains graphene in a QED_{2+1} is given below [41]:

$$H_0 = \hbar v_F \sum_{\sigma} \int_{DC} \frac{d^2k}{(2\pi)^2} \Psi^{\dagger}_{\sigma}(\mathbf{k}) H_0(\mathbf{k}) \Psi_{\sigma}(\mathbf{k}) \tag{1.9}$$

where $H_0(\mathbf{k}) = \alpha^1 k_1 + \alpha^2 k_2$ and $\Psi_{\sigma}(\mathbf{k})$ is the 4 - component spinor defined in terms of the creation and annihilation operators of graphene. Here the 4×4 matrices $\alpha^{1,2}$ are the α matrices defined in terms of the pauli spin matrices as $\sigma_3 \bigotimes(\sigma_1, \sigma_2)$ and k_1 and k_2 are $(k_x + ik_y)$ and $(k_x - ik_y)$ respectively.

1.3.3 Dirac Hamiltonian from Tight Binding Hamiltonian

Consider the region close to the Dirac points i.e. at $\mathbf{k} = \mathbf{K}$. Consider the difference in wave vector defined as $\mathbf{q} = \mathbf{k} - \mathbf{K}$ [55]. Now expanding equation (1.7) around $\mathbf{q} = 0$, we obtain,

$$\Delta(\mathbf{q}) = 2e^{-iK_x a_{cc}}\mathbf{q}\cdot\nabla_{\mathbf{k}}\left(e^{3ik_x a_{cc}/2}\cos[\frac{\sqrt{3}}{2}k_y a_{cc}]\right)_{\mathbf{k}=\mathbf{K}} = -\frac{3t}{2a_{cc}}e^{-iK_x a_{cc}}(iq_x - q_y) \tag{1.10}$$

Apart from the overall constant factor,

$$\Delta(\mathbf{q}) = \hbar v_F(q_x + iq_y) + O(q/K)^2 \tag{1.11}$$

where $v_F = \frac{3t}{2a_{cc}} \cong 10^6 m/sec$. If we expand around $\mathbf{K}'$, $\Delta_{\mathbf{K}'}(\mathbf{q}) = \hbar v_F(q_x - iq_y) = \Delta^*_{\mathbf{K}}(\mathbf{q})$. Therefore the Hamiltonian can be written as

$$H \equiv \hbar v_F \begin{pmatrix} 0 & q_x + iq_y \\ q_x - iq_y & 0 \end{pmatrix} \equiv \hbar v_F\, \hat{\sigma}\cdot\mathbf{q} \tag{1.12}$$

Therefore the energy eigenvalue is $E(q) = \pm\hbar v_F|q|$ where $\hat{\sigma}$ are the Pauli spin matrices. We can see that the eigenvalues are functions only of the magnitude of $\mathbf{q}$ and not on the direction. Comparison with equation (1.9) shows that equation (1.12) is the Hamiltonian for mass-less relativistic particle of spin $1/2$ with velocity of light c replaced by the Fermi velocity v_F which is 300 times smaller than velocity of light [55].

1.4 Methods of Synthesis

As mentioned in an earlier section, graphene was not supposed to exist basically due to two reasons. First one is that the usual crystal growth mechanisms fails to grow low dimensional systems because of the large thermodynamic fluctuations at high temperature during growth processes may damage the system and even if they exist they cannot be stable transforming themselves to 3D structures, second reason is the difficulty to isolate the single layer of a 2D material. Even though the conventional methods of crystal growth are not successful in the production of 2D materials, a possibility still remains that they may be produced artificially. That is, we can grow the monolayer on top of a 3D bulk material and then remove it by some means or other in a sufficiently low temperature such that the thermodynamic fluctuations

does not damage the 2D system. Hence, broadly we can say that there are generally two ways of producing graphene, one is from top down (e.g. exfoliation or intercalation) and the other is bottom up (e.g. epitaxial methods). There are many reviews on the method of preparation of graphene [7, 48, 64].

1.4.1 Intercalation compounds

This is a technique used earlier to produce few layer graphene. The method to produce graphene starts with the 3D bulk graphite crystal which has a layered structure with a very weak inter-layer coupling. The inter-layer forces can be made much weaker by inserting some foreign atoms between the layers leading into a separation of layers [65]. But it is almost impossible to produce monolayer graphene using this, at the most this may result in systems with 10 – 15 layers.

1.4.2 Mechanical Exfoliation

Mechanical exfoliation is the way in which Graphene was isolated for the first time. This is also known as the scotch tape technique and is the fastest method to obtain graphene. This method consists of splitting the weakly bonded layers of 3D bulk highly oriented pyrolitic graphite (HOPG) manually to individual layers accompanied by several thicker crystals. That is, rubbing HOPG against another surface. By transferring the one atom thick, hence highly transparent material to a silicon dioxide substrate makes it slightly visible due to the change in interference color compared to bare substrate. This method provides high crystal quality samples of the order of millimeter size which are continuous on macroscopic scale and can be used for fundamental study [9]. This method has the drawback that it cannot be used for the large scale production of graphene. Ultrasonic cleavage is a type of mechanical exfoliation method which produces stable suspensions of graphene crystals of size in the micrometer range. The sonification can be made easy by starting with the graphite intercalation compounds which can help an industrial production of graphene [5].

1.4.3 Epitaxial Growth

Here the graphene layers are grown on 3D substrate materials where the monolayers remain bound to the underlying substrate material which suppresses the fluctuations. After cooling the grown structure, by the method of chemical etching the substrate material can be removed. Silicon carbide is the substrate material mostly chosen for the epitaxial growth because this material automatically offers an insulating environment [66]. When SiC is used for this purpose two different types of products may evolve. That is, graphene may grow on a Si terminated face or on a carbon terminated face. These two have entirely different properties, advantages and disadvantages. Graphene growth on metals such as Iridium, Rubedium and Platinum can also be obtained by the hydrocarbon decomposition at high temperature by chemical vapour deposition (CVD) [67]. These two methods, epitaxy and CVD are limited to certain substrates and are very costly due to the requirement of high temperature and ultra high vacuum.

1.4.4 Other routes

Use of organic precursors, solution based techniques, colloidal suspensions of graphene by sonification of graphite in organic solvents, sonification of graphite oxide in aqueous media followed by deoxygenation [5].

In spite of development of all these techniques, the large scale industrial production of graphene for the technological applications is still a hurdle.

1.5 Optical Studies

Along with the electronic and transport properties of graphene, its optical studies has also attracted much attention due to its several important discoveries. This includes both experimental and theoretical works.

1.5.1 Experimental studies

Experimental techniques includes reflection spectroscopy of graphene which helps to identify graphene for the first time on a silicon dioxide substrate material by interference effects [3, 68]. Infrared reflection spectroscopy can be used to study absorption spectrum of graphene. Another important experimental tool to study the optical effects is Raman spectroscopy which helps to differentiate between the mono-layer and bi-layer samples [69, 70, 71, 72, 73, 74], influence of defects [75] and whose temperature variation finds applications in nanometrology [76, 77]. Reviews on the Raman spectroscopic studies and imaging is available in the literature [42, 78]. Studies reveal the breaking of adiabatic Born-Oppenheimer approximation which can affect the vibrational properties and result in variation of the Raman active peaks in graphene which allow the determination of the effective doping by Raman spectroscopy [79]. As mentioned earlier, an applied gate voltage can shift the Fermi energy due to which there are gate induced optical effects such as modification of optical transitions and gate modulation in mono-layer graphene [80], gate tunable band gap in bi-layer graphene [81] etc. Sources of absorption in different energy regions ranging from terahertz to visible region can be obtained from the study of optical absorption spectra which leads to a better understanding of optical conductivity, carrier densities, scattering time etc [82]. Optical contrast studies especially its angle dependence, of graphene on a dielectric substrate helps a better and fast detection of mono-layer samples [83, 84, 85]. Optical conductivity studies in the high energy region has been studied by reflection contrast spectroscopy [86]. Confocal Rayleigh scattering microscopy can be used to identify graphene layers and when combined with Raman scattering provides structural identification [87]. Identification of the thickness of graphene layers can also be done with the contrast spectroscopy [88]. Many body effects are studied by examining the Dirac charge dynamics by infrared spectroscopy [89]. Infrared spectroscopy of Landau levels in graphene deduces the band velocity along with the many body effects to the infrared transition energies [90]. A review on the optical spectroscopic studies gives an overview of the linear transmission and reflection optical studies of graphene based structures [43]. Other studies includes the experimental determination of universal optical conductance [26], optical reflectivity and transmission measurements and the non-universal conductivity behavior at low photon energies [91], measurement of fine structure constant from mono-layer transparency [92], far infrared transmission experiments on few layer graphene [93], contrast analysis by optical microscopy to monitor graphene cleanness [84] etc.

1.5.2 Theoretical studies

Theoretical studies on graphene started with the study of the 3D bulk material, graphite. This is because graphite has a layered structure and to theoretically model graphite it is necessary to consider the simplest situation of a single layer which is really graphene. It started with the band structure calculation of graphite by Wallace [58] and a few others [94, 95] followed by several optical studies in graphite [96, 97, 98, 99]. Even though theoretical background for graphene was available from almost 50 years ago, only after its experimental realization in 2004 an active study of various theoretical aspects of graphene has started. One of the most important theoretical study of the optical properties of graphene is the calculation of optical conductivity. A detailed calculation of the general expression for the optical conductivity elements are there in the literature which can be applied for any frequency range and also at any temperature [100]. Starting from a 2 + 1 dimensional Dirac Lagrangian conductivity tensor elements are derived using Kubo formula. There is a review also available in the literature which connects the tight binding model and quantum electrodynamics of Dirac fermions [41]. Electro and Magneto optical response of graphene and the anomalous absorption in graphene are well studied [101, 102, 103, 104]along with the theoretical calculation of universal ac optical conductivity [27] and the sum rules for optical and Hall conductivities [105]. Based on the general formula for optical graphene conductivity microwave response is separately studied which shows some unusual behavior of the Dirac quasi particles in graphene [106]. Optical conductivity calculations of graphene and related systems like bi-layer graphene are also done in specific regions of the electromagnetic spectrum such as visible region, far infrared region etc. some of them are applicable even beyond the Dirac cone approximation [107, 108, 109, 110, 111, 112, 113, 114, 115, 116, 117, 118]. There are a number of studies which deals the substrate effects on graphene, its visible criteria, contrast analysis etc [119, 120]. Optical constants such as reflection and transmission coefficients have also been analyzed theoretically in different regions of the EM spectrum which studies the effect of doping, biasing etc [121, 122, 123, 124, 125, 126]. Influence of spin orbit coupling, excitons, many body effects are also recent considerations in this field of theoretical optical study [127, 128, 129, 130].

1.6 Applications

Graphene has many potential applications in various fields ranging from nanotechnology to medicine. It has many technological as well as device applications ranging from hydrogen storage devices [131] to batteries. It is believed that graphene has an important role in future electronics which can enable the faster and smaller transistors that consumes less energy [132]. Other applications are in sensors [133], conducting transparent films in solar cells and liquid crystal devices [134], ultra capacitors [135], bacterium bio-devices and label-free DNA sensors [136].

Chapter 2

Free Standing Graphene

This chapter discusses the freestanding form of graphene. The main tool used to study the system is Maxwell's equations. The first section describes the problem under consideration followed by a description of the tools used for study. A general description of the quantities under study are included as the next section and finally the results are discussed in detail with the help of few plots. The highlight of this chapter is the angular dependence of the optical reflection and transmission coefficients.

2.1 Problem Description

Mono-layer graphene sheet in the free standing state is considered for study in chapter 2. Freely suspended graphene is important because we don't have to worry about the disorder effects. Most of the disorder in graphene comes from the interaction of graphene with its substrate upon which it is deposited. Consider the graphene sheet to be kept in *xy* plane. An electromagnetic wave with a wave vector $\mathbf{q}_0$ is incident on the sheet at an arbitrary angle θ_0. The incident wave vector is considered to have all the three components along the three Cartesian directions. The schematic of the situation is shown in Fig. 2.1. Throughout this work the electric field is expressed in general as a linear combination of its polarization components in different directions. In this way the incident electric field denoted by $\mathbf{E}_{ext}(\mathbf{r}, t)$ in real space

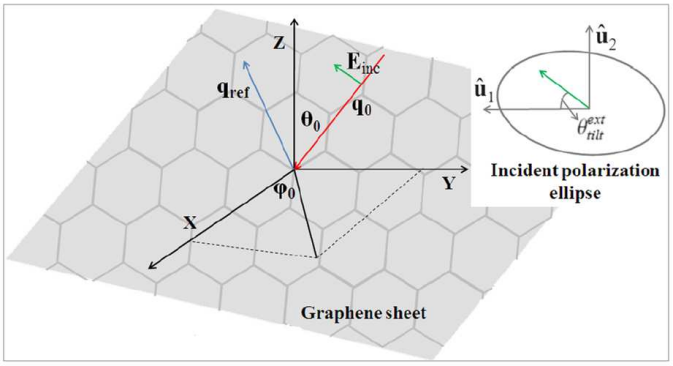

FIGURE 2.1: Schematic of the situation under study. A graphene sheet is placed in the x-y plane. Parameters involved in the study are explained in the figure. Red arrow shows the incident wave with wave vector $\mathbf{q}_0$ and blue arrow shows the reflected wave with wave vector $\mathbf{q}_{ref}$. Arrow perpendicular to the incident wave is the incident electric field. Two polarization directions with the definition of tilt angle is shown on the upper part of the figure.

can be written as

$$\mathbf{E}_{ext}(\mathbf{r},t) = e^{i\mathbf{q}_{0,\parallel}\cdot\mathbf{r}_{\parallel} + iq_{0,z}z - ic|q_0|t} \sum_{\nu=1,2} \hat{\mathbf{u}}_\nu^{ext} E_\nu^{ext} \tag{2.1}$$

Here $\hat{\mathbf{u}}_\nu^{ext}$ are the unit vectors in the two directions of polarization which are defined in a general way as given below:

$$\hat{\mathbf{u}}_1^\alpha = \frac{\hat{\mathbf{e}}_z \times \hat{\mathbf{q}}_\alpha}{|\hat{\mathbf{e}}_z \times \hat{\mathbf{q}}_\alpha|} \quad ; \quad \hat{\mathbf{u}}_2^\alpha = \frac{\hat{\mathbf{u}}_1^\alpha \times \hat{\mathbf{q}}_\alpha}{|\hat{\mathbf{u}}_1^\alpha \times \hat{\mathbf{q}}_\alpha|} \tag{2.2}$$

Also E_ν^{ext} is the components of incident electric field along the unit vectors defined in equation (2.2). General form of this quantity can be written as

$$E_1^\alpha = |E^\alpha| \cos\theta_{tilt}^\alpha \, e^{i\delta_1^\alpha} \quad ; \quad E_2^\alpha = |E^\alpha| \sin\theta_{tilt}^\alpha \, e^{i\delta_2^\alpha} \tag{2.3}$$

where $|E^{ext}|$ is the amplitude of incident electric field which is independent of position and time, α is a parameter which takes care of the different situations namely (inc,ref,tran), θ_{tilt}^α is the tilt angle of the polarization ellipse in the corresponding situation and δ_1^α is the magnitude of polarization in the $\hat{\mathbf{u}}_1^\alpha$ direction and δ_2^α is magnitude of polarization in the $\hat{\mathbf{u}}_2^\alpha$ direction. In the reciprocal domain the incident electric field is given by the Fourier transform of the real space electric field vector.

$$\mathbf{E}_{ext}(\mathbf{q}_\parallel, q_z, \omega) = \delta^3(\mathbf{q}_0 - \mathbf{q})\, \delta(c|q_0| - \omega) \sum_{\nu=1,2} \hat{\mathbf{u}}_\nu E_\nu^{ext} \tag{2.4}$$

To derive the electric field emerging from the graphene surface due to incident wave Maxwell's equations are used and is discussed in the next section.

2.2 Maxwell's Equations

Maxwell's equations representing the present system under study is given in CGS units below,

$$\vec{\nabla} \cdot \vec{\mathbf{E}} = 4\pi\rho \quad ; \quad \vec{\nabla} \times \vec{\mathbf{E}} = -\frac{1}{c}\frac{\partial \mathbf{B}}{\partial t}$$

$$\vec{\nabla} \cdot \vec{\mathbf{B}} = 0 \quad ; \quad \vec{\nabla} \times \vec{\mathbf{B}} = \frac{4\pi}{c}\mathbf{J} + \frac{1}{c}\frac{\partial \mathbf{E}}{\partial t} \tag{2.5}$$

Here graphene is modelled as a highly conducting material without any dielectric properties. This is because refraction does not take place in a one atom thick material - the transmitted beam moves in the same direction as the incident beam. with current density denoted by **J** whose components are

$$J_a(\mathbf{r}, \omega) = \int \sum_b \sigma_{a,b}(\mathbf{r}', \omega)\, E_{ext,b}(\mathbf{r} - \mathbf{r}', \omega)\, d^3r' \tag{2.6}$$

where $\sigma_{a,b}$ in the above definition is the elements of optical conductivity tensor of graphene. Graphene as we all know being a 2D material, hence the conductivity can be represented by a 2×2 matrix. As it is mentioned at the start, in this study the graphene sheet is placed in the *xy* plane, which makes the *z* component of the induced current density vanish, i.e. $J_z^{ind} = 0$. Equations (2.5) can be solved using Fourier transform technique with the help of few other basic equations (equation of continuity, electric and magnetic field in terms of vector potential etc.) to obtain the emergent electric field. The Fourier transform of a general field $\mathbf{F}(\mathbf{r}, t)$ is defined as below:

$$\mathbf{F}(\mathbf{r}, t) = \int_{-\infty}^{\infty} d^2\mathbf{q}_{\parallel} \int_{-\infty}^{\infty} dq_z \int_{-\infty}^{\infty} d\omega\, \mathbf{F}(\mathbf{q}_{\parallel}, q_z, \omega)\, e^{i\mathbf{q}_{\parallel}\cdot\mathbf{r}_{\parallel}}\, e^{iq_z z}\, e^{-i\omega t} \tag{2.7}$$

The gauge is chosen such that the scalar potential is zero.

2.3 Emergent Electric Field : Reflection and Transmission

Using the information given in the above section, Maxwell's equations are solved to obtain the emergent electric field as given below (The details of the calculation are given in Appendix A):

$$\mathbf{E}_{emerg}(\mathbf{r},t) = e^{i\mathbf{q}_{0,\|}\cdot\mathbf{r}_{\|}}\, e^{-ic|q_0|t}\, \Big(\mathbf{E}_{emerg,1}(z)\,\Theta(-z) + \mathbf{E}_{emerg,2}(z)\,\Theta(z)\Big) \tag{2.8}$$

where

$$\mathbf{E}_{emerg,1}(z) = \sum_{\nu=1,2} \hat{\mathbf{u}}_{\nu}^{ext} E_{\nu}^{ext}\, e^{iq_{0,z}z} - 2\pi \left[\left(\hat{\mathbf{e}}_z - \frac{\mathbf{q}_{0,\|}}{q_{0,z}}\right)\frac{1}{c|q_0|}\,\mathbf{q}_{0,\|}\cdot\mathbf{K}^{ext} + \frac{|q_0|}{q_{0,z}c}\,\mathbf{K}^{ext}\right] e^{-iq_{0,z}z} \tag{2.9}$$

$$\mathbf{E}_{emerg,2}(z) = \left(\sum_{\nu=1,2} \hat{\mathbf{u}}_{\nu}^{ext} E_{\nu}^{ext} + 2\pi \left[\left(\hat{\mathbf{e}}_z + \frac{\mathbf{q}_{0,\|}}{q_{0,z}}\right)\frac{1}{c|q_0|}\,\mathbf{q}_{0,\|}\cdot\mathbf{K}^{ext} - \frac{|q_0|}{q_{0,z}c}\,\mathbf{K}^{ext}\right]\right) e^{iq_{0,z}z} \tag{2.10}$$

Here $\mathbf{K}^{ext} = \overline{\overline{\sigma}}(\mathbf{q}_{0,\|},\omega)\cdot\sum_{\nu=1,2}\hat{\mathbf{u}}_{\nu}^{ext}E_{\nu}^{ext}$ If the entire space is divided into two parts $z<0$ and $z>0$, there are two parts in the former which are the incident part and the reflected part and only transmitted part exists in the latter region.

$$\mathbf{E}_{ref}(\mathbf{r},t) = -2\pi\left[\left(\hat{\mathbf{e}}_z - \frac{\mathbf{q}_{0,\|}}{q_{0,z}}\right)\frac{1}{c|q_0|}\,\mathbf{q}_{0,\|}\cdot\mathbf{K}^{ext} + \frac{|q_0|}{q_{0,z}c}\,\mathbf{K}^{ext}\right] e^{i(\mathbf{q}_{0,\|}\cdot\mathbf{r}_{\|} - c|q_0|t - q_{0,z}z)} \tag{2.11}$$

$$\mathbf{E}_{tran}(\mathbf{r},t) = \left(\sum_{\nu=1,2} \hat{\mathbf{u}}_{\nu}^{ext} E_{\nu}^{ext} + 2\pi \left[\left(\hat{\mathbf{e}}_z + \frac{\mathbf{q}_{0,\|}}{q_{0,z}}\right)\frac{1}{c|q_0|}\,\mathbf{q}_{0,\|}\cdot\mathbf{K}^{ext} - \frac{|q_0|}{q_{0,z}c}\,\mathbf{K}^{ext}\right]\right) e^{i(\mathbf{q}_{0,\|}\cdot\mathbf{r}_{\|} - c|q_0|t + q_{0,z}z)} \tag{2.12}$$

Just as in the case of incident electric field (equation (2.1)), the real space vectors of reflected and transmitted electric fields can be expressed in terms of its polarization components.

$$\mathbf{E}_{ref}(\mathbf{r},t) = e^{i\mathbf{q}_{ref,\|}\cdot\mathbf{r}_{\|} + iq_{ref,z}z - ic|q_{ref}|t} \sum_{\nu=1,2} \hat{\mathbf{u}}_{\nu}^{ref} E_{\nu}^{ref} \tag{2.13}$$

$$\mathbf{E}_{tran}(\mathbf{r},t) = e^{i\mathbf{q}_{tran,\|}\cdot\mathbf{r}_{\|} + iq_{tran,z}z - ic|q_{tran}|t} \sum_{\nu=1,2} \hat{\mathbf{u}}_{\nu}^{tran} E_{\nu}^{tran} \tag{2.14}$$

where $\mathbf{q}_{ref} = \left(q_{0,x}, q_{0,y}, -q_{0,z}\right)$ and $\mathbf{q}_{tran} = \left(q_{0,x}, q_{0,y}, q_{0,z}\right)$ with $|q_{ref}| = |q_{tran}| = |q_0|$. Unit vectors along the polarization directions of the reflected and transmitted field is defined in equation (2.2) with α as ref or $tran$. Similarly the general equations for the components of reflected and transmitted electric field along the polarization directions are also given in equation (2.3). The polarization components of the reflected and transmitted electric field can be obtained from equations (2.11, 2.12, 2.13, 2.14) in the following way,

$$E_{\nu}^{ref} = e^{-i\mathbf{q}_{0,\parallel}\cdot\mathbf{r}_{\parallel} + iq_{0,z}z + ic|q_0|t}\, \mathbf{E}_{ref}(\mathbf{r}, t) \cdot \hat{\mathbf{u}}_{\nu}^{ref} \tag{2.15}$$

$$E_{\nu}^{tran} = e^{-i\mathbf{q}_{0,\parallel}\cdot\mathbf{r}_{\parallel} - iq_{0,z}z + ic|q_0|t}\, \mathbf{E}_{tran}(\mathbf{r}, t) \cdot \hat{\mathbf{u}}_{\nu}^{tran} \tag{2.16}$$

To proceed further, that is to calculate any physically interesting quantity we need to know about the conductivity tensor of graphene.

2.3.1 Optical Conductivity

If a system is placed in an external electric field, a redistribution of charges occurs in it due to which currents are induced. For small fields, the induced currents are proportional to the inducing field. In that way optical conductivity denoted by σ is a linear response function relating the current $\mathbf{J}$ to an applied transverse electric field $\mathbf{E}$, which is the vector form of Ohm's law $\mathbf{J} = \sigma\mathbf{E}$. If the electric field is steady, then the above given response function is called "electrical conductivity" and if the applied electric field is alternating, then the same is called "optical conductivity". In the Ohm's law equation, the conductivity is written as a proportionality constant which is a scalar. But this is only a special case. In the most general case this response function is a tensor. It is seen that the current density and the electric field are both vectors and conductivity in general has to have a tensor form (in general, it is a 2^{nd} rank tensor) to make the relation mathematically true. Physical insight to the tensor form of conductivity can be obtained by thinking that the external applied electric field and the induced current density are not in same direction. i.e. $\mathbf{J} = \overline{\overline{\sigma}} \cdot \mathbf{E}$. Therefore $\overline{\overline{\sigma}}$ being a 2^{nd} rank tensor can be represented in the form of matrices. Hence σ_{ab} is the linear response function relating the current $\mathbf{J}$ in the a direction to an applied transverse electric field $\mathbf{E}$ in the b direction. In the general form, if the conductivity tensor elements are all different, it is called anisotropic which contains information about the anisotropic nature of the medium

also. Within this anisotropic limit itself, there can be many possibilities: (a) diagonal elements equal and off diagonal elements equal (b) diagonal elements are unequal. Then even if the off-diagonal elements vanishes the medium and the tensor can be anisotropic. If the conductivity tensor has all its diagonal elements equal with vanishing off-diagonal elements, then it is said to be isotropic which gives us the information that the medium is also isotropic.

As mentioned in one of the earlier sections, conductivity tensor for graphene being a $2D$ material is a 2×2 matrix, that is it can be represented as $\begin{pmatrix} \sigma_{xx} & \sigma_{xy} \\ \sigma_{yx} & \sigma_{yy} \end{pmatrix}$. Under different physical conditions there will be restrictions to the tensor components which are discussed below. There is a large amount of literature which study optical conductivity in graphene. One of the best references in this area is by Gusynin et. al. [100] which calculates the optical conductivity of graphene for a general case with arbitrary frequency and temperature, starting from the conventional $\mathbf{QED}_{2+1}$ Lagrangian Density. The situation is such that an external magnetic field $B = \vec{\nabla} \times \vec{\mathbf{A}}^{ext}$ is applied perpendicular to the plane, i.e. along the positive z axis and corresponding vector potential in the symmetric gauge $\mathbf{A}^{ext} = (-By/2, Bx/2)$. Here throughout the study the energy unit is considered as Kelvin.

$$\begin{aligned}\sigma_{ij}(\Omega) = \frac{e^2 v_F^2 \, |eB| \, N_f}{2\pi^2 c \, \Omega} \sum_{n=0}^{\infty} \int_{-\infty}^{\infty} d\omega \, (\delta_{ij} \left[n_F(\omega) - n_F(\omega') \right] \\ \times Re \left[\Pi^1_{n,n+1}(\omega, \omega') + \Pi^1_{n+1,n}(\omega, \omega') - \Pi^2_{n,n+1}(\omega, \omega') - \Pi^2_{n+1,n}(\omega, \omega') \right] \\ - \epsilon_{ij} \, sgn(eB) \left[n_F(\omega) - n_F(\omega') \right] Im \left[\Pi^1_{n,n+1}(\omega, \omega') - \Pi^1_{n+1,n}(\omega, \omega') \right] \\ + \epsilon_{ij} \, sgn(eB) \left[n_F(\omega) + n_F(\omega') \right] Im \left[\Pi^2_{n,n+1}(\omega, \omega') - \Pi^2_{n+1,n}(\omega, \omega') \right]) \end{aligned} \tag{2.17}$$

Here v_F is the Fermi velocity of the carriers in graphene which is of the order of $10^{-6}\ m/s$, B is the applied magnetic field, N_f is the number of spin components and $N_f = 2$ corresponds to the physical case, Ω is the incident wave frequency, $n_F(\omega) = \frac{1}{e^{\frac{\omega-\mu}{T}}+1}$ is the Fermi distribution function, δ_{ij} is the Kronecker delta function which will vanish for $i \neq j$, ϵ_{ij} is an antisymmetric function with $\epsilon_{12} = 1$. Also

$$\Pi^1_{n,m}(\omega,\omega') = \frac{\left(\omega' + i\Gamma'\right)\ (\omega - i\Gamma)\ -\ \Delta^2}{[\omega - \omega' - i\,(\Gamma + \Gamma')]\ [\omega + \omega' - i\,(\Gamma - \Gamma')]\ +\ 2B(n-m)} \times\left[\frac{1}{(\omega' + i\Gamma')^2 - M_n^2} - \frac{1}{(\omega - i\Gamma)^2 - M_m^2}\right]$$

$$\Pi^2_{n,m}(\omega,\omega') = \frac{\left(\omega' + i\Gamma'\right)\ (\omega + i\Gamma)\ -\ \Delta^2}{[\omega - \omega' + i\,(\Gamma - \Gamma')]\ [\omega + \omega' + i\,(\Gamma + \Gamma')]\ +\ 2B(n-m)} \times\left[\frac{1}{(\omega' + i\Gamma')^2 - M_n^2} - \frac{1}{(\omega + i\Gamma)^2 - M_m^2}\right]$$

Here $B = \frac{v_F^2\ |eB|}{c}$, $M_n = \sqrt{\Delta^2 + \frac{2nv_F^2\ |eB|}{c}}$, $\Gamma(\omega)$ is the frequency dependent impurity scattering rate and Δ is the gap in the quasi particle spectrum. Equation (2.17) gives some general properties of the graphene conductivity tensor. It is clear from equation (2.17) that the diagonal components of the conductivity tensor are equal and the off-diagonal components are of equal magnitude but opposite sign. i.e. $\sigma_{xx} = \sigma_{yy}$ and $\sigma_{xy} = -\sigma_{yx}$. This is because in the equation for the diagonal part, the Kronecker delta is present and in the off-diagonal part an antisymmetric function appears. The source of this antisymmetric function is the presence of Pauli spin matrices in the Hamiltonian. Therefore one can see that in a perpendicular magnetic field the system has a conductivity tensor with its diagonal elements equal whereas the off-diagonal elements equal and opposite in sign. But this general equation of conductivity elements is extremely complicated and it is very difficult to get an analytical result in a general situation. Therefore some special cases of equation (2.17) is appreciable. The microwave response in the high magnetic field limit simplifies the general conductivity equation to a large extent [106] and is given below:

$$\sigma_{xx}(\Omega,T) = \frac{e^2 N_f \Gamma}{2\pi h\,\Omega}\ Im\left[\psi\left(\frac{\Gamma + i(\mu + \Omega + \Delta)}{2\pi T} + \frac{1}{2}\right) - \psi\left(\frac{\Gamma + i(\mu - \Omega + \Delta)}{2\pi T} + \frac{1}{2}\right) + (\Delta \to -\Delta)\right] \tag{2.18}$$

$$\sigma_{xy}(\Omega,T) = -\frac{e^2 N_f\ sgn(eB)}{\pi h}\,(Im\left[\psi\left(\frac{\Gamma+i(\mu+\Delta)}{2\pi T}+\frac{1}{2}\right)+(\Delta\rightarrow-\Delta)\right] - \frac{\Gamma}{2\Omega}Re\left[\psi\left(\frac{\Gamma+i(\mu+\Omega+\Delta)}{2\pi T}+\frac{1}{2}\right)-\psi\left(\frac{\Gamma+i(\mu+\Omega+\Delta)}{2\pi T}+\frac{1}{2}\right)+(\Delta\rightarrow-\Delta)\right]) \tag{2.19}$$

Here $\psi(x)$ is the digamma function, μ is the chemical potential, T is the temperature and the impurity scattering rate Γ is taken as frequency independent. Two pieces of information can be obtained about the off-diagonal conductivity element from equation (2.19), (i) in the presence of an external magnetic field, it depends significantly on $sgn(eB)$ (ii) it is an anti-symmetric function of the chemical potential. To consider conductivity as a dimensionless quantity, the definition of fine structure constant is used with the choice of $c = 1$. By choosing some specific values for the parameters like Δ, Γ, T etc. the numerical value of the conductivity can be obtained in the high magnetic field limit of microwave region.

The microwave region is important because of the interesting features shown by the material in its microwave response, for example, the peculiarity of Landau levels in graphene. Landau level quantization is the quantization of the cyclotron orbits of charged particles in magnetic fields. As a result, the charged particles can only occupy orbits with discrete energy values, called Landau levels. The Landau levels are in general degenerate, with the number of electrons per level directly proportional to the strength of the applied magnetic field. But contrary to this, in graphene, the energy of the lowest Landau level is independent of the applied magnetic field. Therefore even in the presence of high magnetic field the lowest Landau level remains unshifted while all other levels shift to higher energies. The conductivity tensor is affected on the low frequency side which is helpful for the study of the development of the gap induced by the magnetic field. It has also been observed in many planar systems with a Dirac-like spectrum of quasi-particle excitations that a high magnetic field limit is very useful for the study of Quantum effects [102].

At this stage it is desirable to think about another situation when the conductivity tensor isotropic, i.e. when the off-diagonal elements vanishes and the diagonal elements are equal. From equation (2.19) it is clear that it happens (i) in the absence of externally applied magnetic field or (ii) when the chemical potential is zero. In the latter case, the diagonal conductivity is obtained by taking the $\mu \rightarrow 0$ limit of equation (2.18). In the former case the diagonal

conductivity in the zero scattering limit at T = 0 is given below:

$$\sigma_{xx}(\Omega) = \frac{\pi e^2 N_f}{h}\,\delta(\Omega)\,\frac{(\mu^2-\Delta^2)\,\theta(\mu^2-\Delta^2)}{|\mu|} + \frac{\pi e^2 N_f}{4h}\,\frac{\Omega^2+4\Delta^2}{\Omega^2}\,\theta\left(\frac{|\Omega|}{2} - max\,\{|\mu|,\,\Delta\}\right) \tag{2.20}$$

Here it is seen that in the isotropic limit, the conductivity tensor become diagonal. But the diagonal tensor does not mean that the medium is isotropic because it can be possible that the tensor is diagonal and still the medium anisotropic which happens when the diagonal elements are unequal. And a fully anisotropic system is characterized with all the elements of the conductivity elements different. As we can see there are various parameters in the above given conductivity equations. By choosing appropriate values for them we can obtain numerical values to the conductivity tensor elements with the help of which various studies can be done using the emergent electric field discussed above.

2.4 Optical Coefficients

Optical quantities discussed in this section are coefficient of reflection, coefficient of transmission and polarization of the reflected wave.

2.4.1 Reflection coefficient

Reflection coefficient is the ratio of reflected wave to incident wave at the point of reflection and it can be either amplitude ratio or intensity ratio depending upon which it is called amplitude reflection coefficient or intensity reflection coefficient. In a general way it is expressed in terms of the ratio of the Poynting's vectors (denoted by **S**) of the incident wave and the reflected wave perpendicular to the plane. i.e. $R = \frac{\mathbf{S}_{ref,z}}{\mathbf{S}_{inc,z}}$ where $\mathbf{S} = \mathbf{E}^* \times \mathbf{B}$. Here **B** is the magnetic field. This will finally reduce to $R = \frac{|\mathbf{E}_{ref}|^2}{|\mathbf{E}_{ext}|^2}$ which becomes $R = \frac{|E_1^{ref}|^2 + |E_2^{ref}|^2}{|E^{ext}|^2}$. Substituting for E_1^{ref} and E_2^{ref} obtained from equation (2.15), the final equation for the reflection coefficient is obtained as

$$R^{fr} = r_1^{fr}\,\cos^2\theta_{tilt}^{ext} + r_2^{fr}\,\sin^2\theta_{tilt}^{ext} + r_3^{fr}\,\sin 2\theta_{tilt}^{ext} \tag{2.21}$$

where

$$
\begin{aligned}
r_1^{fr} = \frac{\pi^2}{2} & (3\sigma_{xy}^2 - 2\sigma_{xy}\sigma_{yx} + 3\sigma_{yx}^2 + (\sigma_{xx} - \sigma_{yy})^2 + \sec^2\theta_0\,[3\sigma_{xx}^2 + (\sigma_{xy} + \sigma_{yx})^2 + 2\sigma_{xx}\sigma_{yy} \\
& + 3\sigma_{yy}^2 + 2\,(-2\sigma_{xx}^2 + \sigma_{xy}^2 - \sigma_{yx}^2 + 2\sigma_{yy}^2 + (\sigma_{xy}^2 - \sigma_{yx}^2)\cos 2\theta_0)\cos 2\phi_0 \\
& - 2\,(3\sigma_{xx}\sigma_{xy} + \sigma_{xx}\sigma_{yx} + \sigma_{xy}\sigma_{yy} + 3\sigma_{yx}\sigma_{yy} + (\sigma_{xy} - \sigma_{yx})\,(\sigma_{xx} - \sigma_{yy})\cos 2\theta_0)\sin 2\phi_0] \\
& + [(\sigma_{xx} - \sigma_{xy} - \sigma_{yx} - \sigma_{yy})\,(\sigma_{xx} + \sigma_{xy} + \sigma_{yx} - \sigma_{yy})cos4\phi_0 \\
& + 2\,(\sigma_{xy} + \sigma_{yx})\,(\sigma_{xx} - \sigma_{yy})\sin 4\phi_0]\tan^2\theta_0)
\end{aligned}
$$

$$
\begin{aligned}
r_2^{fr} = \frac{\pi^2}{4} & [5\sigma_{xx}^2 + 7\sigma_{xy} - 2\sigma_{xy}\sigma_{yx} + 7\sigma_{yx}^2 - 2\sigma_{xx}\sigma_{yy} + 5\sigma_{yy}^2 + 4\,(\sigma_{xx}^2 - 2\sigma_{xy}^2 + 2\sigma_{yx}^2 \\
& - 4\sigma_{yy}^2)\cos 2\phi_0 - (\sigma_{xx} - \sigma_{xy} - \sigma_{yx} - \sigma_{yy})(\sigma_{xx} + \sigma_{xy} + \sigma_{yx} - \sigma_{yy})\cos 4\phi_0 \\
& + 4\,(3\sigma_{xx}\sigma_{xy} - \sigma_{xx}\sigma_{yx} - \sigma_{xy}\sigma_{yy} + 3\sigma_{yx}\sigma_{yy})\sin 2\phi_0 + 2\cos 2\theta_0(\sigma_{xx} + \sigma_{yy} \\
& + (\sigma_{xx} - \sigma_{yy})\cos 2\phi_0 + (\sigma_{xy} + \sigma_{yx})\sin 2\phi_0)^2 - 2(\sigma_{xy} + \sigma_{yx})(\sigma_{xx} - \sigma_{yy})\sin 4\phi_0]
\end{aligned}
$$

$$
\begin{aligned}
r_3^{fr} = \frac{\pi^2}{2} & [-2(\sigma_{xx}\sigma_{xy} + \sigma_{yx}\sigma_{yy})(3 + \cos 2\theta_0)\cos 2\phi_0 \sec\theta_0 + (\sigma_{xx}^2 - \sigma_{xy}^2 + \sigma_{yx}^2 - \sigma_{yy}^2) \\
& (3 + \cos 2\theta_0)\sec\theta_0 \sin 2\theta_0 + \sin\theta_0\,(2\,(\sigma_{xy} - \sigma_{yx})\,(\sigma_{xx} + \sigma_{yy}) \\
& + 2\,(\sigma_{xy} + \sigma_{yx})\,(\sigma_{xx} - \sigma_{yy})\cos 4\phi_0 + (\sigma_{xx} + \sigma_{xy} + \sigma_{yx} - \sigma_{yy}) \\
& (-\sigma_{xx} + \sigma_{xy} + \sigma_{yx} + \sigma_{yy})\sin 4\phi_0)\tan\theta_0]
\end{aligned}
$$

where σ_{xx}, σ_{xy}, σ_{yx} and σ_{yy} are the components of the conductivity tensor, θ_0 is the incident angle, ϕ_0 is the azimuthal angle (angle between the component of incident wave vector in the xy plane and the x axis) and θ_{tilt}^{ext} is the tilt angle of the incident polarization ellipse. From the above equations it is clear that reflection coefficient is a function of various parameters related to both the incident wave $(\theta_0, \phi_0, \theta_{tilt}^{ext})$ and the material medium which is graphene $(\sigma_{xx}, \sigma_{xy}, \sigma_{yx}, \sigma_{yy})$. In different situations in which conductivity tensor has various forms (discussed in an earlier subsection) we can see the difference in the dependence of reflection coefficient.

(i) When $\sigma_{xx} = \sigma_{yy}$ and $\sigma_{xy} = \sigma_{yx}$
(ii) When $\sigma_{xx} = \sigma_{yy}$ and $\sigma_{xy} = -\sigma_{yx}$
(iii) When $\sigma_{xx} = \sigma_{yy}$ and $\sigma_{xy} = \sigma_{yx} = 0$
(iv) When $\sigma_{xx} \neq \sigma_{yy}$ and $\sigma_{xy} = \sigma_{yx} = 0$

Here case (ii) and case (iii) are discussed in detail in an earlier subsection and the equations for conductivity tensor in these limit are given by eqns (2.18, 2.19, 2.20). Other two cases may be important when the sources of anisotropy is something else other than the magnetic field. Case (iv) is important when the system is placed in an in-plane electric field. Then the diagonal elements become unequal with the vanishing off-diagonal elements. This situation is explained in Strikha et. al. [104]. Case(ii), (iii) and (iv) are discussed in detail below (in the result section).

2.4.2 Transmission Coefficient

Transmission coefficient describes either the amplitude or the intensity of a transmitted wave relative to an incident wave. The coefficient can be defined in terms of the Poynting's vector, that is $T = \frac{\mathbf{S}_{tran,z}}{\mathbf{S}_{inc,z}}$ where $\mathbf{S}$ is the Poynting's vector. This reduces to the equation $T = \frac{|\mathbf{E}_{ref}|^2}{|\mathbf{E}_{ext}|^2}$ which becomes $T = \frac{|E_1^{tran}|^2 + |E_2^{tran}|^2}{|E^{ext}|^2}$. Substituting for E_1^{tran} and E_2^{tran} from equations (2.16), the final equation for the transmission coefficient is obtained as

$$T^{fr} = t_1^{fr} \cos^2\theta_{tilt}^{ext} + t_2^{fr} \sin^2\theta_{tilt}^{ext} + t_3^{fr} \sin 2\theta_{tilt}^{ext} \tag{2.22}$$

where

$$\begin{aligned} t_1^{fr} = \frac{1}{2}(2 + \pi^2 [3\sigma_{xy}^2 - 2\sigma_{xy}\sigma_{yx} + 3\sigma_{yx}^2 + (\sigma_{xx} - \sigma_{yy})^2] + \pi (4\sec\theta_0 [-\sigma_{xx} - \sigma_{yy} \\ + (\sigma_{xx} - \sigma_{yy})\cos 2\phi_0 + (\sigma_{xy} + \sigma_{yx})\sin 2\phi_0] + \pi \sec^2\theta_0 [3\sigma_{xx}^2 + (\sigma_{xy} + \sigma_{yx})^2 + 3\sigma_{yy}^2 \\ + 2(-2\sigma_{xx}^2 + 2\sigma_{xy}^2 - \sigma_{yx}^2 + 2\sigma_{yy}^2 + (\sigma_{xy}^2 - \sigma_{yx}^2)\cos 2\theta_0)\cos 2\phi_0 - 2(3\sigma_{xx}\sigma_{xy} \\ + \sigma_{xx}\sigma_{yx} + \sigma_{xy}\sigma_{yy} + 3\sigma_{yx}\sigma_{yy} + (\sigma_{xy} - \sigma_{yx})(\sigma_{xx} - \sigma_{yy})\cos 2\theta_0)\sin 2\phi_0] + \pi [(\sigma_{xx} - \sigma_{xy} \\ - \sigma_{yx} - \sigma_{yy})(\sigma_{xx} + \sigma_{xy} + \sigma_{yx} - \sigma_{yy})\cos 4\phi_0 + 2(\sigma_{xy} + \sigma_{yx})(\sigma_{xx} - \sigma_{yy})\sin 4\phi_0]tan^2\theta_0)) \end{aligned}$$

$$t_2^{fr} = \frac{1}{4}(4 + \pi^2\,[5\sigma_{xx}^2 + 7\sigma_{xy}^2 - 2\sigma_{xy}\sigma_{yx} + 7\sigma_{yx}^2 - 2\sigma_{xx}\sigma_{yy} + 5\sigma_{yy}^2] - 8\pi\cos\theta_0\,[\sigma_{xx} + \sigma_{yy} + (\sigma_{xx} - \sigma_{yy})\cos 2\phi_0 + (\sigma_{xy} + \sigma_{yx})\sin 2\phi_0] + \pi^2\,[(3\sigma_{xx}^2 + (\sigma_{xy} + \sigma_{yx})^2 + 2\sigma_{xx}\sigma_{yy} + 3\sigma_{yy}^2)\cos 2\theta_0 + 4\,(\sigma_{xx}^2 - 2\sigma_{xy}^2 + 2\sigma_{yx}^2 - \sigma_{yy}^2 + (\sigma_{xx}^2 - \sigma_{yy}^2)\cos 2\theta_0)\cos 2\phi_0 - 2\,(\sigma_{xx} - \sigma_{xy} - \sigma_{yx} - \sigma_{yy})\,(\sigma_{xx} + \sigma_{xy} + \sigma_{yx} - \sigma_{yy})\cos 4\phi_0 \sin^2\theta_0 + 4\,(3\sigma_{xx}\sigma_{xy} - \sigma_{xx}\sigma_{yx} - \sigma_{xy}\sigma_{yy} + 3\sigma_{yx}\sigma_{yy} + (\sigma_{xy} + \sigma_{yx})(\sigma_{xx} + \sigma_{yy})\cos 2\theta_0)\sin 2\phi_0 - 4\,(\sigma_{xy} + \sigma_{yx})(\sigma_{xx} - \sigma_{yy})\sin^2\theta_0 \sin 4\phi_0])$$

$$t_3^{fr} = \frac{\pi}{2}\,(2\cos 2\phi_0\,[2\,(\sigma_{xy} + \sigma_{yx}) - \pi\,(\sigma_{xx}\sigma_{xy} + \sigma_{yx}\sigma_{yy})\,(3 + \cos 2\theta_0)\sec\theta_0] + [4\,(-\sigma_{xx} + \sigma_{yy})\cos\theta_0 + \pi\,(\sigma_{xx}^2 - \sigma_{xy}^2 + \sigma_{yx}^2 - \sigma_{yy}^2)\,(3 + \cos 2\theta_0)]\sec\theta_0 \sin 2\phi_0 + 2\pi\,(\sigma_{xy} - \sigma_{yx})\,(\sigma_{xx} + \sigma_{yy})\sin\theta_0 \tan\theta_0 + 2\pi\,(\sigma_{xy} + \sigma_{yx})\,(\sigma_{xx} - \sigma_{yy})\cos 4\phi_0 \sin\theta_0 \tan\theta_0 - \pi\,(\sigma_{xx} - \sigma_{xy} - \sigma_{yx} - \sigma_{yy})\,(\sigma_{xx} + \sigma_{xy} + \sigma_{yx} - \sigma_{yy})\sin\theta_0 \sin 4\phi_0 \tan\theta_0)$$

The explanations of various parameters are mentioned in the previous subsection. Similar to reflection coefficient, transmission coefficient also is a function of both incident wave parameters $(\theta_0, \phi_0, \theta_{tilt}^{ext})$ and the material parameters $(\sigma_{xx}, \sigma_{xy}, \sigma_{yx}, \sigma_{yy})$. Here also various situations under which form of the conductivity tensor changes has been considered to see the difference.

2.4.3 Reflected Polarization

This quantity measures the polarization of the reflected wave in terms of the polarization of the incident wave. This can be obtained from the formula $e^{-i\delta^{ref}} = \frac{\left(E_1^{ref}\right)^*\left(E_2^{ref}\right)}{|E_1^{ref}|\,|E_2^{ref}|}$. After substituting for the two polarization components of the reflected electric field from equation (2.15) we obtain the equation for reflected polarization as given below,

$$e^{-i\delta_{fr}^{ref}} = \frac{n_1^{fr} + in_2^{fr}}{\sqrt{d_1^{fr}\,d_2^{fr}}} \tag{2.23}$$

where $\delta_{fr}^{ref} = \delta_{1,fr}^{ref} - \delta_{2,fr}^{ref}$ is the polarization of the reflected light.

$$
\begin{aligned}
n_1^{fr} = & -\pi^2 \sec\theta_0 \left[-\sigma_{xx} - \sigma_{yy} + (\sigma_{xx} - \sigma_{yy})\cos 2\phi_0 + (\sigma_{xy} + \sigma_{yx})\sin 2\phi_0\right]\left[\sigma_{xy} - \sigma_{yx}\right. \\
& \left. + (\sigma_{xy} + \sigma_{yx})\cos 2\phi_0 + (-\sigma_{xx} + \sigma_{yy})\sin 2\phi_0\right]\cos^2\theta_{tilt}^{ext} + \pi^2\cos\theta_0\left[\sigma_{xx} + \sigma_{yy}\right. \\
& \left. + (\sigma_{xx} - \sigma_{yy})\cos 2\phi_0 + (\sigma_{xy} + \sigma_{yx})\sin 2\phi_0\right]\left[-\sigma_{xy} + \sigma_{yx} + (\sigma_{xy} + \sigma_{yx})\cos 2\phi_0\right. \\
& \left. + (-\sigma_{xx} + \sigma_{yy})\sin 2\phi_0\right]\sin^2\theta_{tilt}^{ext} + \pi^2\left[-(\sigma_{xx} + \sigma_{xy} - \sigma_{yx} + \sigma_{yy})(\sigma_{xx} - \sigma_{xy} + \sigma_{yx} + \sigma_{yy})\right. \\
& \left. + (\sigma_{xx} - \sigma_{xy} - \sigma_{yx} - \sigma_{yy})(\sigma_{xx} + \sigma_{xy} + \sigma_{yx} - \sigma_{yy})\cos 4\phi_0\right. \\
& \left. + 2(\sigma_{xy} + \sigma_{yx})(\sigma_{xx} - \sigma_{yy})\sin 4\phi_0\right]\sin\theta_{tilt}^{ext}\cos\theta_{tilt}^{ext}\cos\delta^{ext}
\end{aligned}
$$

$$
n_2^{fr} = 4\pi^2\left(-\sigma_{xy}\sigma_{yx} + \sigma_{xx}\sigma_{yx}\right)\sin\theta_{tilt}^{ext}\cos\theta_{tilt}^{ext}\sin\delta^{ext}
$$

$$
\begin{aligned}
d_1^{fr} = & \left[\pi^2\sec^2\theta_0\left(\sigma_{xx} + \sigma_{yy} - (-\sigma_{xx} + \sigma_{yy})\cos 2\phi_0 - (\sigma_{xy} + \sigma_{yx})\sin 2\phi_0\right)^2\right]\cos^2\theta_{tilt}^{ext} \\
& + \left[\pi^2\left(-\sigma_{xy} + \sigma_{yx} - (\sigma_{xy} + \sigma_{yx})\cos 2\phi_0 + (-\sigma_{xx} + \sigma_{yy})\sin 2\phi_0\right)^2\right]\sin^2\theta_{tilt}^{ext} \\
& - 4\pi^2\sec\theta_0\left[\sigma_{yy}\cos^2\phi_0 - (\sigma_{xy} + \sigma_{yx})\cos\phi_0\sin\phi_0 + \sigma_{xx}\sin^2\phi_0\right]\left[\sigma_{yx}\cos^2\phi_0\right. \\
& \left. + (-\sigma_{xx} + \sigma_{yy})\cos\phi_0\sin\phi_0 - \sigma_{xy}\sin^2\phi_0\right]\sin 2\theta_{tilt}^{ext}\cos\delta^{ext}
\end{aligned}
$$

$$
\begin{aligned}
d_2^{fr} = & \left[\pi^2\left(\sigma_{xy} - \sigma_{yx} + (\sigma_{xy} + \sigma_{yx})\cos 2\phi_0 + (-\sigma_{xx} + \sigma_{yy})\sin 2\phi_0\right)^2\right]\cos^2\theta_{tilt}^{ext} \\
& + \left[\pi^2\cos^2\theta_0\left(\sigma_{xx} + \sigma_{yy} + (\sigma_{xx} - \sigma_{yy})\cos 2\phi_0 + (\sigma_{xy} + \sigma_{yx})\sin 2\phi_0\right)^2\right]\sin^2\theta_{tilt}^{ext} \\
& - 4\pi^2\cos\theta_0\left[\sigma_{xy}\cos^2\phi_0 + (-\sigma_{xx} + \sigma_{yy})\cos\phi_0\sin\phi_0 - \sigma_{yx}\sin^2\phi_0\right]\left[\sigma_{xx}\cos^2\phi_0\right. \\
& \left. + (\sigma_{xy} + \sigma_{yx})\cos\phi_0\sin\phi_0 + \sigma_{yy}\sin^2\phi_0\right]\sin 2\theta_{tilt}^{ext}\cos\delta^{ext}
\end{aligned}
$$

By simultaneously solving the real and imaginary parts of equation (2.23) we can study the behavior of reflected polarization in terms of other parameters. Different restrictions on the conductivity tensor elements (as discussed in an earlier sub section) reduces the complications of the above given equation which are discussed in the next section.

2.5 Results and Discussion

Each of the afore mentioned optical quantities are discussed in this section taking into account different limiting cases separately. In each of the cases, viz. isotropic, anisotropic, incident

linear polarization, the coefficients are studied with the help of a number of plots.

2.5.1 Isotropic Case

Isotropic limit of the conductivity tensor is one of the important and interesting limiting case. This happens when the off-diagonal elements of the conductivity tensor vanishes and when the diagonal elements are equal. i.e. $\sigma_{xx} = \sigma_{yy}$ and $\sigma_{xy} = \sigma_{yx} = 0$. From equation (2.17), it is clear that vanishing of the off-diagonal conductivity elements happens in two different ways. (i) when the external applied static magnetic field is zero (ii) when the chemical potential is zero. This implies that the anisotropic nature of the optical conductivity tensor can be invoked by the magnetic field applied or by electrostatic doping of the material. As discussed in chapter 1, graphene band structure contains two inequivalent pairs of Dirac cones. Zero chemical potential implies that, out of these two cones one cone in each pair is full and the other is empty. Positive chemical potential makes the carriers electrons and the negative chemical potential signifies the carriers as holes.

As we can see below in the isotropic limit, the coefficients are functions of only the diagonal conductivity and the angle parameters θ_{tilt}^{ext} and θ_0. Out of these the conductivity can be obtained for the first case (for $B = 0$) from equation (2.20) and for the second case (for $\mu = 0$) from equation (2.19) by fixing values for the parameters like gap, impurity scattering rate etc. For example, for zero applied magnetic field with the choice of $\mu = 4K$ and $\Omega = 9.6K$ in equation (2.20) the diagonal element $\sigma_{xx} = 1.82 \times 10^{-3}$ (when $\Delta = 0K$) and 2.54×10^{-3} (when $\Delta = 3K$). For zero electrostatic doping case, $\sigma_{xx} = 2.404 \times 10^{-5}$ (with $\Delta = 0K$) and 2.402×10^{-5} (with $\Delta = 3K$). As such there is nothing special about the value of $3K$ chosen for the gap in the calculation for conductivity. As discussed above, the numerical values of the graphene conductivity tensor for this study is taken from the reference Gusynin et. al. [106] and we have chosen the value $3K$ for Δ since this reference also does the same.

Note that the conductivity tensor elements are in units of c where c is taken as unity throughout this calculation and all the energy equivalent quantities are expressed in units of "Kelvin". At this stage, the general equation for the reflection coefficient (2.21), transmission coefficient (2.22) and reflected polarization (2.23) reduces to a much simpler form as given below and is discussed below in detail. All studies in this chapter are done in the microwave

region of the electromagnetic spectrum and more specifically for an incident energy $\Omega = 200\ GHz$.

2.5.1.1 Reflection coefficient

In the isotropic limit, the reflection coefficient reduces to a simpler form

$$R_{iso}^{fr} = 4\pi^2\sigma_{xx}^2\left(\cos^2\theta_{tilt}^{ext}\sec^2\theta_0 + \cos^2\theta_0\sin^2\theta_{tilt}^{ext}\right) \tag{2.24}$$

With a fixed conductivity, R_{iso}^{fr} is a function of two angle parameters which are the incident angle and the tilt angle of the incident polarization ellipse and clearly the reflection coefficient is independent of the azimuthal angle of the incident wave. The nature of the coefficient with respect to one of the angle parameters with a fixed value of the other one is considered in the $B = 0$ situation (mentioned above) of isotropic nature (Fig. 2.2).

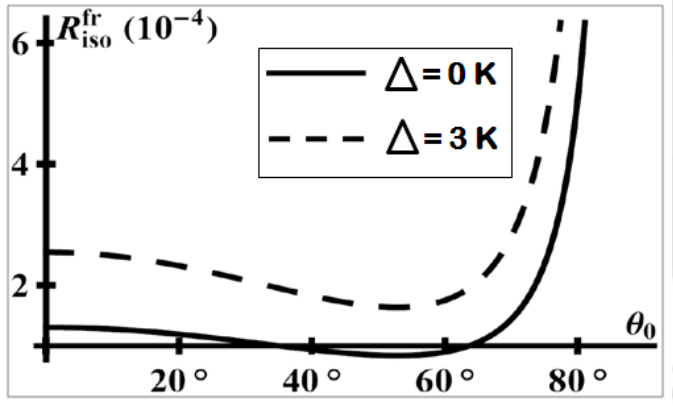

FIGURE 2.2: Reflection coefficient versus incident angle when the graphene conductivity tensor is isotropic (Incident photon energy is fixed to a value $\Omega = 200\ GHz$). Here the solid curve shows the situation with zero gap in the graphene quasi-particle spectrum and dashed curves represents that with a finite gap.

Fig. 2.2 shows the variation of R_{iso}^{fr} with respect to θ_0 with tilt angle fixed. This contains two curves that corresponds to the zero gap and a finite gap situation. The gap factor denoted by Δ is coming through the dependence of reflection coefficient on conductivity tensor. The second possibility of the isotropy, which is $\mu = 0$, the reflection coefficient becomes extremely small ($\sim 10^{-8}$) compared to the first case and the effect of gap is also not significant, therefore it is not included in the plot. The influence of gap on the reflected intensity as can be seen from Fig. 2.2 is to increase it but the effect decreases as the angle of incidence increases. Another

interesting case is the situation when the wave is incident normal to the plane of the material. Then the isotropic reflection coefficient solely depends on the diagonal conductivity only, i.e. $R_{iso}^{fr,\perp} = 4\pi^2\sigma_{xx}^2$. All together we can see that the magnitude of the reflection coefficient is very small which is expected and proved by experiments. Experiments show that the reflectance in graphene is less than 0.1% at optical frequencies [92].

Consider the special situation, when the incident wave is linearly polarized. That is when there is no phase difference between the two polarization amplitudes the obvious way of which is when $\delta^{ext} = 0$. With reference to the plane of incidence, a simple classification of linearly polarized light becomes possible. Two kinds of linearly polarized light are defined in the literature. One is known as p-polarized where the electric field vector is parallel to the plane of incidence and s-polarized light where the electric field vector is perpendicular to the plane of incidence. In other words, the two types namely, $s-$ polarization and $p-$ polarization refer to a situation where the tilt angle of the incident polarization ellipse are 0 and $\pi/2$ respectively. For both the extreme cases, the angle dependence of R_{iso}^{fr} is through the incident angle only. For $s-$ polarization it is $\sec^2\theta_0$ and $p-$ polarization it is $\cos^2\theta_0$. For this reason, in the $s(p)-$ polarization case, the reflected intensity is minimum (maximum) at normal incidence and in the other way round for gracing incidence. It is already seen that reflection coefficient is small, but it further decreases in the case of $p-$ polarization compared with the $s-$ polarization (because of the dependence on the incident angle).

2.5.1.2 Transmission Coefficient

In the isotropic limit, the transmission coefficient reduces to a much simpler form as given below:

$$T_{iso}^{fr} = \cos^2\theta_{tilt}^{ext}(1 - 2\pi\sigma_{xx}\sec\theta_0)^2 + (1 - 2\pi\sigma_{xx}\cos\theta_0)^2\sin^2\theta_{tilt}^{ext} \tag{2.25}$$

With fixed diagonal conductivity, as in the case of reflection coefficient, T_{iso}^{fr} is a function of only two angle parameters (the incident angle and the tilt angle) as in the case of isotropic reflection coefficient, that is its independent of the other parameters like azimuthal angle and incident polarization. Only the case with $B = 0$ is discussed here because the other case does not show much variation and is always close to unity through out the whole range of variation of the parameter.

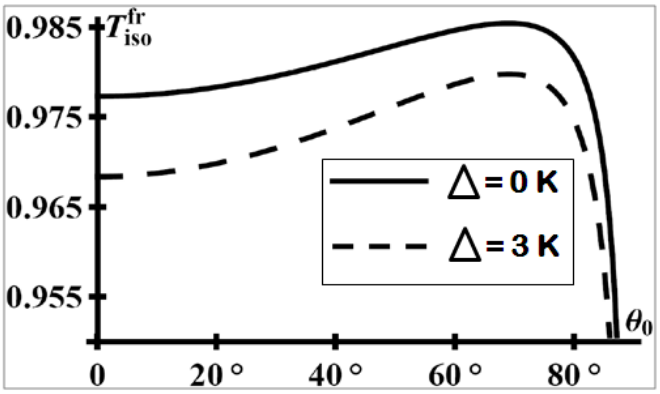

FIGURE 2.3: Transmission coefficient versus incident angle when the graphene conductivity tensor is isotropic (Incident photon energy is fixed to a value $\Omega = 200\ GHz$). The solid curve demonstrates the zero gap situation in the graphene quasi-particle spectrum and dashed curves represents that with a finite gap.

Fig. 2.3 shows the variation with respect to incident angle with tilt angle fixed which contains two curves, the solid one showing the zero gap situation and the dashed curve shows the finite gap situation. The influence of gap as can be seen, decreases the transmission coefficient (contrary to reflection coefficient) which is more visible in the small incident angles. Transmitted intensity is maximum at small angle of incidence and it slowly decreases as it approaches the grazing incidence. At normal incidence, we can see that the transmission coefficient depends only on the diagonal conductivity element and is given by $T_{iso}^{fr,\perp} = (1 - 2\pi\sigma_{xx})^2$. It is seen that the transmission coefficient is very large which is one of the special characteristics of graphene (high optical transparency). It is known that in the higher energy regions of the electromagnetic spectrum such as visible region, the optical conductivity tensor is a universal constant whose value is $\frac{e^2}{4\hbar}$. By taking σ_{xx} as the universal constant in our study, the transmission coefficient for mono-layer graphene shows exact matching with one of the experimental finding for the same [92]. From the present study it is also clear that in monolayer graphene the absorption is very small and is easily found out in the case of normal incidence using the conservation theorem, i.e. $1 - R - T$ which gives a value 0.023 when $\sigma_{xx} = \frac{e^2}{4\hbar}$. The conservation theorem for a general case in monolayer graphene is derived in Appendix A. The transmitted intensity and absorption for monolayer graphene matches perfectly with one of the experimental observations by Nair et. al. [92].

In the extreme limits of linear incident polarization, the only parameter upon which the transmitted intensity depends is on the incident angle. For $s-$ polarization the dependence is

$(1 - 2\sigma_{xx} \sec\theta_0)^2$ and for $p-$ polarization it is $(1 - 2\sigma_{xx} \cos\theta_0)^2$. The behavior of the transmission coefficient with the $s-$ and $p-$ polarized incident wave with respect to incident angle is exactly opposite that of the reflection coefficient. When the incident angle is small, both the reflection and transmission for s and p polarized incident wave coincides. As θ_0 increases, the T with $s-$ polarized wave increases and that with $p-$ polarized incidence decreases which is in the other way for reflection coefficient. Therefore in the case of transmission, in contrary to reflection coefficient, the $p-$ polarized incident wave increases the transmitted intensity.

2.5.1.3 Reflected Polarization

In the isotropic limit, the reflected polarization reduces to

$$e^{-i\delta^{ref}}|_{iso,fr} = -\frac{\cos\theta^{ext}_{tilt} \sin\theta^{ext}_{tilt} e^{-i\delta^{ext}}}{\sqrt{\cos\theta^{ext}_{tilt} \sin\theta^{ext}_{tilt}}} = -e^{-i\delta^{ext}} sgn(\sin 2\theta^{ext}_{tilt}) \tag{2.26}$$

In contrast to the other two quantities namely the reflection coefficient and transmission coefficient, it is seen that the polarization of the reflected wave is dependent only on the incident polarization in the isotropic limit. The qualitative behavior of reflected polarization depends on the sign of $\sin 2\theta^{ext}_{tilt}$ also. Since the reflected polarization is independent of the conductivity, the two cases of isotropic limits makes no difference and also the gap does not enter into the picture. Therefore we can think that the isotropic limit makes polarization of the reflected wave from graphene sheet deprived of the any material specific parameters. From equation (2.26) it is understood that the real and imaginary part of reflected polarization shows an oscillatory behavior with respect to incident polarization. By simultaneously solving the equations of $\cos\delta^{ref}$ and $\sin\delta^{ref}$ reflected polarization can be obtained. From the equation for reflected polarization given by (2.26) we can infer that the polarization of reflected wave is either equal to the incident polarization or there is a 180^0 difference between the two polarizations. Hence the key point in this study is that the phase shift (either 180^0 or 0^0) between the incident and reflected polarization can be found out from θ^{ext}_{tilt} and the magnitude of reflected polarization from the incident polarization.

The two extreme cases of incident polarization, i.e. $s-$ and $p-$ polarization are taken in to consideration in this limit and is explained in Fig. 2.4. It shows the behavior of real and imaginary parts of the reflected polarization with respect to incident polarization There are different curves which shows the real and imaginary parts with s and p polarized incidence.

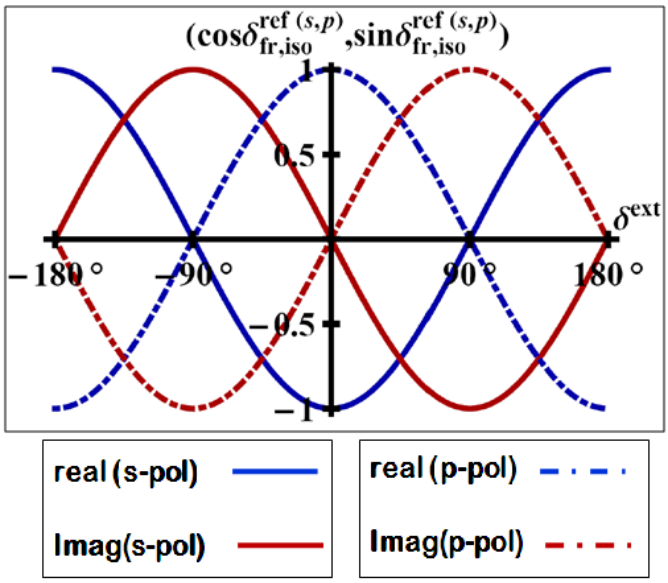

FIGURE 2.4: Polarization of the reflected wave from mono-layer free standing graphene versus incident polarization when the incident wave is linearly polarized in an extreme way and the conductivity tensor is isotropic (Incident photon energy is fixed to a value $\Omega = 200\,GHz$). Here the solid curves are for s polarized incident waves and dot-dashed curves are for p polarized incident waves. The blue curves shows the behavior of real part of the reflected polarization and the red curves shows the imaginary part of reflected polarization.

The variation is oscillatory as given by equation (2.26) with respect to incident polarization. That is for an $s-$ polarized incident wave, the real part of reflected polarization varies as $-\cos\delta^{ext}$ and imaginary part varies as $\sin\delta^{ext}$. Similarly, for $p-$ polarized incident wave, the real part varies as $\cos\delta^{ext}$ and imaginary part as $-\sin\delta^{ext}$.Following table gives an idea about δ^{ref} for different ranges of values of δ^{ext}.

$s-$ **polarization**		$p-$ **polarization**	
δ^{ext}	δ^{ref}	δ^{ext}	δ^{ref}
$(0, \frac{\pi}{2})$	$(0, \frac{\pi}{2})$	$(0, \frac{\pi}{2})$	$(-\frac{\pi}{2}, -\pi)$
$(\frac{\pi}{2}, \pi)$	$(\frac{\pi}{2}, \pi)$	$(\frac{\pi}{2}, \pi)$	$(0, -\frac{\pi}{2})$
$(0, -\frac{\pi}{2})$	$(0, -\frac{\pi}{2})$	$(0, -\frac{\pi}{2})$	$(\frac{\pi}{2}, \pi)$
$(-\frac{\pi}{2}, -\pi)$	$(-\frac{\pi}{2}, -\pi)$	$(-\frac{\pi}{2}, -\pi)$	$(0, \frac{\pi}{2})$

Table.1: Reflected polarization for different ranges of incident polarization for s and p polarized incident wave

When the incident wave is linearly polarized with $\delta^{ext} = 0$, the imaginary part of the reflected polarization is always zero which implies that δ^{ref} is either 0 or $\pm\pi$ and the real part depends on $sgn(\sin 2\theta^{ext}_{tilt})$ and is either $+1$ or -1. Therefore when the incident polarization vanishes, reflected polarization is determined by tilt angle (whether it is 0 or $\pm\pi$). More specifically, sign of $-\sin 2\theta^{ext}_{tilt}$ determines the value of reflected polarization if $\delta^{ext} = 0$.

In this section, mainly the isotropic nature of different optical quantities are studied with respect to different angle parameters. The situation in which the incident polarization is linear (three different cases) is also studied. From the equations derived in this section we can obtain information about the conductivity tensor of mono-layer graphene by knowing the reflection and transmission coefficients. That is, we derive equations for the conductivity tensor elements in terms of the reflection and transmission coefficients. This is explained in Appendix A.

2.5.2 Anisotropic Case

The conductivity tensor of graphene may also be anisotropic in different ways as discussed earlier.

(i) When the diagonal elements are equal and the off-diagonal elements are equal and opposite in sign ($\sigma_{xx} = \sigma_{yy} = \sigma_1$ and $\sigma_{xy} = -\sigma_{yx} = \sigma_2$)

(ii) When the diagonal elements are different and the off-diagonal elements are zero ($\sigma_{xx} \neq \sigma_{yy}$ and $\sigma_{xy} = \sigma_{yx} = 0$)

(iii) When the diagonal elements are equal and the off- diagonal elements are equal and same in sign ($\sigma_{xx} = \sigma_{yy} = \sigma_1$ and $\sigma_{xy} = \sigma_{yx} = \sigma_2$)

(iv) When the diagonal elements and off diagonal elements are all different ($\sigma_{xx} \neq \sigma_{yy}$ and $\sigma_{xy} \neq \sigma_{yx}$)

Only the first two situations enumerated above are considered in this section. The first situation given above happens when graphene is in an externally applied static magnetic field denoted by **B**. This is discussed in Gusynin et. al. [100] where it is explained mathematically that in the presence of an externally applied perpendicular magnetic field the conductivity

tensor can have such a form. In the second case listed above, the conductivity tensor is diagonal but the diagonal elements are not equal which means that the properties are not same along the two directions. This can be possible by the application of an in-plane external static electric field. This situation is explained in detail by Strikha et. al. [104]. The third case listed above may be possible if there is an in-plane electric field and the electric field is applied in a direction away from the principal axes of the material. If the applied electric field is such that the difference between the diagonal elements are so small, then the off-diagonal elements will have a non-zero magnitude of the order of difference between the diagonal elements. The last situation can be possible when the material is highly anisotropic due to various external agents or a combination of them. In this section most of the attention goes to the first condition which can be named "off-diagonal anisotropy" and is possible in the presence of a static perpendicular magnetic field (according to Gusynin et. al.). The numerical value of the conductivity tensor elements for this situation is obtained from equations in the microwave region (2.18) and (2.19) by fixing the parameters as in the case of isotropic limit. For example, with $\Gamma = 4K$, $\mu = -6K$, $T = 0.5K$, $\Omega = 9.6K$ one gets $\sigma_{xx} = \sigma_{yy} = 6.28 \times 10^{-4}$ and $\sigma_{xy} = -\sigma_{yx} = 1.78 \times 10^{-3}$ for $\Delta = 0K$ (zero gap in the quasi-particle spectrum) and $\sigma_{xx} = \sigma_{yy} = 5.83 \times 10^{-4}$ and $\sigma_{xy} = \sigma_{yx} = 1.63 \times 10^{-3}$ with a finite gap (for example $3K$). Note that all the parameters given above are expressed in an energy equivalent unit Kelvin and the conductivity when expressed in terms of the fine structure constant has the unit of 'c' and in this calculation 'c' is taken as unity. In the second case, which can be named "diagonal anisotropy", as discussed in Strikha et. al. [104], the diagonal conductivity elements can be taken as $\sigma_{xx} = \sigma + \frac{\Delta\sigma}{2}$ and $\sigma_{yy} = \sigma - \frac{\Delta\sigma}{2}$, where σ is taken as the universal optical conductivity $\frac{e^2}{4\hbar}$ and $\Delta\sigma$ is chosen randomly to be a small quantity compared to σ, say of the order of 10^{-4} which is consistent with Strikha et. al. As in the isotropic case, here also the reflection coefficient, transmission coefficient and reflected polarization are considered for study with incident photon energy in the microwave region i.e. with $\Omega = 200\ GHz$.

2.5.2.1 Reflection Coefficient

When $\sigma_{xx} = \sigma_{yy} = \sigma_1$ and $\sigma_{xy} = -\sigma_{yx} = \sigma_2$.

$$R^{fr}_{off} = 2\pi^2 \left[2\cos^2\theta^{ext}_{tilt}(\sigma_2^2 + \sigma_1^2\sec^2\theta^{ext}_{tilt}) + (\sigma_1^2 + 2\sigma_2^2 + \sigma_1^2\cos 2\theta_0)\sin^2\theta^{ext}_{tilt} + 2\sigma_1\sigma_2\cos\delta^{ext}\sin\theta_0\tan\theta_0\sin 2\theta^{ext}_{tilt}\right] \quad (2.27)$$

When $\sigma_{xx} \neq \sigma_{yy}$ and $\sigma_{xy} = \sigma_{yx} = 0$

$$\begin{aligned} R^{fr}_{diag} = & ([5\sigma_1^2 - 2\sigma_1\sigma_4 + 5\sigma_4^2 + 2\cos 2\theta_0\,(\sigma_1 + \sigma_4 + (\sigma_1 - \sigma_4)\cos 2\phi_0)^2 \\ & + (\sigma_1 - \sigma_4)\,(4\,(\sigma_1 + \sigma_4)\cos 2\phi_0 + (-\sigma_1 + \sigma_4)\cos 4\phi_0)]\sin^2\theta^{ext}_{tilt} \\ & + 2\,(\sigma_1 - \sigma_4)\cos\delta^{ext}\sin 2\theta^{ext}_{tilt}\,[(\sigma_1 + \sigma_4)\,(3 + \cos 2\theta_0)\sec\theta_0\sin 2\phi_0 \\ & + (-\sigma_1 + \sigma_4)\sin\theta_0\sin 4\phi_0\tan\theta_0] + 2\cos^2\theta^{ext}_{tilt}\,[(3\sigma_1^2 + 2\sigma_1\sigma_4 + 3\sigma_4^2 \\ & + 4\,(-\sigma_1^2 + \sigma_4^2)\cos 2\phi_0)\sec^2\theta_0 + (\sigma_1 - \sigma_4)^2(1 + \cos 4\phi_0\tan^2\theta_0)]) \end{aligned} \tag{2.28}$$

where $\sigma_{xx} = \sigma_1$ and $\sigma_{yy} = \sigma_4$. We can see that the first case is clearly different from the other case because in it the reflection coefficient is a function of all the parameters except the azimuthal angle where as in the other case, the azimuthal angle dependence is coming in to picture. Reflection coefficients of both the above given cases are plotted with respect to each of the parameters with the others fixed as explained earlier.

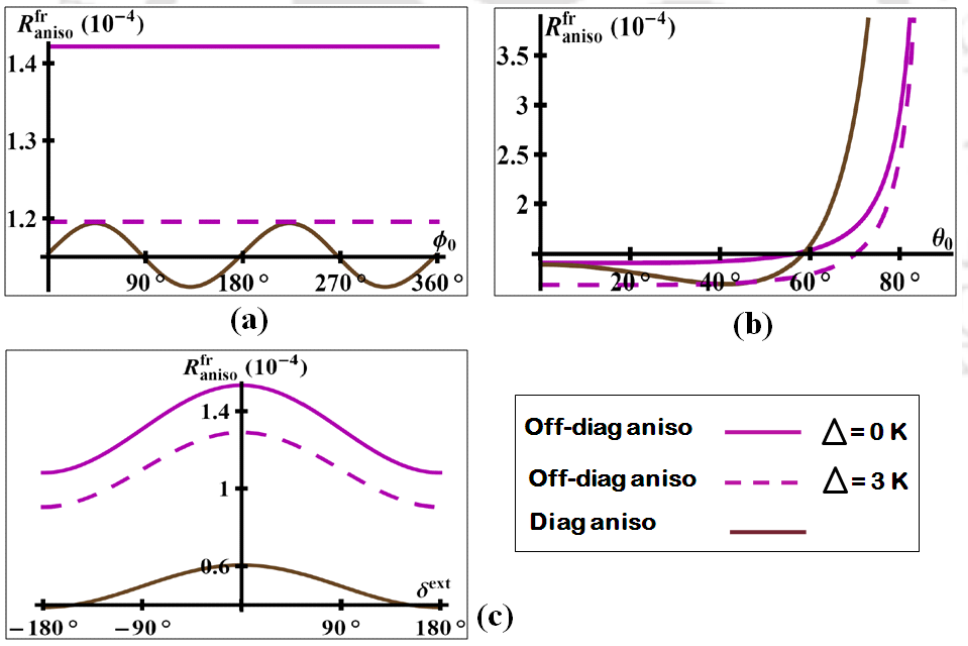

FIGURE 2.5: Reflection coefficient versus various angle parameters. This figure has three parts (a) behavior with respect to azimuthal angle (b) variation with respect to incident angle (c) variation with respect to incident polarization. In this figure the solid magenta curve shows the situation with off diagonal anisotropy with zero gap and dashed magenta curve shows that with finite gap and solid brown curve shows the behavior with diagonal anisotropic situation. Here incident photon energy is fixed to a value with frequency 200 *GHz*

Fig. 2.5 has three parts which shows the anisotropic reflection coefficient versus azimuthal angle, incident angle and the incident polarization respectively for the two types of anisotropic situations mentioned above. Each of these panels has three curves, where the magenta curve is for off-diagonal anisotropic situation (solid one for zero gap case and dashed one for finite gap case). The brown curves are for diagonal anisotropic situation. From each of the panels we can see that the effect of gap is to decrease the magnitude of the reflection coefficient.

From Fig. 2.5a, it is clear that when the anisotropy is such that the off-diagonal element is equal in magnitude and opposite sign, the azimuthal angle dependence is washed out. But for a diagonal type of anisotropy, azimuthal angle variation comes in to picture. Fig. 2.5b shows variation with respect to incident angle. For small angle of incidence the variation is almost constant and the reflected intensity increases with incident angle. The effect of gap in the case of off-diagonal anisotropy is more visible with small angle of incidence. The last part of the figure shows the variation of reflection coefficient with respect to the incident polarization. We can see that the behavior is similar in both the kinds of anisotropy. The extremely small magnitude of reflected intensity can be observed in the anisotropic limiting case also.

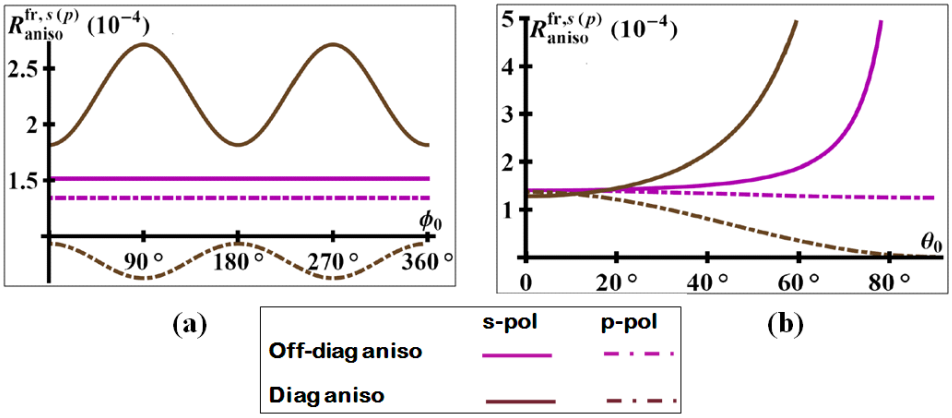

FIGURE 2.6: Reflection coefficient versus various angle parameters when the conductivity tensor is anisotropic and the incident wave is linearly polarized. This figure has two parts (a) behavior with respect to azimuthal angle (b) variation with respect to incident angle. The solid curves for incident *s* polarized wave and dot-dashed curves for incident *p* polarized wave. The magenta curve shows the situation with off diagonal anisotropy and brown curve shows the behavior with diagonal anisotropic situation. Here incident photon energy is fixed to a value $\Omega = 200\ GHz$

Consider the special case where the incident wave is linearly polarized. First let us consider the extreme cases as discussed in the isotropic limit, viz. *s*– and *p*– polarization. In this limit, the reflection coefficients for both the above mentioned cases of anisotropy are shown in

Fig. 2.6. Here R_{aniso} is a function of incident angle for both the type of anisotropy and for diagonal anisotropy it is a function of azimuthal angle also. In both the cases, we can see that the $p-$ polarization decreases the reflection coefficient. Fig. 2.6a, shows the variation of reflection coefficient with respect to azimuthal angle where off-diagonal anisotropic situation shows a constant behavior whereas the diagonal anisotropic situation shows an oscillatory behavior. The diagonal anisotropic behavior of reflected intensity with s and p polarized incident wave shows a $\pi/2$ phase shift. Fig. 2.6b shows the variation with respect to incident angle where the qualitative behavior of both the type of anisotropy are similar. The reflected intensity with s polarized incident wave increases where as that of p polarized incident wave decreases with incident angle and approaches a minimum at gracing incidence. The third route to linear incident polarization is when $\delta^{ext} = 0$ where the reflection coefficient is a function of azimuthal angle, incident angle and tilt angle of the incident polarization ellipse. The behavior with respect to azimuthal angle and the incident angle are similar to that of $s-$ polarization case

All together in this subsection the reflection coefficient is studied when the graphene conductivity is anisotropic. Two different kinds of anisotropy are considered here and in each case variation with respect to various parameters are studied by fixing the conductivity tensor elements. It is important to highlight one of the main observations obtained from this study which is the significance of azimuthal angle dependence which indicates the type of anisotropy present in the material. It is believed that as the strength of azimuthal angle dependence increases with the strength of diagonal anisotropy.

2.5.2.2 Transmission Coefficient

When $\sigma_{xx} = \sigma_{yy} = \sigma_1$ and $\sigma_{xy} = -\sigma_{yx} = \sigma_2$

$$T_{off}^{fr} = \cos^2\theta_{tilt}^{ext}\left[1 + 4\pi^2\sigma_2^2 + 4\pi\sigma_1 \sec\theta_0\left(-1 + \pi\sigma_1 \sec\theta_0\right)\right] + \sin^2\theta_{tilt}^{ext} + 2\pi\left[\left(-2\sigma_1\cos\theta_0 + \pi\left(\sigma_1^2 + 2\sigma_2^2 + \sigma_1^2\cos 2\theta_0\right)\right)\sin^2\theta_{tilt}^{ext} + 2\pi\sigma_1\sigma_2\cos\delta^{ext}\sin\theta_0\sin 2\theta_{tilt}^{ext}\tan\theta_0\right] \quad (2.29)$$

When $\sigma_{xx} \neq \sigma_{yy}$ and $\sigma_{xy} = \sigma_{yx} = 0$

$$
\begin{aligned}
T^{fr}_{diga} = \frac{1}{4}\Big([4 + \pi^2 (5\sigma_1^2 - 2\sigma_1\sigma_4 + 5\sigma_4^2) - 8\pi \cos\theta_0 (\sigma_1 + \sigma_4 + (\sigma_1 - \sigma_4)\cos 2\phi_0) \\
+ \pi^2 ((3\sigma_1^2 + 2\sigma_1\sigma_4 + 3\sigma_4^2)\cos 2\theta_0 + 2(\sigma_1 - \sigma_4)(4(\sigma_1 + \sigma_4)\cos^2\theta_0 \cos 2\phi_0 \\
+ (-\sigma_1 + \sigma_4)\cos 4\phi_0 \sin^2\theta_0))]\sin^2\theta^{ext}_{tilt} + 2\pi(\sigma_1 - \sigma_4)\cos\delta^{ext}\sin 2\theta^{ext}_{tilt}[(-4\cos\theta_0 \\
+ \pi(\sigma_1 + \sigma_4)(3 + \cos 2\theta_0))\sin 2\phi_0 + \pi(-\sigma_1 + \sigma_4)\sin\theta_0 \sin 4\phi_0 \tan\theta_0] \\
+ 2\cos^2\theta^{ext}_{tilt}[2 + \pi^2(\sigma_1 - \sigma_4)^2 + \pi(-4(\sigma_1 - \sigma_4)\cos 2\phi_0 \sec\theta_0(-1 + \pi(\sigma_1 \\
+ \sigma_4)\sec\theta_0) + \sec\theta_0(-4(\sigma_1 + \sigma_4) + \pi(3\sigma_1^2 + 2\sigma_1\sigma_4 + 3\sigma_4^2)\sec\theta_0) \\
+ \pi(\sigma_1 - \sigma_4)^2 \cos 4\phi_0 \tan^2\theta_0)]\Big)
\end{aligned}
\tag{2.30}
$$

where $\sigma_{xx} = \sigma_1$ and $\sigma_{yy} = \sigma_4$. The first case is different from the second because of the azimuthal angle dependence of the diagonal anisotropic situation. Transmission coefficients of both the above given cases are shown in the plots given below with respect to incident angle.

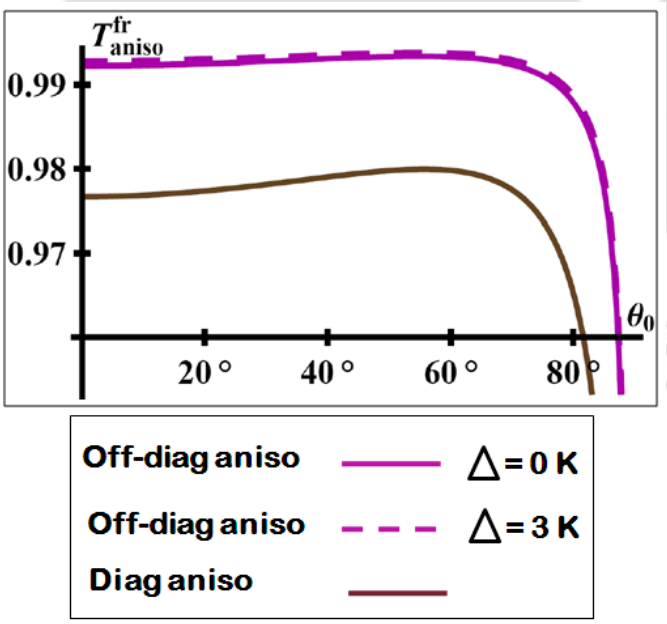

FIGURE 2.7: Transmission coefficient versus incident angle when the optical conductivity tensor is anisotropic. Both types of anisotropic situations are shown in the figure, magenta solid curve shows the situation with zero gap off diagonal anisotropic conductivity tensor and dashed magenta curve that with finite gap. The brown solid curve shows the diagonal anisotropic situation. Here incident photon energy is fixed to a value $\Omega = 200\ GHz$

Fig. 2.7 shows the behavior of transmitted intensity with respect to incident angle. The high optical transparency is evident in the anisotropic limit also. The intensity is maximum at normal incidence and remains constant and as the incident angle approaches the gracing incidence, the transmitted intensity goes to minimum. Here the magenta curve shows the off diagonal anisotropic situation with zero gap shown by the solid line whereas the finite gap situation is shown by the dashed line. The brown curve is for the behavior of diagonal anisotropic situation. Here unlike in the case of reflection coefficient, the effect of gap on transmission coefficient is to increase the transmitted intensity but the increase is very small compared to the magnitude of transmission coefficient.

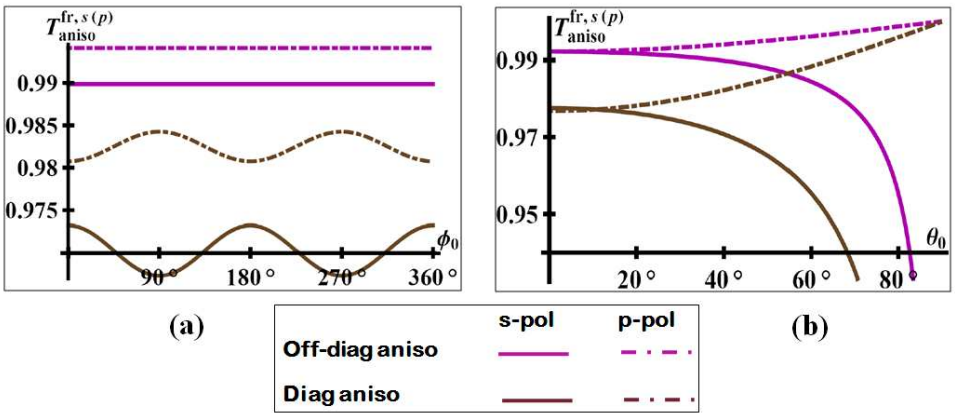

FIGURE 2.8: Transmission coefficient versus various angle parameters when the conductivity tensor is anisotropic and the incident wave is linearly polarized. This figure has two parts (a) behavior with respect to azimuthal angle (b) variation with respect to incident angle. The solid curves for incident s polarized wave and dot-dashed curves for incident p polarized wave. The magenta curve shows the situation with off diagonal anisotropy and brown curve shows the behavior with diagonal anisotropic situation. Here incident photon energy is fixed to a value $\Omega = 200\ GHz$

Now moving towards the extreme cases of linear polarization of incident waves, the transmission coefficient is function of azimuthal and incident angles. The variation with respect to those two parameters are shown in Fig. 2.8. Fig. 2.8a shows the variation with respect to azimuthal angle and Fig. 2.8b shows that with respect to incident angle. Unlike in the reflection coefficient case, we can see that the $p-$ polarized incident wave increases the transmitted intensity. There is a phase shift of $\pi/2$ in the behavior of transmitted intensity with respect to azimuthal angle for s and p polarized incident wave with diagonal anisotropy. For small angle of incidence, the transmitted intensity with $s-$ polarized incident intensity and p polarized intensity coincides and is more or less constant. But as the angle of incidence increases

the transmitted intensity with s polarized wave slowly decreases and a sharp decrease is observed for the gracing incidence. In the $p-$ polarized incident wave situation, the transmitted intensity increases with the incident angle. In transmission, the behavior of $s-$ and $p-$ polarization cases is opposite to that observed in reflection situation. The $s-$ polarization incidence of transmission behaves as $p-$ polarization case of reflection and vice verse. The next case is when the incident polarization is zero. Then the transmission coefficient is a function of azimuthal angle, incident angle and the tilt angle. The behavior of transmission coefficient with respect to ϕ_0 and θ_0 is similar to the behavior explained in Fig. 2.8 with the $s-$ polarized incidence.

In this subsection the study of transmission coefficient with respect to various parameters are discussed when the conductivity tensor elements of graphene is anisotropic in two different ways. The observation made for reflection coefficient regarding the the dependence of azimuthal angle is true for transmission case also. If it is to be checked experimentally it will be convenient to do with transmission since the magnitude of reflected intensity is too small to measure.

2.5.2.3 Reflected Polarization

When $\sigma_{xx} = \sigma_{yy} = \sigma_1$ and $\sigma_{xy} = -\sigma_{yx} = \sigma_2$

$$e^{-i\delta^{ref}}|_{off}^{fr} = \frac{n_{1,off}^{fr} + in_{2,off}^{fr}}{\sqrt{d_{1,off}^{fr}\, d_{2,off}^{fr}}} \tag{2.31}$$

where

$$n_{1,off}^{fr} = \sigma_1\sigma_2\,(\cos^2\theta_{tilt}^{ext}\sec\theta_0 - \cos\theta_0\sin^2\theta_{tilt}^{ext}) + (-\sigma_1^2+\sigma_2^2)\cos\delta^{ext}\cos\theta_{tilt}^{ext}\sin\theta_{tilt}^{ext}$$

$$n_{2,off}^{fr} = (\sigma_1^2+\sigma_2^2)\cos\theta_{tilt}^{ext}\sin\theta_{tilt}^{ext}\sin\delta^{ext}$$

$$d_{1,off}^{fr} = (\sigma_2^2\cos^2\theta_{tilt}^{ext} + \sigma_1\cos\theta_0\sin\theta_{tilt}^{ext}\,(-2\sigma_2\cos\delta^{ext}\cos\theta_{tilt}^{ext} + \sigma_1\cos\theta_0\sin\theta_{tilt}^{ext}))$$

$$d_{2,off}^{fr} = \sigma_1^2\cos^2\theta_{tilt}^{ext}\sec^2\theta_0 + \frac{\sigma_2}{2}\,(\sigma_2\,(1-\cos 2\theta_{tilt}^{ext}) + 2\sigma_1\sec\theta_0\sin 2\theta_{tilt}^{ext}\cos\delta^{ext})$$

When $\sigma_{xx} \neq \sigma_{yy}$ and $\sigma_{xy} = \sigma_{yx} = 0$

$$e^{-i\delta^{ref}}|^{fr}_{diag} = \frac{n^{fr}_{1,diag} + in^{fr}_{2,diag}}{\sqrt{d^{fr}_{1,diag}\, d^{fr}_{2,diag}}} \tag{2.32}$$

where

$$\begin{aligned} n^{fr}_{1,diag} = \frac{\pi^2}{2} &(\cos\delta^{ext}\,(-(\sigma_1+\sigma_4)^2 + (\sigma_1-\sigma_4)^2\cos 4\phi_0)\sin 2\theta^{ext}_{tilt} + 2\,(\sigma_1-\sigma_4) \\ &(\cos^2\theta^{ext}_{tilt}(-\sigma_1-\sigma_4+(\sigma_1-\sigma_4)\cos 2\phi_0)\sec\theta_0 - \cos\theta_0\,(\sigma_1+\sigma_4 \\ &+(\sigma_1-\sigma_4)\cos 2\phi_0)\sin^2\theta^{ext}_{tilt})\sin 2\phi_0) \end{aligned}$$

$$n^{fr}_{2,diag} = 2\pi^2\sigma_1\sigma_4\sin\delta^{ext}\sin 2\theta^{ext}_{tilt}$$

$$\begin{aligned} d^{fr}_{1,diag} = \pi^2(&\cos^2\theta_0(\sigma_1+\sigma_4+(\sigma_1-\sigma_4)\cos 2\phi_0)^2\sin^2\theta^{ext}_{tilt} + 4(\sigma_1-\sigma_4)\cos\delta^{ext}\cos\theta_0 \\ &\cos\phi_0\sin 2\theta^{ext}_{tilt}\sin\phi_0(\sigma_1\cos^2\phi_0+\sigma_4\sin^2\phi_0) + (\sigma_1-\sigma_4)^2\cos^2\theta^{ext}_{tilt}\sin^2 2\phi_0) \end{aligned}$$

$$\begin{aligned} d^{fr}_{2,diag} = \pi^2(&\cos^2\theta^{ext}_{tilt}(\sigma_1+\sigma_4+(-\sigma_1+\sigma_4)\cos 2\phi_0)^2\sec^2\theta_0 + (\sigma_1-\sigma_4)(4\cos\delta^{ext}\cos\phi_0 \\ &\sec\theta_0\sin 2\theta^{ext}_{tilt}\sin\phi_0(\sigma_4\cos^2\phi_0+\sigma_1\sin^2\phi_0) + (\sigma_1-\sigma_4)\sin^2\theta^{ext}_{tilt}\sin^2 2\phi_0)) \end{aligned}$$

The main difference between the two kinds of anisotropy is explicitly seen from the equations (2.31, 2.32) where azimuthal angle dependence is absent in the first case and it is present in the other case. It is seen that both the real and imaginary parts of the polarization of reflected wave is functions of incident angle, tilt angle and the incident polarization. The variation with respect to incident angle is given in Fig. 2.9 which has two parts: Fig. 2.9a shows the behavior of $\cos\delta^{ref}_{fr}$ and Fig. 2.9b shows $\sin\delta^{ref}_{fr}$ with respect incident angle. Each panel has two curves in it, the magenta curves showing the off-diagonal anisotropic situation and the brown curves shows that of diagonal anisotropy. All the plots in this section is for zero gap. The finite gap situation is also studied, but the effect of gap cannot be seen in any of the case, therefore it is not included. We can see that the real part is almost constant up to relatively larger angle of incidence for diagonal anisotropy and decreases as the incident angle approaches gracing incidence. For off-diagonal anisotropy the real part of reflected polarization slowly increases with the incident angle. For the chosen set of parameters the

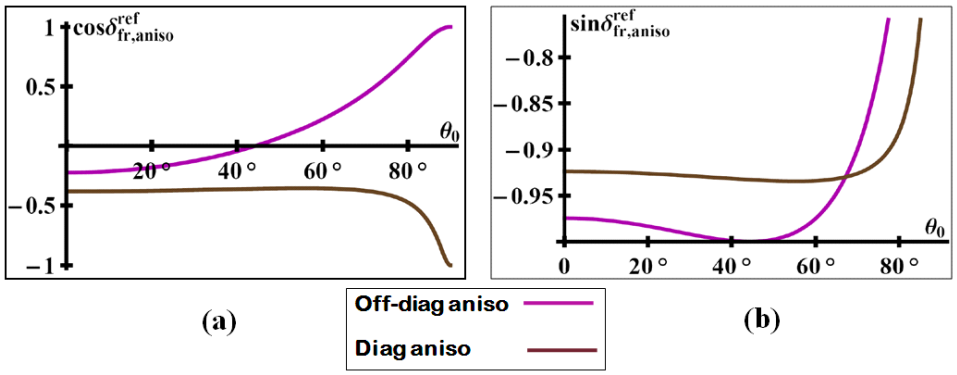

FIGURE 2.9: Reflected polarization versus incident angle. This figure has two parts (a) behavior of real part of reflected polarization (b) behavior of imaginary part of the reflected polarization. In both of them, the magenta curves shows the off-diagonal anisotropic situation and diagonal anisotropic situation is shown by brown curves. Here incident photon energy is fixed to a value $\Omega = 200\ GHz$

real part of reflected polarization varies between negative and positive values for off diagonal anisotropy whereas it remains in the negative axis for diagonal anisotropy. Fig. 2.9b which shows the variation of $\sin\delta^{ref}_{fr}$ for both types of anisotropy and can see that they have negative magnitude for the whole range of incident angle. In the off-diagonal anisotropic situation, imaginary part of reflected polarization first decreases followed by a minimum and finally increases as θ_0 increases. But in the diagonal anisotropic situation, the behavior remains constant and finally increases rapidly when θ_0 approaches gracing incidence. Fig. 2.10 shows

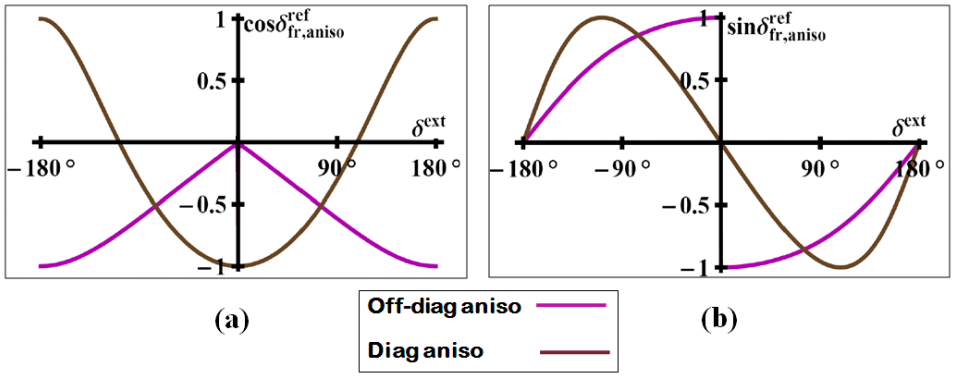

FIGURE 2.10: Reflected polarization versus incident polarization. This figure has two parts (a) behavior of real part of reflected polarization (b) behavior of imaginary part of the reflected polarization. In both of them, the magenta curves shows the off-diagonal anisotropic situation and diagonal anisotropic situation is shown by brown curves. Here incident photon energy is fixed to a value $\Omega = 200\ GHz$

the behavior of $\cos\delta^{ref}_{fr}$ and $\sin\delta^{ref}_{fr}$ with respect to incident polarization. Fig. 2.10a shows

the behavior of real part and Fig. 2.10 shows that of imaginary part. Each of the panels has two curves in it of which the magenta curves show the off-diagonal anisotropic case and the brown one shows the diagonal anisotropic situation. We can see that in both the sections of Fig. 2.10, the diagonal anisotropic situation behaves in a simple way. That means the real part of reflected polarization behaves as $-\cos\delta^{ext}$ and imaginary part of reflected polarization varies as $-\sin\delta^{ext}$. But in the off-diagonal anisotropic situation, the behavior of both real and imaginary parts of δ^{ref}_{fr} is rather complex and can be seen in Fig. 2.10. At incident polarization close to 0^0, the real part shows a maximum and decreases to the negative side of the axis as the incident polarization varies. The imaginary part of the reflected polarization shows a large discontinuity as the incident polarization approaches zero.

Consider the case of linearly polarized incident wave in the anisotropic limit. For off-diagonal anisotropy, the reflected polarization vanishes for an $s-$ polarized incident wave and $\pm\pi$ for $p-$ polarized incident wave. For diagonal anisotropy, reflected polarization is either 0 or $\pm\pi$ depending upon the sign of the product $-(\sigma_1 - \sigma_4 \sin 2\phi_0)$ for both $s-$ and $p-$ polarization. When the incident wave is linearly polarized in such a way that the incident polarization itself is zero for an arbitrary value of θ^{ext}_{tilt}, the reflected polarization is again 0 or $\pm\pi$ depending upon the value of tilt angle for both off-diagonal anisotropy and diagonal anisotropy.

In this subsection we have given a detailed study of the reflected polarization with respect to various parameters under different conditions, i.e. for a general polarization, linear polarization, the conductivity being anisotropic in different ways etc. A comparative study is done here taking into consideration the different situations. Here the reflected polarization is not given as such, but the behavior of real and imaginary parts of it is studied and a simultaneous solution of these two quantities leads to information about the reflected polarization (as discussed in section Isotropic Limit).

2.5.3 Conclusions

This chapter discusses the system of one graphene sheet in its free standing form. In freely suspended graphene as its name suggests, it is expected that there are no disorder due to the substrate. Response of the material in the form of emergent field is calculated in this chapter when a plane electromagnetic wave is allowed to fall on the system at an arbitrary angle. The

emergent electric fields are obtained by solving Maxwell's equations for the system. Using the emergent electric fields, various physically important quantities have been calculated and studied with respect to various angle parameters related to the incident wave. Parameters related to the material, i.e. elements of the conductivity tensor, are fixed throughout the study. To start with, the conductivity tensor is assumed to have the general form with all of its elements different. Then due to the presence and absence of different external sources the components has to obey certain symmetry conditions which leads to constraints to the tensor components which makes the conductivity tensor to appear in different forms. Broadly, one can say that the conductivity tensor can be isotropic or anisotropic. The anisotropy can be of different types. Here in this chapter, the isotropy in the conductivity tensor is achieved in two different ways, when the externally applied magnetic field is absent or when there is no electrostatic doping in the material (i.e. when $B = 0$ or $\mu = 0$). Now among the different kinds of anisotropy, only two cases are considered for a detailed study. One is when a static external magnetic field is applied perpendicular to the plane of graphene (off-diagonal anisotropy, i.e. $\sigma_{xx} = \sigma_{yy} = \sigma_1$ and $\sigma_{xy} = -\sigma_{yx} = \sigma_2$) and the other is when there is only an in plane electric field applied externally (diagonal anisotropy, i.e. $\sigma_{xy} \neq \sigma_{yy}$ and $\sigma_{xy} = \sigma_{yx} = 0$). Both these limits are studied very carefully and compared with each other. This study in the off-diagonal anisotropic limit is restricted to the microwave region in the high magnetic field limit in which the conductivity tensor elements can be obtained from Gusynin et. al. To study the diagonal anisotropy diagonal elements are taken to be $\Delta\sigma$ which is a very small quantity added (subtracted) to universal optical conductivity quantum.

The optical quantities considered for study in this chapter are the reflection coefficient, transmission coefficient and the reflected polarization. Now for a detailed study, different limiting cases of the incident wave parameters are also considered, namely the linear polarization limit, normal incidence etc. Therefore altogether a comparative study is done between the forms of the conductivity tensor and the different limits of the incident wave parameters. The main result of this study is that, one can obtain information about the optical conductivity of graphene by studying the different optical quantities (included in Appendix A). Any two out of the three quantities together can obtain the conductivity tensor for graphene. One can see that the magnitude of the reflection coefficient is extremely small (less than 0.01%) as expected from experiments which may make it difficult to measure and see the variation. For this reason the transmission coefficient along with the reflected polarization can be studied to get the information about the tensor elements. The second important suggestion is that,

the azimuthal angle dependence can provide information about the form of the conductivity tensor. From the study it is clear that the azimuthal angle dependence of the optical quantities are absent if the tensor is either isotropic or off-diagonally anisotropic. There are many such issues discussed in various sections of the chapter which are important in one sense or the other.

Chapter 3

Substrate - Graphene

In this chapter, the system under study is a graphene sheet deposited on a non-magnetic dielectric substrate. The main tool used here for analyzing the substrate graphene is Maxwell's equations. The first section of this chapter describes the problem under study followed by the description of the tools used for study. The same optical quantities are studied for this case as in the case of freely suspended graphene. Therefore only a brief description is included in this chapter. Finally the results are discussed in detail with the help of various plots. In each stage the study is compared with that of the suspended graphene results.

3.1 Problem Description

In this chapter, a mono-layer graphene sheet deposited on a substrate material is considered for study. Free standing case considered in chapter 2 is important and it has its own advantages that it is devoid of the disorder effects that may arise due to the interaction between the substrate and graphene. The studies done in the freestanding case (explained in chapter 2), is taken as a reference for the present study which helps to investigate the influence of the presence of substrate material on the optical properties of graphene. Therefore here a similar route is followed as in the case of free standing graphene.

A monolayer graphene sheet deposited on top of a substrate material is arranged in the xy plane at $z = 0$. An electromagnetic wave with a wave vector $\mathbf{q}_0$ is incident on the sheet at an

arbitrary angle θ_0 with respect to the normal to the plane (z axis). The incident wave vector is considered to have all three components and it is expressed in terms of the incident angle and the azimuthal angle (angle between the projection of the incident wave vector in the xy plane and x axis). Here there are a number of electric fields that has to be dealt with, each of which is expressed in terms of elliptically polarized states, i.e. as a linear combination of its polarization components in different directions. For example, the real space representation of an electric field in general is given as

$$\mathbf{E}_\alpha(\mathbf{r},t) = e^{i\mathbf{q}_{\alpha,\parallel}\cdot\mathbf{r}_\parallel + iq_{\alpha,z}z - ic|q_\alpha|t}\sum_{\nu=1,2}\hat{\mathbf{u}}_\nu^\alpha E_\nu^\alpha \tag{3.1}$$

where α can be the incident, reflection or transmission case. Here $\hat{\mathbf{u}}_\nu^\alpha$ are the unit vectors defining the polarization directions of the respective electric fields which are defined in equation (2.2). Also E_ν^α are the electric field components along the polarization directions which can be expressed in terms of the tilt angle of the polarization ellipse and the corresponding polarization components is given in equation (2.3). Here $|E^\alpha|$ is electric field amplitude which is independent of position and time, θ_{tilt}^α is the tilt angle of the polarization ellipse and δ_1^α and δ_2^α are the polarization components in the direction of unit vectors defined by the equation (2.2). From equation (3.1) with α as *inc*, the incident electric field in real space can be written as $\mathbf{E}_{ext}(\mathbf{r},t) = e^{i\mathbf{q}_{0,\parallel}\cdot\mathbf{r}_\parallel + iq_{0,z}z - ic|q_0|t}\sum_{\nu=1,2}\hat{\mathbf{u}}_\nu^{ext}E_\nu^{ext}$. Corresponding vector in the reciprocal domain is obtained by the Fourier transform (definition given in equation (2.7)) of the incident electric field. Using this technique the incident electric field in the frequency domain can be written as $\mathbf{E}_{ext}(\mathbf{q}_\parallel,q_z,\omega) = \delta^3(\mathbf{q}_0-\mathbf{q})\,\delta(c|q_0|-\omega)\sum_{\nu=1,2}\hat{\mathbf{u}}_\nu^{ext}E_\nu^{ext}$. The notations used in this chapter matches with that in chapter 2 which enables an easy comparison. The next step is to derive the equations for the emergent electric field from graphene surface deposited on a substrate material, using Maxwell's equations. The substrate material is considered as a nonmagnetic dielectric material represented by a dielectric constant ϵ.

3.2 Maxwell's Equations

Maxwell's equations representing substrate-graphene is given in CGS units below,

$$\vec{\nabla}\cdot\vec{\mathbf{D}} = 4\pi\rho_{gr} \quad ; \quad \vec{\nabla}\times\vec{\mathbf{E}} = -\frac{1}{c}\frac{\partial\mathbf{B}}{\partial t}$$

$$\vec{\nabla} \cdot \vec{\mathbf{B}} = 0 \quad ; \quad \vec{\nabla} \times \vec{\mathbf{B}} = \frac{4\pi}{c}\mathbf{J}_{gr} + \frac{1}{c}\frac{\partial \mathbf{D}}{\partial t} \tag{3.2}$$

where $\mathbf{D} = \varepsilon(z)\,\mathbf{E}$. Here the z dependent quantity $\varepsilon(z)$ is the dielectric constant of the substrate material and is defined as $\varepsilon(z) = \Theta(-z) + \epsilon\,\Theta(z)$. The system under study, i.e. substrate-graphene, consists of two parts, one is substrate and the other is graphene. Out of these the substrate material, as mentioned earlier being a perfect dielectric, makes no contribution towards the induced current or charge density of the combined system. This is the reason why the subscript "gr" is given to the charge and current density in the Maxwell's equations, which means that the current in the system is solely due to the graphene conductivity. $\mathbf{J}_{gr}$ and ρ_{gr} are the induced charge and current densities on the whole system due to the external incident field. The induced current density in the system due to incident field is taken as $\mathbf{J}_{gr}(z) = -\frac{1}{c}\,\overline{\overline{\sigma}} \cdot \partial_t \mathbf{A}_{ext}(z = 0)\,\delta(z)$. Here $\overline{\overline{\sigma}}$ is the graphene conductivity tensor which is a represented by a 2×2 matrix. Since the system which is a two dimensional material is placed in the xy plane, the z component of the induced current density vanishes, that is $J_z = 0$. Maxwell's equations given above can be solved with the help of boundary conditions and some other basic equations to get the emergent electric field which are discussed in the next section. The gauge is chosen such that the scalar potential is zero.

3.3 Emergent Electric Field : Reflection and Transmission

With the help of boundary conditions, Maxwell's equations can be solved to obtain the emergent electric field. The emergent field consists of two parts which exists in two different spaces with respect to the $z = 0$ plane. For $z < 0$ there exists the reflected part of the emergent field and in $z > 0$ the transmitted part of the field. The equations for each of them are given below: (The details of the calculation are given in Appendix B)

$$\mathbf{E}^{sg}_{ref}(\mathbf{r}, t) = e^{i\mathbf{q}_{0,\parallel}\cdot\mathbf{r}_{\parallel} \,-\, iq_{0,z}z \,-\, ic|q_0|t}\, \frac{\mathbf{K}^r_1\, E_{ext,x}(0) + \mathbf{K}^r_2\, E_{ext,y}(0)}{c\left(q_{0,z} + q'_{0,z}\right)\left(q^2_{0,x} + q^2_{0,y} + q_{0,z}\, q'_{0,z}\right)} \tag{3.3}$$

where

$$K^{r}_{(1,x)(2,y)} = c\left(q_{0,z} - q^{'}_{0,z}\right)\left(\mp q^{2}_{0,x} \pm q^{2}_{0,y} + q_{0,z}\, q^{'}_{0,z}\right) - 4\pi|q_0|\,(q^{2}_{0,y(x)}\,\sigma_{xx(yy)} + q_{0,z}\, q^{'}_{0,z}\,\sigma_{xx(yy)} - q_{0,x}\, q_{0,y}\,\sigma_{yx(xy)})$$

$$K^{r}_{(2,x)(1,y)} = -2\left(c\, q_{0,x}\, q_{0,y}\left(q_{0,z} - q^{'}_{0,z}\right) + 2\pi|q_0|\left(q^{2}_{0,y(x)}\,\sigma_{xy(yx)} + q_{0,z}\, q^{'}_{0,z}\,\sigma_{xy(yx)} - q_{0,x}\, q_{0,y}\,\sigma_{yy(xx)}\right)\right)$$

$$K^{r}_{(1,z)(2,z)} = -\left(c\, q_{0,x(y)}\left(q_{0,z} - q^{'}_{0,z}\right)\left(q^{2}_{0,x} + q^{2}_{0,y} - q_{0,z}\, q^{'}_{0,z}\right) + 4\pi|q_0|q_{0,z}\, q^{'}_{0,z}\left(q_{0,x}\,\sigma_{xx(xy)} + q_{0,y}\,\sigma_{yx(yy)}\right)\right)$$

$$\mathbf{E}^{sg}_{tran}(\mathbf{r},t) = e^{i\mathbf{q}_{0,\|}\cdot\mathbf{r}_{\|} + iq_{0,z}z - ic|q_0|t}\,\frac{\mathbf{K}^{t}_{1}\,E_{ext,x}(0) + \mathbf{K}^{t}_{2}\,E_{ext,y}(0)}{c\left(q_{0,z} + q^{'}_{0,z}\right)\left(q^{2}_{0,x} + q^{2}_{0,y} + q_{0,z}\, q^{'}_{0,z}\right)} \tag{3.4}$$

where

$$K^{t}_{(1,x)(2,y)} = 2\left[c\, q^{2}_{0,y(x)}\, q_{0,z} + c\left(q^{2}_{0,x} + q^{2}_{0,z}\right)q^{'}_{0,z} - 2\pi|q_0|\left(q^{2}_{0,y}\,\sigma_{xx(yy)} + q_{0,z}q^{'}_{0,z}\,\sigma_{xx(yy)} - q_{0,x}q_{0,y}\,\sigma_{yx(xy)}\right)\right]$$

$$K^{t}_{(2,x)(1,y)} = -2\left[c\, q_{0,x}\, q_{0,y}\left(q_{0,z} - q^{'}_{0,z}\right) + 2\pi|q_0|\left(q^{2}_{0,y(x)}\,\sigma_{xy(yx)} + q_{0,z}\, q^{'}_{0,z}\,\sigma_{xy(yx)} - q_{0,x}\, q_{0,y}\,\sigma_{yy(xx)}\right)\right]$$

$$K^{t}_{(1,z)(2,z)} = -2\left[c\, q_{0,x(y)}\,|q_0| - 2|q_0|\, q_{0,z}\left(q_{0,x}\,\sigma_{xx(xy)} + q_{0,y}\,\sigma_{yx(yy)}\right)\right]$$

Here $q^{'}_{0,z}$ is the z component of the transmitted wave vector which is $\sqrt{\mathbf{q}^{2}_{0,\|} + \epsilon\,|q_0|^2}$ (see Appendix B). For deriving the above equations the conductivity tensor for graphene is taken to be in its most general form with its components unequal. i.e. $\begin{pmatrix} \sigma_{xx} & \sigma_{xy} \\ \sigma_{yx} & \sigma_{yy} \end{pmatrix}$. The correctness of the above equations are checked by two limiting cases: (i) ϵ tends to unity (ii) $\overline{\overline{\sigma}}$ tends to zero limit. The former is the situation when the system is free standing. i.e. suspended graphene discussed in chapter 2. It is seen that in this limit, equations (3.3, 3.4) reduce to the corresponding equations in chapter 2. The second limit signifies the situation in which there is no graphene but only the dielectric substrate material. The amplitude reflection and transmission coefficients using equations (3.3, 3.4), in the $\overline{\overline{\sigma}}$ tends to zero limit matches with the well known results of a dielectric material given in text books (see ref [137]). From the general equation for an electric field given by equation (3.1), the reflected and transmitted

electric fields in real space can be written in terms of its polarization components as given below:

$$\mathbf{E}^{sg}_{ref}(\mathbf{r},t) = e^{i\mathbf{q}_{ref,\parallel}\cdot\mathbf{r}_{\parallel} + iq_{ref,z}z - ic|q_{ref}|t} \sum_{\nu=1,2} \hat{\mathbf{u}}^{ref}_{\nu} E^{ref,sg}_{\nu} \tag{3.5}$$

$$\mathbf{E}^{sg}_{tran}(\mathbf{r},t) = e^{i\mathbf{q}_{tran,\parallel}\cdot\mathbf{r}_{\parallel} + iq_{tran,z}z - ic|q_{tran}|t} \sum_{\nu=1,2} \hat{\mathbf{u}}^{tran}_{\nu} E^{tran,sg}_{\nu} \tag{3.6}$$

Here $\mathbf{q}_{ref} = \{q_{0,x}, q_{0,y}, q_{0,z}\}$ and $\mathbf{q}_{tran} = \{q_{0,x}, q_{0,y}, q^{'}_{0,z}\}$ with $|q_{ref}| = |q_0|$ and $|q_{tran}| = |q_0|\sqrt{-\sin^2\theta_0 + \epsilon}$. Polarization directions are defined by the unit vectors given by equation (2.2). The description of the other terms in the above equations are also given in the beginning of this chapter. For example, the reflected and transmitted components of the electric field in the two polarization directions are given by equation (2.3). Solving the general equations for reflected and transmitted electric field given by equations (3.5, 3.6) and the emergent electric field given by equations (3.3, 3.4) simultaneously, we can get the polarization components of the reflected and transmitted electric field, that is

$$E^{ref,sg}_{\nu} = e^{-i\mathbf{q}_{0,\parallel}\cdot\mathbf{r}_{\parallel} + iq_{0,z}z + ic|q_0|t}\, \mathbf{E}^{sg}_{ref}(\mathbf{r},t)\cdot\hat{\mathbf{u}}^{ref}_{\nu} \tag{3.7}$$

$$E^{tran,sg}_{\nu} = e^{-i\mathbf{q}_{0,\parallel}\cdot\mathbf{r}_{\parallel} - iq^{'}_{0,z}z + ic|q_{tran}|t}\, \mathbf{E}^{sg}_{tran}(\mathbf{r},t)\cdot\hat{\mathbf{u}}^{tran}_{\nu} \tag{3.8}$$

To calculate the physically interesting quantities such as coefficient of reflection which are explained in chapter 2, it is important to know about the conductivity tensor of graphene.

3.3.1 Optical Conductivity

The general idea about the quantity - optical conductivity, its tensor form and anisotropy are discussed in chapter 2 in detail. As explained in the previous section, conductivity tensor of graphene, a two dimensional material, can be represented by a 2×2 matrix. Graphene conductivity is also discussed in chapter 2. In this chapter, the main source of conductivity data is from reference [100] which gives the general equation of the anisotropic conductivity in the presence of a perpendicular external magnetic field for an arbitrary frequency and temperature. This is given as equation (2.17) in chapter 2. With the external agent as the perpendicular magnetic field, the components of the conductivity elements are subjected to the constrains $\sigma_{xx} = \sigma_{yy} = \sigma_1$ and $\sigma_{xy} = -\sigma_{yx} = \sigma_2$. i.e. the diagonal elements are equal and the

off-diagonal elements are equal but of opposite in sign. This is visible from equation (2.17) of chapter 2. Avoiding the complicated general form of the conductivity tensor, here also we have chosen the microwave response in high magnetic field limit as in the case of previous chapter and is given in equations (2.18, 2.19) in chapter 2. A large amount of literature available in the field of conductivity studies in graphene shows that at higher energy regions of the electromagnetic spectrum, the graphene conductivity tensor becomes independent of the incident wavelength and may be taken as approaching the universal dynamical conductivity given by $\frac{e^2}{4\hbar}$ [106, 118]. In other words, the tensor becomes just a simple number. But as in the earlier chapter here too we are interested in studying reflection/transmission coefficients with the anisotropic graphene conductivity tensor in its various limits. This is possible more easily in the microwave region. Also graphene conductivity is well studied in the microwave region by Gusynin et. al. [106] who give a well defined equation for its conductivity tensor. They also show that microwaves are an exceptional tool of graphene's unusual dynamics. Their study reveals that microwave response of Dirac quasiparticles has several anomalous properties both in the presence and absence of a strong magnetic field. Gusynin et. al. [106] shows that the microwave response of graphene reflects the Dirac nature of quasi-particles in this material, which include the intra-band and inter-band contributions to the conductivity with zero magnetic field and also at large fields.

Two pieces of information can be obtained from equation (2.19) about the off-diagonal conductivity element: (i) in the presence of an external magnetic field it depends significantly on $sgn(eB)$ (ii) it is an anti-symmetric function of the chemical potential. To consider conductivity as a dimensionless quantity, the definition of fine structure constant is used with the choice of $c = 1$. By choosing some specific values for the parameters like Δ, Γ, T etc. the numerical value of the conductivity can be obtained in the high magnetic field limit of microwave region. The importance of microwave region and the high magnetic field limits are explained in chapter 2. The isotropic limit of the conductivity tensor is clear from equation (2.19), i.e. the situation under which the off-diagonal elements of the conductivity tensor vanishes. It happens in two different ways as mentioned earlier, (i) when there is no electrostatic doping ($\mu = 0$) or (ii) when there is no external applied magnetic field. Out of these the zero chemical potential limit can be obtained from equation (2.18) and the conductivity for the zero magnetic field is given by equation (2.20) in chapter 2 Different cases of the form of conductivity tensor are discussed below, that is (i) when the conductivity is isotropic and diagonal (ii) when the conductivity is anisotropic and diagonal (iii) when it is non-diagonal

anisotropic etc. One can obtain the numerical value of the conductivity elements in different limits by choosing appropriate values for the parameters appearing in the equations and study different optical quantities using the emergent electric field discussed above.

3.4 Optical Coefficients

Three quantities are studied in this section, the coefficient of reflection, coefficient of transmission and the reflected polarization. This is described in detail in chapter 2, therefore only a brief discussion is given here.

3.4.1 Reflection Coefficient

Reflection coefficient is the fraction of reflected intensity relative to the incident intensity. In EM theory, it is defined in terms of the Poynting's vector for incident and reflected wave. i.e. $R^{sg} = \frac{\mathbf{S}^{sg}_{ref,z}}{\mathbf{S}_{inc,z}}$ where $\mathbf{S} = \mathbf{E}^* \times \mathbf{B}$. This will reduce to a simplified form $R^{sg} = \frac{|\mathbf{E}^{sg}_{ref}|^2}{|\mathbf{E}_{ext}|^2}$, which ultimately becomes $R^{sg} = \frac{|E_1^{ref,sg}|^2 + |E_2^{ref,sg}|^2}{|E^{ext}|^2}$.

Its a complicated system to solve, the general equation for reflection coefficient is therefore equally complicated. Substituting for the reflection components of the electric field along the polarization directions obtained from equation (3.7) we can obtain the reflection coefficient as give below:

$$R^{sg} = r_1^{sg} \cos^2\theta_{tilt}^{ext} + r_2^{sg} \sin^2\theta_{tilt}^{ext} + r_3^{sg} \sin 2\theta_{tilt}^{ext} \tag{3.9}$$

where

$$\begin{aligned} r_1^{sg} = {} & \frac{1}{(\eta + \cos\theta_0)^2} \times [(\eta - \cos\theta_0)^2 - 4\pi(-\eta + \cos\theta_0)\,(\sigma_{xx} + \sigma_4 + (-\sigma_{xx} + \sigma_{yy})\cos 2\phi_0 \\ & - (\sigma_{xy} + \sigma_{yx})\sin 2\phi_0) + \frac{1}{(-1 - 2\eta\cos\theta_0 + \cos 2\theta_0)^2} \times 4\pi^2((-1 - 2\eta\cos\theta_0 + \cos 2\theta_0)^2 \\ & (\sigma_{xx} + \sigma_{yy} + (-\sigma_{xx} + \sigma_{yy})\cos 2\phi_0 - (\sigma_{xy} + \sigma_{yx})\sin 2\phi_0)^2) + 4\eta^2(\sigma_{xy} - \sigma_{yx} \\ & + (\sigma_{xy} + \sigma_{yx})\cos 2\phi_0 + (-\sigma_{xx} + \sigma_{yy})\sin 2\phi_0)^2] \end{aligned}$$

$$
\begin{aligned}
r_2^{sg} = & \frac{\cot^2\theta_0}{16\,(\eta+\cos\theta_0)^2} \times [16\sin^2\theta_0\sin^2\phi_0\,((-4\pi\sigma_{yy}-\eta+\cos\theta_0)\cos\phi_0+4\pi\sigma_{xy}\sin\phi_0)^2 \\
& + 16\cos^2\phi_0\ \sin^2\theta_0\,(4\pi\sigma_{yx}\cos\phi_0+(-4\pi\sigma_{xx}-\eta+\cos\theta_0)\sin\phi_0)^2 \\
& + 16\sin^2\theta_0\,((4\pi\sigma_{yy}+\eta-\cos\theta_0)\cos\phi_0-4\pi\sigma_{xy}\sin\phi_0)\,(4\pi\sigma_{yx}\cos\phi_0+(-4\pi\sigma_{xx}-\eta \\
& + \cos\theta_0)\sin\phi_0)\sin 2\phi_0 + \frac{1}{(\eta\cos\theta_0+\sin^2\theta_0)^2} \times (\sin\theta_0\,(1+4\eta(2\pi(\sigma_{xx}+\sigma_{yy})+\eta) \\
& + 8\pi\eta\,((\sigma_{xx}-\sigma_{yy})\cos 2\phi_0+(\sigma_{xy}+\sigma_{yx})\sin 2\phi_0))-(4\eta+\cos 3\theta_0)\tan\theta_0)^2]
\end{aligned}
$$

$$
\begin{aligned}
r_3^{sg} = & \frac{-2\pi\cot\theta_0}{(\eta+\cos^2\theta_0)^2\,(-1-2\eta\cos\theta_0+\cos 2\theta_0)^2} \times [8\pi\sin\theta_0\,(\eta^2\,(\sigma_{xx}+\sigma_{yy} \\
& + (\sigma_{xx}-\sigma_{yy})\cos 2\phi_0+(\sigma_{xy}+\sigma_{yx})\sin 2\phi_0)\,(\sigma_{xy}-\sigma_{yx}+(\sigma_{xy}+\sigma_{yx})\cos 2\phi_0 \\
& + (-\sigma_{xx}+\sigma_{yy})\sin 2\phi_0)-(\eta\cos\theta_0+\sin^2\theta_0)^2\,(-\sigma_{xx}-\sigma_{yy}+(\sigma_{xx}-\sigma_{yy})\cos 2\phi_0 \\
& + (\sigma_{xy}+\sigma_{yx})\sin 2\phi_0)\,(-\sigma_{xy}+\sigma_{yx}+(\sigma_{xy}+\sigma_{yx})\cos 2\phi_0+(-\sigma_{xx}+\sigma_{yy})\sin 2\phi_0)) \\
& + (-\eta+\cos\theta_0)\,(-2\eta\,(-1+2\eta\cos\theta_0+\cos 2\theta_0)\,(\sigma_{xy}-\sigma_{yx}+(\sigma_{xy}+\sigma_{yx})\cos 2\phi_0 \\
& + (-\sigma_{xx}+\sigma_{yy})\sin 2\phi_0)-\cos\theta_0\,(-1-2\eta\cos\theta_0+\cos 2\theta_0)^2\,(-\sigma_{xy}+\sigma_{yx} \\
& + (\sigma_{xy}+\sigma_{yx})\cos 2\phi_0+(-\sigma_{xx}+\sigma_{yy})\sin 2\phi_0))\ \tan\theta_0]
\end{aligned}
$$

Here $\eta = \sqrt{-\sin^2\theta_0+\epsilon}$ is the z component of transmitted wave vector. θ_0 is the incident angle, ϕ_0 is the azimuthal angle which is the angle between the components of incident wave vector in the xy plane and the x axis and θ_{tilt}^{ext} is the tilt angle of the incident polarization ellipse. The above equation shows that the reflection coefficient in general is a function of the parameters related to incident wave, the material medium and also the substrate material. It is seen that in the limit $\epsilon \to 1$, equation (3.9) reduces to that of freely suspended graphene.

At this stage it is desirable to think of the different possibilities of the ways in which the conductivity tensor components are related. As mentioned in chapter 2, there are four different ways. (i) The situation when the diagonal elements are equal and the off-diagonal elements are also equal (ii) The diagonal elements equal but the off diagonal elements are equal and of opposite sign (in the presence of an external magnetic field given by Gusynin et. al. [106]) (iii) The diagonal elements are equal and the off-diagonal elements vanish (in the absence of external magnetic field or electrostatic doping given by Gusynin et. al. [106]) (iv) With

unequal diagonal elements and the vanishing off-diagonal elements (in the presence of an in-planar electric field given by Strikha et. al. [104]). The situations related to Gusynin's results (cases (ii) and (iii)) are discussed in an earlier subsection in this chapter and also in chapter 2. The conductivity tensor elements in these two limits are given by equations (2.18, 2.19, 2.20). The other two cases mentioned above becomes important when there is an anisotropy not due the magnetic field.

3.4.2 Transmission Coefficient

Transmission coefficient is the ratio of transmitted and incident intensity. This may be defined in general in terms of Poynting's vector for transmitted and incident wave. i.e. $T^{sg} = \frac{\mathbf{S}^{sg}_{tran,z}}{\mathbf{S}_{inc,z}}$ where $\mathbf{S}$ is the Poynting's vector. This can be written in a simplified form as $T^{sg} = \frac{|\mathbf{E}^{sg}_{tran}|^2}{|\mathbf{E}_{ext}|^2}$ which becomes $\frac{|E_1^{tran,sg}|^2 + |E_2^{tran,sg}|^2}{|E^{ext}|^2}$. Substituting for the polarization components, the general equation for transmission coefficient is obtained as given below:

$$T^{sg} = t_1^{sg} \cos^2\theta_{tilt}^{ext} + t_2^{sg} \sin^2\theta_{tilt}^{ext} + t_3^{sg} \sin 2\theta_{tilt}^{ext} \tag{3.10}$$

where

$$\begin{aligned} t_1^{sg} = {} & \frac{4}{(\eta+\cos\theta_0)^2(-1-2\eta\cos\theta_0+\cos 2\theta_0)^2} \times [\cos^2\theta_0\,(-1-2\eta\cos\theta_0+\cos 2\theta_0)^2 \\ & + 2\pi\cos\theta_0(-1-2\eta\cos\theta_0+\cos 2\theta_0)^2\,(-\sigma_{xx}-\sigma_{yy}+(\sigma_{xx}-\sigma_{yy})\cos 2\phi_0 \\ & + (\sigma_{xy}+\sigma_{yx})\sin 2\phi_0) + 16\pi^2\,(2\eta\cos\theta_0\sin^2\theta_0\,(\sigma_{yy}\cos^2\phi_0-(\sigma_{xy}+\sigma_{yx})\cos\phi_0\sin\phi_0 \\ & + \sigma_{xx}\sin^2\phi_0)^2 + \frac{1}{4}\sin^4\theta_0\,(\sigma_{xx}+\sigma_{yy}(-\sigma_{xx}+\sigma_{yy})\cos 2\phi_0-(\sigma_{xy}+\sigma_{yx})\sin 2\phi_0)^2 \\ & + \cos^2\theta_0\,(\sigma_{xy}^2\cos^4\phi_0\sin^2\theta_0+2\sigma_{xy}\,(-\sigma_{xx}+\sigma_{yy})\cos^3\phi_0\sin^2\theta_0\sin\phi_0 \\ & + (\sigma_{xx}^2+\sigma_{yx}^2)\,\eta^2\sin^2\phi_0+\sigma_{yx}^2\sin^2\theta_0\sin^4\phi_0+\cos^2\phi_0\,((\sigma_{xy}^2+\sigma_{yy}^2)\,\eta^2+(-2\sigma_{xy}\sigma_{yx} \\ & + (\sigma_{xx}-\sigma_{yy})^2)\sin^2\theta_0\sin^2\phi_0)-((\sigma_{xx}\sigma_{xy}+\sigma_{yx}\sigma_{yy})\,\eta^2+\sigma_{yx}\,(-\sigma_{xx}+\sigma_{yy}) \\ & \sin^2\theta_0\sin^2\phi_0)\ \sin 2\phi_0))] \end{aligned}$$

$$t_2^{sg} = \frac{8\cos^2\theta_0}{(\eta+\cos\theta_0)^2\,(-1-2\eta\cos\theta_0+\cos 2\theta_0)^2} \times [1+2\eta^2-\cos 2\theta_0+2\pi\cos\theta_0\,(-1-2\eta^2 + \cos 2\theta_0)\,(\sigma_{xx}+\sigma_{yy}+(\sigma_{xx}-\sigma_{yy})\cos 2\phi_0+(\sigma_{xy}+\sigma_{yx})\sin 2\phi_0)+8\pi^2(2\eta\cos\theta_0 \sin^2\theta_0(\sigma_{yx}\cos^2\phi_0+(-\sigma_{xx}+\sigma_{yy})\cos\phi_0\sin\phi_0-\sigma_{xy}\sin^2\phi_0)^2+\frac{1}{4}\sin^4\theta_0(-\sigma_{xy}+\sigma_{yx} + (\sigma_{xy}+\sigma_{yx})\cos 2\phi_0+(-\sigma_{xx}+\sigma_{yy})\sin 2\phi_0)^2+\cos^2\theta_0(\sigma_{xx}^2\cos^4\phi_0\sin^2\theta_0 + 2\sigma_{xx}(\sigma_{xy}+\sigma_{yx})\cos^3\phi_0\sin^2\phi_0+(\sigma_2^2+\sigma_{yy}^2)\,\eta^2\sin^2\phi_0+\sigma_{yy}^2\sin^2\theta_0\sin^4\phi_0 + \cos^2\phi_0((\sigma_{xx}^2+\sigma_{yx}^2)\,\eta^2+((\sigma_{xy}+\sigma_{yx})^2+2\sigma_{xx}\sigma_{yy})\sin^2\theta_0\sin^2\phi_0) + ((\sigma_{xx}\sigma_{xy}+\sigma_{yx}\sigma_{yy})\,\eta^2+(\sigma_{xy}+\sigma_{yx})\,\sigma_{yy}\sin^2\theta_0\sin^2\phi_0)\sin 2\phi_0))]$$

$$t_3^{sg} = \frac{\pi\cos\theta_0}{(\eta+\cos\theta_0)^2\,(-1-2\eta\cos\theta_0+\cos 2\theta_0)^2} \times [(4\,((\sigma_{xy}+\sigma_{yx})\eta-4\pi\,(\sigma_{xx}\sigma_{xy}+\sigma_{yx}\sigma_{yy}) (1+2\eta^2))+2\,(3\,(\sigma_{xy}+\sigma_{yx})-8\pi\,(\sigma_{xx}\sigma_{xy}+\sigma_{yx}\sigma_{yy})\,\eta+14\,(\sigma_{xy}+\sigma_{yx})\,\eta^2)\,\cos\theta_0 - 16\pi\,(\sigma_{xx}\sigma_{xy}+\sigma_{yx}\sigma_{yy})\,(-1+2\eta^2)\cos 2\theta_0+(-7\,(\sigma_{xy}+\sigma_{yx})+16\pi\,(\sigma_{xx}\sigma_{xy} + \sigma_{yx}\sigma_{yy})\,\eta+4\,(\sigma_{xy}+\sigma_{yx})\,\eta^2)\cos 3\theta_0-4\,(\sigma_{xy}+\sigma_{yx})\,\eta\cos 4\theta_0 + (\sigma_{xy}+\sigma_{yx})\,\cos 5\theta_0)\cos 2\phi_0+4\,(\sigma_{xy}-\sigma_{yx})\,(-4\eta+(3+4\eta\,(2\pi\,(\sigma_{xx}+\sigma_{yy}) + \eta))\cos\theta_0-4\,(\pi\,(\sigma_{xx}+\sigma_{yy})+\eta)\cos 2\theta_0+\cos 3\theta_0)\sin^2\theta_0-16\pi\,(\sigma_{xy}+\sigma_{yx}) (\sigma_{xx}-\sigma_{yy})\,(-2\eta\cos\theta_0+\cos 2\theta_0)\cos 4\phi_0\sin^2\theta_0+(4\,(-\sigma_{xx}+\sigma_{yy})\,\eta+8\pi\,(\sigma_{xx}^2 - \sigma_{xy}^2+\sigma_{yx}^2-\sigma_{yy}^2)\,(1+2\eta^2)+(-6\sigma_{xx}+6\sigma_{yy}+8\pi\,(\sigma_{xx}^2-\sigma_{xy}^2+\sigma_{yx}^2-\sigma_{yy}^4)\,\eta + 28\,(-\sigma_{xx}+\sigma_{yy})\,\eta^2)\cos\theta_0+8\pi\,(\sigma_{xx}^2-\sigma_{xy}^2+\sigma_{yx}^2-\sigma_{yy}^2)\,(-1+2\eta^2)\cos 2\theta_0 + (7\sigma_{xx}-7\sigma_{yy}+8\pi\,(-\sigma_{xx}^2+\sigma_{xy}^2-\sigma_{yx}^2+\sigma_{yy}^2)\,\eta+4\,(-\sigma_{xx}+\sigma_{yy})\,\eta^2)\cos 3\theta_0 + 4\,(\sigma_{xx}-\sigma_{yy})\,\eta\cos 4\theta_0+(-\sigma_{xx}+\sigma_{yy})\cos 5\theta_0)\sin 2\phi_0+8\pi\,(\sigma_{xx}-\sigma_{xy}-\sigma_{yx}-\sigma_{yy}) (\sigma_{xx}+\sigma_{xy}+\sigma_{yx}-\sigma_{yy})\,(-2\eta\cos\theta_0+\cos 2\theta_0)\sin^2\theta_0\sin 4\phi_0]$$

The parameters appearing in these equations are the same as those in the case of reflection coefficient. The transmission coefficient as can be seen is a function of (i) angle parameters which is specific about the incident wave (ii) material (graphene) parameters, the components of the conductivity tensor (iii) the dielectric constant ϵ. It is seen that in the limit $\epsilon \to 1$, equation (3.10) reduces to that of freely suspended graphene. The behavior of transmission coefficient under various situations are studied in the next section.

3.4.3 Reflected Polarization

Reflected polarization is the polarization of reflected part of the emergent field defined by the equation (as mentioned in chapter 2 also), $e^{-i\,\delta^{ref}}|_{sg} = \frac{\left(E_1^{ref,sg}\right)^* \left(E_2^{ref,sg}\right)}{|E_1^{ref,sg}|\,|E_2^{ref,sg}|}$. Substituting for the polarization components of the electric field the reflected polarization can be written as

$$e^{-i\,\delta^{ref}}|_{sg} = \frac{n_1^{sg} + i\,n_2^{sg}}{\sqrt{d_1^{sg}\,d_2^{sg}}} \tag{3.11}$$

where

$$\begin{aligned}
n_1^{sg} = {} & \frac{1}{(\eta+\cos\theta_0)^2\,(\eta\cos\theta_0+\sin^2\theta_0)} \times [-2\pi\eta\,[(-2\pi\,(\sigma_{xx}+\sigma_{yy}) - \eta + \cos\theta_0 \\
& + 2\pi\,(\sigma_{xx}-\sigma_{yy})\cos 2\phi_0 + 2\pi\,(\sigma_{xy}+\sigma_{yx})\sin 2\phi_0)\,(\sigma_{xy}-\sigma_{yx} + (\sigma_{xy}+\sigma_{yx})\cos 2\phi_0 \\
& + (-\sigma_{xx}+\sigma_{yy})\sin 2\phi_0)]\cos^2\theta_{tilt}^{ext} + \pi\cos\theta_0\,[(-\sigma_{xy}+\sigma_{yx} + (\sigma_{xy}+\sigma_{yx})\cos 2\phi_0 \\
& + (-\sigma_{xx}+\sigma_{yy})\sin 2\phi_0)\,(-4\eta - \cos 3\theta_0 + \cos\theta_0\,(1 + 4\eta\,(2\pi\,(\sigma_{xx}+\sigma_{yy}) + \eta) \\
& + 8\pi\eta\,((\sigma_{xx}-\sigma_{yy})\cos 2\phi_0 + (\sigma_{xy}+\sigma_{yx})\sin 2\phi_0)))]\sin^2\theta_{tilt}^{ext} + (-4\pi^2\eta\cos\theta_0 \\
& [(\sigma_{xy}-\sigma_{yx} + (\sigma_{xy}+\sigma_{yx})\cos 2\phi_0 + (-\sigma_{xx}+\sigma_{yy})\sin 2\phi_0)\,(-\sigma_{xy}+\sigma_{yx} \\
& + (\sigma_{xy}+\sigma_{yx})\cos 2\phi_0 + (-\sigma_{xx}+\sigma_{yy})\sin 2\phi_0)] + [(-2\pi\,(\sigma_{xx}+\sigma_{yy}) - \eta + \cos\theta_0 \\
& + 2\pi\,(\sigma_{xx}-\sigma_{yy})\cos 2\phi_0 + 2\pi\,(\sigma_{xy}+\sigma_{yx})\sin 2\phi_0)\,(-4\eta - \cos 3\theta_0 + \cos\theta_0(1 \\
& + 4\eta\,(2\pi\,(\sigma_{xx}+\sigma_{yy}) + \eta) + 8\pi\eta\,((\sigma_{xx}-\sigma_{yy})\cos 2\phi_0 + (\sigma_{xy}+\sigma_{yx})\sin 2\phi_0)))]) \\
& \sin\theta_{tilt}^{ext}\cos\theta_{tilt}^{ext}\cos\delta^{ext}]
\end{aligned}$$

$$\begin{aligned}
n_2^{sg} = {} & \frac{1}{(\eta+\cos\theta_0)^2\,(\eta\cos\theta_0+\sin^2\theta_0)} \times [(-4\pi^2\eta\cos\theta_0\,[(\sigma_{xy}-\sigma_{yx} + (\sigma_{xy}+\sigma_{yx})\cos 2\phi_0 \\
& + (-\sigma_{xx}+\sigma_{yy})\sin 2\phi_0)\,(-\sigma_{xy}+\sigma_{yx} + (\sigma_{xy}+\sigma_{yx})\cos 2\phi_0 + (-\sigma_{xx}+\sigma_{yy})\sin 2\phi_0)] \\
& - [(-2\pi\,(\sigma_{xx}+\sigma_{yy}) - \eta + \cos\theta_0 + 2\pi\,(\sigma_{xx}-\sigma_{yy})\cos 2\phi_0 + 2\pi\,(\sigma_{xy}+\sigma_{yx})\sin 2\phi_0) \\
& (-4\eta - \cos 3\theta_0 + \cos\theta_0(1 + 4\eta\,(2\pi\,(\sigma_{xx}+\sigma_{yy}) + \eta) + 8\pi\eta\,((\sigma_{xx}-\sigma_{yy})\cos 2\phi_0 \\
& + (\sigma_{xy}+\sigma_{yx})\sin 2\phi_0)))])\sin\theta_{tilt}^{ext}\cos\theta_{tilt}^{ext}\sin\delta^{ext}]
\end{aligned}$$

$$
\begin{aligned}
d_1^{sg} \;=\; & \frac{1}{(\eta+\cos\theta_0)^2}\times[(-2\pi\,(\sigma_{xx}+\sigma_{yy})-\eta+\cos\theta_0+2\pi\,(\sigma_{xx}-\sigma_{yy})\cos 2\phi_0 \\
& +2\pi\,(\sigma_{xy}+\sigma_{yx})\sin 2\phi_0)^2\cos^2\theta_{tilt}^{ext}+16\pi^2\cos^2\theta_0\,(-\sigma_{yx}\cos^2\phi_0 \\
& +(\sigma_{xx}-\sigma_{yy})\cos\phi_0\sin\phi_0+\sigma_2\sin^2\phi_0)^2\sin^2\theta_{tilt}^{ext}+2\pi\;\cos\theta_0\,[(-2\pi(\sigma_{xx}+\sigma_{yy}) \\
& -\eta+\cos\theta_0+2\pi\,(\sigma_{xx}-\sigma_{yy})\cos 2\phi_0+2\pi\,(\sigma_{xy}+\sigma_{yx})\sin 2\phi_0) \\
& (-\sigma_{xy}+\sigma_{yx}+(\sigma_{xy}+\sigma_{yx})\cos 2\phi_0+(-\sigma_{xx}+\sigma_{yy})\sin 2\phi_0)]\sin 2\theta_{tilt}^{ext}\cos\delta^{ext}]
\end{aligned}
$$

$$
\begin{aligned}
d_2^{sg} \;=\; & \frac{1}{-2(\eta+\cos\theta_0)^2\,(\sin^2\theta_0+\eta\cos\theta_0)^2}\times[16\pi^2\eta^2\,(\sigma_{xy}-\sigma_{yx}+(\sigma_{xy}+\sigma_{yx})\cos 2\phi_0 \\
& +(-\sigma_{xx}+\sigma_{yy})\sin 2\phi_0)^2\cos^2\theta_{tilt}^{ext}+\frac{1}{4}(4\eta+\cos 3\theta_0-\cos\theta_0\,(1+4\eta\,(2\pi\,(\sigma_{xx}+\sigma_{yy}) \\
& +\eta)+8\pi\eta\,((\sigma_{xx}-\sigma_{yy})\cos 2\phi_0+(\sigma_{xy}+\sigma_{yx})\sin 2\phi_0)))^2\sin^2\theta_{tilt}^{ext}-2\pi\eta\,[(\sigma_{xy}-\sigma_{yx} \\
& +(\sigma_{xy}+\sigma_{yx})\cos 2\phi_0+(-\sigma_{xx}+\sigma_{yy})\sin 2\phi_0)\,(-4\eta-\cos 3\theta_0 \\
& +\cos\theta_0\,(1+4\eta\,(2\pi\,(\sigma_{xx}+\sigma_{yy})+\eta)+8\pi\eta\,((\sigma_{xx}-\sigma_{yy})\cos 2\phi_0 \\
& +(\sigma_{xy}+\sigma_{yx})\sin 2\phi_0)))]\sin 2\theta_{tilt}^{ext}\cos\delta^{ext}]
\end{aligned}
$$

From equation (3.11), the reflected polarization can be obtained by solving the equations for real and imaginary parts simultaneously. The behavior of this quantity with respect to its various parameters in different limits are explained in the coming section. It is seen that in the limit $\epsilon \to 1$, equation (3.11) reduces to that of freely suspended graphene.

From the equations for all the three coefficients it is clear that with the conductivity in its general form the equations are very complicated compared to the free standing results and therefore various limiting cases are considered in the next section.

3.5 Results and Discussion

This section discusses various limiting cases of the results given in the last section. For example, the isotropic limit of the conductivity tensor of graphene, different types of anisotropy, the situation with the incident wave being linearly polarized etc.

3.5.1 Isotropic Case

As mentioned in chapter 2, isotropic limit is one of the important limits, in which the off-diagonal elements of the conductivity tensor vanishes and the diagonal elements become equal. This limit can be obtained in two different ways which are explained in Gusynin et. al. [106] as well in chapter 2 in detail. One is when there is no external magnetic field and the other when the electrostatic doping is absent. Absence of electrostatic doping actually indicates that the chemical potential is zero. The significance of zero, positive and negative chemical potentials are explained in chapter 2.

From equations (3.9,3.10,3.11) it is clear that in the isotropic limit, the coefficients are functions of diagonal conductivity, dielectric constant, incident angle and tilt angle of the incident polarization ellipse. Now to proceed further it is important to have information about the diagonal conductivity of graphene. This for the case of $B = 0$ can be obtained from equation (2.20) by choosing appropriate values for the parameters. Therefore for $\mu = 4K$ and $\Omega = 9.6K$, $\sigma_{xx} = 1.82 \times 10^{-3}$ when Δ the gap in the quasi-particle spectrum is zero and $2.54{\times}10^{-3}$ for $\Delta = 3K$. For the case of $\mu = 0$, equation (2.18) gives $\sigma_{xx} = 2.404{\times}10^{-5}$ for zero gap and 2.402×10^{-5} for a finite gap for the same set of parameters. Each of the coefficients given by the equations (3.9, 3.10, 3.11) are discussed below in the limit of $\sigma_{xy} = \sigma_{yx} = 0$ and $\sigma_{xx} = \sigma_{yy} = \sigma_1$. For all the cases discussed in this section the incident wave is taken to be in the microwave region and more specifically at 200 *GHz*.

3.5.1.1 Reflection coefficient

In the isotropic limit, equation (3.9) reduces to the following form,

$$R_{iso}^{sg} = \frac{(4\pi\sigma_1 + \eta - \cos\theta_0)^2 \cos^2\theta_{tilt}^{ext}}{(\cos\theta_0 + \eta)^2} + \frac{(4\eta - (1 + 4\eta\ (4\pi\sigma_1 + \eta))\cos\theta_0 + \cos 3\theta_0)^2 \sin^2\theta_{tilt}^{ext}}{16\ (\epsilon\cos\theta_0 + \eta)^2} \tag{3.12}$$

where $\eta = \sqrt{-\sin^2\theta_0 + \epsilon}$. Here it is seen that the reflection coefficient of the substrate-graphene is a function of two angle parameters, the diagonal conductivity and the dielectric constant of the substrate material. In this limit it is clear that the reflection coefficient is independent of azimuthal angle which was the case for suspended graphene also. In comparison with the suspended graphene, there is an additional dependence on dielectric constant due to the presence of substrate.

Similar to that in the case of freely suspended graphene, the two different routes to isotropic limit are considered in this chapter. Unlike in the case of suspended graphene, in this situation the magnitude of reflection coefficient when $\mu = 0$ is comparable to that at $B = 0$. Two different quantities are considered for study in the case of substrate-graphene, (i) reflection coefficient of substrate-graphene denoted by R^{sg} (ii) difference in reflection coefficient of the substrate- graphene and that of the dielectric substrate denoted by $R^{sg} - R^{s}$. By the study of latter, the effect of substrate material become more evident. In the following plots, the variation of R^{sg} and $R^{sg} - R^{s}$ with respect to each of the angle parameters are given with the others fixed.

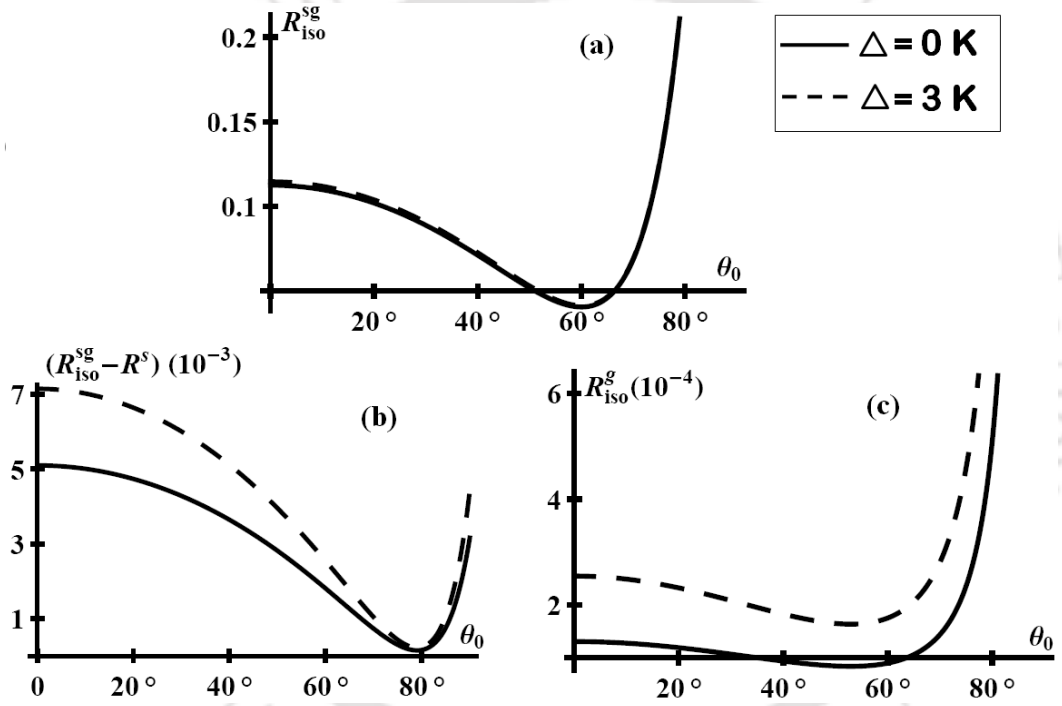

FIGURE 3.1: Reflection coefficient versus incident angle when the graphene conductivity tensor is isotropic and the incident energy is at 200 *GHz*. This figure has three parts: (a) substrate-graphene (b) difference reflection between substrate-graphene and pure substrate material (c) free- standing graphene. Solid curve shows the zero gap situation and the dashed curves are for finite gap situation in each of the cases.

Fig. 3.1 shows the variation of reflection coefficient with respect to incident angle. This figure has three parts which shows the behavior of substrate-graphene, substrate-graphene with the contribution of the pure substrate subtracted out and also the free standing graphene which enables an easy comparison between different situations. Here each of the plots has two curves in it, solid curve showing the zero gap situation whereas the dashed curves showing the

finite gap case in the quasi particle spectrum. In this plot only $B = 0$ situation is shown. The plot is self explanatory. Fig. 3.1b and 3.1c makes the comparison between the substrate and free standing situations easy and it is made for the same set of parameters. The increase in the magnitude of reflection compared to the free standing case is evident from the figure. The effect of gap is not so prominent, but it is clear that the presence of gap increases the reflected intensity. In comparison with the suspended graphene, the variation with respect to incident angle shows a well defined minimum unlike in the case of suspended graphene in which it is broad. The reflected intensity first decreases, goes through a minimum as the incident angle increases and then again increases as the incident angle approaches the gracing incidence. Also Fig. 3.1b signifies the fact that the reflection intensity of substrate graphene is always greater than that due to substrate situation only. The effect of gap can be more observable when the substrate contribution is subtracted out which is given in Fig. 3.1b. It can be seen that the influence of gap is not uniform, it is more visible at small incident angles and the effect is very less visible at angles close to gracing incidence. Behavior of reflected intensity of the substrate- graphene can be studied with respect to other parameter like tilt angle that shows an oscillatory behavior which is not included here.

Consider the situation in which the incident wave is normal to the plane containing the system under study, then the reflection coefficient takes the form $R_{iso}^{sg,\perp} = \frac{(-1+\sqrt{\epsilon}+4\pi\ \sigma_1)^2}{(1+\sqrt{\epsilon})^2}$. Note that the reflection coefficient depends only on the substrate material and the diagonal conductivity of graphene, the limit of ϵ tends to unity is easily checked here. The value of the diagonal conductivity is sensitive to gap and the way in which the isotropic nature is obtained which makes it easy to distinguish between the different situations at normal incidence.

The situation in which the incident wave is linearly polarized is interesting where the reflection coefficient becomes only a function of incident angle for fixed conductivity and fixed substrate material. The two extreme situations of this case are when $\theta_{tilt}^{ext} = 0$ at which $R_{iso,s}^{sg} = \frac{(4\pi\sigma_1-\cos\theta_0+\eta)^2}{(\cos\theta_0+\eta)^2}$ and $\theta_{tilt}^{ext} = \pi/2$ at which $R_{iso,p}^{sg} = \frac{(\eta-\cos\theta_0(\epsilon+4\pi\sigma_1\eta))^2}{(\epsilon\cos\theta_0+\eta)^2}$. Vanishing incident polarization is not important in the isotropic limit because in this limit the reflected intensity is not a function of it. The behavior of reflected intensity with respect to incident angle with *s* and *p* - polarized incidence resembles the behavior of a dielectric substrate which is discussed in detail in a separate section.

3.5.1.2 Transmission Coefficient

In the isotropic limit, equation (3.10) becomes,

$$T_{iso}^{sg} = \frac{4\,(-2\pi\sigma_1 + \cos\theta_0)^2 \cos^2\theta_{tilt}^{ext}}{(\eta + \cos\theta_0)^2} + \frac{4\,\epsilon\,\cos^2\theta_0\,(1 - 2\pi\,\sigma_1\cos\theta_0)^2 \sin^2\theta_{tilt}^{ext}}{(\eta + \cos\theta_0)^2\,(\eta\cos\theta_0 + \sin^2\theta_0)^2} \tag{3.13}$$

As in the case of reflection coefficient, transmission coefficient is also a function of only the angle parameters, incident angle and the tilt angle if the conductivity is fixed with a given substrate material. The isotropic limit is devoid of any azimuthal angle dependence. Different cases of isotropic limit are considered, for example the $B = 0$ limit and $\mu = 0$ limit. Two quantities are considered for the study, one is the transmission coefficient for substrate-graphene and the difference in transmission coefficient of substrate graphene and the pure dielectric material denoted by $T^{sg} - T^{s}$.

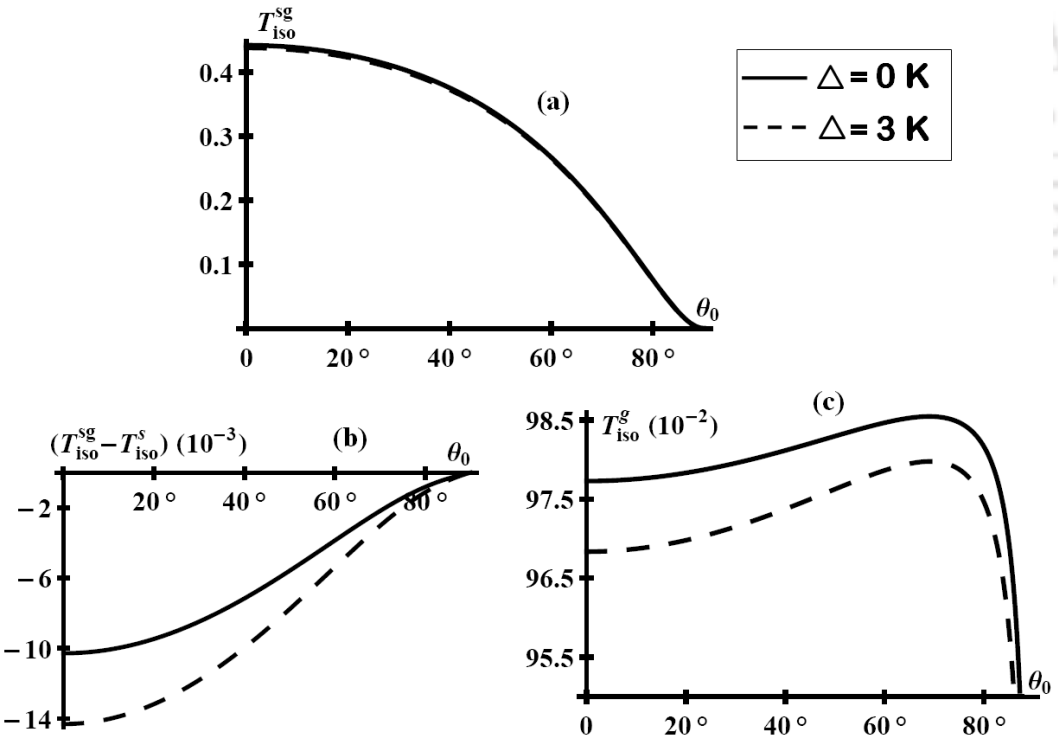

FIGURE 3.2: Transmission coefficient versus incident angle when the graphene conductivity tensor is isotropic. Here the incident energy is in the microwave region, specifically 200 *GHz*. This figure has three parts: (a) substrate-graphene (b) difference transmission between substrate-graphene and pure substrate material (c) free- standing graphene. Solid curve shows the zero gap situation and the dashed curves are for finite gap situation in each of the cases.

Fig. 3.2 shows the behavior of substrate-graphene with respect to incident angle. Fig. 3.2a shows the substrate graphene while Fig. 3.2b showing the transmitted intensity after subtracting out the substrate contribution. The last part Fig. 3.2c shows this property for free standing graphene which enables us to to make a comparison between substrate and free standing graphene. These three plots are drawn for the same set of parameters. As in the reflection study, there are two curves in each plot, the solid curve showing the vanishing gap situation whereas the finite gap situation is shown by the dashed curves. From the figures in this section it is evident that unlike in the case of reflection coefficient the gap decreases the transmitted intensity. A clear difference between the two systems can be seen in this figure. The free standing transmission coefficient is almost constant in the beginning and then increases slowly and at gracing incidence it decreases sharply. But in the substrate-graphene case, the transmission coefficient shows a very slow decrease with respect to incident angle. Note that the magnitude of transmitted intensity is decreased. If we compare with the reflection and transmission, the reflected intensity variation with the substrate contribution subtracted out is always positive throughout the full range of its parameters values whereas that in transmission the variation is always negative for the full range of its parameter values. This gives the difference in influence of substrate on the two coefficients. The reflected intensity fraction is increased by the presence of substrate material while the transmitted fraction is decreased by its presence. The effect of gap in the band structure is not very evident in the variation of transmission coefficient. To see the influence, the contribution of substrate material should be subtracted out. One can see that the influence of gap is not uniform, it is high at the small angle incidence and decreases towards the gracing incidence. The variation with respect to tilt angle of the incident polarization ellipse shows a qualitatively similar behavior to that of the free standing situation.

If the incidence is normal to the plane containing substrate- graphene, the transmission coefficient reduces to $T_{iso}^{sg,\perp} = \frac{4\ (1-2\pi\ \sigma_1)^2}{(1+\sqrt{\epsilon})^2}$. The transmission coefficient depends on the dielectric constant (depends on the substrate material chosen) and the conductivity element which represents the graphene sheet. Note that in the limit $\epsilon \to 1$, it reduces to the free standing result at normal incidence. All these limits check the correctness of the present result. The parameter representing gap is entering into the calculation through the conductivity tensor element. The difference between the two cases zero magnetic field and zero chemical potential is also coming into picture through the conductivity tensor. For these reasons the different situations are easily distinguished in the normal incidence limit, because transmission coefficient

dependence only on the conductivity element for a given substrate material.

It is seen here that the effect of the presence of substrate material on the reflection coefficient is to increase it appreciably and in the transmission coefficient is to decrease it considerably. It is clear from the magnitude of both the coefficients that the absorption in substrate-graphene is very large and significant unlike in the case of freely suspended graphene. It is easy to find out a rough idea about the absorption in the normal incidence limit using the conservation theorem, $1 - R - T$ which has the magnitude of approximately 0.6708 when the diagonal conductivity is 1.82×10^{-3} which is approximately one order of magnitude larger compared to the suspended result. The equation for the loss in this case can be calculated using the calculations given in Appendix A using the corresponding electric fields for substrate-graphene.

Turning towards the linearly polarized incidence, the zero incident polarization is irrelevant in the isotropic limit. The two extreme cases of $s-$ polarization and $p-$ polarization are studied for zero gap and zero magnetic field limit. The transmission coefficient with $s-$ polarized incident wave is $T^{sg}_{iso,s} = \frac{4\ (-2\pi\sigma_1+\cos\theta_0)^2}{(\cos\theta_0+\eta)^2}$ and that with $p-$ polarized incident wave is $T^{sg}_{iso,p} = \frac{4\epsilon\cos^2\theta_0\ (1-2\pi\sigma_1\cos\theta_0)^2}{(\epsilon\cos\theta_0+\eta)^2}$.

3.5.1.3 Reflected Polarization

In the isotropic limit, the reflected polarization reduces as given below:

$$e^{-i\ \delta^{ref}}|_{iso,sg} = sgn[\ (4\pi\sigma_1 + \eta - \cos\theta_0)\ (4\eta - (1 + 4\eta\ (4\pi\sigma_1 + \eta))\cos\theta_0 + \cos 3\theta_0)\sin\theta^{ext}_{tilt}\cos\theta^{ext}_{tilt}\ ]\ e^{-i\ \delta^{ext}} \tag{3.14}$$

It can be seen that the quantitative behavior of reflected polarization depends only on the incident polarization. The behavior is qualitatively dependent on the sign of the above given product in the right hand side of equation (3.14). Since there is no dependence on the conductivity (only on its sign), the two different situations $B = 0$ and $\mu = 0$ is not distinguishable in this study. The case is similar with the influence of gap, it cannot be observed in this study. By solving the real and imaginary parts of the above equation, the behavior of reflected polarization can be studied and can be calculated exactly. Reflected polarization for free standing

situation is not dependent on incident angle. But the qualitative behavior of reflected polarization for substrate-graphene is depended on the incident angle also. This is shown in Fig. 3.3, the first part of which shows the case of substrate-graphene whereas the second part shows the situation of suspended graphene. These plots are for fixed value of graphene conductivity and tilt angle of incident polarization effect with a given substrate material. The blue curve in these plots shows the real part of reflection polarization whereas the red curves shows the imaginary part. Note the difference between the two systems, substrate graphene shows a step like behavior and the suspended graphene remains the same for the full range of incident angle.

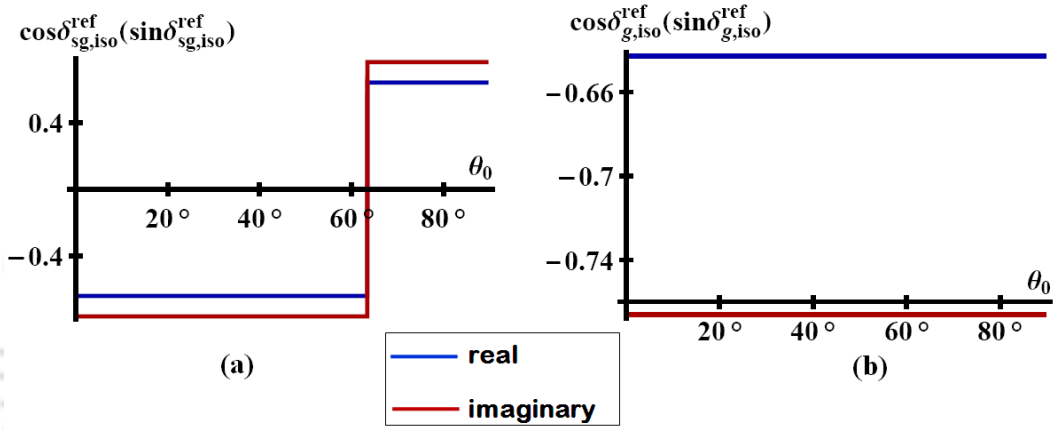

FIGURE 3.3: Reflected polarization versus incident angle when the graphene conductivity tensor is isotropic. This figure has two parts: (a) substrate-graphene (b) free-standing graphene. Blue curve is for real part of the reflection polarization and the red curve is for imaginary part. Here the incident photon energy is in the microwave region, i.e. at 200 *GHz*

The effect of the incident angle and tilt angle for a fixed diagonal conductivity and given substrate material is to make the real and imaginary parts of the reflected polarization to change its sign. The variation of it with respect to the incident polarization is similar to that of free standing case. Fig. 3.4 shows the 3D variation of real and imaginary parts of reflected polarization with respect to incident angle and incident polarization.

Fig. 3.4a shows the behavior of the real part of the reflected polarization and 4b shows that of the imaginary part. The behavior of the real and imaginary parts of reflected polarization is oscillatory with respect to the incident polarization and it is a step like behavior with respect to incident angle which are evident from Fig. 3.4. With respect to tilt angle they change sign at regular intervals and with respect to incident angle they change sign only once whose value depends upon the value of the tilt angle. By simultaneously solving the equations for $\cos\delta^{ref}$

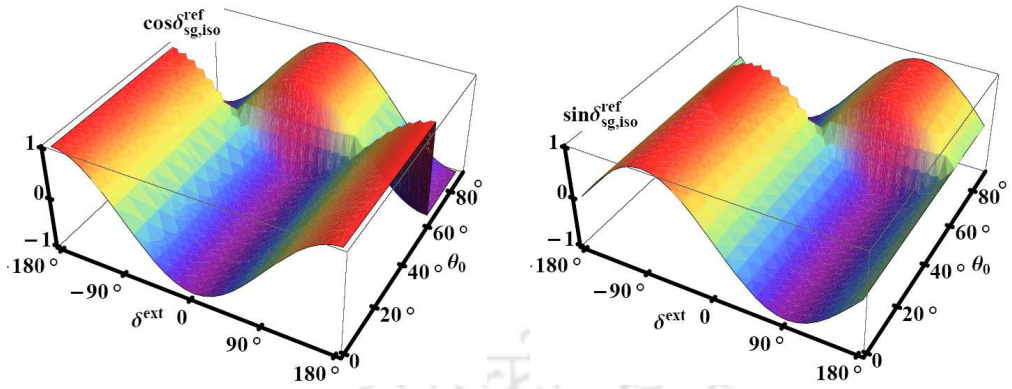

(a) (b)

FIGURE 3.4: Reflected polarization versus incident angle and incident polarization. First part shows the real part and the second part shows the imaginary part. The incident wave is in the microwave region of the electromagnetic spectrum with frequency 200 *GHz*

and $\sin\delta^{ref}$, gives the reflected polarization. It is explained with the help of a example in chapter 2, the method can be applied in this situation also. From equation (3.14), it is clear that the reflected polarization is either equal to the incident polarization or it is 180^0 out of phase to it. The phase shift between the incident and reflected polarization is determined together by the incident angle and tilt angle whereas the magnitude of the reflected polarization is determined by the incident polarization.

Moving towards the extreme cases of linear incident polarization, the reflected polarization in the isotropic limit with $s-$ and $p-$ polarized incidence will become $e^{-i\,\delta^{ref}}|^{s}_{iso,sg} = sgn[\,(4\pi\sigma_1+\eta-\cos\theta_0)\,(4\eta-(1+4\eta\,(4\pi\sigma_1+\eta))\cos\theta_0+\cos 3\theta_0)\,]e^{-i\,\delta^{ext}}$ and $e^{-i\,\delta^{ref}}|^{sg}_{iso,p} = -sgn[\,(4\pi\sigma_1+\eta-\cos\theta_0)\,(4\eta-(1+4\eta\,(4\pi\sigma_1+\eta))\cos\theta_0+\cos 3\theta_0)\,]e^{-i\,\delta^{ext}}$ respectively. From the equations it is clear that for a fixed conductivity element and a given substrate material, elements which determine the reflected polarization are not only the incident polarization but also the incident angle. In the free standing case the reflected polarization with $s-$ and $p-$ incident polarization depends only on the incident polarization. From Fig. 3.4 it is clear that at angle of incidence less than around 65^0, the behavior of the reflected polarization with respect to incident polarization is same as the free standing case, but as the incident angle increases, it becomes exactly opposite to that of free standing case.

Fig. 3.5 shows the plot of the above given expressions which illustrates the behavior of real and imaginary parts of reflected polarization with respect to incident polarization when

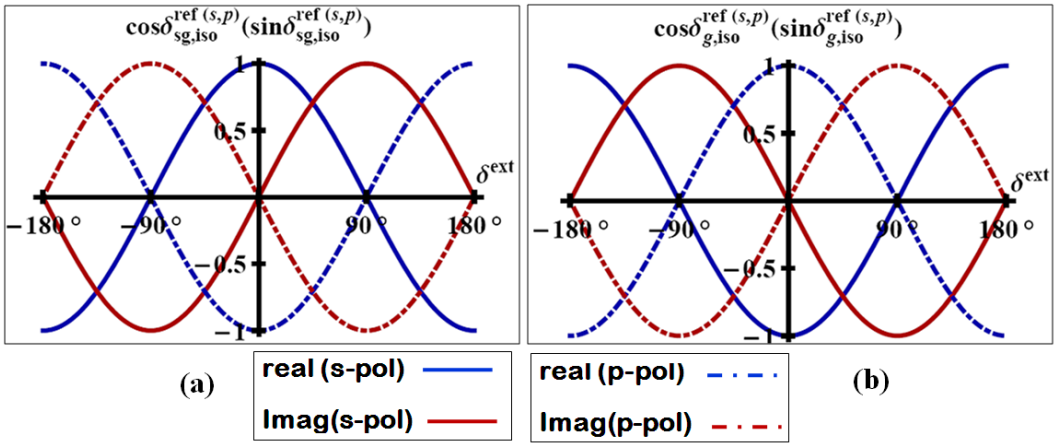

FIGURE 3.5: Real and imaginary parts of reflected polarization versus incident polarization when the incident wave is *s* and *p* - polarized. Left part shows the behavior of substrate-graphene where the right part shows that of the free- standing graphene. Here the blue curves are for real part of reflected polarization and red curves are for imaginary part. The solid curve signifies the situation with *s* - polarized incident wave whereas the dot-dashed curves are for *p* - polarized incident wave. The incident wave is with frequency 200 *GHz*

the incident wave is polarized in an extreme manner (*s* and *p* polarized) with angle of incidence is large (greater than 65^0). This figure has two parts, first showing the behavior of substrate graphene while the other part shows the variation of free standing graphene which is given for a comparative study. Solid curves are for *s* - polarized incident intensity where as dashed dotted curves are for *p* - polarized incident intensity. Blue curve is for real part and red curves signifies the imaginary part. At large incidence, reflected polarization with *s*− polarized intensity in substrate graphene behaves as the reflected polarization with *p*− polarized intensity in suspended graphene, that is there is a 180^0 phase shift between the suspended graphene and substrate graphene with extreme limits of incident polarization and large incident angle. When the incident polarization itself vanishes, then the imaginary part of the reflected polarization also vanishes and this makes the reflected polarization either zero or $\pm\pi$. Now out of these the decision about reflected polarization is done from the value of incident angle and tilt angle.

In this section, the nature of reflection coefficient, transmission coefficient and reflected polarization of light emerging from a substrate graphene are studied in the isotropic limit of the conductivity tensor. In each and every situation we can see a comparison between the present system under study and the system discussed in chapter 2. A similar study is done as in the case of free standing graphene. The general behavior of these quantities remains

the same when one compare between the free standing and substrate-graphene. But a close observation of the optical quantities in various limits such as $B = 0$, $\mu = 0$, $\theta_0 = 0$, $\theta_{tilt}^{ext} \to 0$ and $\theta_{tilt}^{ext} \to \pi/2$ shows a clear difference between the behaviors of the two systems. The three quantities studied gives information about the conductivity tensor of the material.

3.5.2 Anisotropic Case

This section deals with the situation when the conductivity tensor of graphene is anisotropic, it can happen in general two ways, one is when the off diagonal elements are non-zero or with the vanishing off-diagonal elements and unequal diagonal elements. In the first case, there are different possibilities: (i) all the elements can be different (ii) diagonal elements equal and off-diagonal elements also equal (iii) diagonal elements equal but the off-diagonal elements equal and opposite. Out of all these possibilities, only two are considered for study, just as in the case of free standing graphene. The cases under consideration are when i) $\sigma_{xx} = \sigma_{yy} = \sigma_1$ and $\sigma_{xy} = -\sigma_{yx} = \sigma_2$ and ii) $\sigma_{xx} \neq \sigma_{yy}$ and $\sigma_{xy} = \sigma_{yx} = 0$. The first case can be named an off-diagonal anisotropy and the second case can be called diagonal anisotropy. Here the first case, i.e. the off-diagonal anisotropy is well explained in Gusynin et. al. [106] and the source of this anisotropy is either the external magnetic field or the non zero chemical potential. Therefore this situation is well understood and the conductivity tensor in this stage is also known and given by the equations (2.18, 2.19) in the microwave region and in the high magnetic field limit. Numerical value is obtained from these equations by the choice of its parameters, that is if $\Gamma = 4K$, $\mu = -6K$, $T = 0.5K$ and $\Omega = 9.6K$ the diagonal conductivity become 6.28×10^{-4} and the off-diagonal conductivity 1.78×10^{-3} for a zero gap situation and $(5.83 \times 10^{-4}, 1.63 \times 10^{-3})$ for a finite gap of the order of $3K$. Here conductivity elements appears to be dimensionless because c is chosen as unity. The diagonal anisotropy case is studied in Strikha et. al. [104] which says that such kind of anisotropy can be expected in an in-planar electric field. We can guess that it may also happen when there is a structural anisotropy in the material due to disorder or an external agent like strain. Since the behavior of the conductivity tensor under this situation is not clear, this part of the study is done by choosing the diagonal conductivity elements as $\sigma_{xx} = \sigma + \frac{\Delta\sigma}{2}$ and $\sigma_{yy} = \sigma - \frac{\Delta\sigma}{2}$ where σ is taken as the universal optical conductivity $\frac{e^2}{4\hbar}$ and $\Delta\sigma$ is chosen randomly to be a small quantity which is consistent with Strikha et. al. of the order of 10^{-4}.

As in the isotropic limit, here also the three optical quantities are considered for study, viz. coefficient of reflection, coefficient of transmission and the reflected polarization. Here also the incident energy is in the microwave region of the electromagnetic spectrum, specifically at 200 *GHz*.

3.5.2.1 Reflection Coefficient

In the case of off-diagonal anisotropy, i.e. when $\sigma_{xx} = \sigma_{yy} = \sigma_1$ and $\sigma_{xy} = -\sigma_{yx} = \sigma_2$

$$R_{off}^{sg} = r_{1,sg}^{off} \cos^2\theta_{tilt}^{ext} + r_{2,sg}^{off} \sin^2\theta_{tilt}^{ext} + r_{3,sg}^{off} \sin 2\theta_{tilt}^{ext} \cos\delta^{ext} \tag{3.15}$$

$$\begin{aligned} r_{1,sg}^{off} = {} & \frac{1}{(\epsilon\cos\theta_0 + \eta)^2} \times [(-\cos\theta_0 + \eta)\,(8\pi\sigma_1 - \cos\theta_0 + \eta)\,(\sin^2\theta_0 + \cos\theta_0\eta)^2 \\ & + 4\pi^2\,(2\,(-1+2\epsilon)\sigma_2^2 + 2\,((-1+\epsilon)\,\sigma_1^2 + \sigma_2^2)\cos 2\theta_0 + \sigma_1^2\,(1 + 2\epsilon + \cos 4\theta_0) \\ & + 8\sigma_1^2\eta\cos\theta_0\sin^2\theta_0)] \end{aligned}$$

$$\begin{aligned} r_{2,sg}^{off} = {} & \frac{1}{2\,(-\sin^2\theta_0 + \epsilon^2\cos^2\theta_0 + \epsilon\,(1 + 2\cos\theta_0\eta))} \times [(-1 + \epsilon\,(2+\epsilon)) \\ & + 8\pi^2\cos^2\theta_0\,((-2+4\epsilon)\sigma_1^2 + (1+2\epsilon)\sigma_2^2 + 2\,(\sigma_1^2 + (-1+\epsilon)\sigma_2^2)\cos 2\theta_0 + \sigma_2^2\cos 4\theta_0) \\ & + 4\pi\,(2\epsilon\sigma_1 - \pi\sigma_2^2\,(\cos 3\theta_0 + \cos 5\theta_0))\,\eta + \cos 2\theta_0\,(1 + \epsilon^2 + 8\pi\epsilon\sigma_1\eta) \\ & + 4\cos\theta_0\,(2\pi\,(1-2\epsilon)\,\sigma_1 - 2\pi\sigma_1\cos 2\theta_0 + (-\epsilon + 2\pi^2\sigma_2^2)\,\eta)] \end{aligned}$$

$$\begin{aligned} r_{3,sg}^{off} = {} & \frac{1}{2\,(-\sin^2\theta_0 + \epsilon^2\cos^2\theta_0 + \epsilon\,(1 + 2\cos\theta_0\eta))} \times 4\pi\sigma_2\sin^2\theta_0[(-2 + 5\epsilon + \cos 4\theta_0) \\ & + 8\pi\sigma_1\eta - 2\cos 3\theta_0\eta + \cos\theta_0\,(-8\pi\,(-1+\epsilon)\,\sigma_1 - 8\pi\sigma_1\cos 2\theta_0 - 2\,(2+\epsilon)\,\eta) \\ & + \cos 2\theta_0(1 + 3\epsilon + 8\pi\sigma_1\eta)] \end{aligned}$$

In the case of diagonal anisotropy, i.e. when $\sigma_{xx} \neq \sigma_{yy}$ and $\sigma_{xy} = \sigma_{yx} = 0$

$$R_{diag}^{sg} = r_{1,sg}^{diag} \cos^2\theta_{tilt}^{ext} + r_{2,sg}^{diag} \sin^2\theta_{tilt}^{ext} + r_{3,sg}^{diag} \sin 2\theta_{tilt}^{ext} \cos\delta^{ext} \tag{3.16}$$

$$r_{1,sg}^{diag} = \frac{1}{(\epsilon\cos\theta_0+\eta)^2}\times[(-\cos\theta_0+\eta)\,(\sin^2\theta_0+\cos\theta_0\eta)^2\,(4\pi\,(\sigma_1+\sigma_4 + (-\sigma_1+\sigma_4)\cos 2\phi_0) + (-\cos\theta_0+\eta)) + \pi^2\,(4\,(\sigma_1+\sigma_4+(-\sigma_1+\sigma_4)\cos 2\phi_0)^2 (\sin^2\theta_0+\cos\theta_0\eta)^2 + 4\,(\sigma_1-\sigma_4)^2\,(\epsilon-\sin^2\theta_0)\sin^2 2\phi_0)]$$

$$r_{2,sg}^{diag} = \frac{1}{(\epsilon\cos\theta_0+\eta)^2}\times\cot^2\theta_0\,[4\pi^2\,(\sigma_1-\sigma_4)^2\sin^2\theta_0\,(\sin^2\theta_0+\cos\theta_0\eta)^2\sin^2 2\phi_0 + (\sin\theta_0\,(\epsilon+2\pi\,(\sigma_1+\sigma_4)\,\eta+2\pi\eta\,(\sigma_1-\sigma_4)\cos 2\phi_0)-\eta\,\tan\theta_0)^2]$$

$$r_{3,sg}^{diag} = \frac{1}{8\,(\epsilon\cos\theta_0+\eta)^2}\times\pi\cot\theta_0\,[16\pi\,(-\sigma_1+\sigma_4)\cos\phi_0\sin\theta_0\,(2\,(-1+2\epsilon+\cos 2\theta_0) (\sigma_1+\sigma_4+(\sigma_1-\sigma_4)\cos 2\phi_0) + 4\,(\sigma_1+\sigma_4+(-\sigma_1+\sigma_4)\cos 2\phi_0) (\sin^2\theta_0+\cos\theta_0\eta)^2)\sin\phi_0 - 2\,(\sigma_1-\sigma_4)\,(-\cos\theta_0+\eta)\,(2\,(-1+7\epsilon)\cos\theta_0 + (1+2\epsilon)\cos 3\theta_0+\cos 5\theta_0+8\cos 2\theta_0\sin^2\theta_0\eta)\sin 2\phi_0\tan\theta_0]$$

where $\sigma_{xx}=\sigma_1$ and $\sigma_{yy}=\sigma_2$. The basic difference between these two cases is clear from the first glance that is there is no azimuthal angle dependence in the reflection coefficient as in the isotropic limit where as there is azimuthal angle playing a role in the diagonal anisotropic situation. Both these cases the coefficient is a function of incident angle, tilt angle, incident polarization, conductivity tensor elements and the dielectric constant of the substrate material. In this limiting case also, two quantities are considered one is the reflection coefficient of substrate-graphene denoted by R_{aniso}^{sg} and the other is reflection coefficient with the substrate contribution subtracted out denoted by $R_{aniso}^{sg}-R^{s}$ of which the latter helps to understand the actual influence of substrate material on graphene reflection. Influence of gap in the quasi-particle spectrum on the reflected intensity which is coming through the conductivity tensor elements decreases the reflection coefficient unlike that of the isotropic situation. Also the overall increase in the magnitude of reflected intensity due to the presence of substrate material can be understood from the study of reflected intensity with the substrate contribution subtracted out with the reflected intensity from substrate-graphene always greater than that due to the corresponding dielectric material. Dependence with respect to different parameters are studied, the behaviors showing almost similar characteristics of free standing situation. The situation with linearly polarized incidence is included as a separate section which carries various interesting information.

3.5.2.2 Transmission Coefficient

In the case of off-diagonal anisotropy, i.e. when $\sigma_{xx} = \sigma_{yy} = \sigma_1$ and $\sigma_{xy} = -\sigma_{yx} = \sigma_2$.

$$T^{sg}_{off} = t^{off}_{1,sg} \cos^2\theta^{ext}_{tilt} + t^{off}_{2,sg} \sin^2\theta^{ext}_{tilt} + t^{off}_{3,sg} \sin 2\theta^{ext}_{tilt} \cos\delta^{ext} \tag{3.17}$$

$$\begin{aligned} t^{off}_{1,sg} = {} & \frac{1}{2(\epsilon\cos\theta_0+\eta)^2} \times [-32\pi\epsilon\,\sigma_1\cos^3\theta_0 + 4\cos^2\theta_0\,(\epsilon\,(1+8\pi^2\,(\sigma_1^2+\sigma_2^2)) \\ & + \cos 2\theta_0\,(-1+\epsilon+\cos 2\theta_0)) - 32\pi^2\sigma_1^2\cos 2\theta_0\sin^2\theta_0 + 2\cos\theta_0\,(16\pi\sigma_1\cos 2\theta_0\sin^2\theta_0 \\ & + (1+8\pi^2\sigma_1^2)\,\eta) - \eta\,((1+16\pi^2\sigma_1^2)\cos 3\theta_0 + \cos 5\theta_0 + 16\pi\sigma_1\sin^2 2\theta_0)] \end{aligned}$$

$$\begin{aligned} t^{off}_{2,sg} = {} & \frac{1}{(\epsilon\cos\theta_0+\eta)^2} \times 4\cos^2\theta_0\,[\epsilon\,(1+2\pi^2\,(\sigma_1^2+\sigma_2^2)) + 2\pi\,(-\pi\sigma_2^2\eta\,\cos 3\theta_0 \\ & + \pi\cos 2\theta_0\,(\epsilon\,(\sigma_1^2+\sigma_2^2) - 2\sigma_2^2\,\sin^2\theta_0) + \cos\theta_0\,(-2\epsilon\sigma_1+\pi\eta\,\sigma_2^2))] \end{aligned}$$

$$\begin{aligned} t^{off}_{3,sg} = {} & \frac{1}{(\epsilon\cos\theta_0+\eta)^2} \times 8\pi\sigma_2\cos\theta_0\sin^2\theta_0\,[-2\pi\sigma_1\cos 2\theta_0 + \cos\theta_0\,(\epsilon+\cos 2\theta_0 \\ & + 4\pi\eta\,\sigma_1 - 2\eta\,\cos\theta_0)] \end{aligned}$$

In the case of diagonal anisotropy, i.e. when $\sigma_{xx} \neq \sigma_{yy}$ and $\sigma_{xy} = \sigma_{yx} = 0$.

$$T^{sg}_{diag} = t^{diag}_{1,sg} \cos^2\theta^{ext}_{tilt} + t^{diag}_{2,sg} \sin^2\theta^{ext}_{tilt} + t^{diag}_{3,sg} \sin 2\theta^{ext}_{tilt} \cos\delta^{ext} \tag{3.18}$$

where

$$\begin{aligned} t^{diag}_{1,sg} = {} & \frac{1}{(\epsilon\cos\theta_0+\eta)^2} \times [4\cos^2\theta_0\,(\sin^2\theta_0+\eta\,\cos\theta_0)^2 - 8\pi\cos\theta_0\,(\sigma_1+\sigma_4+(-\sigma_1 \\ & + \sigma_4)\cos 2\phi_0)\,(\sin^2\theta_0+\eta\,\cos\theta_0)^2 + 4\pi^2\,((\sigma_1+\sigma_4+(-\sigma_1+\sigma_4)\cos 2\phi_0)^2\sin^4\theta_0 \\ & + 2\cos\theta_0\,(\sigma_1+\sigma_4+(-\sigma_1+\sigma_4)\cos 2\phi_0)^2\eta\,\sin^2\theta_0 + 4\cos^2\theta_0\,(\sigma_1^2\,\eta^2\sin^2\phi_0 \\ & + \cos^2\phi_0\,(\sigma_4^2\,\eta^2 + (\sigma_1-\sigma_4)^2\sin^2\theta_0\sin^2\phi_0)))] \end{aligned}$$

$$t_{2,sg}^{diag} = \frac{1}{(-\sin^2\theta_0 + \epsilon^2\cos^2\theta_0 + \epsilon\,(1+2\cos\theta_0\eta))} \times 4\cos^2\theta_0\,[\epsilon - 2\pi\epsilon\cos\theta_0\,(\sigma_1+\sigma_4 + (\sigma_1-\sigma_4)\cos 2\phi_0) + 4\pi^2\cos^2\theta_0\,(\epsilon\,\sigma_4^2\sin^2\phi_0 + \cos^2\phi_0\,(\epsilon\,\sigma_1^2 - (\sigma_1-\sigma_4)^2\sin^2\theta_0\sin^2\phi_0)) + \pi^2\,(\sigma_1-\sigma_4)^2\sin^2\theta_0\,(\sin^2\theta_0 + 2\eta\,\cos\theta_0)\sin^2 2\phi_0]$$

$$t_{3,sg}^{diag} = \frac{1}{(-\sin^2\theta_0 + \epsilon^2\cos^2\theta_0 + \epsilon\,(1+2\cos\theta_0\eta))} \times \pi\,(\sigma_1-\sigma_4)\cos\theta_0\,[4\pi(\sigma_1+\sigma_4 + (-\sigma_1+\sigma_4)\cos 2\phi_0)\sin^4\theta_0\sin 2\phi_0 + \cos\theta_0\,(-1-6\epsilon-2\,(-1+\epsilon)\cos 2\theta_0 - \cos 4\theta_0 + 2\eta\,(\cos 3\theta_0 + 4\pi\,(\sigma_1+\sigma_4+(-\sigma_1+\sigma_4)\cos 2\phi_0)\sin^2\theta_0))\sin 2\phi_0 + \cos^2\theta_0\,(-4\eta\,\cos\phi_0\sin\phi_0 - 16\pi\,\cos\phi_0\sin^2\theta_0\sin\phi_0\,(\sigma_4\cos^2\phi_0 + \sigma_1\sin^2\phi_0) + 8\pi\epsilon\,(\sigma_1+\sigma_4)\sin 2\phi_0)]$$

where $\sigma_{xx} = \sigma_1$ and $\sigma_{yy} = \sigma_4$. It is seen that the main difference between the two cases of anisotropy, namely the diagonal and off-diagonal anisotropy, is that there is no azimuthal angle dependence in the transmission coefficient for off-diagonal anisotropy whereas the diagonal anisotropic situation shows an azimuthal angle dependence. Except for this, both are functions of incident angle, tilt angle and the incident polarization, conductivity tensor elements for graphene and dielectric constant of the substrate material. The study of transmission coefficient goes in parallel with the reflection coefficient,that is two quantities are of importance here the transmission coefficient of substrate graphene denoted by T_{aniso}^{sg} and the transmission coefficient without the purely substrate contribution denoted by $T_{aniso}^{sg} - T^{s}$. These quantities are studied with respect to various angle parameters for both the types of anisotropy. A decrease in magnitude of transmission coefficient is clear from the study due to presence of substrate. Influence of gap in the quasi-particle spectrum in transmitted intensity is to increase it in the case of off-diagonal anisotropy unlike the situation in isotropic limit. Also the differential transmission coefficient is always negative for the full range of parameter values which shows that the transmitted intensity of substrate-graphene is always less than that of its corresponding dielectric material alone.

In this section, the situation when the incident wave is linearly polarized it studied in detail. First two extreme cases are considered, by now it is clear that one is $s-$ polarization and the other is $p-$ polarization. Fig. 3.6 shows the variation of transmitted intensity of substrate graphene with respect to incident angle when the incident wave is linearly polarized

in an extreme way.

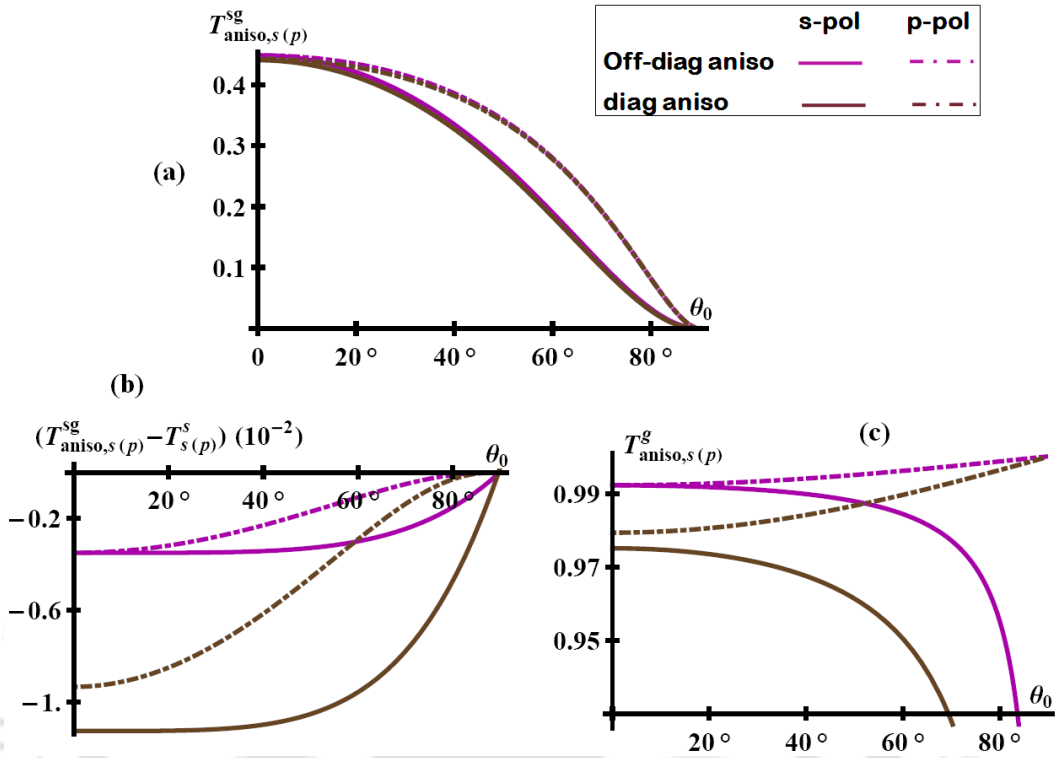

FIGURE 3.6: Transmission coefficient versus incident angle with anisotropic graphene conductivity tensor when the incident wave is linearly polarized. This figure has three parts (a) substrate-graphene (b) difference in transmission intensity between substrate-graphene and dielectric substrate (c) free-standing situation. Here the solid curves are for *s* - polarized incidence case and dot-dashed curves are for *p* - polarized incidence. The magenta curve is with the off-diagonal anisotropy and brown curves are for diagonal anisotropic situation. Here the incident photon is considered with frequency in the microwave region i.e. say at 200 *GHz*

The figure has three parts, Fig. 3.6a shows the variation of substrate-graphene, Fig. 3.6b shows the behavior of differential transmission coefficient and the third part Fig. 3.6c shows the suspended results for a comparative study. Each of the curves many curves in it of which the brown curves are for diagonal anisotropic situation and magenta curves are for off-diagonal anisotropic case. The solid curves are with the incident wave *s* - polarized and the dash-dotted curves are with incident light being *p* - polarized. We can see the difference in behavior of transmitted intensity in the two systems, substrate graphene and suspended graphene for different kinds of anisotropy. To make sure the influence of substrate on graphene transmission and to differentiate between the anisotropy, the differential transmission coefficient is

also given whose magnitude is always negative which implies the decrease in magnitude of the substrate-graphene compared to the simple dielectric material as seen earlier.

Fig. 3.6b shows a clear distinction between the different anisotropic situations. When compared with the free standing situation we can see that both the cases, the $s-$ polarized incidence and $p-$ polarized incidence is behaving in an entirely different way in substrate-graphene. Instead of a sharp decrease in magnitude for angle of incidence close to gracing incidence which was the case in free standing case, the $s-$ polarized incidence shows a smooth decrease in transmitted intensity. The $p-$ polarized incidence shows an entirely different behavior compared to the free standing case, i.e. a smooth decrease in magnitude as the angle of incidence increases but through a different path compared to the $s-$ polarized incidence. In the free standing case it is a smooth increase as can be seen from Fig. 3.6c. The trivial case of linearly polarized incidence, which is when the incident polarization is vanishing, the behavior is similar to that of the general case of anisotropy.

3.5.2.3 Comparison of Reflection and Transmission

A comparison between the reflection and transmission coefficient is done with respect to the dielectric constant. This is to observe the effect of different substrate materials on the optical properties of graphene. This study is explained with the help of Fig. 3.7. Note that the reflection coefficient increases with dielectric constant whereas the transmission coefficient decreases. In Fig. 3.7, all the cases of anisotropy together with the isotropic condition for zero gap situation is plotted. The solid curves are for reflection and dotted curves are for transmission. Isotropic behavior is highlighted with green curves, the off-diagonal anisotropic situations with magenta curves whereas the diagonal anisotropic cases with brown curves. We can see from the figure that all the situations merge into a single curve for both reflection and transmission. To observe the difference between the various situations, the purely substrate contribution can be subtracted out which is shows as Fig. 3.7b. We can see that the isotropic case and the diagonal anisotropy are very close in magnitude. The behavior is same for all the cases.

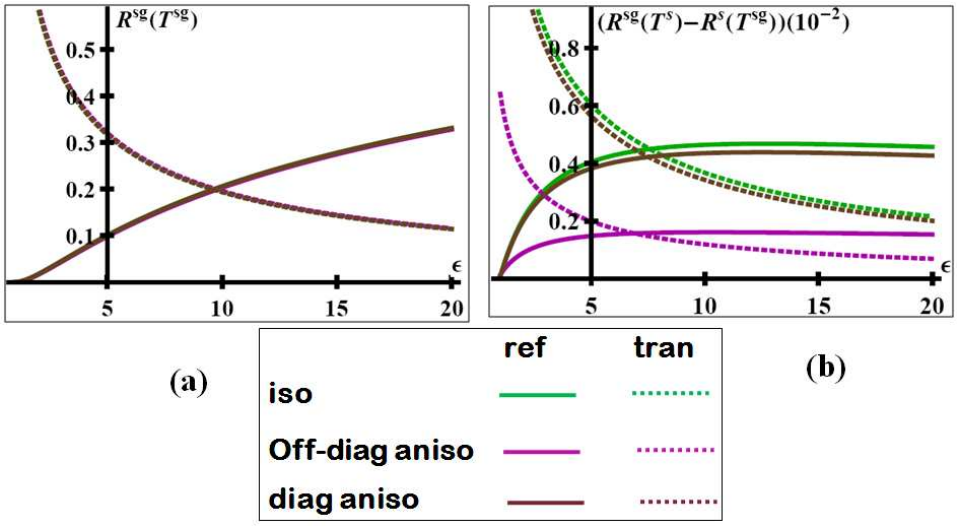

FIGURE 3.7: Reflection and transmission coefficient of substrate graphene as a function of the dielectric constant of the substrate where the incident wave being at 200 *GHz*. This figure has two parts, the left part shows the reflection and transmission intensity of substrate-graphene where as the right part shows the difference intensity of reflected and transmitted wave between the substrate-graphene and dielectric substrate. Here the solid curve is for reflection and dashed curve is for transmission. Isotropic situation is represented by the green curves, off-diagonal anisotropic limit is shown by the magenta curves and diagonal anisotropic case is given by the brown colored curves.

3.5.2.4 Reflected Polarization

When $\sigma_{xx} = \sigma_{yy} = \sigma_1$ and $\sigma_{xy} = -\sigma_{yx} = \sigma_2$

$$e^{i\,\delta^{ref}}|^{sg}_{off} = \frac{n^{sg}_{1,off} + i\, n^{sg}_{2,off}}{\sqrt{d^{sg}_{1,off}\, d^{sg}_{2,off}}} \tag{3.19}$$

$$\begin{aligned} n^{sg}_{1,off} = {} & \frac{1}{(\cos\theta_0 + \eta)\,(\epsilon\cos\theta_0 + \eta)} \times [4\pi\sigma_2\,(\epsilon + 4\pi\eta\,\sigma_1 - (\sin^2\theta_0 + \eta\,\cos\theta_0))\cos^2\theta^{ext}_{tilt} \\ & - 4\pi\sigma_2\cos\theta_0\,(-\eta + \cos\theta_0\,(\epsilon + 4\pi\eta\,\sigma_1))\sin^2\theta^{ext}_{tilt} + (16\pi^2\eta\,\sigma_2^2\cos\theta_0 \\ & + \frac{1}{2}(8\pi\eta\,\sigma_1\cos^2\theta_0 + ((-1 + 3\epsilon + (1+\epsilon)\cos 2\theta_0) + 8\pi\eta\,\sigma_1) - 2\cos\theta_0\,(8\pi\epsilon\,\sigma_1 \\ & - 4\pi\sigma_1\sin^2\theta_0 + ((1+\epsilon) + 16\pi^2\sigma_1^2)\,\eta)))sin\theta^{ext}_{tilt}\cos\theta^{ext}_{tilt}\cos\delta^{ext}] \end{aligned}$$

$$n^{sg}_{2,off} = \frac{1}{(\cos\theta_0+\eta)\,(\epsilon\cos\theta_0+\eta)} \times [(16\pi^2\eta\,\sigma_2^2\cos\theta_0 - \frac{1}{2}(8\pi\eta\,\sigma_1\cos^2\theta_0 + ((-1+3\epsilon + (1+\epsilon)\cos 2\theta_0) + 8\pi\eta\,\sigma_1) - 2\cos\theta_0\,(8\pi\epsilon\,\sigma_1 - 4\pi\sigma_1\sin^2\theta_0 + ((1+\epsilon) + 16\pi^2\sigma_1^2)\,\eta)))sin\theta^{ext}_{tilt}\cos\theta^{ext}_{tilt}\sin\delta^{ext}]$$

$$d^{sg}_{1,off} = \frac{1}{(\cos\theta_0+\eta)^2} \times [(4\pi\sigma_1 - \cos\theta_0+\eta)^2\cos^2\theta^{ext}_{tilt} + 16\pi^2\sigma_2^2\cos^2\theta_0\sin^2\theta^{ext}_{tilt} + 4\pi\sigma_2\cos\theta_0\,(4\pi\sigma_1 - \cos\theta_0+\eta)\sin 2\theta^{ext}_{tilt}\cos\delta^{ext}]$$

$$d^{sg}_{2,off} = \frac{1}{(\epsilon\cos\theta_0+\eta)^2} \times [16\pi^2\eta^2\sigma_2^2\cos^2\theta^{ext}_{tilt} + (\eta - \cos\theta_0\,(\epsilon+4\pi\eta\,\sigma_1))^2\sin^2\theta^{ext}_{tilt} - 4\pi\sigma_2\,(\eta^2 + \cos\theta_0\,(\epsilon\,\eta + 4\pi\eta^2\sigma_1))\sin 2\theta^{ext}_{tilt}\cos\delta^{ext}]$$

When $\sigma_{xx} \neq \sigma_{yy}$ and $\sigma_{xy} = \sigma_{yx} = 0$

$$e^{i\,\delta^{ref}}|^{sg}_{diag} = \frac{n^{sg}_{1,diag} + i\,n^{sg}_{2,diag}}{\sqrt{d^{sg}_{1,diag}\,d^{sg}_{2,diag}}} \tag{3.20}$$

$$n^{sg}_{1,diag} = \frac{1}{(\cos\theta_0+\eta)\,(\epsilon\cos\theta_0+\eta)} \times [-2\pi\eta\,(\sigma_1-\sigma_4)\,(2\pi\,(\sigma_1+\sigma_4) - \cos\theta_0 + 2\pi\,(-\sigma_1+\sigma_4)\cos 2\phi_0+\eta)\sin 2\phi_0\cos^2\theta^{ext}_{tilt} - 2\pi\,(\sigma_1-\sigma_4)\cos\theta_0((-1+ 2\pi\eta\,(\sigma_1-\sigma_4)\cos\theta_0\cos 2\phi_0) + \cos\theta_0\,(\epsilon + 2\pi(\sigma_1+\sigma_4)\,\eta))\sin 2\phi_0\sin^2\theta^{ext}_{tilt} + (-16\pi^2\eta\,(\sigma_1-\sigma_4)^2\cos\theta_0\cos^2\phi_0\sin^2\phi_0 - (2\pi\,(\sigma_1+\sigma_4) - \cos\theta_0 + 2\pi\,(-\sigma_1+\sigma_4)\cos 2\phi_0+\eta)\,((-1+2\pi\,(\sigma_1-\sigma_4)\cos\theta_0\cos 2\phi_0)\,\eta + \cos\theta_0(\epsilon + 2\pi\,(\sigma_1+\sigma_4)\,\eta)))\sin\theta^{ext}_{tilt}\cos\theta^{ext}_{tilt}\cos\delta^{ext}]$$

$$n^{sg}_{2,diag} = \frac{1}{(\cos\theta_0+\eta)\,(\epsilon\cos\theta_0+\eta)} \times [(-16\pi^2\eta\,(\sigma_1-\sigma_4)^2\cos\theta_0\cos^2\phi_0\sin^2\phi_0 + (2\pi\,(\sigma_1+\sigma_4)-\cos\theta_0+2\pi\,(-\sigma_1+\sigma_4)\cos 2\phi_0+\eta)\,((-1+2\pi\,(\sigma_1 - \sigma_4)\cos\theta_0\cos 2\phi_0)\,\eta+\cos\theta_0\,(\epsilon+2\pi\,(\sigma_1+\sigma_4)\,\eta)))\sin\theta^{ext}_{tilt}\cos\theta^{ext}_{tilt}\sin\delta^{ext}]$$

$$d^{sg}_{1,diag} = \frac{1}{(\cos\theta_0+\eta)^2} \times [(2\pi\,(\sigma_1+\sigma_4)-\cos\theta_0+\eta+2\pi\,(-\sigma_1+\sigma_4)\cos 2\phi_0)^2\cos^2\theta^{ext}_{tilt} + 16\pi^2\,(\sigma_1-\sigma_4)^2\cos^2\theta_0\cos^2\phi_0\sin^2\phi_0\sin^2\theta^{ext}_{tilt} + 2\pi\,(\sigma_1-\sigma_4)\cos\theta_0\,(2\pi(\sigma_1+\sigma_4) - \cos\theta_0+\eta+2\pi\,(-\sigma_1+\sigma_4)\cos 2\phi_0)\sin 2\phi_0\sin 2\theta^{ext}_{tilt}\cos\delta^{ext})]$$

$$d^{sg}_{2,diag} = \frac{1}{(\epsilon\cos\theta_0+\eta)^2} \times [4\pi^2\eta^2\,(\sigma_1-\sigma_4)^2\eta^2\sin^2 2\phi_0\cos^2\theta^{ext}_{tilt} + ((-1+2\pi\,(\sigma_1 - \sigma_4)\cos\theta_0\cos 2\phi_0)\,\eta+\cos\theta_0\,(\epsilon+2\pi\,(\sigma_1+\sigma_4)\,\eta))^2\sin^2\theta^{ext}_{tilt} + 2\pi\,(\sigma_1-\sigma_4) (-\epsilon+\sin^2\theta_0+\cos\theta_0(\pi\,(-1+2\epsilon+\cos 2\theta_0)\,(\sigma_1+\sigma_4+(\sigma_1-\sigma_4)\cos 2\phi_0) + \epsilon\,\eta))\sin 2\phi_0\sin 2\theta^{ext}_{tilt}\cos\delta^{ext}]$$

where $\sigma_{xx} = \sigma_1$ and $\sigma_{yy} = \sigma_2$. It is clear from the equations (3.19, 3.20) that the off-diagonal anisotropy is different from diagonal anisotropy by its azimuthal angle independence. Note that both the real and imaginary parts of the polarization of reflected wave is a function of incident, angle, tilt angle of the incident polarization ellipse and the incident polarization.

Fig. 3.8 shows the variation of the real and imaginary parts of reflected polarization with respect to the incident angle. This figure has two parts Fig. 3.8a showing the behavior of real part of reflected polarization and Fig. 3.8b shows that of imaginary part. Each of the figures consists of several curves, of which the dark curves are for substrate-graphene whereas the lighter curves are for free standing graphene. Brown curves shows the behavior with diagonal anisotropy and the magenta curves shows that with off-diagonal anisotropy. We can compare the two systems and see the difference in behavior. Both the diagonal and off-diagonal anisotropic situation shows a constant behavior for the real part of reflected polarization followed by a sharp increase or decrease at a particular incident angle which is determined by the tilt angle of the incident polarization ellipse. In the free standing situation the variation of the real part in both the anisotropic cases is slow and it shows an extreme value only at gracing incidence. Similarly, the imaginary part given in Fig. 3.8b shows a step like behavior and

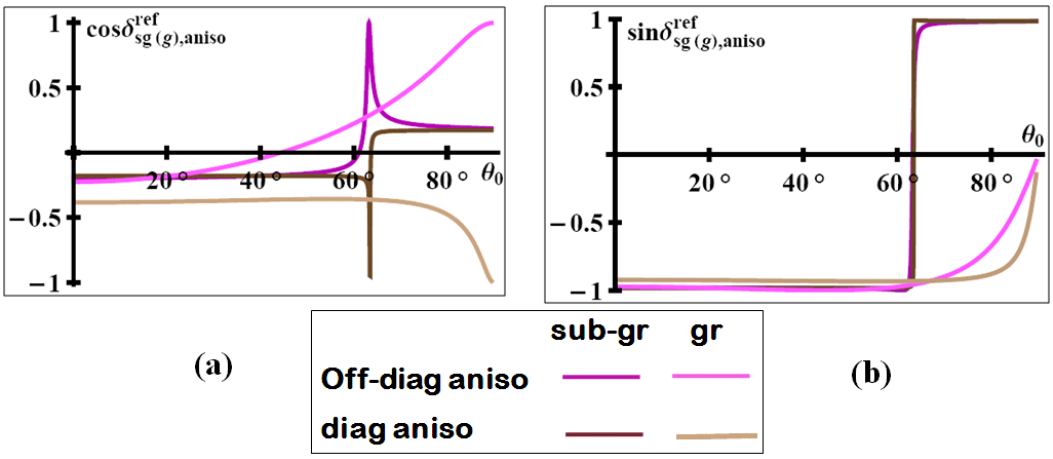

FIGURE 3.8: Reflected polarization versus incident angle when the graphene has different types of anisotropy with incident photon in the microwave region of the electromagnetic spectrum with frequency 200 *GHz*. The left part of the figure shows the behavior of real part and the right part shows that of imaginary part. In each of the figure the behavior of substrate-graphene (dark) and free-standing (light) are shown. Magenta curves are for off-diagonal anisotropy and brown curves are for diagonal anisotropy.

shows a sharp shift from its value of −1 to +1 at a particular angle of incidence in substrate-graphene for both the anisotropic situations which is entirely different from its corresponding free standing situation which are shown in the same figure.

The behavior of reflected polarization can be studied using equations (3.19, 3.20) with respect to other parameters also in general case and also in special limits like linearly polarized incidence.

In short, in this subsection, the situation with the conductivity tensor of graphene being anisotropic is discussed. Mainly, three coefficients are studied, reflection, transmission and the reflected polarization. Two different kinds of anisotropy is considered for study, the off-diagonal and diagonal. Variation of the coefficients with respect to each of the parameters is studied and some of them is discussed in detail with the help of various plots. In each stage the results are compared with that of the free standing case for a clear understanding of the two situations. For getting a clear picture about the influence of substrate material on graphene, the differential coefficients are also considered for study in the case of reflection and transmission.

3.5.3 Brewster's Law

This section discusses a well known phenomena in optics known as Brewster's law, related to substrate-graphene. For an easy comparison with the standard study in a dielectric material, the amplitude reflection coefficient is preferred instead of intensity reflection coefficient. This study is done in both the limits: with the conductivity tensor being isotropic and anisotropic. Fig. 3.9a shows the variation of amplitude reflection coefficient of substrate graphene versus the incident angle. Even though only two curves are prominently visible in the figure, there are many curves which signifies different situations. The solid curves are for the situation with incident wave as s - polarized and the dashed-dotted curves are for the case with incident wave p - polarized. Green curves are with isotropic conductivity tensor, magenta curves are with conductivity tensor being off-diagonal and brown curves are for conductivity tensor being diagonal. Even though the different situations cannot be distinguished from each other we can see signatures of Brewster's phenomenon.

In general, Brewster's law explains the phenomenon: polarization by reflection. According to this law, for a certain angle of incidence a monochromatic light is entirely polarized upon reflection. The refracted beam is partially polarized, but the reflected beam is completely polarized parallel to the reflecting surface (s - polarization). This means that at this particular angle known as Brewster's angle, the $p-$ polarized intensity vanishes with a non-zero $s-$ polarized intensity. From Fig. 3.9a, we can see that at a value of incident angle close to 63^0, the $p-$ polarized intensity vanishes with a non zero value of the $s-$ polarized intensity. Fig. 3.9a depicts that this is a signature of Brewster's phenomena in graphene deposited on a substrate material. The portion of Fig. 3.9a around the incident angle 63^0 is enlarged and shown as an inset which shows the reflected amplitude with p - polarized incident wave. From the inset the exact position and magnitude of the minimum can be made clear. The inset shows that the isotropic case and the diagonal anisotropic case really goes to zero reflection when the incident wave is $p-$ polarized. The angle at which the reflected amplitude with p - polarized incident wave approaches zero is the Brewster's angle and this angle lies very close to each other in the case of isotropic and diagonal anisotropic case the exact value of which is 63.4^0. Note that the Brewster's minimum with off-diagonal conductivity tensor is much higher than the other two cases and the angle also shifts by a small amount to the left. We can see that if the strength of the diagonal anisotropy increases the Brewster's angle shift towards right. For a comparative study with the free standing situation, the corresponding

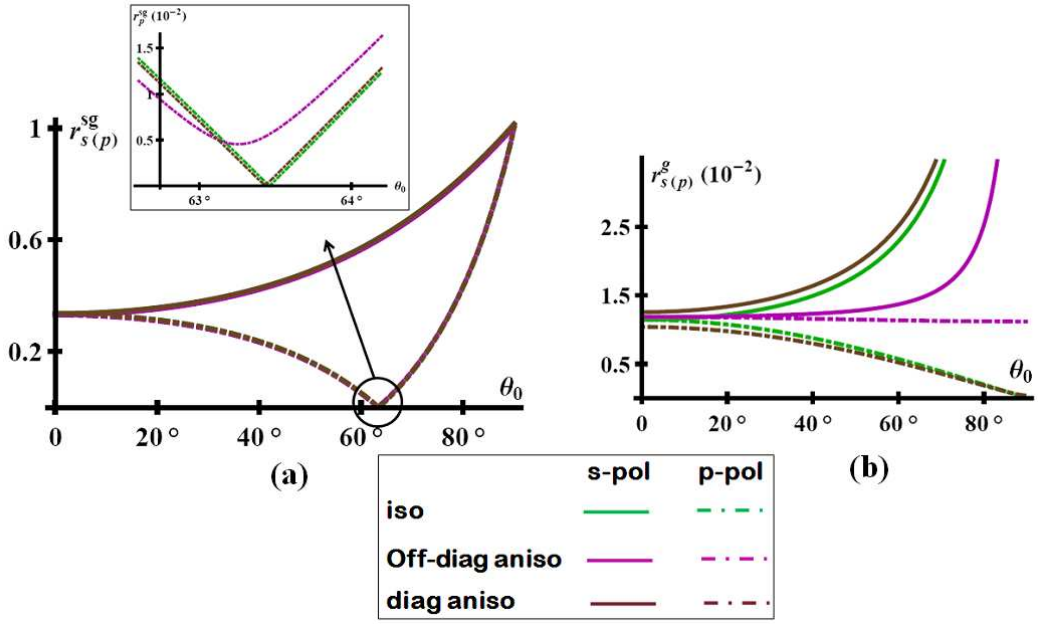

FIGURE 3.9: Brewster's Law: Amplitude reflection coefficient versus incident angle when the incident wave is *s* and *p* - polarized with frequency 200 *GHz*. This figure has two parts (a) substrate-graphene (b) free-standing graphene. The inset of (a) shows the reflected amplitude when the incident wave is *p* - polarized and incident angle is close to Brewster's angle. This shows that the Brewster's minimum for different forms of the conductivity tensor is different. Here the solid curve is for the case with *s* - polarized incident wave and dot-dashed curves are for the case with *p* - polarized incident wave. Blue curve is for the isotropic situation, magenta curve is for off-diagonal anisotropic conductivity tensor and brown curves are for diagonal anisotropic conductivity tensor.

behavior is shown as Fig. 3.9b which shows the same amplitude reflection coefficient versus incident angle. We can see that no such phenomena can be observed in this case, since the *p* - polarized situation goes to minimum only at gracing angle. In the free standing situation, the different types of anisotropy can be distinguished which may be due to the small magnitude of reflection coefficient compared to the substrate graphene.

To know how graphene is affected by the presence of substrate material in detail, the substrate contribution is subtracted out from the amplitude reflection coefficient ($r^{sg}_{s(p)} - r^{s}_{s(p)}$) and is plotted versus incident angle in Fig. 3.10. It is seen from the plot that there is very sharp change in magnitude of the difference reflection coefficient with an incident $p-$ polarized wave at an angle close to 63^0. The figure clearly demonstrates a change in sign and it gives an impression that that there is a finite discontinuity of about 0.1 in magnitude. But if the portion close to 63^0 is enlarged it is seen that, in reality it is a continuous behavior. The

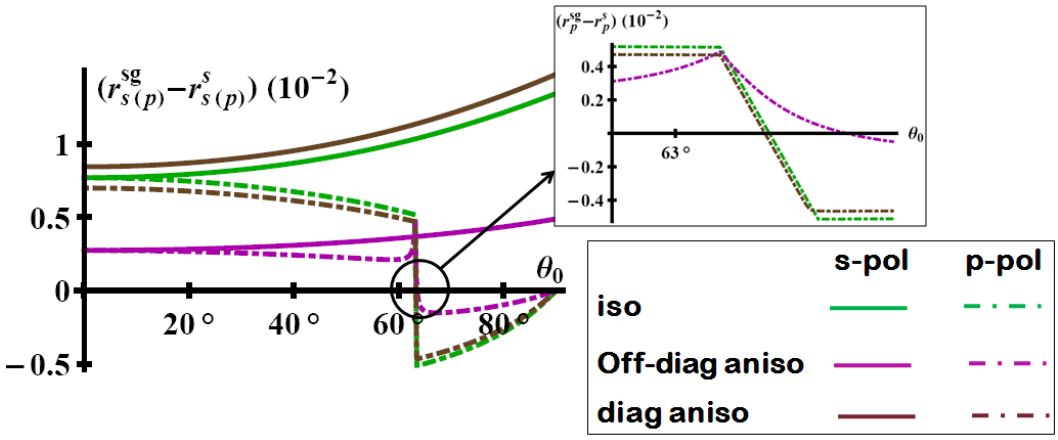

FIGURE 3.10: Brewster's Law: Difference in reflected amplitude between the substrate-graphene and a purely dielectric substrate material versus incident angle when the incident wave is *s* and *p* - polarized and with a frequency 200 *GHz*. Inset shows the reflected amplitude difference when the incident wave is *p* - polarized and the incident angle close to Brewster's angle. This highlights the discontinuous like part of the original figure and shows that it is not a discontinuity at all and the continuous behavior depends largely on the form of conductivity tensor. Here the solid curve is for the case with *s* - polarized incident wave and dot-dashed curves are for the case with *p* - polarized incident wave. Blue curve is for the isotropic situation, magenta curve is for off-diagonal anisotropic conductivity tensor and brown curves are for diagonal anisotropic conductivity tensor.

enlarged portion is shown as an inset to Fig. 3.10. We can see that, below a particular angle close to 63^0, the reflection coefficient due to substrate-graphene leads in magnitude that of the situation with a pure dielectric substrate; but above this angle it is just the reverse. The inset showing the apparent discontinuity (it has a really steep but finite slope) in amplitude reflection coefficient without substrate contribution with a $p-$ polarized incident wave shows how the different cases of anisotropy varies from each other. The difference between the diagonal and off diagonal anisotropy is clearly understandable where the discontinuity reduces to a kink. The magnitude of the discontinuity is large when the conductivity tensor is isotropic and it reduces an appreciable amount with off-diagonal anisotropy. Hence in all the cases, the isotropic as well as the anisotropic cases, close to the Brewster's angle, the variation in difference reflection coefficient with respect to incident angle is so sharp that it appears like a discontinuity when observed in a large scale.

The observation of Brewster's phenomenon itself is a difference between the free standing situation and the substrate graphene.

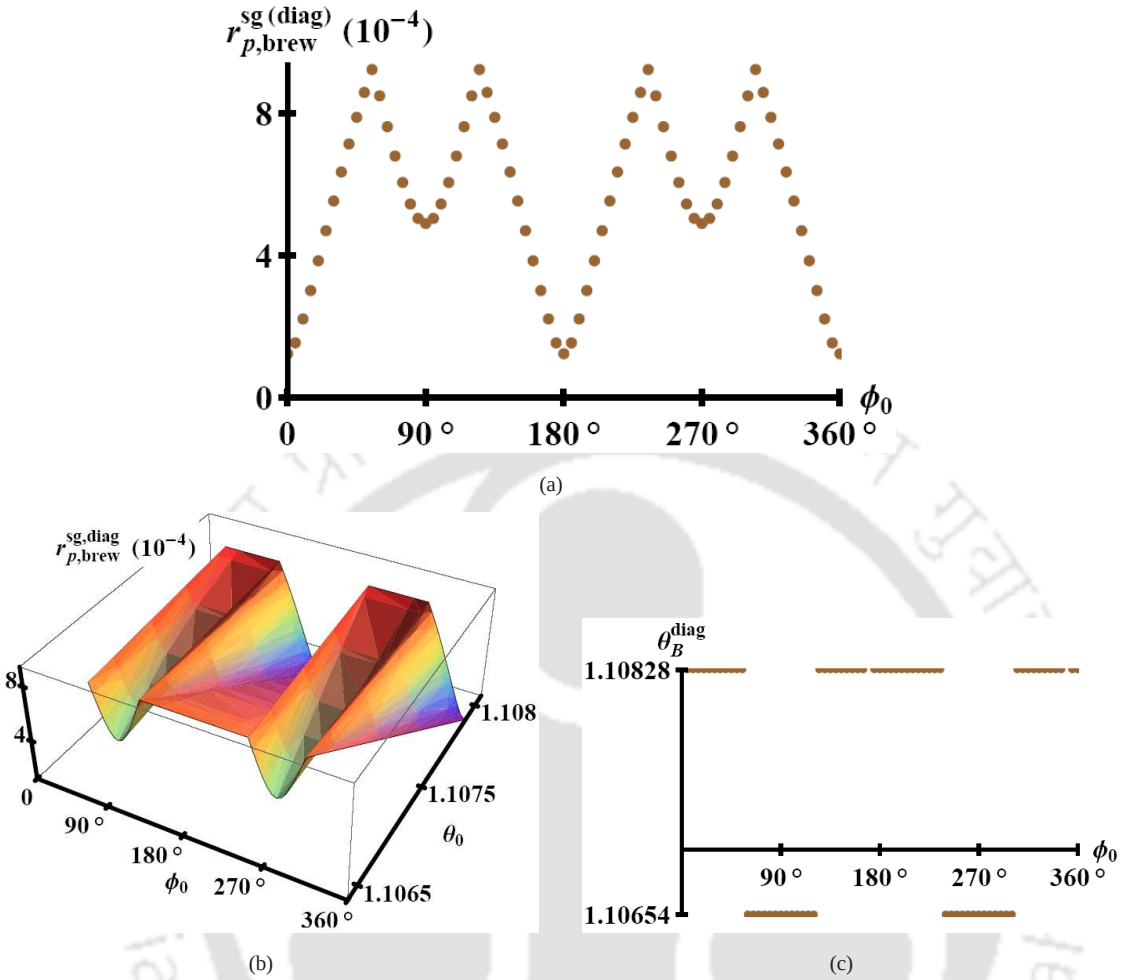

FIGURE 3.11: Fig. (a) shows the amplitude reflection coefficient of substrate-graphene at Brewster's angle versus azimuthal angle of the p - polarized incident wave when the graphene conductivity has a diagonal anisotropy. Fig. (b) shows its 3D variation with respect to incident angle and azimuthal angle. Fig. (c) shows the azimuthal angle dependence of Brewster's angle. In all the cases the incident photon frequency is 200 GHz

It is clear from equations (3.15,3.16) that the off-diagonal anisotropic situation is independent of azimuthal angle as in the isotropic limit whereas there is an azimuthal angle dependence in the diagonal anisotropic case. Therefore there is a dependence of reflection coefficient on the azimuthal angle even if the incident wave is linearly polarized. This is important in the sense that it is possible to observe Brewster's phenomena for more than one angle of incidence or in other words there are two angle parameters (θ_0 and ϕ_0) associated with the Brewster's phenomena observed in substrate graphene unlike in the case of an ordinary material. Fig. 3.11a shows the amplitude reflection coefficient of substrate-graphene

at Brewster's angle against the azimuthal angle when the incident wave is p - polarized, that is the figure shows the variation of Brewster's minimum with respect to azimuthal angle and can be seen that the actual minimum occurs at $\phi_0 = 0, \pi$ or 2π. There are two local minima occurring at $\frac{\pi}{2}$ and $\frac{3\pi}{2}$. To make the situation more clear a 3D variation with respect to incident angle and azimuthal angle is shown in the second part of the figure, Fig. 3.11b. This will help to find out the actual incident angle at which the Brewster's phenomena is observed at a high degree of accuracy. This study reveals that the reflected amplitude with $p-$ polarized incident intensity is not going to zero at Brewster's angle if the graphene conductivity tensor is anisotropic but goes to a minimum whose value oscillates with the azimuthal angle with a period of π. Therefore in contrast to the situation with a dielectric material the Brewster's angle is determined not only by the incident angle but also by the azimuthal angle. This study is important because it gives a way to get the Brewster's angle in a high degree of accuracy. The variation of Brewster's angle with respect to azimuthal angle is shown in the last part of the figure, Fig. 3.11c. We can see that the Brewster's angle varies between 63.3^0 and 63.4^0 at regular intervals of the azimuthal angle. Even though the variation in Brewster's angle is very small of the order of 0.1^0, it is important to understand the dependence on the azimuthal angle. It is expected that the Brewster's angle varies considerable when the anisotropy involved in the system is very strong.

One may get a feeling at this stage that the Brewster's phenomenon explained here may only be due to substrate because of its extreme resemblance with the Brewster's law of a general dielectric material But as can be noted from the plots just described (Fig. 3.10), the anisotropic behavior of the graphene conductivity tensor makes the Brewster's phenomena in graphene on a substrate, different from that in a purely dielectric material, which is mainly the azimuthal angle dependence of the Brewster's minimum and the Brewster's angle. One can understand that the presence of substrate acts as a platform for the observation of Brewster's law in graphene.

3.6 Conclusions

In this chapter the system considered for study is the substrate- graphene. i.e. a 2D graphene sheet deposited on a dielectric material with dielectric constant ϵ. The substrate material is

considered to be a non-magnetic perfect dielectric material. The chapter previous to this considered the free standing graphene for study using various optical quantities. In this chapter also a similar route is followed for an easy comparison of the present system with the free standing situation. Study done in the free standing system is considered as a reference to the present study and a comparison is made in each stage to check the correctness as well as to understand the influence of the presence of substrate material on the optical properties of pure graphene. This is the main aim of this study. Plane electromagnetic wave is incident on the system at an arbitrary angle and the emergent field from the system is calculated by solving Maxwell's equations for the system using the boundary conditions. Presence of substrate material is evident from the dielectric constant appearing in Maxwell's equations. The emergent field has two parts - reflection and transmission with help of which various physically important quantities have been calculated. It is found that they are functions of various parameters related to the incident wave (which are the angle parameters) and also the parameters specific about the material (conductivity tensor elements) and the substrate material (dielectric constant). With respect to each of these parameters behavior of the system has been studied by fixing the conductivity tensor elements. The correctness of the equations are checked with the help of two different limits, one when the conductivity tends to zero and the dielectric constant tends to unity. The former gives rise to the free standing situation and the latter the perfect dielectric results, which is well studied in most of the optics text books. Initially the conductivity tensor is considered to have its most general form, i.e. with all its elements different from each other just as in the case of freely suspended graphene. Then depending upon the different external fields acting on the system the conductivity tensor takes various forms. The first division can be made, as the isotropic and anisotropic limits which can be of different types. Isotropy can be due to the absence of magnetic field or due to the absence of doping. Anisotropy can be of different types, but only two of them are considered here as in the free standing situation. One is when $\sigma_{xx} = \sigma_{yy} = \sigma_1$ and $\sigma_{xy} = -\sigma_{yx} = \sigma_2$ and the other is when $\sigma_{xx} \neq \sigma_{yy}$ and $\sigma_{xy} = \sigma_{yx} = 0$ which are named as off- diagonal anisotropy and diagonal anisotropy respectively. These different limits are studied separately with respect to various parameters and compared with each other. The numerical value of the conductivity elements for the isotropic situation and off-diagonal anisotropy are taken from Gusynin et. al. [106] by the proper choice of the parameters. Information about the diagonal anisotropic conductivity tensor is obtained from Strikha et. al. [104].

Optical coefficients considered for study in this chapter are the coefficient of reflection,

coefficient of transmission and the polarization of the reflected wave. To understand the effect of substrate on these coefficients, coefficients with the substrate contribution subtracted out are also considered for study, which enables one an easy comparison with the reference system, the suspended graphene. A detailed study has been done, by considering different limiting cases of various parameters. For example the linear polarization limit, normal incidence, diagonal anisotropy, off-diagonal anisotropy, isotropic situation etc. The main comparative study in this chapter is done between the two systems, the substrate-graphene and the free standing situation. Then within that a comparison between the isotropic and anisotropic situations and also between different anisotropic situations are also taken into account. Optical quantities mentioned above are studied with respect to each of the angle parameters, dielectric constant. The whole study is done within the microwave region of the electromagnetic spectrum.

The main output obtained from this study is the difference between the substrate-graphene and the freestanding graphene. How the presence of substrate affects the optical properties of free standing situation. It is found that the presence of substrate increases the reflection coefficient and decreases the transmission coefficient. The effect of gap on some cases are decreased due to the substrate and in some cases it is indistinguishable. The change in magnitude of the coefficients are the first things to be noticed with substrate graphene. Variation of transmission and reflection with respect to different substrate materials also has been studied. The second point to be noted in this case is the linear incident polarization. The well known phenomena in optics called ″ Brewster's law ″ is observed in this system which was not found in the suspended graphene. For a particular set of parameters chosen, it is found here that with a substrate material with dielectric constant 3.9 (silicon dioxide), the Brewster's angle is close to 63^0. In the suspended graphene the reflection with $p-$ polarized incidence goes to a minimum only at gracing incidence which is the reason why this phenomenon is not observed in that system. The main peculiarity of Brewster's phenomenon in graphene is the additional dependence of Brewster's angle on the azimuthal angle. The minimum observed in reflection with $p-$ polarized incidence may not be the actual minimum and the actual minimum of reflected intensity, i.e. perfect polarization by reflection, is obtained by tuning not only the incident angle but also the azimuthal angle which can help for an accurate measurement of the Brewster's angle. This may be technologically important for applications in which a perfectly polarized light is needed. There are other differences discussed in the text of this

chapter which differentiates between the substrate-graphene and the corresponding free standing situation by which one can actually study the change in properties due to the presence of the substrate material. As a whole it is seen that the presence of substrate affects the optical properties of graphene, both in its magnitude and behavior.

Chapter 4

Bi-layer Graphene

In the previous two chapters (2, 3) two different systems were considered, namely mono-layer graphene in its free-standing form and mono-layer graphene deposited on a substrate. There are various other systems related to mono-layer graphene. In this chapter a system of two mono-layer graphene (bi-layer graphene) is considered. This study is done based on the results of suspended mono-layer graphene. A series summation method is used to derive the emergent electric field for this two layer system.

We consider the two monolayers as being independent. However this assumption is known to fail quite strongly when the incident light is in the microwave region and is still questionable in the optical region. Pioneering works [138], [122] have considered interlayer coupling effects by incorporating the band structure of a bilayer system which is very different from that of a monolayer. These works have evaluated the optical conductivity of a bilayer from first principles, by taking into account the modified band structure. Our aim in this work is more modest. We wish to retain our simple minded picture of independent layers and incorporate these effects of modified band structure indirectly by asserting that the independent monolayers have an effective or renormalized conductivity that depends on the number of layers in the system. This renormalized conductivity has to be fitted from either experimental data or by a comparison with detailed theoretical works such as [138], [122]. However this approach clearly compromises the predictive power of our model. Thus for the bilayer system, our independent layer assumption is likely to be of limited applicability, except when we consider the incident wavelength to be in the soft X-ray region. In this case, inter-layer effects $t_\perp$ may be ignored (the parameter $(\frac{t_\perp}{\hbar\nu})^2$ is small). The plots in the soft X-ray region demonstrate a

sensitive dependence of reflection coefficient on the incident angle primarily due to the path length which produces a large phase shift caused by the X-ray travelling between the two layers. The independent layer model is still included since it is a precursor for the treatment of the multilayer system in the subsequent chapters when we treat the issue of renormalization of the monolayer conductivity in a more careful, albeit phenomenological manner.

As in previous chapters, initially the situation under consideration is described in detail followed by the explanation of the method of calculation of the emergent field. Various optical quantities are studied in this chapter such as coefficient of reflection. Finally the results are discussed in detail with the help of a few plots.

4.1 Problem Description

A free standing bi-layer graphene sheet is considered for study in this chapter. By bi-layer graphene we mean a collection of two free standing (renormalized) mono-layer graphene layers lying one on top of the other and separated by a distance of d which is of the order of 3.35 Å. As we have remarked earlier, in our approach, the monolayer graphene sheets have a renormalized conductivity due to the very different nature of the band structure of the bilayer. Instead of working from first principles, we use a phenomenological interpolation scheme to estimate this renormalized value by comparing with refined theoretical approaches and experiments that do take into account effects of band structure. This procedure is described in detail in the next chapter. Here we merely quote the value of the renormalized effective monolayer reflection matrix (G-matrix) for a bilayer as has been deduced in the next chapter. The value for the renormalized G-matrix we have deduced in chapter (5) in the context of a bilayer is $G_{eff} = -0.01162$.

The bi-layer system is important because it is the simplest two dimensional structure after graphene and also because of potential technological applications due to the fact that it can develop a tunable band gap by the application of an electric field [139, 140, 141]. Bi-layer graphene considered for study consists of two equivalent mono-layer graphene sheets placed one on top of other which are assumed to have the same properties, especially optical conductivity. However as mentioned earlier, due to strong coupling between layers, especially at longer-wavelengths, such as infra-red and microwave, we have to assume an effective or

renormalized conductivity. The system is kept in the xy plane, one layer at $z = 0$ and the other at $z = d$. As mentioned in the previous chapters, an electromagnetic wave with a wave vector $\mathbf{q}_0$ is incident on the system at an arbitrary angle θ_0. The incident wave vector has all the three Cartesian components. From the general form of electric field in terms of its components along the polarization directions (discussed in chapter 3) the incident electric field can be written as, $\mathbf{E}_{ext}(\mathbf{r},t) = e^{i\ \mathbf{q}_{0,\parallel}\cdot\mathbf{r}_{\parallel}\ +\ iq_{0,z}z\ -ic|q_0|t}\sum_{\nu=1,2}\hat{\mathbf{u}}_{\nu}^{ext}E_{\nu}^{ext}$. Here $\hat{\mathbf{u}}_{\nu}^{ext}$ are the unit vectors in the two directions of polarization as defined in chapter 2. And E_{ν}^{ext} are the components of the incident electric field along the above mentioned unit vectors the general representation of which is also given in earlier chapters. To calculate the emergent electric field from the bi-layer graphene surface we have made use of the mono-layer results and is discussed in the next section.

4.2 Emergent Electric Field: Method of Series Summation

Consider the emergent electric field for suspended mono-layer graphene given in chapter 2 (see equations (2.11, 2.12)) which can be expressed in a compact form as given below: The reflected field in mono-layer graphene:

$$\mathbf{E}_{ref}^{mono}(\mathbf{r},t) = e^{i\mathbf{q}_{0,\parallel}\cdot\mathbf{r}_{\parallel}\ -\ iq_{0,z}z\ -\ ic|q_0|t}\ G_{1,r}\cdot\mathbf{E}_{inc}(0) \tag{4.1}$$

where $\mathbf{E}_{inc}(0) = \sum_{\nu=1,2}\hat{\mathbf{u}}_{\nu}^{ext}E_{\nu}^{ext}$ and $G_{1,r}$ is a 3×3 matrix and is given below:

$$G_{1,r} = \begin{pmatrix} \frac{2\pi\left(-|q_0|^2\sigma_{xx}+q_{0,x}\left(q_{0,x}\sigma_{xx}+q_{0,y}\sigma_{yx}\right)\right)}{c|q_0|q_{0,z}} & \frac{2\pi\left(-|q_0|^2\sigma_{xy}+q_{0,x}\left(q_{0,x}\sigma_{xy}+q_{0,y}\sigma_{yy}\right)\right)}{c|q_0|q_{0,z}} & 0 \\ \frac{2\pi\left(q_{0,x}q_{0,y}\sigma_{xx}+\left(-|q_0|^2+q_{0,y}^2\right)\sigma_{yx}\right)}{c|q_0|q_{0,z}} & \frac{2\pi\left(q_{0,x}q_{0,y}\sigma_{xy}+\left(-|q_0|^2+q_{0,y}^2\right)\sigma_{yy}\right)}{c|q_0|q_{0,z}} & 0 \\ -\frac{2\pi\left(q_{0,x}\sigma_{xx}+q_{0,y}\sigma_{yx}\right)}{c|q_0|} & -\frac{2\pi\left(q_{0,x}\sigma_{xy}+q_{0,y}\sigma_{yy}\right)}{c|q_0|} & 0 \end{pmatrix} \tag{4.2}$$

The transmitted field in mono-layer graphene:

$$\mathbf{E}_{tran}^{mono}(\mathbf{r},t) = e^{i\mathbf{q}_{0,\parallel}\cdot\mathbf{r}_{\parallel}\ +\ iq_{0,z}z\ -\ ic|q_0|t}\ G_{1,t}\cdot\mathbf{E}_{inc}(0) \tag{4.3}$$

where $G_{1,t}$ is a 3×3 matrix and is given below:

$$G_{1,t} = \begin{pmatrix} \frac{c|q_0|q_{0,z}+2\pi\left(-|q_0|^2\sigma_{xx}+q_{0,x}\left(q_{0,x}\sigma_{xx}+q_{0,y}\sigma_{yx}\right)\right)}{c|q_0|q_{0,z}} & \frac{2\pi\left(-|q_0|^2\sigma_{xy}+q_{0,x}\left(q_{0,x}\sigma_{xy}+q_{0,y}\sigma_{yy}\right)\right)}{c|q_0|q_{0,z}} & 0 \\ \frac{2\pi\left(q_{0,x}q_{0,y}\sigma_{xx}+\left(-|q_0|^2+q_{0,y}^2\right)\sigma_{yx}\right)}{c|q_0|q_{0,z}} & \frac{c|q_0|q_{0,z}+2\pi\left(q_{0,x}q_{0,y}\sigma_{xy}+\left(-|q_0|^2+q_{0,y}^2\right)\sigma_{yy}\right)}{c|q_0|q_{0,z}} & 0 \\ \frac{2\pi\left(q_{0,x}\sigma_{xx}+q_{0,y}\sigma_{yx}\right)}{c|q_0|} & \frac{2\pi\left(q_{0,x}\sigma_{xy}+q_{0,y}\sigma_{yy}\right)}{c|q_0|} & 1 \end{pmatrix} \tag{4.4}$$

It is seen that the two matrices for reflection and transmission do not commute in the most general situation. In the limiting case of normal incidence where $q_{0,x} = q_{0,y} = 0$ and $q_{0,z} = |q_0|$, the matrices commute.

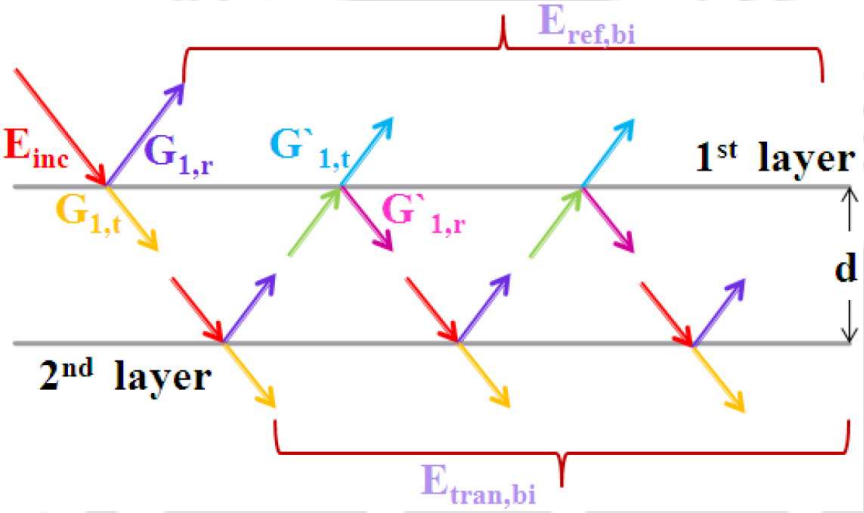

FIGURE 4.1: Schematic of bi - layer graphene which shows multiple reflection when an electromagnetic wave is incident on it (red arrow). $G_{1,r}$ and $G_{1,t}$ are the reflection and transmission matrices of mono - layer system and $G'_{1,r}$ and $G'_{1,t}$ are the reflection and transmission matrices of mono - layer system with z component of the wave vector in the opposite direction, d is the distance between the layers.

As mentioned in the earlier paragraph, with bi-layer graphene there are two separate monolayers which makes the wave transmitted from first layer incident on the second layer by travelling a distance d and there is room for multiple reflection which makes the effective reflection and transmission from the system, a series of terms. Therefore we must take care of this effect also when the system consists of more than one layer. This is explained in Fig. 4.1. Here we can see that each time the wave encounters a layer except for the first time, it has to travel a distance d which adds a path difference appreciable only in the X-ray region between the waves ultimately emerging from the system as effective reflection and transmission. Hence in the emergent field of bi-layer system, both reflection and transmission matrices

of mono-layer graphene denoted by $G_{1,r}$ and $G_{1,t}$ are made use of. Reflected and transmitted field from the bi-layer graphene can also be written in a matrix form as

$$\mathbf{E}_{ref,bi}(\mathbf{r},t) = e^{i\mathbf{q}_{0,\|}\cdot\mathbf{r}_{\|} - iq_{0,z}z - ic|q_0|t}\, G_{2,r}\cdot\mathbf{E}_{inc}(0) \tag{4.5}$$

$$\mathbf{E}_{tran,bi}(\mathbf{r},t) = e^{i\mathbf{q}_{0,\|}\cdot\mathbf{r}_{\|} + iq_{0,z}z - ic|q_0|t}\, G_{2,t}\cdot\mathbf{E}_{inc}(0) \tag{4.6}$$

where $G_{2,r}$ and $G_{2,t}$ are the reflection and transmission matrices of bi-layer system. It is written in terms of corresponding matrices of mono-layer graphene as given below:

$$G_{2,r} = G_{1,r} + G^{'}_{1,t}\cdot G_{1,r}\cdot\frac{1}{\mathbf{I}_3 - G^{'}_{1,r}\cdot G_{1,r}\, e^{2i\, q_{0,z}d}}\cdot G_{1,t}\, e^{2i\, q_{0,z}d} \tag{4.7}$$

$$G_{2,t} = G_{1,t}\cdot\frac{1}{\mathbf{I}_3 - G^{'}_{1,r}\cdot G_{1,r}\, e^{2i\, q_{0,z}d}}\cdot G_{1,t}\, e^{i\, q_{0,z}d} \tag{4.8}$$

Here $\mathbf{I}_3$ is the 3×3 identity matrix and the matrices with primes are the corresponding matrices for reflection and transmission for mono-layer system with negative z component of the incident wave vector, that is $G^{'}_{1,r}$ is the matrix for reflection if it is travelling towards $z > 0$ region and $G^{'}_{1,t}$ is the matrix for transmission if it is travelling towards $z < 0$ region. This kind of treatment is needed for the transversality condition to be satisfied. (By transversality we mean that $\mathbf{q}\cdot\mathbf{E} = 0$ where $\mathbf{q}$ is the wave vector for the particular situation and $\mathbf{E}$ is the corresponding electric field). The exponential factors in equations (4.7, 4.8) are due to the path difference between the waves each time when it interact with any of the layers. Out of the four matrices for mono-layer graphene, the matrices which commute are $G_{1,r}$ and $G^{'}_{1,t}$ and $G_{1,t}$ with $G^{'}_{1,r}$ in a general situation of oblique incidence. But when it comes to normal incidence, all the matrices commute with each other. Turning to the matrices for bi-layer graphene given by equations (4.7, 4.8), they don't commute with each other except when the wave is incident normal to the surface. The details of above equations are included as Appendix C. This method of finding out the emergent fields of a layered system is well known and explained in various text books on Optics [142]. Unfortunately, in this situation there is no limiting case in which the bi-layer system reduces to that of a mono-layer, that is there is no limit in which $G_{2,r}$ tends to $G_{1,r}$ and $G_{2,t}$ tends to $G_{1,t}$. But the correctness of the result is ensured by comparison with the results of standard text books.

Here each mono-layer is assumed to possess a conductivity defined by the $2D$ conductivity tensor denoted by $\overline{\overline{\sigma}}$ with all its elements different from each other. The components of the reflection and transmission matrix in terms of the conductivity tensor elements are given in Appendix C. Equations (4.5, 4.6) along with equations (4.7, 4.8) can be used to obtain the optical coefficients.

As in the case of incident electric field given by equation (2.1), the general representation of reflected and transmitted field for bi-layer can be written as,

$$\mathbf{E}^{bi}_{ref}(\mathbf{r},t) = e^{i\mathbf{q}_{ref,\parallel}\cdot\mathbf{r}_{\parallel} + iq_{ref,z}z - ic|q_{ref}|t}\sum_{\nu=1,2}\hat{\mathbf{u}}^{ref}_{\nu}E^{ref}_{\nu} \tag{4.9}$$

$$\mathbf{E}^{bi}_{tran}(\mathbf{r},t) = e^{i\mathbf{q}_{tran,\parallel}\cdot\mathbf{r}_{\parallel} + iq_{tran,z}z - ic|q_{tran}|t}\sum_{\nu=1,2}\hat{\mathbf{u}}^{tran}_{\nu}E^{tran}_{\nu} \tag{4.10}$$

where $\mathbf{q}_{ref}$ has components $\left(q_{0,x}, q_{0,y}, -q_{0,z}\right)$ and $\mathbf{q}_{tran}$ has components $\left(q_{0,x}, q_{0,y}, q_{0,z}\right)$ such that $|q_{ref}| = |q_{tran}| = |q_0|$. The unit vectors defining the polarization directions of electric field for reflection and transmission along with the polarization components of the electric field vectors along these directions can be obtained from the general equations for them (2.2, 2.3) given in chapter 2. Combining all these, the polarization components for the reflected and transmitted wave is obtained by taking the dot product of equation (4.5, 4.6) with the corresponding unit vectors.

The $\overline{\overline{\sigma}}$ appearing in the equations for emergent electric field of bi-layer graphene is the mono-layer optical conductivity tensor and it is discussed in detail in previous chapters. $\overline{\overline{\sigma}}$ being a 2^{nd} rank tensor is represented by a 2×2 matrix and has all of its elements different from each other in general. The fully anisotropic case with all the conductivity elements different being complicated, as can be seen from Appendix C, various limiting cases are considered, the most important of which are the isotropic limit ($\sigma_{xx} = \sigma_{yy}$ and $\sigma_{xy} = \sigma_{yx} = 0$), which is realized in different physical conditions as explained in earlier chapters. The study of optical coefficients derived above in the isotropic limit of the conductivity tensor is discussed in this chapter. The numerical value for the conductivity tensor elements in this limit pointed out above is taken from the references [26, 92] which suggests constant value of universal dynamical conductivity for the same.

4.3 Optical Coefficients

Three optical quantities namely reflection coefficient, transmission coefficient and polarization of the reflected wave are considered for study in this chapter. All these quantities are explained in detail in the previous chapters. Coefficient of reflection is the ratio of the reflected wave to incident wave at the point of reflection, i.e. $R = \frac{|\mathbf{E}_{ref}|^2}{|\mathbf{E}_{ext}|^2}$. Transmission coefficient is the ratio of the transmitted wave to incident wave at the point of transmission, i.e. $T = \frac{|\mathbf{E}_{tran}|^2}{|\mathbf{E}_{ext}|^2}$. Polarization of the reflected wave in terms of incident polarization is obtained from the formula $e^{-i\,\delta^{ref}} = \frac{(E_1^{ref})^*\,(E_2^{ref})}{|E_1^{ref}|\,|E_2^{ref}|}$. After substituting for the above quantities, the equations for the coefficients become complicated because of multiple reflection effects, but it has the following form.

$$\begin{aligned} R^{bi} &= [(r_1 + r_2\cos 2s\cos\theta_0 + r_3\cos 4s\cos\theta_0)\cos^2\theta_{tilt}^{ext} + (r_4 + r_5\cos 2s\cos\theta_0 \\ &\quad + r_6\cos 4s\cos\theta_0)\sin^2\theta_{tilt}^{ext} + (r_7\cos\delta^{ext} + r_8\cos(2s\cos\theta_0 + \delta^{ext}) + r_9\cos(2s\cos\theta_0 - \delta^{ext}) \\ &\quad + r_{10}\cos(4s\cos\theta_0 + \delta^{ext}) + r_{11}\cos(4s\cos\theta_0 - \delta^{ext}))\sin 2\theta_{tilt}^{ext}]/(d_1 + d_2\cos 2s\cos\theta_0 \\ &\quad + d_3\cos 4s\cos\theta_0) \end{aligned} \tag{4.11}$$

$$\begin{aligned} T^{bi} &= [(t_1 + t_2\cos 2s\cos\theta_0 + t_3\cos 4s\cos\theta_0)\cos^2\theta_{tilt}^{ext} + (t_4 + t_5\cos 2s\cos\theta_0 \\ &\quad + t_6\cos 4s\cos\theta_0)\sin^2\theta_{tilt}^{ext} + (t_7\cos\delta^{ext} + t_8\cos(2s\cos\theta_0 + \delta^{ext}) + t_9\cos(2s\cos\theta_0 - \delta^{ext}) \\ &\quad + t_{10}\cos(4s\cos\theta_0 + \delta^{ext}) + t_{11}\cos(4s\cos\theta_0 - \delta^{ext}))\sin 2\theta_{tilt}^{ext}]/(d_1 + d_2\cos 2s\cos\theta_0 \\ &\quad + d_3\cos 4s\cos\theta_0) \end{aligned} \tag{4.12}$$

$$\begin{aligned} e^{i\,\delta^{ref}}|_{bi} &= ([(p_1 + (p_2 + p_3)\cos 2s\cos\theta_0 + (p_4 + p_5)\cos 4s\cos\theta_0)\cos^2\theta_0 \\ &\quad + (p_6 + (p_7 + p_8)\cos 2s\cos\theta_0 + (p_9 + p_{10})\cos 4s\cos\theta_0)\sin^2\theta_0 \\ &\quad + ((p_{11} + p_{16})\cos\delta^{ext} + (p_{12} + p_{18})\cos(2s\cos\theta_0 - \delta^{ext}) \\ &\quad + (p_{13} + p_{17})\cos(2s\cos\theta_0 + \delta^{ext}) + (p_{14} + p_{20})\cos(4s\cos\theta_0 - \delta^{ext}) \\ &\quad + (p_{15} + p_{19})\cos(4s\cos\theta_0 + \delta^{ext}))\sin\theta_{tilt}^{ext}\cos\theta_{tilt}^{ext}] \\ &\quad + i\,[((p_{12} - p_{18})\sin(2s\cos\theta_0 - \delta^{ext}) + (p_{13} - p_{17})\sin(2s\cos\theta_0 + \delta^{ext}) \\ &\quad + (p_{14} - p_{20})\sin(4s\cos\theta_0 - \delta^{ext}) + (p_{15} - p_{19})\sin(4s\cos\theta_0 \\ &\quad + \delta^{ext}))\sin\theta_{tilt}^{ext}\cos\theta_{tilt}^{ext}])/\sqrt{d_{1p}\;\;d_{2p}} \end{aligned} \tag{4.13}$$

where

$$
\begin{aligned}
d_{1p} &= (n_1 + n_2 \cos 2s \cos\theta_0 + n_3 \cos 4s \cos\theta_0) \cos^2\theta_{tilt}^{ext} + (n_4 + n_5 \cos 2s \cos\theta_0 \\
&\quad + n_6 \cos 4s \cos\theta_0) \sin^2\theta_{tilt}^{ext} + (n_7 \cos\delta^{ext} + n_8 \cos(2s\cos\theta_0 + \delta^{ext}) \\
&\quad + n_9 \cos(2s\cos\theta_0 - \delta^{ext}) + n_{10} \cos(4s\cos\theta_0 + \delta^{ext}) \\
&\quad + n_{11} \cos(4s\cos\theta_0 - \delta^{ext})) \sin 2\theta_{tilt}^{ext} \\
d_{2p} &= (m_1 + m_2 \cos 2s \cos\theta_0 + m_3 \cos 4s \cos\theta_0) \cos^2\theta_{tilt}^{ext} + (m_4 + m_5 \cos 2s \cos\theta_0 \\
&\quad + m_6 \cos 4s \cos\theta_0) \sin^2\theta_{tilt}^{ext} + (m_7 \cos\delta^{ext} + m_8 \cos(2s\cos\theta_0 + \delta^{ext}) \\
&\quad + m_9 \cos(2s\cos\theta_0 - \delta^{ext}) + m_{10} \cos(4s\cos\theta_0 + \delta^{ext}) \\
&\quad + m_{11} \cos(4s\cos\theta_0 - \delta^{ext})) \sin 2\theta_{tilt}^{ext}
\end{aligned}
$$

Here r, t, d, p, n, m are complicated functions of elements of the conductivity tensor (σ_{xx}, σ_{xy}, σ_{yx}, σ_{yy}) and the angle parameters, θ_0, ϕ_0. θ_{tilt}^{ext} is the tilt angle of the incident polarization ellipse, δ^{ext} is the incident polarization and s is the product of the magnitude of incident wave vector ($|q_0|$) and the distance between the layers, i.e. $|q_0|\, d$ (small for optical fields). Note that the form of the coefficients is entirely different from the mono-layer system. The s dependence is unique to the bi-layer system as compared to the mono-layer system and this is because of the multiple reflection effects. By simultaneously solving the real and imaginary parts of the reflected polarization equation, we can study the behavior of reflected polarization in terms of its parameters. Optical coefficients explained in the above mentioned equations are studied in one of the important limits of the conductivity tensor explained in an earlier section, viz. isotropic limit which is considered for study in the next section and compared with the mono-layer situation.

4.4 Results and Discussion

A comparative study of the two systems, the bi-layer graphene and the free standing mono-layer graphene, has been done in this section. Isotropic limit of the conductivity tensor is studied here.

4.4.1 Isotropic Case

As mentioned in the earlier chapters, this is one of the important and interesting limiting cases. This happens when the off-diagonal elements of the conductivity tensor vanishes and when the diagonal elements become equal. i.e. $\sigma_{xx} = \sigma_{yy} = \sigma_1$ and $\sigma_{xy} = \sigma_{yx} = 0$. In this limit the coefficients are functions only of the diagonal conductivity, incident angle and the tilt angle of the incident polarization. The bilayer is investigated in the same manner as the monolayer where the three quantities, reflection, transmission and polarization coefficients, are taken for study. But they do not show much difference from that of the mono-layer system in this limit.

We can see that the bi-layer system and hence its equations are complicated especially due to multiple reflection. While the path length traversed in one reflection is small compared to the wavelength in the optical region or microwave region, there are changes in the amplitude of the reflected wave which contribute cumulatively in multiple reflections. In addition, in the soft X-ray region, there are phase changes caused by the fact that path length even in one reflection is comparable to the wavelength. This manifests itself in a characteristic periodic behavior of the reflection coefficient on the incident angle (see Fig. 4.2a), something absent for longer wavelengths. In earlier chapters, the microwave region of the electromagnetic spectrum was studied where the conductivity tensor is known by the study of Gusynin et. al. [106]. It is known that [26, 92] the high frequency dynamic conductivity in graphene should be a universal constant equal to $\frac{e^2}{4\hbar}$. Therefore the isotropic limit with the diagonal conductivity element given by the universal constant is useful for the study of high energy limit of the coefficients, such as soft X-ray region.

The reflection coefficient versus incident angle for both the systems, that is free standing mono-layer and the bi-layer system in the soft X-ray region is shown in Fig. 4.2a. In this figure the solid curve shows the behavior of reflected intensity of the mono-layer graphene and the dashed curve shows that of bi-layer system. One can see that the amplitude of oscillation increases with the incident angle. For this study, we have used the universal dynamic conductivity for the calculation.

Fig. 4.2b shows the transmission coefficient of mono-layer and bi-layer system in the high energy range (visible). Here the solid curve is for the mono-layer system, dashed curve is for the bi-layer system and the dotdashed curve is for the bilayer system taking into consideration the effects due to triagonal warping, finite energy effects etc. Here we can see that there

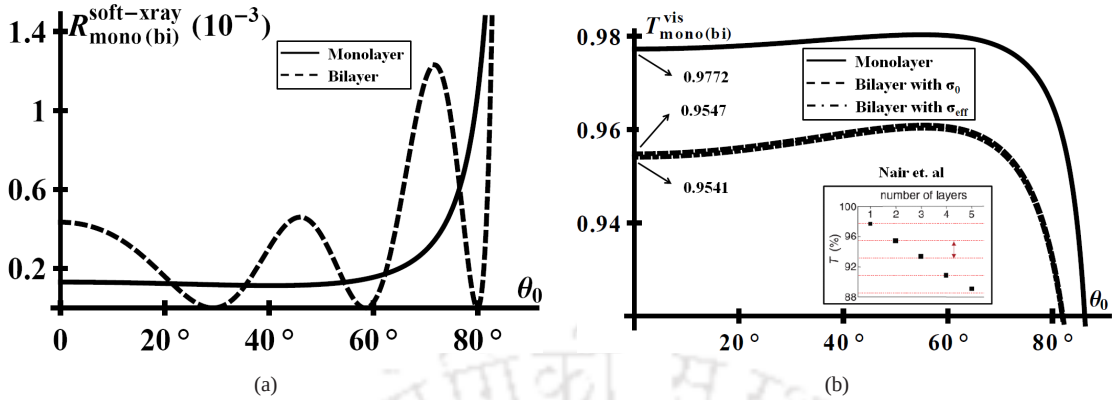

FIGURE 4.2: Reflection and Transmission coefficient of mono - layer (solid) and bi - layer (dashed) graphene as a function incident angle. Reflection coefficient (a) is plotted in the soft X-ray region where the reflection coefficient of bi-layer is influenced considerably by multiple reflection effects which results in the periodic behavior of the reflected intensity. The transmission coefficient (b) is plotted in the visible region where the mono-layer and bi-layer transmitted intensity is compared with the result of an experimental observation by Nair et. al. [92] shown as the inset. Here the solid curve shows the behavior of monolayer system, dashed curve for bilayer system and the dotdashed curve which lie very close to the dashed curve is for bilayer graphene with effective conductivity due to several effects such as trigonal warping, finite energy effects due to nonlinearity etc.

is no significant difference in magnitude as well as behavior between the system used with universal dynamic conductivity and that with effective dynamical conductivity. We can see a decrease in magnitude of the transmitted intensity when it comes to a bi-layer system. Fig. 4.2b inset shows the experimental result given by Nair et. al. [92] by which it is clear that the result given by the current study matches with that of Nair et. al. for both mono-layer and bi-layer situation. The effective conductivity does not change the transmitted intensity much even at normal incidence as can be seen from the figure. The study done in Nair et. al. is for normal incidence and in the visible region. With incident wave in the visible region of the electromagnetic spectrum, the current study also shows the same magnitude of reflection for normal incidence [see when $\theta_0 = 0$ region in Fig. 4.2b] i.e. close to 98% for monolayer and close to 95% for bi-layer graphene which proves the correctness of the treatment followed in this study. To check the correctness of the general equations (4.11, 4.12, 4.13) of coefficients derived in the earlier section, conservation of the coefficients is checked by deriving the equation for the loss coefficient by substituting the series summation solution into Maxwell's equations.

4.5 Conclusions

In this chapter, the system under study is bi-layer graphene, which is a combination of two mono-layer layers separated by a distance 3.35 Å. Due to presence of this extra layer there are multiple reflection effects that become relevant. Further, effects due to inter-layer interaction, trigonal warping and so on are taken into account phenomenologically by postulating that each independent layer possesses a renormalized conductivity which depends on the number of layers, which is determined by an interpolation scheme in the next chapter. The electromagnetic response of the system is studied through three quantities such as the coefficient of reflection, coefficient of transmission and the polarization of reflected wave. Electromagnetic wave is incident on the system at an arbitrary angle and the emergent field is studied based on the results of mono-layer system explained in chapter 2. The mono-layer results are used to derive the emergent electric fields for the bi-layer system by the use of series summation method. Using this field, i.e. the electric field of the reflected wave and that of the transmitted wave, the above mentioned physically important quantities have been calculated. The form of the equations for these coefficients are different compared to the mono-layer system. This is the difference in bi-layer system as compared to the mono-layer situation where the energy of the incident wave enters only through the conductivity tensor elements. The bi-layer optical coefficients are functions of other parameters also as in the case of mono-layer graphene. i.e. the angle parameters which represents the incident electromagnetic plane wave and the conductivity tensor elements which represents the material under study. Optical studies done here uses isotropic conductivity tensor.

Graphene, in its mono-layer form is a very rich area of research. But as is known, it is extremely difficult to prepare it in the mono-layer form. Therefore it is always important to confirm after the sample preparation that it is a mono-layer system. There are references available in the literature which describe various experimental methods to distinguish the mono-layer system from the bi-layer and multi-layer system. For example AFM techniques, Raman studies etc. explained in chapter 1. The position and intensity of the peaks in the Raman spectra varies in mono-layer, bi-layer and multi-layer systems [69, 70, 71, 72, 73, 74]. The main aim of this study is to distinguish between the two systems using theoretical techniques. Results of the mono-layer system which is already considered in chapter 2 serves as the reference for the present study. In this chapter, a comparison between the two systems

is done to find out ways to distinguish between the systems. In the isotropic limit, for bi-layer system, the study is extended to the higher energy region (soft X-rays) which shows a noticeable difference between the behavior of mono-layer and bi-layer reflected intensity with respect to incident angle. (oscillation of the bi-layer reflected intensity with respect to the incident angle due to multiple reflection effects). The result obtained for the bi-layer system and the mono-layer system in the visible region of the electromagnetic spectrum at normal incidence shows perfect matching with one of the references in the literature [92], thereby strengthening our surmise that inter-layer effects are suppressed in the visible region at least for the few layer system. Even though the results obtained in this chapter may not look very exciting, the mathematical framework for the bi-layer system is important and necessary to proceed to the next stage of few layer graphene (included in the next chapter).

Chapter 5

Multi-layer Graphene

As we have seen in the last few chapters, we have studied mono-layer graphene, substrate graphene and bi-layer graphene. Besides these, multi-layer graphene is also of interest to the scientific community. In this chapter we study multi-layer graphene. In few-layer graphene, each of the layers are separated by a distance of the order of angstroms, more specifically 3.35 Å [143, 144]. This study is important because it is very difficult to extract a single layer of graphene in experiments [7]. Although it is true that a simple act like writing with a pencil may lead to the production of graphene [11], the experimental needs demand careful preparation of a sample for a fundamental study. A single layer graphene was not supposed to exist due to its two dimensional nature [4], but was proved to exist by Geim and Novoselov in 2005 [3] for which they were awarded the Nobel Prize in 2010. Starting with the attempt by scientists in University of Manchester (UK) and the Institute for Microelectronics Technology (Russia) [3, 9] where the team employed a technique known as mechanical exfoliation of the graphite crystals, there are by now a variety of methods developed for the production of graphene which is discussed in chapter 1. For instance epitaxial growth, silicon carbide reduction, hydrazine reduction, sodium reduction of ethanol, various chemical deposition methods and so on [11]. Even then, it is extremely difficult to produce a pure mono-layer graphene layer. Most methods of production yield a statistical distribution of samples with different number of layers. From these samples one is now faced with the task of identifying samples with the fewest number of layers. Therefore it is always important to distinguish between different samples for example, mono-layer, bi-layer, few-layers and multi-layer graphene. In other words it is necessary to find a method to ascertain the thickness of the sample one has

prepared. There are a few experimental techniques for doing this such as, Raman spectroscopic studies [70], Auger electron spectroscopy [145], reflection and contrast spectroscopy [88] and so on. Even though there are many experimental techniques used to distinguish between the the multi-layer and mono-layer systems, determination of the actual number of layers in the sample is still a hurdle. This is important since many properties of graphene may depend sensitively on the number of layers. A combination of optical microscopy and Raman spectroscopy has been used as a method for determining the number of layers (layer number determined by their optical contrast) and for the study of the electronic transport properties [88]. Here we present an effective method to actually count the number of layers through the transmission coefficient in the optical frequency range. The method involves deriving a formula for the transmission coefficient versus the number of layers using theoretical methods. In the process one finds that there is a significant deviation from the prediction of Beer's law in the case of few-layer graphene.

In this work, the multi-layer system is studied iteratively, by making use of the results for mono-layer free standing system which has been studied earlier using Maxwell's equations as a starting point. We derive the properties of the n - layer system taking into account, multiple reflection effects. We begin with a description of the problem under study followed by the method used to study the few-layer system and discuss the consequences of multiple reflections and the effect it has on the reflection and transmission coefficients. This section also has the recursion relation that relates reflection and transmission amplitudes between systems that have one more or one less number of layers. These relations are solved subsequently by analytical methods. This is followed by a discussion of results obtained through this work, such as plots that highlight deviation from Beer's law in case of the few-layer system and also a plot of the transmission coefficient versus number of layers obtained using this work at optical wavelengths upto five layers and a superimposed plot of the same from experiments namely Nair et. al. [92] showing nearly exact agreement with our theory. Our initial approach was to ignore interlayer coupling effects that possibly alter the effective conductivity of each monolayer and also effects such as trigonal warping that alter the conductivity of monolayers as well. Even this rather oversimplified model shows remarkable agreement with experiment [92] as we have already mentioned. Later it was pointed out by reviewers that our model may fail to reproduce results of graphite when extrapolated to a large number of layers. This is to be expected since our simplistic model fails to take into account the band structure of graphite. Indeed our approach is purely phenomenological and no band structure calculations

are involved. Rather our intention is to use the band structure results of others to come up with a interpolation scheme that enables a method for counting the number of layers of multilayer graphene by examining the transmission of (visible) light through the sample. Hence we have considered a refinement of our approach that involves treating multilayer graphene as a collection of independent monolayers but with an effective conductivity to be determined so as to smoothly interpolate between few-layers all the way to graphite. This necessarily involves diluting the predictive power of our model since more parameters have to be introduced that have to be fitted from experiment. However the observation that the original simplistic model agrees with experiments up to five layers means that we may suspect that the effects of interlayer coupling and trigonal warping on the *effective conductivity of each monolayer* does not make its presence felt until the number of layers is large (compared to five). We discuss these issues at length in this chapter and investigate to what extent the predicted deviation from Beer's Law is insensitive to such detailed considerations.

5.1 Problem Description

This chapter tries to understand the multi-layer system which is assumed to be placed in the *xy* plane. Basic constituent of a layered structure like few-layer graphene is the mono-layer graphene explained in chapter 2. Hence this study is based on the work described in chapter 2 which describes the optical constants of a free standing mono-layer graphene [146] by deriving an expression for the reflected and transmitted electric field from the system when a plane electromagnetic wave is incident at an arbitrary angle. Here the multi-layer system is considered to be kept in the *xy* plane and an electromagnetic wave with a wave vector $\mathbf{q}_0$ is incident on the sheet at arbitrary angle θ_0. The incident wave vector has in general all the three components along the Cartesian directions. Most of the notations used in this chapter are similar to those used in the earlier three chapters. Due to the presence of many layers, there is multiple reflection from each of the layers which makes the effective reflection and transmission from the multi-layer systems sum of series of terms, as in the case of bi-layer. Bi-layer which has only two layers is the simplest situation in which to study multiple reflection effects. The same phenomenon namely, multiple reflection makes the calculation of the emergent electric field extremely difficult to handle. The reflection and transmission from an n layer system depends on both the reflection and transmission from each of the

layers which makes the equations complicated. During this process one has to take care of the transversality conditions of electric field (By transversality we mean that $\mathbf{q} \cdot \mathbf{E} = 0$ where $\mathbf{q}$ is the wave vector for the chosen situation and $\mathbf{E}$ is the corresponding electric field) which means the fields with wave-vectors whose projection on the unit normal to the layers is positive has to be treated differently from the fields whose projection is negative.

5.2 Emergent Electric Fields : Reflection and Transmission

In this section, a general situation of arbitrary incidence is considered for study. The situation explained above is understood as follows. Consider the incident electric field denoted by $\mathbf{E}_{ext}(\mathbf{r}, t)$. When this field is incident on a mono-layer free standing graphene, the emergent electric fields that is, the reflected and the transmitted fields are derived in chapter 2 and they are denoted by $\mathbf{E}^{mono}_{ref}(\mathbf{r}, t)$ and $\mathbf{E}^{mono}_{tran}(\mathbf{r}, t)$. As can be seen from chapter 2, these fields are functions of the elements of the conductivity tensor of graphene, the components of the incident wave vector, the tilt angle of the incident polarization ellipse and also of the incident polarization. But in chapter 4 which dealt with bi-layer graphene these fields are written in a more compact way, using a matrix for reflection and transmission denoted by $G_{1,r}$ and $G_{1,t}$. That is $\mathbf{E}^{mono}_{ref}(\mathbf{r}, t) = e^{i\mathbf{q}_{0,\parallel}\cdot\mathbf{r}_{\parallel} - iq_{0,z}z - ic|q_0|t}\, G_{1,r} \cdot \mathbf{E}_{inc}(0)$ and $\mathbf{E}^{mono}_{tran}(\mathbf{r}, t) = e^{i\mathbf{q}_{0,\parallel}\cdot\mathbf{r}_{\parallel} + iq_{0,z}z - ic|q_0|t}\, G_{1,t} \cdot \mathbf{E}_{inc}(0)$. Here $\mathbf{E}_{inc}(0) = \sum_{\nu=1,2} \hat{\mathbf{u}}^{ext}_{\nu}\, E^{ext}_{\nu}$ is the amplitude of the wave incident on the system where $\hat{\mathbf{u}}^{ext}_{\nu}$ are the unit vectors which defines the polarization directions of the incident wave and E^{ext}_{ν} are the components of the incident electric field along these polarization directions. Also $G_{1,r}$ and $G_{1,t}$ are reflection and transmission matrices for mono-layer graphene in the free standing form which are 3×3 non-commuting matrices for an arbitrary incidence as given by equations (4.2, 4.4) in chapter 4. As can be seen, these matrices depend on the components of the wave vector incident as well as the conductivity tensor elements of grapene. In a similar way the system with 2 layers can be defined by the electric field denoted by $\mathbf{E}^{bi}_{ref}(\mathbf{r}, t)$ and $\mathbf{E}^{bi}_{tran}(\mathbf{r}, t)$ and can be written as $\mathbf{E}^{bi}_{ref}(\mathbf{r}, t) = e^{i\mathbf{q}_{0,\parallel}\cdot\mathbf{r}_{\parallel} - iq_{0,z}z - ic|q_0|t}\, G_{2,r} \cdot \mathbf{E}_{inc}(0)$ and $\mathbf{E}^{bi}_{tran}(\mathbf{r}, t) = e^{i\mathbf{q}_{0,\parallel}\cdot\mathbf{r}_{\parallel} + iq_{0,z}z - ic|q_0|t}\, G_{2,t} \cdot \mathbf{E}_{inc}(0)$. These matrices $G_{2,r}$ and $G_{2,t}$ can be expressed in terms of $G_{1,r}$ and $G_{1,t}$ as explained in chapter 4. Reflection and transmission matrices for bi-layer is the sum of an infinite series because of multiple reflections. The bi-layer case may be understood as follows. The transmitted electric field from layer 1 is incident on layer 2 after travelling a distance d (inter-layer separation). A part of it is reflected from layer 2 and a

part of it transmitted from layer 2. This transmitted part contributes to the second term in the series for effective transmission of bi-layer graphene. Now the reflected part from the second layer again travels a distance d, one part of which is transmitted from the first layer towards $z < 0$ and contributes as the second term in the series for the effective reflection matrix. This continues and the reflection and transmission matrices in terms of matrices for the mono-layer graphene is given as in equations (4.7, 4.8) in chapter 4.

The n - layer system can also be represented in a similar form using the n - layer reflection and transmission matrices denoted by $G_{n,r}$ and $G_{n,t}$ respectively. That is $\mathbf{E}_{n,ref}(\mathbf{r},t) = e^{i\mathbf{q}_{0,\|}\cdot\mathbf{r}_\| - iq_{0,z}z - ic|q_0|t}\, G_{n,r}\cdot\mathbf{E}_{inc}(0)$ and $\mathbf{E}_{n,tran}(\mathbf{r},t) = e^{i\mathbf{q}_{0,\|}\cdot\mathbf{r}_\| + iq_{0,z}z - ic|q_0|t}\, G_{n,t}\cdot\mathbf{E}_{inc}(0)$. To solve the n - layer system, we think of it as a combination of $(n-1)$ - layer system and a mono-layer, with a distance 3.35 Å between consecutive layers. Fig. 5.1 shows the schematic of the situation under study where the red arrow represents the initial incident wave. Fig. 5.1 illus-

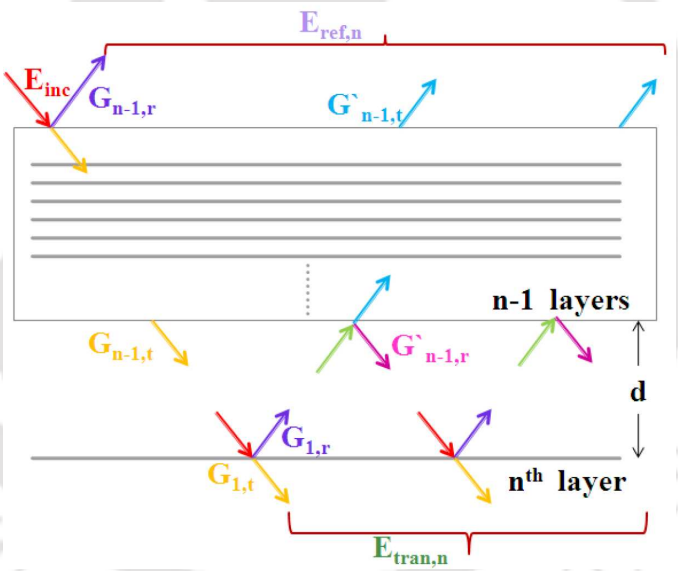

FIGURE 5.1: Schematic of n - layer graphene which shows multiple reflection when an electromagnetic wave is incident on it (red arrow). $G_{n-1,r}$ and $G_{n-1,t}$ are the reflection and transmission matrices of $n-1$ - layer system and $G'_{n-1,r}$ and $G'_{n-1,t}$ are the reflection and transmission matrices of $n-1$ - layer system with z component of the wave vector in the opposite direction, d is the distance between consecutive layers and $G_{1,r}$ and $G_{1,t}$ are the reflection and transmission matrices of mono-layer system.

trates multiple reflection phenomena due to more than one layer which makes the effective reflection and transmission from the n - layer system a sum of contributions from an infinite number of terms incorporating destructive and constructive interference effects. Our main aim is to write down a recursion relation for G_n's in terms of G_{n-1}'s and G_1's and finally to solve

those relations and find out a way to represent the n - layer matrices purely in terms of the mono-layer matrices. The recursion relation derived using methods similar to those outlined in the text-book by Jenkins and White[142], is obtained by summing the appropriate series that takes into account these effects leading to the following results:

$$G_{n+1,r} = G_{n,r} + G'_{n,t} \cdot G_{1,r} \cdot \frac{1}{\mathbf{I}_3 - G'_{n,r} \cdot G_{1,r}\, e^{2i\ q_{0,z}d}} \cdot G_{n,t}\, e^{2i\ q_{0,z}d} \tag{5.1}$$

$$G_{n+1,t} = G_{1,t} \cdot \frac{1}{\mathbf{I}_3 - G'_{n,r} \cdot G_{1,r}\, e^{2i\ q_{0,z}d}} \cdot G_{n,t}\, e^{iq_{0,z}d} \tag{5.2}$$

where n is the number of layers, with $n = 1$ corresponding to bi-layer graphene. Here $q_{0,z}$ is the z component of the incident wave vector and d is the inter-layer separation in few-layer graphene which is equal to 3.35 Å. Here $G_{n,r}$ and $G_{n,t}$ are the reflection and transmission matrices for the n layer system respectively and $G'_{n,r}$ and $G'_{n,t}$ are the reflection and transmission matrices with the z - component of the incident wave vector in the opposite direction. Similar set of equations for the primed matrices can be written by priming the above equations on both sides with the condition $G'' = G$.

$$G'_{n+1,r} = G'_{n,r} + G_{n,t} \cdot G'_{1,r} \cdot \frac{1}{\mathbf{I}_3 - G_{n,r} \cdot G'_{1,r}\, e^{2i\ q_{0,z}d}} \cdot G'_{n,t}\, e^{2i\ q_{0,z}d} \tag{5.3}$$

$$G'_{n+1,t} = G'_{1,t} \cdot \frac{1}{\mathbf{I}_3 - G_{n,r} \cdot G'_{1,r}\, e^{2i\ q_{0,z}d}} \cdot G'_{n,t}\, e^{iq_{0,z}d} \tag{5.4}$$

All the matrices given in the above equations are in general complex 3×3 matrices except the mono-layer matrices which are real matrices. Also $n+1$ layer matrices depends on the n layer matrices and the mono-layer matrix. Correctness of equations (5.1, 5.2) has been checked by deriving the equations for the simplest case of bi-layer graphene and then comparing it with equations (4.7, 4.8). The matrices $G_{n,r}$ ($G'_{n,r}$) and $G_{n,t}$ ($G'_{n,t}$) do not commute with each other whereas $G_{n,r}$ ($G_{n,t}$) commutes with $G'_{n,t}$ ($G'_{n,r}$) in the general situation of arbitrary incidence. The exponential factor appearing in equations (5.1, 5.2) are due to phase changes suffered by light that undergoes multiple reflection [see for example [142]] . As may be seen, the general situation is complicated and simplifying assumptions are necessary in order to solve these equations analytically.

5.3 Isotropic Limit at Normal Incidence

In these limits, the equations (5.1, 5.2) simplify to a large extent. Here two limits are considered. The isotropic limit means the general 2×2 conductivity tensor of graphene becomes a diagonal matrix with equal diagonal elements, hence can be considered as numbers. In the normal incidence limit, the G matrices commute with each other. In this situation, G matrices of the mono-layer can be related to each other in the following way: $G^{'}_{1,r} = -G_{1,r}$, $G_{1,t} = 1 + G_{1,r}$ and $G^{'}_{1,t} = 1 - G_{1,r}$. This makes the n - layer reflection matrices in the two different directions related to each other as $G^{'}_{n,r} = -G_{n,r}$. Substituting these relations into the general equations for the $n+1$ layer matrices they become as follows:

$$G_{n+1,r} = G_{n,r} + G^{'}_{n,t} \cdot G_{1,r} \cdot \frac{1}{\mathbf{I}_2 + G_{n,r} \cdot G_{1,r}\, e^{2i\ |q_0|d}} \cdot G_{n,t}\, e^{2i\ |q_0|d} \tag{5.5}$$

$$G_{n+1,t} = (\mathbf{I}_2 + G_{1,r}) \cdot \frac{1}{\mathbf{I}_2 + G_{n,r} \cdot G_{1,r}\, e^{2i\ |q_0|d}} \cdot G_{n,t}\, e^{i|q_0|d} \tag{5.6}$$

$$G^{'}_{n+1,r} = -G_{n,r} - G_{n,t} \cdot G_{1,r} \cdot \frac{1}{\mathbf{I}_2 + G_{n,r} \cdot G_{1,r}\, e^{2i\ |q_0|d}} \cdot G^{'}_{n,t}\, e^{2i\ |q_0|d} \tag{5.7}$$

$$G^{'}_{n+1,t} = (\mathbf{I}_2 - G_{1,r}) \cdot \frac{1}{\mathbf{I}_2 + G_{n,r} \cdot G_{1,r}\, e^{2i\ |q_0|d}} \cdot G^{'}_{n,t}\, e^{i|q_0|d} \tag{5.8}$$

Taking the ratio of the n - layer transmission matrices in opposite directions one gets,

$$\frac{G_{n+1,t}}{G^{'}_{n+1,t}} = \frac{1 + G_{1,r}}{1 - G_{1,r}} \quad \frac{G_{n,t}}{G^{'}_{n,t}} = \left(\frac{1 + G_{1,r}}{1 - G_{1,r}}\right)^{n+1} \tag{5.9}$$

Substituting this in equation (5.5, 5.6), the $n+1$ layer reflection and transmission matrices become,

$$G_{n+1,r} = G_{n,r} + \left(\frac{1-G_{1,r}}{1+G_{1,r}}\right)^n \frac{G_{n,t}^2 \cdot G_{1,r}\, e^{2i\,|q_0|d}}{1+G_{n,r}\cdot G_{1,r}\, e^{2i\,|q_0|d}} \tag{5.10}$$

$$G_{n+1,t} = \frac{(1+G_{1,r})\cdot G_{n,t}\, e^{i|q_0|d}}{1+G_{n,r}\cdot G_{1,r}\, e^{2i\,|q_0|d}} \tag{5.11}$$

For convenience, we work in the limit $|q_0|d$ much less than unity (with wavelength larger than those of soft X-rays), in this limit the equations simplify as follows :

$$G_{n+1,r} = G_{n,r} + \left(\frac{1-G_{1,r}}{1+G_{1,r}}\right)^n \frac{G_{n,t}^2 \cdot G_{1,r}}{1+G_{n,r}\cdot G_{1,r}} \tag{5.12}$$

$$G_{n+1,t} = \frac{(1+G_{1,r})\cdot G_{n,t}}{1+G_{n,r}\cdot G_{1,r}} \tag{5.13}$$

In the limit $|q_0|d \ll 1$, all the matrices become real. From the form of mono-layer reflection and transmission matrices given in equations (4.2,4.4), one may identify $G_{1,r}$ and $G_{1,t}$ with $\left(-\frac{2\pi\sigma_1}{c}\right)$ and $\left(1-\frac{2\pi\sigma_1}{c}\right)$ respectively where σ_1 is the optical conductivity of graphene. Therefore for positive values of σ_1, one can see that $G_{1,r}$ is always negative. We considered the region, $-1 < G_{1,r} < 0$ and solved for $G_{n,r}$ and $G_{n,t}$ numerically and found that the relation $G_{n,t} = 1 + G_{n,r}$ is always valid. Using this in an analytical solution leads to a self-consistent proof of this assumption. This way, one may obtain a general solution for an n layer system. Putting all the information together we observe, (i) $G_{n,r}$ tends to -1 as n tends to ∞ (ii) $G_{n,t}$ tends to 0 as n tends to ∞ (iii) $G_{n,t} = 1 + G_{n,r}$ for all n. Hence the general equations for the n - layer system may be solved as follows:

$$G_{n,r} = \frac{1-\lambda^n}{1+\lambda^n} \qquad \& \qquad G_{n,t} = \frac{2}{1+\lambda^n} \tag{5.14}$$

where $\lambda = \frac{1-G_{1,r}}{1+G_{1,r}}$ which is always greater than unity. The correctness of this solution can be checked by substituting in equations (5.12 and 5.13).

5.4 Beer-Lambert's Law

Beer-Lambert's law has been used traditionally, as a simple means of characterizing the nature of light matter interactions. According to this law, the light transmitted through a certain thickness of solid or liquid enclosed in a transparent cell is exponentially smaller than that of the incident light due to its extinction along the path. This law finds its application in a variety of fields from physics to biotechnology. In physics it is applied in optics, laser technology, material science and so on. Medicine and biology is one of the most important non-physics field in which the law has a significant role. For example, Beer's law is used as a model in the study of plant structures to spot the relationship between light penetration and leaf area [147], cell counting techniques in micro-culture to study growth factors [148]. The relevance of Beer's law can also be found, for instance in the field of corneal refractive surgery [149]. A review article is available in the literature which describes the application of this law in near infrared spectroscopy in the medical field [150]. Highly scattering media such as human tissue are also studied based on microscopic Beer-Lambert's law for the understanding of concentration of absorbing substances [151]. Some modifications to this law have been noted in the field of near infrared spectroscopy which measure several important quantities such as change in cerebral hemoglobin oxygenation, redox rate and so on [152]. In physical sciences, study of electro-chromism in amorphous and poly-crystalline thin films [153], the study of optically anisotropic systems [154] employ Beer's law. An analytical solution of two level energy rate equations is given in Abitan et. al. [155] which incorporates a correction to Beer's Law utilizing the Lambert-W function that can be used to describe absorption in optical media with a complicated structure of energy levels. Beer-Lambert's law has been employed for the study of electromagnetic wave propagation under low visibility conditions where corrections to this law have been found to be needed for a satisfactory analysis [156]. The application of the law and deviations from its predictions can been seen in the optical bleaching effect shown by various solutions illuminated by laser sources [157]. Effects such as scattering and absorption of light that does not obey Beer-Lambert's law can be observed in human cells [158]. In short, Beer-Lambert's law, which is a mathematical way of expressing how light is absorbed by matter, with its generalizations and modifications is one of the most important tools for the study of light propagation in matter.

According to Beer-Lambert's law, there is a logarithmic dependence between the transmission of the light through a substance and the product of the attenuation constant and the

path length (that is, the distance the light travels through the material). Mathematically, it is described by an exponentially decaying dependence between the transmission coefficient of light through a substance and the path length. This may be written as $I_t = I_0 e^{-\alpha L}$ where I_t is the transmitted intensity, I_0 the incident intensity, α the attenuation constant for the material and L is the path length.

In the present study, we have found that the transmitted intensity for n-layer graphene is $\frac{I_t}{I_0} = \frac{4}{(1+\lambda^n)^2}$. We have already seen in the previous section that $\lambda = \frac{1 - G_{1,r}}{1 + G_{1,r}}$ and it is greater than unity in the selected region of $G_{1,r}$. Setting $\lambda = e^{\frac{\alpha d}{2}} > 1$ makes $G_{n,t} = \frac{2}{1+e^{\frac{n\alpha d}{2}}} = \frac{2}{1+e^{\frac{\alpha L}{2}}}$ where $L = n\,d$. We define reflection and transmission coefficients as $R_n = |G_{n,r}|^2$ and $T_n = |G_{n,t}|^2$. In the limit of $\alpha L \gg 1$, $T_n = |G_{n,t}|^2 = 4e^{-\alpha L}$. Since λ is greater than unity, for large values of n, $\lambda^n \gg 1$. Take $\lambda^n \simeq 100$ which implies $n\ log_{10}(\lambda) = 2$. Therefore one can see that for Beer's law to be obeyed, the number of layers should be roughly greater than $\frac{2}{log_{10}(\lambda)}$. When the number of layers becomes small compared to this number, a deviation from Beer's law can be observed. However, it is also possible to do the reverse. We may choose a proper attenuation constant so that Beer's Law and our result agree for a *small* number of layers but necessarily differ for large number of layers. This may be achieved for example by choosing $T_{n,Beer} = \lambda^{-n}$. Both these approaches are tried subsequently and a concrete prediction is made that can be tested experimentally.

5.5 Results and Discussion

In the earlier section, we have studied the reflection and transmission coefficient of an n - layer system. As can be seen from equations of n - layer reflection and transmission coefficients, they depend on parameter λ which in turn depends on $G_{1,r}$ that ultimately equals $\frac{-2\pi\sigma_1}{c}$ in the isotropic limit at normal incidence. It is clear therefore that, to study reflection and transmission one should have an idea about the graphene conductivity element σ_1. For this the optical region of the electromagnetic spectrum is considered. This is because in higher energy regions of the electromagnetic spectrum such as the visible region, the optical conductivity is a universal constant [106, 118] whose value is $\frac{e^2}{4\hbar}$ which is different from both the universal d.c. conductivity from theory ($\frac{4e^2}{\pi h}$) and experiments ($\frac{4e^2}{h}$) [9]. In order for us to be able to neglect accumulated phase changes in multiple reflections, we are forced to work in the limit $n|q_0|d \ll 1$. In the optical region it is around 50 layers.

Fig. 5.2a and 5.2b shows the behavior of n - layer reflection coefficient and transmission coefficient as the number of layers increases. In these figures, the number of layers goes from 1 to 50. Here the incident photon energy is considered to be in the visible region as described above. It is clear from the figures that reflection coefficient increases slowly initially as the number of layers increases and rapidly for higher number of layers. Corresponding behavior for transmission coefficient shows a decrease. This is as expected.

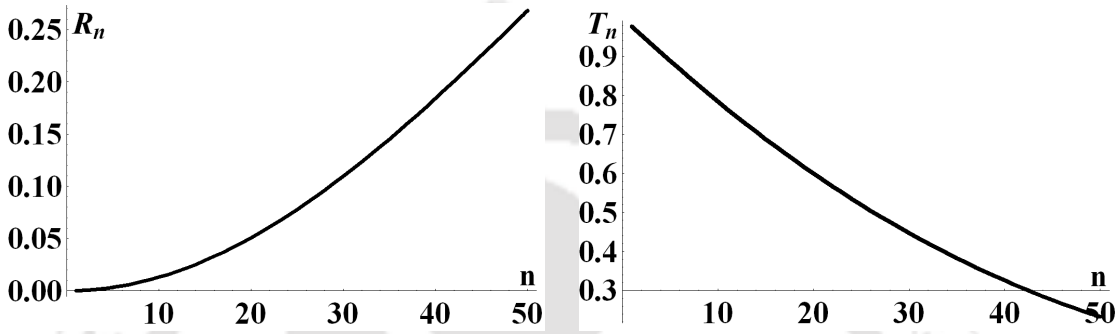

(a) (b)

FIGURE 5.2: Reflection and Transmission coefficient of n - layer system as a function number of layers with the incident photon energy in the visible region.

Fig. 5.3 studies the Beer-Lambert's law where $-ln[T]$ varies with n. In the visible region of the electromagnetic spectrum which is given here, we can see a deviation from linear behavior for number of layers all the way upto 50 layers.

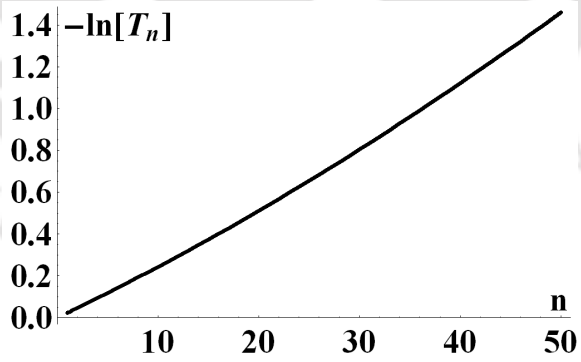

FIGURE 5.3: Beer-Lambert's law: $-log(T_n)$ with respect to the number of layers with incident wave in the visible region

To confirm the deviation from linearity of $-log(T_n)$ versus n, a plot of $ln\left(\frac{G^{beer}_{n,t}}{G_{n,t}}\right)$ is plotted versus the number of layers when the incident energy is in the visible range with conductivity as a constant value equivalent to the universal dynamical conductivity is shown in Fig. 5.4.

According to Beer's law, this plot should have been a horizontal line with ordinate equal to zero. But it is seen that the plot shows a significant deviation from this behavior for all the values of n from 1 to 50.

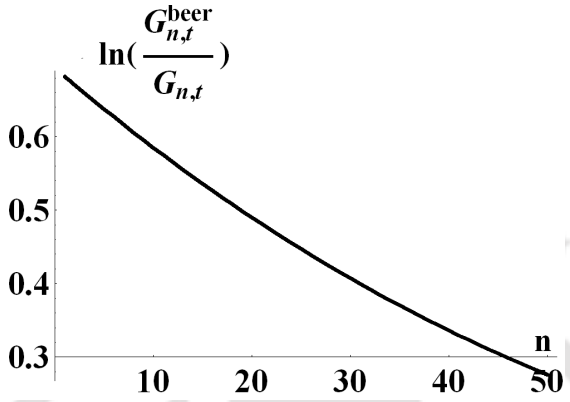

FIGURE 5.4: Deviation from Beer's law: Plot of $-log\left(\frac{G^{beer}_{n,t}}{G_{n,t}}\right)$ versus n. This is to confirm the deviation from Beer's law. The plot is drawn in the visible region with conductivity taken as the universal dynamic conductivity. If Beer's law were obeyed for all the values of n, the plot should have been a straight line parallel to x axis with ordinate zero.

Now we would like to compare the results obtained from the present study with the results obtained from one of the experiments by Nair et. al. [92]. This is given in Fig. 5.5 where the blue dots with an error bar shows the results obtained by Nair et. al. for number of layers from 1 to 5. It is given in the reference that the experimental error bar is 0.1%. The plot with red dots is the present theoretical study with the conductivity chosen to be the universal a.c. conductivity ($\frac{e^2}{4\hbar}$) [106, 118].

We have already shown that $T_n = \frac{4}{(1+\lambda^n)^2}$. In this equation, λ is a quantity which purely depends on the mono-layer conductivity. Therefore if our theory is right, the slope of $log\left(\frac{2}{\sqrt{T_n}} - 1\right)$ versus n should be straight line passing through the origin with slope $log(\lambda)$. Thus this slope indirectly gives us the conductivity of a mono-layer. We plot the same function using a Beer's Law ansatz designed to coincide with our results for small number of layers. This ansatz is $T_{n,Beer} = \lambda^{-n}$. Finally we superimpose on these two plots, the experimental results of Nair et. al. This is shown in Fig. 5.6a. We can see that all the three cases are nearly identical. However, in order to tell the two theories apart we have shown in Fig. 5.6b, the two theoretical plots - our results and Beer's Law, for number of layers upto 50. This clearly shows that Beer's law deviates from linearity whereas our results are perfectly linear (by construction).

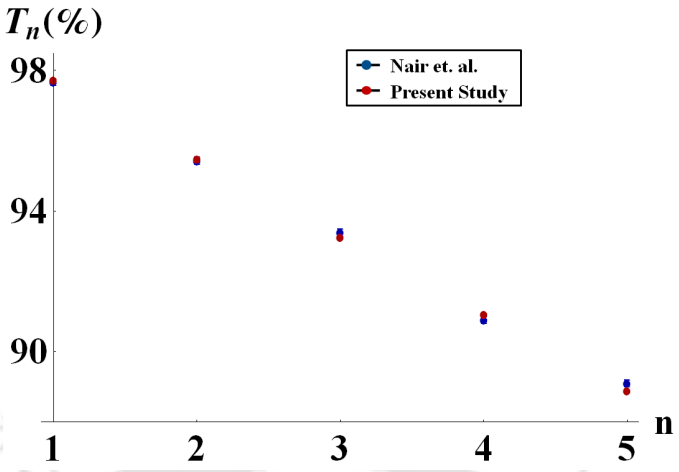

FIGURE 5.5: Comparison with experiment: Plot showing percentage transmission coefficient versus number of layers up to five layers. This plot is in the visible region and uses the universal dynamical conductivity. Here blue dots shows the result obtained by Nair et. al. from experimental observations whereas the red dots shows the results obtained by the present study using the universal ac conductivity. We can see that the results from our study nearly matches with the
experimental observation.

Our theory may be confirmed or refuted simply by extending the experiments of Nair et. al. for number of layers close to 50.

One point is worth stressing. In Beer's law, the attenuation of light in the bulk is caused by mechanisms such as ohmic losses, imaginary part of the dielectric constant and so on. In the few layer graphene system, not only are such effects present within the layer, but equally importantly, destructive interference of light that undergoes multiple reflection between adjacent layers also contributes to attenuation. Thus two physically distinct mechanisms are operative in leading to the Beer's law limit of our results. Ohmic loss is nothing but the $Re(\mathbf{E}^* \cdot \mathbf{J})$ term that exists within each layer. Destructive interference of light between adjacent layers occurs even when light travels in empty space between layers. Both these put together lead to attenuation of light as it passes through multi-layer graphene. However, in the mono-layer case, when there are no interference effects, ohmic loss may be calculated using a (energy) conservation law derived from Maxwell's equations, involving reflection and transmission coefficients. The calculated ohmic loss comes out to be 2.27% and the opacity defined by $1 - T$ becomes 2.28% which nearly matches with the results obtained by Nair et. al. where it is $2.3 \pm 0.1\%$ [92] (more details may be found in Appendix A).

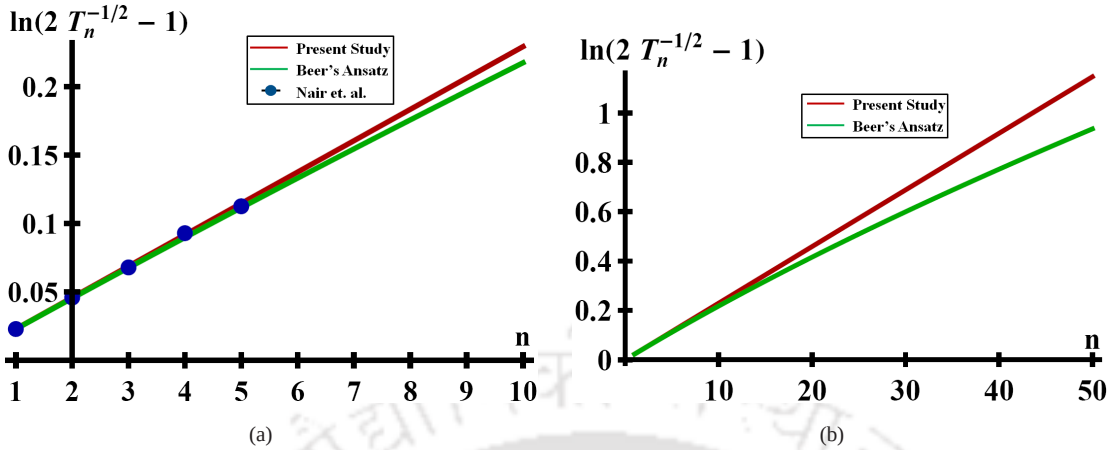

FIGURE 5.6: Comparison between present study and Beer's ansatz: Plot showing $log\left(\frac{2}{\sqrt{T_n}} - 1\right)$ versus n in the visible region. Red line shows the result from present study whereas the green line is for results obtained by using Beer Law ansatz. The blue dots are results from experiments for upto five layers by Nair et. al. (a) It is seen that the three results are nearly identical upto five layers. (b) Deviation from Beer's law can be observed as the number of layers increases.

To conclude, this section studies the optical coefficients of multi-layer system in the isotropic limit at normal incidence. Beer's law is studied along with a deviation from the Beer's law shown by the system when the number of layers is small. The study also enables one to obtain the conductivity element of a monolayer graphene system by studying the multilayer graphene system. This study shows a close resemblance with the experimental observations for the transmitted intensity upto five layers (experimental limit) as well as the monolayer opacity in the visible region.

5.6 Effects of Trigonal warping, Nonlinearity and Inter-layer interaction

Till now we have modelled the multi-layer system as a collection of independent monolayers with conductivity of each monolayer given by the universal value. However, this is clearly an oversimplification. In hindsight, it is somewhat of a coincidence that the independent layer model with the universal conductivity is in nearly exact agreement with the experiments upto

five layers. One obvious test is to extrapolate to an infinite number of layers and see if our formulas reproduce the optical absorption coefficient of graphite. Predictably it does not. Indeed the absorption coefficient of bulk graphite is four times less than the corresponding quantity from our independent layer model for infinite number of layers. We may then attribute this rather significant difference to inter-layer effects and also perhaps to cumulative changes in effective monolayer conductivity due to intra-layer effects such as trigonal warping, next-nearest neighbor interactions, finite energy effects due to nonlinearity in the energy spectrum etc. In this section we attempt to take into account these effects in a phenomenological manner by continuing to assert that the multilayer system consists of n-independent monolayers but the conductivity of each monolayer is replaced by an effective conductivity that depends on the total number of layers of the system. Clearly this approach immediately takes away all predictive power of our model unless we can convince ourselves that the effective conductivity may be interpolated using a simple function with few parameters and also that the effective conductivity of each monolayer is nearly independent of the number of layers for a few tens of layers at least. In what follows we describe one such interpolation scheme that could do this.

As discussed already, the calculations done in the earlier sections enable us to study the transmission coefficient of a few layer graphene system. The few-layer system is modelled using an independent layer approximation with the interlayer distance of the order of 3.35Å. Even though we are successful in writing down the recursion relation which is a general expression, for practical computations, we restrict ourselves to the isotropic limit of the conductivity tensor with a beam incident perpendicular to the system. This solves the recurrence relation provided the number of layers is such that $n|q_0 d| \ll 1$ (around 50 layers for optical wavelengths). We have chosen the visible region of the electromagnetic spectrum for the present study where the effects of interlayer interaction can be considered small [92], and the multilayer system can be considered as a collection of nearly independent layers. It is known that interlayer coupling effects are important when the quantity $(\frac{t_\perp}{\Omega_{inc}})^2 \sim 1$ [92]. From tight binding calcualtions, we know that the interplanar hopping energy denoted by $t_\perp$ has the magnitude of $\approx 0.3eV$ and hence $(\frac{t_\perp}{\Omega_{inc}})^2 \ll 1$ in the visible region [92]. The large amount of literature in this area instructs us to think about various factors which may affect the band structure of a monolayer graphene leading to corrections to the conductivity even in the visible energy range. Effects such as trigonal warping, next nearest neighbor interaction etc. have been discussed in the literature. Stauber et. al. [112] proved next-nearest neighbor interaction

to be very small in magnitude in the infrared region. Still this may make its presence felt in a cumulative effect on the effective conductivity of each monolayer for large number of layers. It can be seen from Nair et. al. that the above mentioned effects may actually change the graphene conductivity in the visible region from the universal value of the dynamical conductivity. It can be noted down from the reference that particularly in the green light region, the variation from the universal value is approximately 2% and it is an increase. In the extreme limits of visible range it goes beyond 4% [See Fig. S4 of supplementary material of [92]]. We focus on green light as the data for this wavelength appear more robust. In addition, we may suspect that inter-layer interactions also cause cumulative changes to the effective conductivity of each monolayer in a multi-layer sample. To accommodate all these effects, we can define an effective monolayer reflection matrix denoted by $G^{eff}_{1,r}(n)$ which depends on the number of layers n in the system and is given by the following interpolation formula:

$$G^{eff}_{1,r}(n) = G^{eff}_{1,r}(1) + \frac{\Delta G^{(ii)}_{1,r}\,(n-1)}{1 + (n-2)\frac{\Delta G^{(ii)}_{1,r}}{\Delta G^{sat}_{1,r}}} \tag{5.15}$$

This expression has two contributions. The first term is the effective reflection matrix for monolayer taking into consideration the effects due to nonlinearity in the energy spectrum as well the triangular warping. The second term is due to the cumulative effect of a large number of layers on the effective conductivity of each monolayer. The first contribution can be written as

$$G^{eff}_{1,r}(1) = G^{0}_{1,r}(1) + \Delta G^{(i)}_{1,r} \tag{5.16}$$

where $\Delta G^{(i)}_{1,r}$ is $\pm 4\%$ of $1.02 G^{0}_{1,r}(1)$ with $G^{0}_{1,r}(1) = -2\pi\sigma_0$ where σ_0 is the universal dynamic conductivity, as described earlier around green light in the visible spectrum [Fig. S2 of the supplementary material of [92]]. An estimate of the parameter $\Delta G^{sat}_{1,r}$ can be made from the experimental value of the extinction coefficient of 3D graphite available in the literature [159] in the green light region. Now $\Delta G^{(ii)}_{1,r}$ can be thought of as the effect due to inter-layer interaction and other effects which influences the band structure of a few layer system. The term involving this quantity cumulatively changes the effective G for each monolayer as the number of layers increases. Thus our prediction of a systematic and well-defined deviation from Beer's law for small number of layers is valid only if $\Delta G^{(ii)}_{1,r}$ is sufficiently small and positive. It cannot be zero either since for large number of layers we have to reproduce the graphite result. The magnitude of this quantity is estimated by examining the difference between the

effective monolayer G when there two layers in the system and when there is only one layer. As this is difficult to ascertain the value of this quantity from existing experimental data, we have chosen a suitable small value broadly consistent with these data. As we have seen in an earlier section, our results without considering all these effects, i.e. with the conductivity as the universal constant value is able to reproduce the experimental results given by Nair et. al. for few layer system up to five layers. This in turn means that the parameter $\Delta G^{(ii)}_{1,r}$ that determines cumulative effects on effective monolayer conductivity is small. The smallness of this quantity is critical to ensuring that our prediction of a systematic deviation from Beer's law for small number of layers continues to be valid. Using the analytical expression for the transmission coefficient derived from the present theory and the experimental results by Nair et. al. [Fig. S3 from supplementary results of [92]] we choose a suitable small value of $\Delta G^{(ii)}_{1,r} = 7.4 \times 10^{-5}$ that falls in a range that can be surmised from this data.

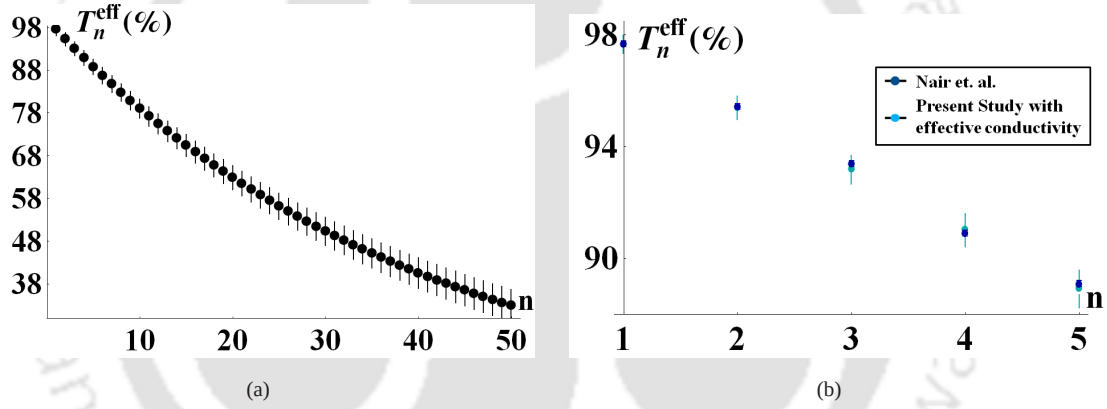

FIGURE 5.7: Plot showing effective percentage transmission versus number of layers. Transmission of a multilayer system taking into consideration the influences of trigonal warping, finite energy effects, interlayer interactions etc. (a) Prediction of transmission coefficient upto 50 layers with incident wave in the visible region. (b) Comparison between effective tranmission data and the experimental observations upto 5 layers. We can see that the average value of effective transmission matches with the experimental values atleast upto five layers.

Fig. 5.7a shows the percentage transmission coefficient versus the number of layers with incident photon energy in the green light region of the visible spectrum. This figure shows the effective transmission coefficient of a multi-layer graphene system taking into account a few additional factors which influences the transmission coefficient as mentioned in the above paragraphs. This is the transmission coefficient calculated using the effective monolayer reflection matrices given by equation (5.15). The vertical lines in the plot show the error bars in the calculation whereas the dots shows the average effective transmission. Fig. 5.7b compares

the results obtained by effective transmission for five layers with the experimental results. Here the cyan dots show the results obtained by the present study with the effective reflection matrix and the blue dots show the experimental observations with 0.1% error bars. We can see that the average effective transmission lies nearly close to the experimental data points which confirms the facts that at least for up to five layers the few layer system in the optical region can indeed be considered as a collection of independent layers (with possibly a renormalized conductivity) which agrees with the conclusion made by Nair et. al.(Supplementary material of [92])

To conclude, this section proposes a refinement to the model of earlier chapters wherein effects of trigonal warping, nonlinearity in energy spectrum and interlayer coupling are included in a phenomenological manner by postulating that the n-layer system is a collection of independent monolayers but each layer possessing an effective conductivity that depends on the total number of layers. A simple interpolation formula for this effective conductivity is proposed that enables the absorption coefficient of graphite to be reproduced as well as ensure that for small number of layers our original simple model of truly independent layers continues to be valid. This in turn means that the prediction of the systematic deviation from Beer's law is testable experimentally.

5.7 Conclusions

We have studied the transmission and reflection of light incident on a few layer graphene system by modelling it as a collection of conducting planes separated by a distance of 3.35Å. The importance of the multi-layer system is that the process of preparation of a mono-layer usually leads to the production of multi-layers. The main focus of this study is to propose a reliable way of counting the number of layers in a few-layer graphene system. Reflection and transmission coefficients of an n - layer system is derived in this work which enables one to study the limits of applicability of Beer-Lambert's law in this system. The study is done in the visible region of the electromagnetic spectrum The dependence of the transmission coefficient on conductivity allows one to extract the mono-layer conductivity by an experimental determination of the transmission coefficient of the few-layer system. A comparison of our findings in the optical region with the experimental work of Nair et.al. shows an exact match for systems up to five layers (experimental limit). However, Beer's Law with a proper choice

of the attenuation constant is also shown to reproduce these experimental findings. We therefore propose that an extension of the experimental results for larger number of layers will validate or refute our theory and set it apart from Beer's Law. While these results are most appealing when the n-layer system can be considered as being a set truly independent layers, we have also conducted a detailed phenomenological study of the potential consequences of including inter-layer coupling effects as well as nonlinearities and other effects that modify the conductivity of a single layer. We find that under optimistic scenarios our simple-minded predictions of deviations from Beer's Law appears to be robust upto a few tens of layers. In addition, using Maxwell's equations, we have obtained a matching result for mono-layer opacity $(1 - T)$ with one of the experimental observations in the visible wavelength region.

Chapter 6

Summary and outlook

As the title of this thesis suggests, this work is on carbon based systems which are two dimensional. Till 2004 it was believed that a 2D material cannot be made because it is not possible to have a long range crystalline order in two dimension because of the large thermodynamic fluctuations which makes them highly unstable. In 2004 2D carbon named graphene came into existence for which the pioneers Dr. A. K. Geim and Dr. K. S. Novoselov from Manchester University received the 2010 Nobel prize. Graphene defined as a densely packed material made purely out of carbon atoms arranged in hexagonal lattice shows many attractive, interesting and exotic properties such as the linear dispersion near low energies, fractional Quantum Hall Effect, electric field effects etc. There are many experimental and theoretical works ongoing on the different aspects of this material which made this a rich area of research. Even if this is the case, the optical properties of graphene are one of the most unexplored aspects of this new material. There are a few experimental and theoretical works available in this subarea, but still it is less visited compared to the electronic and transport properties. Also due to the high degree of expectation and enthusiasm in this field, a number of related materials have also attracted attention which are substrate-graphene, bi-layer graphene, few layer graphene, graphene nanoribbons, graphane etc.

The main focus of this thesis is the study of optical properties of graphene and some of its related systems. A theoretical formulation is developed for mono-layer graphene using some well-known but elementary physics equations. A purely classical study is done here. Maxwell's equations are used to determine the electric field emerging from different systems

under study. Wherever it is useful and convenient, other methods like series summation methods are also used to solve the equations related to the system. The systems under study in this work are mono-layer free standing graphene, substrate-graphene, bi-layer graphene and few layer graphene of which the formulation made for free standing mono-layer graphene plays an important role in the subsequent study in other related systems. The optical coefficients under study in these systems are the coefficient of reflection, coefficient of transmission and polarization of reflected wave. The situation under study for all the systems considered in this work is explained in the next few lines. The system under study is exposed to a plane electromagnetic wave and the wave is incident on the system at an arbitrary angle. For this system we have calculated the field reflected and transmitted from the systems by solving either Maxwell's equations or by using series summation methods. Then using these emergent fields the optical coefficients are derived and studied with respect to various parameters.

In chapter 2, the system under study is freely suspended graphene which is not supposed to have any disorder effects due to the presence of substrate material. This system is modeled as a conducting medium of one atom thickness, i.e. perfectly two dimensional. Maxwell's equations are solved to derive equations for reflected and transmitted electric fields and general analytical expressions for reflection coefficient, transmission coefficient and reflected polarization are derived. These general equations are functions of various parameters related to the system as well as the incident wave. The system dependent parameters are the optical conductivity elements. In various limits of these parameters, such as conductivity and several angle parameters, the above mentioned optical quantities behave in different ways. A few examples are the isotropic limit, linearly polarized incidence limit, diagonal anisotropic limit, off-diagonal anisotropic limit etc. These results obtained for mono-layer reflection, shows a small value for this quantity which is as expected by experiments and the transmission results also matches with the experimental observations available in this area. Loss coefficient associated with mono-layer graphene derived from energy conservation arguments show excellent agreement with the experimental findings. Azimuthal angle dependence of optical quantities gives hints about the form of optical conductivity tensor of graphene. In addition, this study provides a way to express the polarization of the reflected wave in terms of the polarization of incident wave.

Even if graphene is extremely interesting and important, in order for it to be practically useful, it has to be deposited on a substrate material. This situation is explained in chapter 3 where the influence of a substrate material on optical properties of graphene is considered for

study. A similar route given in chapter 2 has been followed in this system also. The system under study in this chapter can be considered as a combination of a conducting graphene sheet and a dielectric substrate material. We have assumed here that the presence of substrate does not alter the chemical structure of graphene. Maxwell's equations for this system is solved separately with the use of boundary conditions and derived general equations for the emergent electric field, which include reflection and transmission. The correctness of these equations has been checked at different stages of the calculations in various limits at which it should reduce to some of the well known results. Using the reflected and transmitted electric fields, the optical quantities mentioned above has been calculated and as discussed in the case of earlier chapter, they are functions of a few parameters which under several limits produces some interesting limits. At each stage of study, a comparison with the corresponding situations in free standing situation is made which helps to relate and differentiate the two systems. One of the important limiting cases is the situation when the incident light is linearly polarized. If the behavior of reflected amplitude is seen with respect to incident angle, a phenomenon which describes the polarization by reflection can be observed. The only difference in this case is that the minimum observed in the reflected amplitude with *p* polarized incident wave is not only decided by the conventional parameter as in the case of ordinary materials which is the Brewster (incident) angle but also an additional parameter namely the azimuthal angle. It is also important to note that the position of the minimum varies with the type of anisotropy present in the system.

The next system which is immediately related to graphene is bi-layer graphene which is a combination of two monolayers separated by a distance of 3.35 Å. Even though it is not a perfectly two dimensional material, it is considered to be that way because of the angstrom order distance separating them. We continue to model the bilayer (multilayer) system as being composed of two (many) independent monolayers but with the conductivity of each monolayer suitably renormalized to account for the effects of trigonal warping, non-linearity in the energy spectrum and inter layer hopping. This is done at a phenomenological level and not at the band structure level. We propose an interpolation formula for the effective conductivity of each graphene monolayer and determine the parameters in this interpolation but making contact with the experimental findings for bulk graphite and also with the theoretical/experimental studies for a bilayer. Due to the presence of one extra layer there are effects of multiple reflection which is responsible for the phase factors appearing the equations derived for effective reflection and transmission for bi-layer graphene. The system is solved using series

summation method which is effective in taking care of the multiple reflection due to which the reflection and transmission becomes a sum of an infinite series. Thus the main difference between the general equations for bi-layer and mono-layer systems are the multiple reflection effects between layers that can lead to construvtive or destructive interference. The reflected intensity shows an oscillation with respect to incident angle if the incident wave is in the high energy region (soft X-ray) in the case of bi-layer graphene. Another important result in this section is the perfect matching of the bi-layer transmission at normal incidence and with visible frequency with one of the experimental results available in the literature. The importance of this study is that it acts as the basis for deriving a general result for multi-layer graphene which is explained in the next chapter.

Among the experimental techniques for synthesizing graphene, the most convenient, fast and successful method is mechanical exfoliation. But most of the time, graphene is surrounded by a number of multi-layered flakes. Hence it is always important to distinguish between the different samples produced while synthesis. It is also important to count the number of layers. This is the objective of chapter 5. In chapter 5, multi-layer system is considered for study. This is a combination of n number of graphene layers each having similar properties especially the optical conductivity and each separated by a distance of 3.35 Å. Due to the presence of a large number of mono-layers, multiple reflection effects in this system is extremely large and it is taken care of by the use of series summation method to derive the reflection and transmission. A general recurrence relation has been derived for the reflection and transmission which is extremely complicated due to the non-commutative property of different matrices present in the general equations. The limit of normal incidence and isotropic conductivity tensor simplifies the general situation to a large extent and in these limits the equations can be exactly solved which results in a general solution for the reflection and transmission for an n layer system. Using this result the reflection and transmission has been studied with respect to number of layers and found out that upto five layers (experimental limit) the results obtained from present study matches with one of the experimental observations available in the literature. The results obtained enables us to study the well known rule in optics known as Beer-Lambert's law for a multi-layer graphene system. In the small n (number of layers) limit, it appears that transmission deviates from Beer's law. Hence a comparison is made between the present results and the results obtained from a Beer's law ansatz in the small n limit. The experimental results shows perfect matching with both of the

results upto five layers. The availability of experimental results for larger number of layers will validate the correctness of this formulation developed for multi-layer graphene.

A few concluding remarks mark the end of our journey into the fascinating world of graphene. This thesis made an effort to understand the mono-layer graphene and some of its related systems with the help of a few well-known optical quantities such as coefficient of reflection, coefficient of transmission and reflected polarization from a theoretical point of view. This work proposes a method for detecting the optical anisotropy of graphene and parameters associated with it (with anisotropy being defined as the propensity for the current density to point in a direction different from the applied field). It also recommends a method for determining the number of layers in multi-layer graphene by studying transmission as a function of number of layers which shows a marked departure from Beer's law for a small number of layers. This work also sheds light on the behavior of the polarization of electromagnetic waves reflected from graphene and its related systems. It also represents a less well-studied aspect of graphene viz. the optical properties from a physical optics point of view in contrast with the more well-studied Dirac fermion aspects. This is simple and understandable in the sense that it uses only well established fundamental laws and equations. This study and the theoretical formulation developed for graphene gives such a thorough understanding of the optical properties of graphene which can prompt further studies along these lines keeping this study as the starting point.

Appendix A

Free standing mono-layer graphene: Detailed calculations

A.1 Emergent electric field

The incident electric field has the form as given by equation (2.1) in real space and equation (2.4) in reciprocal space. In general, $\mathbf{E} = -\frac{1}{c}\frac{\partial A}{\partial t}$ where A is the vector potential which in Fourier space becomes

$$\mathbf{E}(\mathbf{q}\omega) = \frac{i\omega}{c}\mathbf{A}(\mathbf{q},\omega) \tag{A.1}$$

Since the graphene sheet is assumed to be kept in the xy plane as mentioned in chapter 2, the current density **J** appearing in equation (free-max-eqn) does not have any component in the z direction. That is $J_z(\mathbf{r},t) = 0$. From equations (2.6, 2.7) we can get the current density:

$$\mathbf{J}(\mathbf{q}_{\|},z,\omega) = \overline{\overline{\sigma}}(\mathbf{q}_{\|},\omega)\cdot\mathbf{E}_{ext}(\mathbf{q}_{\|},z=0,\omega)\,\delta(z) \tag{A.2}$$

From the continuity equation

$$\nabla\cdot\mathbf{J} + \frac{\partial\rho}{\partial t} = 0 \tag{A.3}$$

we can get the charge density denoted by ρ in equation (2.5) as

$$\rho(\mathbf{q}_{\|},z,\omega) = \frac{\mathbf{q}_{\|}\cdot\overline{\overline{\sigma}}(\mathbf{q}_{\|},\omega)\cdot\mathbf{E}_{ext}(\mathbf{q}_{\|},z=0,\omega)\,\delta(z)}{\omega} \tag{A.4}$$

From one of the first Maxwell's equation given in equation (2.5) which connects the charge density and the electric field: $\nabla \cdot \mathbf{E} = 4\pi\rho$, we can get the following equation:

$$i\mathbf{q}_{\parallel} \cdot \mathbf{A}(\mathbf{q}_{\parallel}, z, \omega) + \partial_z A_z(\mathbf{q}_{\parallel}, z, \omega) = \frac{4\pi c}{i\omega} \frac{\mathbf{q}_{\parallel} \cdot \mathbf{J}(\mathbf{q}_{\parallel}, z, \omega)}{\omega} \tag{A.5}$$

From the fourth Maxwell's equation given by equation (2.5) connecting the magnetic field and the rate of change of electric field: $\nabla \times \mathbf{B} = \frac{4\pi}{c}\mathbf{J} + \frac{1}{c}\frac{\partial \mathbf{E}}{\partial t}$, we will get

$$\begin{aligned}(i\mathbf{q}_{\parallel} + \hat{e}_z\,\partial_z)\left[(i\mathbf{q}_{\parallel}) \cdot \mathbf{A}(\mathbf{q}_{\parallel}, z, \omega) + \partial_z A_z(\mathbf{q}_{\parallel}, z, \omega)\right] - (\mathbf{q}_{\parallel}^2 + \partial_z^2)\mathbf{A}(\mathbf{q}_{\parallel}, z, \omega) \\ = \frac{4\pi}{c}\mathbf{J}(\mathbf{q}_{\parallel}, z, \omega) + \frac{\omega^2}{c^2}\mathbf{A}(\mathbf{q}_{\parallel}, z, \omega)\end{aligned} \tag{A.6}$$

Substituting equations (A.2, A.5) in equation (A.6) we can get

$$\begin{aligned}\left(\frac{\omega^2}{c^2} - \mathbf{q}_{\parallel}^2 + \partial_z^2\right)\mathbf{A}(\mathbf{q}_{\parallel}, z, \omega) = (i\mathbf{q}_{\parallel} + \hat{e}_z\partial_z)\left[\frac{4\pi c}{i\omega}\frac{\mathbf{q}_{\parallel} \cdot \overline{\overline{\sigma}}(\mathbf{q}_{\parallel}, \omega) \cdot \mathbf{E}_{ext}(\mathbf{q}_{\parallel}, z = 0, \omega)\,\delta(z)}{\omega}\right] \\ - \frac{4\pi}{c}\overline{\overline{\sigma}}(\mathbf{q}_{\parallel}, \omega) \cdot \mathbf{E}_{ext}(\mathbf{q}_{\parallel}, z = 0, \omega)\,\delta(z)\end{aligned} \tag{A.7}$$

After a few substitutions and algebra we can get the electric field as given below:

$$\begin{aligned}\mathbf{E}(\mathbf{q}_{\parallel}, z, \omega) = \frac{2i}{c|q_0|(q_{0,z}^2 - q_z^2)}(\mathbf{q}_{0,\parallel} + \hat{e}_z q_z)\,\mathbf{q}_0 \cdot \overline{\overline{\sigma}}(\mathbf{q}_{0,\parallel}, c|q_0|) \cdot \delta(\omega - c|q_0|)\,\delta^2(\mathbf{q}_{0,\parallel} - \mathbf{q}_{\parallel}) \sum_{\nu=1,2} \hat{\mathbf{u}}_\nu E_\nu^{ext} \\ - \frac{i|q_0|}{(q_{0,z}^2 - q_z^2)}\frac{4\pi}{c}\overline{\overline{\sigma}}(\mathbf{q}_{0,\parallel}, c|q_0|) \cdot \delta(\omega - c|q_0|)\,\delta^2(\mathbf{q}_{\parallel} - \mathbf{q}_{0,\parallel}) \sum_{\nu=1,2} \hat{\mathbf{u}}_\nu E_\nu^{ext}\,\frac{1}{2\pi}\end{aligned} \tag{A.8}$$

By repeated inverse Fourier transform of equation (A.8) we will get the emergent electric field as shown in equation (2.8)

A.2 Conductivity from optical coefficients

We have discussed in detail the reflection and transmission coefficients of free standing mono-layer graphene in chapter (1) and they are given by equations (2.21, 2.22). We also know that the linearly polarized incidence can be taken care of in three ways, (i) when θ_{tilt}^{ext} tends to zero which is called s - polarization (ii) when θ_{tilt}^{ext} tends to $\frac{\pi}{2}$ which is called p - polarization (iii) when $\delta^{ext} = 0$, this is when the difference between the polarization components vanishes.

To make the situation simple, we can consider the normal incidence limit of equations (2.21, 2.22). Let us denote the reflection and transmission coefficients in the above mentions limits as R_s (reflection coefficient with s polarized incidence), R_p (reflection coefficient with p polarized incidence), T_s (transmission coefficient with s polarized incidence), T_p (transmission coefficient with p polarized incidence). The equations for the above mentioned quantities are given below:

$$R_s^{\perp} = 4\pi^2(\sigma_{xy}^2 + \sigma_{yy}^2) \tag{A.9}$$

$$R_p^{\perp} = 4\pi^2(\sigma_{xx}^2 + \sigma_{yx}^2) \tag{A.10}$$

$$T_s^{\perp} = 4\pi^2\sigma_{xy}^2 + (1 - 2\pi\sigma_{yy})^2 \tag{A.11}$$

$$T_p^{\perp} = 4\pi^2\sigma_{yx}^2 + (1 - 2\pi\sigma_{xx})^2 \tag{A.12}$$

Solving the system of equations for $\sigma_{xx}, \sigma_{xy}, \sigma_{yx}$ and σ_{yy} we get,

$$\sigma_{xx} = \frac{1 + R_p - T_p}{4\pi} \tag{A.13}$$

$$\sigma_{yy} = \frac{1 + R_s - T_s}{4\pi} \tag{A.14}$$

$$\sigma_{xy} = \pm \frac{\sqrt{-1 + 2R_s - R_s^2 + 2T_s + 2R_sT_s - T_s^2}}{4\pi} \tag{A.15}$$

$$\sigma_{yx} = \pm \frac{\sqrt{-1 + 2R_p - R_p^2 + 2T_p + 2R_pT_p - T_p^2}}{4\pi} \tag{A.16}$$

A.3 Conservation theorem in monolayer graphene

Poynting's vector by definition is given by,

$$\mathbf{S} = \frac{c}{4\pi} Re\,(\mathbf{E} \times \mathbf{B}^*) \tag{A.17}$$

where **E** and **B** are the electric and magnetic field. Using Maxwell's equations the conservation law can be derived as follows:

$$\nabla \cdot \mathbf{S} + \frac{1}{8\pi}\frac{\partial}{\partial t}\mathbf{B}^* \cdot \mathbf{B} + \frac{1}{8\pi}\frac{\partial}{\partial t}\mathbf{E}^* \cdot \mathbf{E} = -Re(\mathbf{E}^* \cdot \mathbf{J}) \tag{A.18}$$

where **J** is the current density vector and for a 2D material $\mathbf{J} = \overline{\overline{\sigma}} \cdot \mathbf{E}_{ext}(z=0)\,\delta(z)$.

$$\nabla \cdot \mathbf{S} + \frac{\partial u}{\partial t} = -\delta(z)\, Re\left(\mathbf{E}^*(z=0) \cdot \overline{\overline{\sigma}} \cdot \mathbf{E}_{ext}(z=0)\right) \tag{A.19}$$

where $u = \frac{1}{8\pi}(\mathbf{B}^* \cdot \mathbf{B} + \mathbf{E}^* \cdot \mathbf{E})$. Integrating both sides of the above equation $\int d^2\mathbf{r}_{\parallel} \int_{-\epsilon}^{\epsilon} dz$

$$\int d^2\mathbf{r}_{\parallel}\ (S_z(z=0^+) - S_z(z=0^-)) = -\int d^2\mathbf{r}_{\parallel}\, Re\left(\mathbf{E}^*(z=0) \cdot \overline{\overline{\sigma}} \cdot \mathbf{E}_{ext}(z=0)\right) \tag{A.20}$$

As given in chapter 1, the electric field emerging from graphene when a plane electromagnetic wave $\mathbf{E}_{ext}$ with wave vector $\mathbf{q}_0$ is incident on it at an arbitrary angle θ_0 is given by equation (2.8) from which corresponding magnetic field can be written as,

$$\begin{aligned}\mathbf{B}^* =& \frac{1}{|q_0|}\, e^{ic|q_0|t}\, e^{-i\mathbf{q}_{0,\parallel}\cdot\mathbf{r}_{\parallel}} \left(e^{-iq_{0,z}z}\,(q_{0,z}\hat{e}_z + \mathbf{q}_{0,\parallel}) \times \mathbf{E}^*_{ext} + e^{iq_{0,z}z}\,(-q_{0,z}\hat{e}_z + \mathbf{q}_{0,\parallel}) \times \mathbf{E}^*_{ref}\right)\Theta(-z) \\ &+ \frac{1}{|q_0|}\, e^{ic|q_0|t}\, e^{-iq_{0,z}z}\, e^{-i\mathbf{q}_{0,\parallel}\cdot\mathbf{r}_{\parallel}}\,(q_{0,z}\hat{e}_z + \mathbf{q}_{0,\parallel}) \times \mathbf{E}^*_{tran}\Theta(z)\end{aligned} \tag{A.21}$$

Using the equations (2.8, A.21) for electric field and magnetic field we get,

$$2Re[(\mathbf{E} \times \mathbf{B}^*) \cdot \hat{e}_z] = \frac{2q_{0,z}}{|q_0|}\left(\left[\mathbf{E}_{ext} \cdot \mathbf{E}^*_{ext} - \mathbf{E}_{ref} \cdot \mathbf{E}^*_{ref}\right]\Theta(-z) + \mathbf{E}_{tran} \cdot \mathbf{E}^*_{tran}\Theta(z)\right) \tag{A.22}$$

$$\mathbf{E}(z=0) = \frac{1}{2}e^{-ic|q_0|t}\, e^{i\mathbf{q}_{0,\parallel}\cdot\mathbf{r}_{\parallel}}\left(\mathbf{E}_{ext} + \mathbf{E}_{ref} + \mathbf{E}_{tran}\right) \tag{A.23}$$

$$S_z(z=0^+) = \frac{c}{4\pi}\frac{q_{0,z}}{|q_0|}\,(\mathbf{E}_{tran} \cdot \mathbf{E}_{tran}) \quad ; \quad S_z(z=0^-) = \frac{c}{4\pi}\frac{q_{0,z}}{|q_0|}\left(\mathbf{E}_{ext} \cdot \mathbf{E}_{ext} - \mathbf{E}_{ref} \cdot \mathbf{E}_{ref}\right) \tag{A.24}$$

Substituting equations (A.22, A.23, A.24) in equation (A.20) we can get,

$$\frac{c}{\pi}\frac{q_{0,z}}{|q_0|}\left(\mathbf{E}_{tran} \cdot \mathbf{E}_{tran} - \mathbf{E}_{ext} \cdot \mathbf{E}_{ext} + \mathbf{E}_{ref} \cdot \mathbf{E}_{ref}\right) = -2Re\left[(\mathbf{E}^*_{ext} + \mathbf{E}^*_{ref} + \mathbf{E}^*_{tran}) \cdot \overline{\overline{\sigma}} \cdot \mathbf{E}_{ext}(z=0)\right] \tag{A.25}$$

We know already that the incident, reflected and transmitted intensity has the definition given below:

$$I_{inc} = \frac{q_{0,z}c}{|q_0|}\left(\mathbf{E}_{ext}\cdot\mathbf{E}^*_{ext}\right) \quad ; \quad I_{ref} = \frac{q_{0,z}c}{|q_0|}\left(\mathbf{E}_{ref}\cdot\mathbf{E}^*_{ref}\right) \quad ; \quad I_{tran} = \frac{q_{0,z}c}{|q_0|}\left(\mathbf{E}_{tran}\cdot\mathbf{E}^*_{tran}\right) \tag{A.26}$$

Substituting the above definitions in equation(A.28) we get,

$$\left(I_{inc} - I_{ref} - I_{tran}\right) = 2\pi Re\left((\mathbf{E}^*_{ext} + \mathbf{E}^*_{ref} + \mathbf{E}^*_{tran})\cdot\overline{\overline{\sigma}}\cdot\mathbf{E}_{ext}(z=0)\right) = I_{ohmic} \tag{A.27}$$

Hence $I_{inc} = I_{ref} + I_{tran} + I_{ohmic}$. That is,

$$1 = R + T + L \tag{A.28}$$

where

$$R = \frac{I_{ref}}{I_{inc}} = \frac{\left(\mathbf{E}_{ref}\cdot\mathbf{E}^*_{ref}\right)}{\left(\mathbf{E}_{ext}\cdot\mathbf{E}^*_{ext}\right)} \tag{A.29}$$

$$T = \frac{I_{tran}}{I_{inc}} = \frac{\left(\mathbf{E}_{tran}\cdot\mathbf{E}^*_{tran}\right)}{\left(\mathbf{E}_{ext}\cdot\mathbf{E}^*_{ext}\right)} \tag{A.30}$$

$$L = \frac{I_{ohmic}}{I_{inc}} = \frac{2\pi Re\left[\left(\mathbf{E}^*_{ext} + \mathbf{E}^*_{ref} + \mathbf{E}^*_{tran}\right)\cdot\overline{\overline{\sigma}}\cdot\mathbf{E}_{ext}(z=0)\right]}{\frac{q_{0,z}c}{|q_0|}\left(\mathbf{E}_{ext}\cdot\mathbf{E}^*_{ext}\right)} \tag{A.31}$$

We have already derived the equations for R and T in chapter 1. Substituting for $\mathbf{E}_{ref}$ and $\mathbf{E}_{tran}$ derived in chapter 1 we may obtain the coefficient L as functions of various angle parameters as well as the conductivity tensor elements. Therefore in the isotropic limit at normal incidence these equations reduce to $R = \frac{4\pi^2\sigma_1^2}{c^2}$, $T = \left(1 - \frac{2\pi\sigma_1}{c}\right)^2$ and $L = \frac{4\pi\sigma_1(c-2\pi\sigma_1)}{c^2}$ where σ_1 is the optical conductivity of graphene. In this situation, in the high energy region such as visible energy range, with graphene conductivity as the universal constant $\frac{e^2}{4\hbar}$, we can get mono-layer ohmic loss as 2.27% and opacity defined by $(1-T)$ as 2.28% which matches quite closely with the experimental observation by Nair et.al[92].

Appendix B

Substrate-graphene: Detailed calculations

B.1 Emergent electric field

As discussed in chapter 2, the incident electric field has the form as given by equation (2.1) in real space and (2.4) in reciprocal space. We know in general that $\mathbf{E} = -\frac{1}{c}\frac{\partial A}{\partial t}$ and $\mathbf{B} = \nabla \times \mathbf{A}$. where $\mathbf{A}$ is the vector potential. Substrate-graphene is a combined system of a substrate material and a one atom thick 2D graphene sheet. The substrate material is a dielectric with a dielectric constant ϵ whereas the graphene sheet is a conducting media with conductivity $\overline{\overline{\sigma}}$. For this reason the current density induced in the system due to the incident field is purely due to graphene and is denoted by $\mathbf{J}_{gr}$ which can be written as

$$\mathbf{J}_{gr} = -\frac{1}{c}\,\overline{\overline{\sigma}} \cdot \partial_t \mathbf{A}_{ext}(z=0)\,\delta(z) \tag{B.1}$$

From the fourth Maxwell's equation given by equation (3.2) we get

$$\nabla(\nabla \cdot \mathbf{A}) - \nabla^2 \mathbf{A} = -\frac{4\pi}{c^2}\,\overline{\overline{\sigma}} \cdot \partial_t \mathbf{A}_{ext}(z=0)\,\delta(z) - \frac{\varepsilon(z)}{c^2}\,\frac{\partial^2 \mathbf{A}}{\partial t^2} \tag{B.2}$$

The vector potential in general can be written as

$$\mathbf{A}(\mathbf{r},t) = \left[\Theta(-z)\, e^{i\mathbf{q}_{0,\parallel}\cdot\mathbf{r}_\parallel}\,\left(e^{iq_{0,z}z}\mathbf{A}_{ext}(0) + e^{-iq_{0,z}z}\mathbf{A}_{ref}(0)\right) + \Theta(z)\, e^{i\mathbf{q}'_{0,\parallel}\cdot\mathbf{r}_\parallel + iq'_{0,z}z}\mathbf{A}_{tran}(0)\right] e^{-ic|q_0|t} \tag{B.3}$$

where

$$e^{i\mathbf{q}_{0,\|}\cdot\mathbf{r}_{\|}+iq_{0,z}z}\,\mathbf{A}_{ext}(0)\,e^{-ic|q_0|t}=\mathbf{A}_{ext}(\mathbf{r},t) \tag{B.4}$$

$$e^{i\mathbf{q}_{0,\|}\cdot\mathbf{r}_{\|}-iq_{0,z}z}\,\mathbf{A}_{ref}(0)\,e^{-ic|q_0|t}=\mathbf{A}_{ref}(\mathbf{r},t) \tag{B.5}$$

$$e^{i\mathbf{q}^{'}_{0,\|}\cdot\mathbf{r}_{\|}+iq^{'}_{0,z}z}\,\mathbf{A}_{tran}(0)\,e^{-ic|q_0|t}=\mathbf{A}_{tran}(\mathbf{r},t) \tag{B.6}$$

where $\mathbf{q}^{'}_{0,\|}$ and $q^{'}_{0,z}$ are the parallel and z components of the transmitted part of field respectively. In regions $z>0$ and $z<0$ (that is away from the region $z=0$), we can say that $\nabla\cdot\mathbf{D}=0$ which when substituted in equation (B.2) we will get

$$\nabla^2\mathbf{A}=\frac{\epsilon}{c^2}\frac{\partial^2\mathbf{A}}{\partial t^2} \tag{B.7}$$

From these equations it is also clear that $\nabla\cdot\mathbf{A}_{ext}(\mathbf{r},t)=0$, $\nabla\cdot\mathbf{A}_{ref}(\mathbf{r},t)=0$ and $\nabla\cdot\mathbf{A}_{tran}(\mathbf{r},t)=0$ which implies that

$$(i\mathbf{q}_{0,\|}+\hat{e}_z\,q_{0,z})\cdot\mathbf{A}_{ext}(0)=0 \tag{B.8}$$

$$(i\mathbf{q}_{0,\|}-\hat{e}_z\,q_{0,z})\cdot\mathbf{A}_{ref}(0)=0 \tag{B.9}$$

$$(i\mathbf{q}^{'}_{0,\|}+\hat{e}_z\,q^{'}_{0,z})\cdot\mathbf{A}_{tran}(0)=0 \tag{B.10}$$

From equation (B.7) in $z>0$ region, we an get $|q^{'}_0|=\sqrt{\epsilon}\,|q_0|$.

At this stage we can make a few assumptions, such that $\mathbf{A}_{\|}$ is continuous at $z=0$ and A_z is not. Applying the continuity of $\mathbf{A}_{\|}$ at $z=0$ to the general equation of vector potential given by equation (B.3), the following condition arises

$$e^{i\mathbf{q}_{0,\|}\cdot\mathbf{r}_{\|}}\left(\mathbf{A}_{ext,\|}(0)+\mathbf{A}_{ref,\|}(0)\right)=e^{i\mathbf{q}^{'}_{0,\|}\cdot\mathbf{r}_{\|}}\mathbf{A}_{tran,\|}(0) \tag{B.11}$$

which implies that

$$\mathbf{q}_{0,\parallel} \;=\; \mathbf{q}^{'}_{0,\parallel} \tag{B.12}$$

$$\mathbf{A}_{ext,\parallel}(0) + \mathbf{A}_{ref,\parallel}(0) \;=\; \mathbf{A}_{tran,\parallel}(0) \tag{B.13}$$

Now consider the region in the vicinity of $z = 0$ in which equation (B.2) can be written as

$$\begin{aligned}(i\mathbf{q}_{0,\parallel} \;+\; \hat{e}_z\partial_z)\,(i\mathbf{q}_{0,\parallel}\cdot\mathbf{A}_{\parallel} \;+\; \partial_z A_z) \;-\; (-\mathbf{q}^2_{0,\parallel} \;+\; \partial_z^2)\,(\mathbf{A}_{\parallel} \;+\; \hat{e}_z A_z)\\ =\; -\frac{4\pi}{c^2}\,\overline{\overline{\sigma}}\cdot\partial_t\mathbf{A}_{ext,\parallel}(z=0)\,\delta(z) \;+\; \frac{\varepsilon(z)\omega^2}{c^2}\,(\mathbf{A}_{\parallel} \;+\; \hat{e}_z A_z)\end{aligned} \tag{B.14}$$

Separating out the parallel and z components of equation (B.14), from the z component we will get

$$A_z = \frac{\partial_z(i\mathbf{q}_{0,\parallel}\cdot\mathbf{A}_{\parallel})}{\varepsilon(z)\,|q_0|^2 - \mathbf{q}^2_{0,\parallel}} \tag{B.15}$$

Now to solve for the parallel component of vector potential, integrate the parallel component of equation (B.14) with respect to z within a small interval close to zero which will give the following result:

$$i\mathbf{q}_{0,\parallel}\,(A_{z,+} - A_{z,-}) - \partial_z\mathbf{A}_{\parallel,+} + \partial_z\mathbf{A}_{\parallel,-} = -\frac{4\pi}{c^2}\,\overline{\overline{\sigma}}\cdot\partial_t\mathbf{A}_{ext,\parallel}(z=0) \tag{B.16}$$

Each of the terms in equation (B.16) is given below:

$$\partial_z\mathbf{A}_{\parallel,+} = e^{i\mathbf{q}_{0,\parallel}\cdot\mathbf{r}_{\parallel} \;+\; iq^{'}_{0,z}z}\,(iq^{'}_{0,z})\,\mathbf{A}_{tran,\parallel}(0)\,e^{-i\omega t} \tag{B.17}$$

$$\partial_z\mathbf{A}_{\parallel,-} = iq_{0,z}e^{i\mathbf{q}_{0,\parallel}\cdot\mathbf{r}_{\parallel}}\,\left(e^{iq_{0,z}z}\,\mathbf{A}_{ext,\parallel}(0) \;-\; e^{-iq_{0,z}z}\mathbf{A}_{ref,\parallel}(0)\right)\,e^{-i\omega t} \tag{B.18}$$

$$A_{z,+} = \frac{-e^{i\mathbf{q}_{0,\parallel}\cdot\mathbf{r}_{\parallel} \;+\; iq^{'}_{0,z}z}\,q^{'}_{0,z}\,(\mathbf{q}_{0,\parallel}\cdot\mathbf{A}_{tran,\parallel}(0))\,e^{-i\omega t}}{q^{'2}_{0,z}} \tag{B.19}$$

$$A_{z,-} = \frac{-e^{i\mathbf{q}_{0,\parallel}\cdot\mathbf{r}_{\parallel}}\,q_{0,z}\,\mathbf{q}_{0,\parallel}\cdot\left(e^{iq_{0,z}z}\,\mathbf{A}_{ext,\parallel}(0) \;-\; e^{-iq_{0,z}z}\mathbf{A}_{ref,\parallel}(0)\right)e^{-i\omega t}}{q^2_{0,z}} \tag{B.20}$$

Substituting equations (B.17, B.18, B.19, B.20) in equation (B.16) we get,

$$\mathbf{q}_{0,\|}\left(\frac{-q'_{0,z}\,\mathbf{q}_{0,\|}\cdot\mathbf{A}_{tran,\|}(0)}{q'^{2}_{0,z}}-\frac{-q_{0,z}\,\mathbf{q}_{0,\|}\cdot(\mathbf{A}_{ext,\|}(0)-\mathbf{A}_{ref,\|}(0))}{q^{2}_{0,z}}\right) \tag{B.21}$$
$$-\,q'_{0,z}\,\mathbf{A}_{tran,\|}(0)+q_{0,z}\,(\mathbf{A}_{ext,\|}(0)\,-\,\mathbf{A}_{ref,\|}(0))=\frac{4\pi|q_0|}{c}\overline{\overline{\sigma}}\cdot\mathbf{A}_{ext,\|}(z=0)$$

Solving equations (B.13) and (B.21) simultaneously we will get the parallel components of the vector potential:

$$\mathbf{q}_{0,\|}\left(\frac{1}{q'_{0,z}}+\frac{1}{q_{0,z}}\right)\,(\mathbf{q}_{0,\|}\cdot\mathbf{A}_{tran,\|}(0))+\left(q'_{0,z}+q_{0,z}\right)\mathbf{A}_{tran,\|}=2q_{0,z}\,\mathbf{A}_{ext,\|}(0)\,+\,\frac{2\mathbf{q}_{0,\|}}{q_{0,z}}\,(\mathbf{q}_{0,\|}\cdot\mathbf{A}_{ext,\|}(0))$$
$$-\,\frac{4\pi|q_0|}{c}\overline{\overline{\sigma}}\cdot\mathbf{A}_{ext,\|}(0) \tag{B.22}$$

Equation (B.22) is a vector equation. Separating it into its components we can get the *x* and *y* components of the transmitted part of vector potential. Substituting these in equation (B.13) we can get the corresponding components of reflected part of the vector potential. The *z* component of the total vector potential is already known from equation (B.15). Combining all these components together and making use of equation (A.1), we can get the emergent electric field as given by equations (3.3, 3.4).

Appendix C

Bi-layer-graphene: Detailed calculations

C.1 Bi-layer reflection and transmission matrices

We have seen in chapter 4 that the mono-layer reflection and transmission can be represented in a compact form using the corresponding matrices denoted by $G_{1,r}$ and $G_{1,t}$. These matrices are given in equations (4.2, 4.4). In a similar way the bi-layer reflection and transmission electric fields can be represented in terms the matrices in this system denoted by $G_{2,r}$ and $G_{2,t}$. From the schematic given in Fig. 1 in chapter 4, it is clear that there will be contributions due to multiple reflections. The series for bi-layer graphene representing the effective reflection and transmission which finally converges to equations (4.7) and (4.8) is given below:

$$\begin{aligned}
\mathbf{E}^{bi}_{ref}(\mathbf{r},t) &= e^{i\mathbf{q}_{0,\|}\cdot\mathbf{r}_\|\,-\,iq_{0,z}z\,-\,ic|q_0|t}\,(G_{1,r}+G^{'}_{1,t}G_{1,r}G_{1,t}\,e^{2i\;q_{0,z}d}+G^{'}_{1,t}G_{1,r}G^{'}_{1,r}G_{1,r}G_{1,t}\,e^{4i\;q_{0,z}d}\\
&\quad+G^{'}_{1,t}G_{1,r}G^{'}_{1,r}G_{1,r}G^{'}_{1,r}G_{1,r}\,e^{6i\;q_{0,z}d}+G^{'}_{1,t}G_{1,r}G^{'}_{1,r}G_{1,r}G^{'}_{1,r}G_{1,r}G^{'}_{1,r}G_{1,r}\,e^{8i\;q_{0,z}d}\\
&\quad+.....)\cdot\mathbf{E}_{inc}(0)\\
&= e^{i\mathbf{q}_{0,\|}\cdot\mathbf{r}_\|\,-\,iq_{0,z}z\,-\,ic|q_0|t}\,(G_{1,r}+G^{'}_{1,t}\cdot G_{1,r}\cdot\frac{1}{I_3-G^{'}_{1,r}G_{1,r}\,e^{2i\;q_{0,z}d}}\cdot G_{1,t}\,e^{2i\;q_{0,z}d})\cdot\mathbf{E}_{inc}(0)\\
&= e^{i\mathbf{q}_{0,\|}\cdot\mathbf{r}_\|\,-\,iq_{0,z}z\,-\,ic|q_0|t}\,G_{2,r}\cdot\mathbf{E}_{inc}(0) \qquad \text{(C.1)}
\end{aligned}$$

where $G_{2,r}$ is given by equation (4.7). Similarly the transmitted field from bi-layer system can be written as given below:

$$\begin{aligned}\mathbf{E}^{bi}_{tran}(\mathbf{r},t) &= e^{i\mathbf{q}_{0,\parallel}\cdot\mathbf{r}_{\parallel}+\, iq_{0,z}z\, -\, ic|q_0|t}\,(G_{1,t}\,G_{1,t}e^{iq_{0,z}d} + G_{1,t}G^{'}_{1,r}G_{1,r}G_{1,t}\,e^{3i\;q_{0,z}d} \\ &\quad + G_{1,t}G^{'}_{1,r}G_{1,r}G^{'}_{1,r}G_{1,r}G_{1,t}\,e^{5i\;q_{0,z}d} + G_{1,t}G^{'}_{1,r}G_{1,r}G^{'}_{1,r}G_{1,r}G^{'}_{1,r}G_{1,r}G_{1,t}\,e^{7i\;q_{0,z}d} \\ &\quad + G_{1,t}G^{'}_{1,r}G_{1,r}G^{'}_{1,r}G_{1,r}G^{'}_{1,r}G_{1,r}G^{'}_{1,r}G_{1,r}G_{1,t}\,e^{9i\;q_{0,z}d} + ...)\cdot\mathbf{E}_{inc}(0) \\ &= e^{i\mathbf{q}_{0,\parallel}\cdot\mathbf{r}_{\parallel}\,+\,iq_{0,z}z\,-\,ic|q_0|t}\,G_{1,t}\cdot\frac{1}{I_3 - G^{'}_{1,r}G_{1,r}\,e^{2i\;q_{0,z}d}}\cdot G_{1,t}\,e^{iq_{0,z}d}\cdot\mathbf{E}_{inc}(0) \\ &= e^{i\mathbf{q}_{0,\parallel}\cdot\mathbf{r}_{\parallel}\,+\,iq_{0,z}z\,-\,ic|q_0|t}\,G_{2,t}\cdot\mathbf{E}_{inc}(0) \qquad \text{(C.2)}\end{aligned}$$

where $G_{2,t}$ is given in equation (4.8). The relation between the primed and unprimed matrices appearing in the above equations can be written as $G^{'}_{1,r} = G_{1,r}|_{q_{0,z}=-q_{0,z}}$ and $G^{'}_{1,t} = G_{1,t}|_{q_{0,z}=-q_{0,z}}$. At normal incidence $G_{1,r}$ and $G_{1,t}$ given by equations (4.2, 4.4) reduces to $G_{1,r} = -\frac{2\pi}{c}\,\overline{\overline{\sigma}}$ and $G_{1,t} = I_2 - \frac{2\pi}{c}\,\overline{\overline{\sigma}} = I_2 + G_{1,r}$ where I_2 is the two dimensional identity matrix. Hence at normal incidence $[G_{1,r}, G_{1,t}] = 0$. In the bi-layer case at normal incidence, $G_{2,r} = \frac{2G_{1,r}}{I_2+G^2_{1,r}}$ and $G_{2,t} = \frac{(I_2+G_{1,r})^2}{(I_2+G^2_{1,r})}$ in the limit of $|q_0|d \ll 1$ which makes them commute.

C.2 Components of $G_{2,r}$ and $G_{2,t}$

We can write the matrix form of bi-layer reflection matrix as given below:

$$G_{2,r} = \begin{pmatrix} \frac{a_{r,1}+e^{2i\;q_{0,z}d}b_{r,1}+e^{4i\;q_{0,z}d}c_{r,1}}{f_1+e^{2i\;q_{0,z}d}g_1+e^{4i\;q_{0,z}d}h_1} & \frac{a_{r,2}+e^{2i\;q_{0,z}d}b_{r,2}+e^{4i\;q_{0,z}d}c_{r,2}}{f_1+e^{2i\;q_{0,z}d}g_1+e^{4i\;q_{0,z}d}h_1} & 0 \\ \frac{a_{r,3}+e^{2i\;q_{0,z}d}b_{r,3}+e^{4i\;q_{0,z}d}c_{r,3}}{f_1+e^{2i\;q_{0,z}d}g_1+e^{4i\;q_{0,z}d}h_1} & \frac{a_{r,4}+e^{2i\;q_{0,z}d}b_{r,4}+e^{4i\;q_{0,z}d}c_{r,4}}{f_1+e^{2i\;q_{0,z}d}g_1+e^{4i\;q_{0,z}d}h_1} & 0 \\ \frac{a_{r,5}+e^{2i\;q_{0,z}d}b_{r,5}+e^{4i\;q_{0,z}d}c_{r,5}}{f_1+e^{2i\;q_{0,z}d}g_1+e^{4i\;q_{0,z}d}h_1} & \frac{a_{r,6}+e^{2i\;q_{0,z}d}b_{r,6}+e^{4i\;q_{0,z}d}c_{r,6}}{f_1+e^{2i\;q_{0,z}d}g_1+e^{4i\;q_{0,z}d}h_1} & 0 \end{pmatrix} \qquad \text{(C.3)}$$

where the components are

$$a_{r,1} = 2c^3\pi|q_0|q^3_{0,z}\left(-|q_0|^2\sigma_{xx} + q_{0,x}(q_{0,x}\sigma_{xx} + q_{0,y}\sigma_{yx})\right)$$

$$\begin{aligned}b_{r,1} &= 2\pi c|q_0|q_{0,z}\,[c^2q^2_{0,z}(-|q_0|^2\sigma_{xx} + q_{0,x}(q_{0,x}\sigma_{xx} + q_{0,y}\sigma_{yx})) + 4\pi^2q^2_{0,z}(\sigma_{xy}\sigma_{yx} - \sigma_{xx}\sigma_{yy}) \\ &\quad \times(|q_0|^2\sigma_{yy} - q_{0,y}(q_{0,x}\sigma_{xy} + q_{0,y}\sigma_{yy}))]\end{aligned}$$

$$c_{r,1} = 8\pi^3 c|q_0|q_{0,z}^3(\sigma_{xy}\sigma_{yx} - \sigma_{xx}\sigma_{yy})(|q_0|^2\sigma_{yy} - q_{0,y}\left(q_{0,x}\sigma_{xy} + q_{0,y}\sigma_{yy}\right))$$

$$a_{r,2} = 2c^3\pi|q_0|q_{0,z}^3\left(-|q_0|^2\sigma_{xy} + q_{0,x}(q_{0,x}\sigma_{xy} + q_{0,y}\sigma_{yy})\right)$$

$$b_{r,2} = -2\pi c q_{0,z}\left(|q_0|^2\sigma_{xy} - q_{0,x}(q_{0,x}\sigma_{xy} + q_{0,y}\sigma_{yy})\right)\ (c^2q_{0,z}^2 + 4\pi^2q_{0,z}^2(\sigma_{xy}\sigma_{yx} - \sigma_{xx}\sigma_{yy}))$$

$$c_{r,2} = -8\pi^3 c|q_0|q_{0,z}^3(\sigma_{xy}\sigma_{yx} - \sigma_{xx}\sigma_{yy})(|q_0|^2\sigma_{xy} - q_{0,x}(q_{0,x}\sigma_{xy} + q_{0,y}\sigma_{yy}))$$

$$a_{r,3} = 2c^3\pi|q_0|q_{0,z}^3\left(q_{0,x}q_{0,y}\sigma_{xx} + (-|q_0|^2 + q_{0,y}^2)\sigma_{yx}\right)$$

$$b_{r,3} = 2\pi c q_{0,z}(q_{0,x}q_{0,y}\sigma_{xx} + (-|q_0|^2 + q_{0,y}^2)\sigma_{yx})(c^2q_{0,z}^2 + 4\pi^2q_{0,z}^2(\sigma_{xy}\sigma_{yx} - \sigma_{xx}\sigma_{yy}))$$

$$c_{r,3} = 8\pi^3 c|q_0|q_{0,z}^3\left(|q_0|^2\sigma_{yx} - q_{0,y}(q_{0,x}\sigma_{xx} + q_{0,y}\sigma_{yx})\right)(-\sigma_{xy}\sigma_{yx} - \sigma_{xx}\sigma_{yy})$$

$$a_{r,4} = 2\pi c^3|q_0|q_{0,z}^3\left(q_{0,x}q_{0,y}\sigma_{xy} + \left(-|q_0|^2 + q_{0,y}^2\right)\sigma_{yy}\right)$$

$$b_{r,4} = 2\pi c|q_0|q_{0,z}(c^2q_{0,z}^2(q_{0,x}q_{0,y}\sigma_{xy} + (-|q_0|^2 + q_{0,y}^2)\sigma_{yy}) - 4\pi^2q_{0,z}^2(|q_0|^2\sigma_{xx} - q_{0,x}(q_{0,x}\sigma_{xx} + q_{0,y}\sigma_{yx})(-\sigma_{xy}\sigma_{yx} + \sigma_{xx}\sigma_{yy}))$$

$$c_{r,4} = -8\pi^3 c|q_0|q_{0,z}^3\left(|q_0|^2\sigma_{xx} - q_{0,x}(q_{0,x}\sigma_{xx} + q_{0,y}\sigma_{yx})\right)(-\sigma_{xy}\sigma_{yx} + \sigma_{xx}\sigma_{yy})$$

$$a_{r,5} = -2\pi c^3|q_0|q_{0,z}^4(q_{0,x}\sigma_{xx} + q_{0,y}\sigma_{yx})$$

$$b_{r,5} = -2\pi c|q_0|q_{0,z}^2(c^2q_{0,z}^2(q_{0,x}\sigma_{xx} + q_{0,y}\sigma_{yx}) + 4\pi^3(\sigma_{xy}\sigma_{yx} - \sigma_{xx}\sigma_{yy})(q_{0,x}^2q_{0,y}\sigma_{xy} + (|q_0|^2 - q_{0,y}^2)q_{0,y}\sigma_{yx} - q_{0,x}(q_{0,y}^2(\sigma_{xx} - \sigma_{yy}) + |q_0|^2\sigma_{yy})))$$

$$c_{r,5} = -8\pi^3 c|q_0|q_{0,z}^2(-\sigma_{xy}\sigma_{yx} + \sigma_{xx}\sigma_{yy})(-q_{0,x}^2q_{0,y}\sigma_{xy} + q_{0,y}(-|q_0|^2 + q_{0,y}^2)\sigma_{yx} + q_{0,x}(q_{0,y}^2(\sigma_{xx} - \sigma_{yy}) + |q_0|^2\sigma_{yy}))$$

$$a_{r,6} = -2\pi c^3|q_0|q_{0,z}^4\left(q_{0,x}\sigma_{xy}+q_{0,y}\sigma_{yy}\right)$$

$$b_{r,6} = -2\pi c|q_0|q_{0,z}^2(c^2q_{0,z}^2(q_{0,x}\sigma_{xy}+q_{0,y}\sigma_{yy})+4\pi^2(-\sigma_{xy}\sigma_{yx}+\sigma_{xx}\sigma_{yy})(|q_0|^2(q_{0,y}\sigma_{xx}-q_{0,x}\sigma_{yx}) + q_{0,x}(q_{0,x}^2\sigma_{xy}-q_{0,y}^2\sigma_{yx}+q_{0,x}q_{0,y}(-\sigma_{xx}+\sigma_{yy}))))$$

$$c_{r,6} = -8\pi^3 c|q_0|q_{0,z}^2(|q_0|^2(-q_{0,y}\sigma_{xx}+q_{0,x}\sigma_{xy})+q_{0,x}(-q_{0,x}^2\sigma_{xy}+q_{0,y}^2\sigma_{yx}+q_{0,x}q_{0,y}(\sigma_{xx}-\sigma_{yy}))) \times(\sigma_{xy}\sigma_{yx}-\sigma_{xx}\sigma_{yy})$$

$$f_1 = c^4|q_0|^2q_{0,z}^4$$

$$g_1 = 4\pi^2c^2q_{0,z}^2[\left(q_{0,x}^2\sigma_{xx}+q_{0,x}q_{0,y}(\sigma_{xy}+\sigma_{yx})+q_{0,y}^2\sigma_{yy}\right)^2+|q_0|^4\left(\sigma_{xx}^2+2\sigma_{xy}\sigma_{yx}+\sigma_{yy}^2\right) - 2|q_0|^2(q_{0,x}^2(\sigma_{xx}^2+\sigma_{xy}\sigma_{yx})+q_{0,x}q_{0,y}(\sigma_{xy}+\sigma_{yx})(\sigma_{xx}+\sigma_{yy})+q_{0,y}^2(\sigma_{xy}\sigma_{yx}+\sigma_{yy}^2))]$$

$$h_1 = 16\pi^4|q_0|^2q_{0,z}^4(\sigma_{xy}\sigma_{yx}-\sigma_{xx}\sigma_{yy})^2$$

The matrix form of bilayer transmission matrix is as given below:

$$G_{2,t} = e^{i\,q_{0,z}d}\begin{pmatrix} \frac{a_{t,1}+e^{2i\,q_{0,z}d}b_{t,1}}{f_1+e^{2i\,q_{0,z}d}g_1+e^{4i\,q_{0,z}d}h_1} & \frac{a_{t,2}+e^{2i\,q_{0,z}d}b_{t,2}}{f_1+e^{2i\,q_{0,z}d}g_1+e^{4i\,q_{0,z}d}h_1} & 0 \\ \frac{a_{t,3}+e^{2i\,q_{0,z}d}b_{t,3}}{f_1+e^{2i\,q_{0,z}d}g_1+e^{4i\,q_{0,z}d}h_1} & \frac{a_{t,4}+e^{2i\,q_{0,z}d}b_{t,4}}{f_1+e^{2i\,q_{0,z}d}g_1+e^{4i\,q_{0,z}d}h_1} & 0 \\ \frac{a_{t,5}+e^{2i\,q_{0,z}d}b_{t,5}+e^{4i\,q_{0,z}d}c_{t,5}}{f_1+e^{2i\,q_{0,z}d}g_1+e^{4i\,q_{0,z}d}h_1} & \frac{a_{t,6}+e^{2i\,q_{0,z}d}b_{t,6}+e^{4i\,q_{0,z}d}c_{t,6}}{f_1+e^{2i\,q_{0,z}d}g_1+e^{4i\,q_{0,z}d}h_1} & 1 \end{pmatrix} \quad \text{(C.4)}$$

where the components are

$$a_{t,1} = c^2q_{0,z}^2(c^2|q_0|^2q_{0,z}^2+4\pi c|q_0|q_{0,z}(-|q_0|^2\sigma_{xx}+q_{0,x}(q_{0,x}\sigma_{xx}+q_{0,y}\sigma_{yx}))+4\pi^2(|q_0|^4(\sigma_{xx}^2 + \sigma_{xy}\sigma_{yx})+q_{0,x}(q_{0,x}\sigma_{xx}+q_{0,y}\sigma_{yx})(q_{0,x}^2\sigma_{xx}+q_{0,x}q_{0,y}(\sigma_{xy}+\sigma_{yx})+q_{0,y}^2\sigma_{yy}) - |q_0|^2(q_{0,y}^2\sigma_{xy}\sigma_{yx}+q_{0,x}^2(2\sigma_{xx}^2+\sigma_{xy}\sigma_{yx})+q_{0,x}q_{0,y}(\sigma_{xx}\sigma_{yx}+2\sigma_{xx}\sigma_{yx}+\sigma_{yx}\sigma_{yy}))))$$

$$
\begin{aligned}
b_{t,1} &= 4\pi^2(4\pi^2|q_0|^2q_{0,z}^4(\sigma_{xy}\sigma_{yx}-\sigma_{xx}\sigma_{yy})^2+4\pi c|q_0|q_{0,z}^3(\sigma_{xy}\sigma_{yx}-\sigma_{xx}\sigma_{yy})(|q_0|^2\sigma_{yy}\\
&\quad -q_{0,y}(q_{0,x}\sigma_{xy}+q_{0,y}\sigma_{yy}))+c^2q_{0,z}^2(q_{0,y}(q_{0,x}\sigma_{xy}+q_{0,y}(\sigma_{xy}+\sigma_{yx}))+q_{0,y}^2\sigma_{yy})\\
&\quad +|q_0|^4(\sigma_{xy}\sigma_{yx}+\sigma_{yy}^2)-|q_0|^2(q_{0,x}q_{0,y}\sigma_{xx}\sigma_{xy}+(q_{0,x}^2+q_{0,y}^2)\sigma_{xy}\sigma_{yx}\\
&\quad +q_{0,x}q_{0,y}(2\sigma_{xy}+\sigma_{yx})\sigma_{yy}+2q_{0,y}^2\sigma_{yy}^2)))\\
a_{t,2} &= -4c^2\pi q_{0,z}^2(|q_0|^2\sigma_{xy}-q_{0,x}(q_{0,x}\sigma_{xy}+q_{0,y}\sigma_{yy}))(c|q_0|q_{0,z}+\pi(q_{0,x}(q_{0,x}\sigma_{xx}\\
&\quad +q_{0,y}(\sigma_{xy}+\sigma_{yx}))+q_{0,y}^2\sigma_{yy}-|q_0|^2(\sigma_{xx}+\sigma_{yy})))\\
b_{t,2} &= -4c\pi^2q_{0,z}(|q_0|^2\sigma_{xy}-q_{0,x}(q_{0,x}\sigma_{xy}+q_{0,y}\sigma_{yy}))(4\pi|q_0|q_{0,z}^2(\sigma_{xy}\sigma_{yx}-\sigma_{xx}\sigma_{yy})\\
&\quad +cq_{0,z}(-q_{0,x}(q_{0,x}\sigma_{xx}+q_{0,y}(\sigma_{xy}+\sigma_{yx}))-q_{0,y}^2\sigma_{yy}+|q_0|^2(\sigma_{xx}+\sigma_{yy})))\\
a_{t,3} &= 4c^2\pi q_{0,z}^2(q_{0,x}q_{0,y}\sigma_{xx}+(-|q_0|^2+q_{0,y}^2)\sigma_{yx})(c|q_0|q_{0,z}+\pi(q_{0,x}(q_{0,x}\sigma_{xx}+q_{0,y}(\sigma_{xy}+\sigma_{yx}))\\
&\quad +q_{0,y}^2\sigma_{yy}-|q_0|^2(\sigma_{xx}+\sigma_{yy})))\\
b_{t,3} &= 4\pi^2cq_{0,z}(q_{0,x}q_{0,y}\sigma_{xx}+(-|q_0|^2+q_{0,y}^2)\sigma_{yx})(4\pi|q_0|q_{0,z}^2(\sigma_{xy}\sigma_{yx}-\sigma_{xx}\sigma_{yy})\\
&\quad +cq_{0,z}(-q_{0,x}(q_{0,x}\sigma_{xx}+q_{0,y}(\sigma_{xy}+\sigma_{yx}))-q_{0,y}^2\sigma_{yy}+|q_0|^2(\sigma_{xx}+\sigma_{yy})))\\
a_{t,4} &= c^2q_{0,z}^2(c^2|q_0|^2q_{0,z}^2+4\pi c|q_0|q_{0,z}(q_{0,x}q_{0,y}\sigma_{xy}+(-|q_0|^2+q_{0,y}^2)\sigma_{yy})+4\pi^2(q_{0,y}(q_{0,x}\sigma_{yx}\\
&\quad +q_{0,y}\sigma_{yy})(q_{0,x}(q_{0,x}\sigma_{xx}+q_{0,y}(\sigma_{xy}+\sigma_{yx}))+q_{0,y}^2\sigma_{yy})+|q_0|^4(\sigma_{xy}\sigma_{yx}+\sigma_{yy}^2)\\
&\quad -|q_0|^2(q_{0,x}q_{0,y}\sigma_{xx}\sigma_{xy}+(q_{0,x}^2+q_{0,y}^2)\sigma_{xy}\sigma_{yx}+q_{0,x}q_{0,y}(2\sigma_{xy}+\sigma_{yx})\sigma_{yy}+2q_{0,y}^2\sigma_{yy}^2)))\\
b_{t,4} &= 4\pi^2|q_0|^2(4\pi^2|q_0|^2q_{0,z}^4(\sigma_{xy}\sigma_{yx}-\sigma_{xx}\sigma_{yy})^2-4\pi c|q_0|q_{0,z}^3(|q_0|^2\sigma_{xx}\\
&\quad -q_{0,x}(q_{0,x}\sigma_{xx}+q_{0,y}\sigma_{yx}))(-\sigma_{xy}\sigma_{yx}+\sigma_{xx}\sigma_{yy})+c^2q_{0,z}^2(|q_0|^4(\sigma_{xx}^2+\sigma_{xy}\sigma_{yx})\\
&\quad +q_{0,x}(q_{0,x}\sigma_{xx}+q_{0,y}\sigma_{yx})(q_{0,x}^2\sigma_{xx}+q_{0,x}q_{0,y}(\sigma_{xy}+\sigma_{yx})+q_{0,y}^2\sigma_{yy})\\
&\quad -|q_0|^2(q_{0,y}^2\sigma_{xy}\sigma_{yx}+q_{0,x}^2(2\sigma_{xx}^2+\sigma_{xy}\sigma_{yx})+q_{0,x}q_{0,y}(\sigma_{xx}\sigma_{xy}+2\sigma_{xx}\sigma_{yx}+\sigma_{yx}\sigma_{yy}))))\\
a_{t,5} &= 4c^2\pi q_{0,z}^3(c|q_0|q_{0,z}(q_{0,x}\sigma_{xx}+q_{0,y}\sigma_{yx})+\pi((q_{0,x}\sigma_{xx}+q_{0,y}\sigma_{yx})(q_{0,x}^2\sigma_{xx}\\
&\quad +q_{0,x}q_{0,y}(\sigma_{xy}+\sigma_{yx})+q_{0,y}^2\sigma_{yy})-|q_0|^2(q_{0,x}(\sigma_{xx}^2+\sigma_{xy}\sigma_{yx})+q_{0,y}\sigma_{yx}(\sigma_{xx}+\sigma_{yy}))))
\end{aligned}
$$

$$
\begin{aligned}
b_{t,5} = & -4\pi^2 q_{0,z}(4\pi^2|q_0|^2 q_{0,x}q_{0,z}^2(\sigma_{xy}\sigma_{yx}-\sigma_{xx}\sigma_{yy})^2 - 4\pi c|q_0|q_{0,z}(\sigma_{xy}\sigma_{yx}-\sigma_{xx}\sigma_{yy}) \\
& \times (q_{0,x}^2 q_{0,y}\sigma_{xy} + (|q_0|^2 - q_{0,y}^2)q_{0,y}\sigma_{yx} - q_{0,x}(q_{0,y}^2(\sigma_{xx}-\sigma_{yy}) + |q_0|^2\sigma_{yy})) \\
& + c^2 q_{0,z}^2((q_{0,x}\sigma_{xx}+q_{0,y}\sigma_{yx})(q_{0,x}^2\sigma_{xx} + q_{0,x}q_{0,y}(\sigma_{xy}+\sigma_{yx}) + q_{0,y}^2\sigma_{yy}) \\
& - |q_0|^2(q_{0,x}(\sigma_{xx}^2 + \sigma_{xy}\sigma_{yx}) + q_{0,y}\sigma_{yx}(\sigma_{xx}+\sigma_{yx}))))
\end{aligned}
$$

$$
c_{t,5} = 16\pi^4|q_0|^2 q_{0,x}q_{0,z}^3(\sigma_{xy}\sigma_{yx}-\sigma_{xx}\sigma_{yy})^2
$$

$$
\begin{aligned}
a_{t,6} = & 4c^2\pi q_{0,z}^3(c|q_0|q_{0,z}(q_{0,x}\sigma_{xy}+q_{0,y}\sigma_{yy}) + \pi((q_{0,x}\sigma_{xy}+q_{0,y}\sigma_{yy})(q_{0,x}^2\sigma_{xx} + q_{0,x}q_{0,y}(\sigma_{xy}+\sigma_{yx}) \\
& + q_{0,y}^2\sigma_{yy}) - |q_0|^2(q_{0,x}\sigma_{xy}(\sigma_{xx}+\sigma_{yy}) + q_{0,y}(\sigma_{xy}\sigma_{yx}+\sigma_{yy}^2))))
\end{aligned}
$$

$$
\begin{aligned}
b_{t,6} = & -4\pi^2 q_{0,z}(4\pi^2|q_0|^2 q_{0,y}q_{0,z}^2(\sigma_{xy}\sigma_{yx}-\sigma_{xx}\sigma_{yy})^2 - 4\pi c|q_0|q_{0,z}(-\sigma_{xy}\sigma_{yx}+\sigma_{xx}\sigma_{yy}) \\
& \times (|q_0|^2(q_{0,y}\sigma_{xx} - q_{0,x}\sigma_{xy}) + q_{0,x}(q_{0,x}^2\sigma_{xy} - q_{0,y}^2\sigma_{yx} + q_{0,x}q_{0,y}(-\sigma_{xx}+\sigma_{yy}))) \\
& + c^2 q_{0,z}^2((q_{0,x}\sigma_{xy}+q_{0,y}\sigma_{yy})(q_{0,x}^2\sigma_{xx} + q_{0,x}q_{0,y}(\sigma_{xy}+\sigma_{yx}) + q_{0,y}^2\sigma_{yy}) \\
& - |q_0|^2(q_{0,x}\sigma_{xy}(\sigma_{xx}+\sigma_{yy}) + q_{0,y}(\sigma_{xy}\sigma_{yx}+\sigma_{yy}^2))))
\end{aligned}
$$

$$
c_{t,6} = 16\pi^4|q_0|^2 q_{0,y}q_{0,z}^3(\sigma_{xy}\sigma_{yx}-\sigma_{xx}\sigma_{yy})^2
$$

Bibliography

[1] S. Iijima, J. Cryst. Growth **50**, 675 (1980).

[2] S. Iijima, Nature **354**, 56 (1991).

[3] K. S. Novoselov et al., Science **306**, 666 (2004)

[4] N. D. Mermin, Phys. Rev. **176**, 250 (1968)

[5] R. M-Ballesté, C. G-Navarro, J. G-Herrero and F. Zamora, Nanoscale (online published) (2010)

[6] K. S. Novoselov et al., Proc. Nat. Acad. Sci. **102**, 10451 (2005)

[7] A. K. Geim, Science **324**, 1530 (2009)

[8] M. I. Katsnelson, Mater. Today **10**, 20 (2007)

[9] A. K. Geim and K. S. Novoselov, Nat. Mater. **6**, 183 (2007)

[10] A. K. Geim and P. Kim, Sci. Am. **298**, 68 (2008)

[11] A. H. C. Neto, F. Guinea, N. M. R. Peres, K. S. Novoselov and A. K. Geim, Rev. Mod. Phys. **81**, 109 (2009)

[12] M. I. Katsnelson and K. S. Novoselov, Solid State Commun. **143**, 3 (2007)

[13] M. I. Katsnelson, Euro. Phys. J. B **51**, 157 (2006)

[14] T. M. Rusin and W. Zawadzki, Phys. Rev. B **80**, 045416 (2009)

[15] M. I. Katsnelson, K. S. Novoselov and A. K. Geim, Nat. Phys. **2**, 620 (2006)

[16] N. Stander, B. Huard and D. G-Gordon, Phys. Rev. Lett. **102**, 026807 (2009)

[17] V. Lukose, R. Shankar and G. Baskaran, Phys. Rev. Lett. **98**, 116802 (2007)

[18] K. S. Novoselov et al., Nat. Phys. **2**, 177 (2006)

[19] V. P. Gusynin and S. G. Sharapov, Phys. Rev. Lett. **95**, 146801 (2005)

[20] Y. Zhang, Y-W. Tan, H. L. Stormer and P. Kim, Nature **438**, 201 (2005)

[21] X. Du, I. Skachko, F. Duerr, A. Luican and E. Y. Andrei, Nature **462**, 192 (2009)

[22] K. I. Bolotin, F. Ghahari, M. D. Shulman, H. L. Stormer and P .Kim, Nature **462**, 196 (2009)

[23] V. Singh and M. M. Deshmukh, Phys. Rev. B **80**, 081404(R) (2009)

[24] P. Recher et al., Phys.Rev. B **76**, 235404 (2007)

[25] S. Russo, J. B. Oostinga, D. Wehenkel, H. B. Heersche, S. S. Sobhani, Phys. Rev. B **77**, 085413 (2008)

[26] A. B. Kuzmenko, E. van Heumen, F. Carbone and D. van der Marel, Phys. Rev. Lett. **100**, 117401 (2008)

[27] V. P. Gusynin, S. G. Sharapov and J. P. Carbotte, New J. Phys. **11**, 095013 (2009)

[28] Y. -W. Tan et al., Phys. Rev. Lett. **99**, 245803 (2007)

[29] C. G. Beneventano, P. Giacconi, E. M. Santangelo, R. Soldati, J. Phys. A: Math. Theor. **42**, 275401 (2009)

[30] V. V. Talanov et al., ACS Nano **4**, 3831 (2010)

[31] S. Y. Zhou et al., Nat. Mater. **6**, 770 (2007)

[32] P. Sutter, J. T. Sadowski and E. Sutter, Phys. Rev. B **80**, 245411 (2009)

[33] F. Hiebel, P. Mallet, F. Varchon, L. Magaud and J-. Y. Veuillen, Phys. Rev. B **78**, 153412 (2008)

[34] A. N. Pal, A. A. Bol and A. Ghosh, Appl. Phys. Lett. bf 97, 133504 (2010)

[35] J. M. Caridad et al., J. Appl. Phys. **108**, 084321 (2010)

[36] P. Sutter, M. S. Hybertsen, J. T. Sadowski and E. Sutter, Nano Lett. **9**, 2654 (2009)

[37] K. A. Ritter and J. W. Lyding, Nat. Mater. **8**, 235 (2009)

[38] K. Esaki, M. Sato, M. Kohmoto and B. I. Halperin, Phys. Rev. B **80**, 125405 (2009)

[39] T. Wassmann, A. P. Seitsonen, A. M. Saitta, M. Lazzeri and F. Mauri, Phys. Rev. Lett. **101** 096402 (2008)

[40] X. Jia et al., Science **323**, 1701 (2009)

[41] V. P. Gusynin, S. G. Sharapov and J. P. Carbotte, Int. J. Mod. Phys. B **21**, 4611 (2007)

[42] Z. Ni, Y. Wang, T. Yu and Z. Shen, Nano Res. **1**, 273 (2008)

[43] M. Orlita and M. Potemski, Semicond. Sci. Technol. **25**, 063001 (2010)

[44] N. M. R. Peres, J. Phys. Condens. Matter **21**, 323201 (2009)

[45] N. M. R. Peres, F. Guinea and A. H. C. Neto, Annals of Phys. **321**, 1559 (2006)

[46] K. S. Novoselov et al., Phys. Stat. Sol. b **244**, 4106 (2007)

[47] A. Bostwick et al., Prog. Surf. Sci. **84**, 380 (2009)

[48] M. J. Allen, V. C. Tung and R. B. Kaner, Chem. Rev. **110**, 132 (2010)

[49] V. I. Fal'ko and A. K. Geim, The Eur. Phys. J. Spl. Top. **148**, 1 (2007)

[50] C. N. R. Rao, K. Biswas, K. S. Subrahmanyam and A. Govindaraj, J. Mater. Chem. **19**, 2457 (2009)

[51] A. H. C. Neto, Mater. Today **13**, 12 (2010)

[52] A. K. Geim and A. H. MacDonald, Phys. Today **60**, 35 (2007)

[53] A. C. Neto, F. Guinea and N. M. Peres, Phys. World **19**, 33 (2006)

[54] K. S. Novoselov, Phys. World **22**, 27 (2009)

[55] A. J. Legget, PHYS598PTD (lecture notes 21), Physics Department, University of Illinois, Urbana (Fall 2009) (http://online.physics.uiuc.edu/courses/phys598PTD/fall09/L21.pdf)

[56] C. Kittel, *Introduction to Solid State Physics*, 7^{th} edition, John Wiley and Sons, Singpore, 1996.

[57] N. W. Ashcroft and N. D. Mermin, *Solid State Physics*, Harcourt Brace, Fort Worth, 1976

[58] P. R. Wallace, Phys. Rev. **71**, 622 (1947)

[59] R. Saito, G. Dresselhaus and M. S. Dresselhaus, *Physical Properties of Carbon Nanotubes*, Imperial, London, 1998

[60] S. Reich, J. Maultzsch and C. Thomsen, Phys. Rev. B **66**, 035412 (2002)

[61] C. Bena and G. Montambaux, New. J. Phys. **11**, 095003 (2009)

[62] Y. Hasegawa and R. Konno, H. Nakano and M. Kohmoto, Phys. Rev. B **74**, 033413 (2006)

[63] G. W. Semenoff, Phys. Rev. Lett. **53**, 2449 (1984)

[64] K. S. Subrahmanyam, S. R. C. Vivekchand, A. Govindaraj and C. N. R. Rao, J. Mater. Chem. **18**, 1517 (2008)

[65] M. S. Dresselhaus, G. Dresselhaus, J. E. Fischer and M. J. Moran, *Intercalated Graphite*, North-Holland, Newyork, 1983

[66] W. A. de Heer et al., Solid State Commn. **143**, 92 (2007)

[67] P. W. Sutter, J-I. Flege and E. A. Sutter, Nat. Mater. **7**, 406 (2008)

[68] P. Blake and et al., Appl. Phys. Lett. **91**, 063124 (2007)

[69] Y. Y. Wang, Z. H. Ni, Z. X. Shen, H. M. Wang and Y. H. Wu, Appl. Phys. Lett. **92**, 043121 (2008)

[70] J. S. Park et al., Carbon **47**, 1303 (2009)

[71] D. Graf et al., The Eur. Phys. J. Spl. Top. **148**, 171 (2007)

[72] Y. ying Wang et al., J. Phys. Chem. C **112**, 10637 (2008)

[73] Z. H. Ni et al., Phys. Rev. B **77**, 115416 (2008)

[74] A. C. Ferrari et. al., Phys. Rev. Lett. **97**, 187401 (2006)

[75] A. Das, B. Chakraborty and A. K. Sood, Bull. Mater. Sci. **31**, 579 (2008)

[76] I. Calizo, F. Miao, W. Bao, C. N. Lau and A. A. Balandin, Appl. Phys. Lett. **91**, 071913 (2007)

[77] I. Calizo, A. A. Balandin, W. Bao, F. Miao and C. N. Lau, Nano Lett. **7**, 2645 (2007)

[78] L. M. Malard, M. A. Pimenta, G. Dresselhaus and M. S. Dresselhaus, Phys. Rep. **473**, 51 (2009)

[79] S. Pisana et al., Nat. Mater. **6**, 198 (2007)

[80] F. Wang et al., Science **320**, 206 (2008)

[81] G. Fiori and G. Iannaccone, IEEE Electron Device Lett. **30**, 261 (2009)

[82] J. M. Dawlaty et al., Appl. Phys. Lett. **93**, 131905 (2008)

[83] V. Yu and M. Hilke, Appl. Phys. Lett. **95**, 151904 (2009)

[84] M. Bruna and S. Borini, J. Phys. D: Appl. Phys. **42**, 175307 (2009)

[85] P. E. Gaskell, H. S. Skulason, C. Rodenchuk and T. Szkopek, Appl. Phys. Lett. **94**, 143101 (2009)

[86] Z. Fei et al., Phys. Rev. B **78**, 201402(R) (2008)

[87] C. Casiraghi et al., Nano Lett. **7**, 2711 (2007)

[88] Z. H. Ni et al., Nano Lett. **7**, 2758 (2007)

[89] Z. Q. Li et al., Nat. Phys. **4**, 533 (2008)

[90] Z. Jiang et al., Phys. Rev. Lett. **98**, 197403 (2007)

[91] K. F. Mak et al., Phys. Rev. Lett. **101**, 196405 (2008)

[92] R. R. Nair et al., Science **320**, 1308 (2008)

[93] M. L. Sadowski, G. Martinez, M. Potemski, C. Berger and W. A. de Heer, Solid State Commun. **143**, 123 (2007)

[94] J. C. Slonczewskr and P. R. Weiss, Phys. Rev. **109**, 272 (1958)

[95] J. W. McClure, Phys. Rev. **108**, 612 (1957)

[96] W. S. Boyle and P. Nozières, Phys. Rev. **111**, 782 (1958)

[97] F. Bassani and E. Tosatti, Phys. Lett. **27**, 446 (1968)

[98] A. B. Djurišić and E. H. Li, J. Appl. Phys. **85**, 7404 (1999)

[99] I. Ohlídal and F. Vižďa, J. Mod. Opt. **46**, 2043 (1999)

[100] V. P. Gusynin and S. G. Sharapov, Phys. Rev. B **73**, 245411 (2006)

[101] V. P. Gusynin, S. G. Sharapov and J. P. Carbotte, J. Phys. Condens. Matter **19**,026222 (2007)

[102] V. P. Gusynin, S. G. Sharapov and J. P. Carbotte, Phys. Rev. Lett. **98**, 157402 (2007)

[103] M. Koshino and T. Ando, Phys. Rev. B **77**, 115313 (2008)

[104] M. V. Strikha and F. T. Vasko, Phys. Rev. B **81**, 115413 (2010)

[105] V. P. Gusynin, S. G. Sharapov and J. P. Carbotte, Phys. Rev. B **75**, 165407 (2007)

[106] V. P. Gusynin, S. G. Sharapov and J. P.Carbotte, Phys. Rev. Lett. **96**, 256802 (2006)

[107] L. Hao and L. Sheng, Solid State Commun. **149**, 1962 (2009)

[108] E. G. Mishchenko, Phys. Rev. Lett. **103**, 246802 (2009)

[109] F. T. Vasko and V. Ryzhii, Phys. Rev. B **77**, 195433 (2008)

[110] N. M. R. Peres, T. Stauber and A. H. C. Neto, Europhys. Lett. **84**, 38002 (2008)

[111] E. J. Nicol and J. P. Carbotte, Phys. Rev. B **77**, 155409 (2008)

[112] T. Stauber, N. M. R. Peres and A. H. C. Neto, Phys. Rev. B **78**, 085418 (2008)

[113] T. Stauber, N. M. R. Peres and A. K. Geim, Phys. Rev. B **78**, 085432 (2008)

[114] N. M. Vildanov, J. Phys. Condens. Matter **21**, 445802 (2009)

[115] L. A. Falkovsky and A. A. Varlamov, The Euro. Phys. J. B **56**, 281 (2007)

[116] D. Liu and S. Zhang, J. Phys. Condens. Matter **20**, 175222 (2008)

[117] D. S. L. Abergel, E. McCann and V. I. Fal'ko, The Euro. Phys. J. Spl. Top. **148**, 105 (2007)

[118] T. Ando, Y. Zheng and H. Suzuura, J. Phys. Soc. Jpn. **71**, 1318 (2002)

[119] D. S. L. Abergel, A. Russell and V. I. Fal'ko, Appl. Phys. Lett. **91**, 063125 (2007)

[120] X. Wang, M. Zhao and D. D. Nolte, Appl. Phys. Lett. **95**, 081102 (2009)

[121] L. A. Falkovsky, J. Phys. Conf. Ser. **129**, 012004 (2008)

[122] D. S. L. Abergel and V. I. Fal'ko, Phys. Rev. B **75**, 155430 (2007)

[123] L. A. Falkovsky and S. S. Pershoguba, Phys. Rev. B **76**, 153410 (2007)

[124] L. A. Falkovsky, J. Exp. Theor. Phys. **106**, 575 (2008)

[125] M. Bruna and S. Borini, Appl. Phys. Lett. **94**, 031901 (2009)

[126] J. Nilsson, A. H. C. Neto, F. Guinea and N. M. R. Peres, Phys. Rev. B **76**, 165416 (2007)

[127] D. Prezzi, D. Varsano, A. Ruini, A. Marini and E. Molinari, Phys. Rev. B **77**, 041404(R) (2008)

[128] P. Ingenhoven, J. Z. Bernád, U. Zülicke and R. Egger, Phys. Rev. B **81**, 035421 (2010)

[129] N. M. R. Peres, R. M. Ribeiro and A. H. C. Neto, Phys. Rev. Lett. **105**, 055501 (2010)

[130] L. Yang, M. L. Cohen and S. G. Louie, Nano Lett. **7**, 3112 (2007)

[131] A. Savchenko, Science **323**, 589 (2009)

[132] M. Taghioskoui, Mater. Today **12**, 34 (2009)

[133] D. C. Elias et al., Science **323**, 610 (2009)

[134] F. Schedin et al., Nat. Mater. **6**, 652 (2007)

[135] N. Mohanty and V. Berry, Nano Lett. **8**, 4469 (2008)

[136] P. Blake et al., Nano Lett. **8**, 1704 (2008)

[137] A. Ghatak, *Optics*, 4th Edition, Tata McGraw-Hill Publishing Company, New Delhi, 2008

[138] E. McCann and V. I. Fal'ko, Phys. Rev. Lett. **96**, 086805 (2006)

[139] E. V. Castro et al., Phys. Rev. Lett. **99**, 216802 (2007)

[140] E. V. Castro, N. M. R. Peres, J. M. B. L. dos Santos, F. Guinea and A. H. C. Neto, J. Phys. Conf. Ser. **129**, 012002 (2008)

[141] H. Schmidt et al., Appl. Phys. Lett. **93**, 172108 (2008)

[142] F. A. Jenkins and H. E. White, *Fundamentals of Optics*, McGraw-Hill, 1981

[143] B. Partoens and F. M. Peeters, Phys. Rev. B **74**, 075404 (2006)

[144] M. Nakamura and L. Hirasawa, Phys. Rev. B **77**, 045429 (2008)

[145] M. Xu, D. Fujita, J. Gao and N. Hanagata, ACS Nano **4**, 2937 (2010)

[146] V. Meera and G. S. Setlur, J. Phys. D: Appl. Phys. **42**, 055403 (2009)

[147] K. Foroutan-pour, P. Dutilleul and D. L. Smith, Agron. J. **93**, 333 (2001)

[148] M. H. Oliver, N. K. Harrison, J. E. Bishop, P. J. Cole and G. J. Laurent, J. Cell. Sci. **92**, 513 (1989)

[149] C. Dorronsoro, D. Cano, J. M-Lloves and S. Marcos, Opt. Exp. **14**, 6142 (2006)

[150] H. O-Reece, M. Smith, C. Elwell and J. C. Goldstone, J. Anaest. **82**, 418 (1999)

[151] Y. Tsuchiya and T. Urakami, Opt. Commun. **144**, 269 (1997)

[152] M. Kohl et al., Phys. Med. Biol. **43**, 1771 (1998)

[153] J. Scarminio, A. Urbano and B. Gardes, Mat. Chem. Phys. **61**, 143 (1999)

[154] B. Commoner and D. Lipkin, Science **110**, 41 (1949)

[155] H. Abitan, H. Bohr and P. Buchhave, Appl. Opt. **47**, 5354 (2008)

[156] W. G. Tam and A. Zardecki, Appl. Opt. **21**, 2405 (1982)

[157] M. Andorn and K. H. Bar-Eli, J. Chem. Phys. **55**, 5017 (1971)

[158] B. Mohlenhoff, M. Romeo, M. Diem and B. R. Wood, Bio. Phys. J. **88**, 3635 (2005)

[159] E. D. Palik, *Handbook of Optical Constants of Solids*, Academic Press, San Diego, 1998

Publications

Journal

1. V Meera and G S Setlur, *Beer-Lambert's Law and Few-Layer Graphene* (communicated)

2. V Meera and G S Setlur, *Ellipsometry of Graphene on a Substrate*, Journal of Applied Physics **107**, 033525 (2010)

3. V Meera and G S Setlur, *Conductivity Tensor of Graphene Through Reflection of Microwave Measurements, Journal of Physiscs D: Applied Physics* **42**, 055403 (2009); Erratum: Journal of Physics D: Applied Physics **42**, 139802 (2009)

Vita

Ms. Meera V, born in Kerala, India did her B.Sc. with Physics as main subject in 2001 from C M S College, Kottayam, Kerala and M.Sc. in Physics in 2003 from C M S College, Kottayam, Kerala. She joined IIT Guwahati for Ph.D. in 2005. She was awarded Junior Research Fellowship in 2005 and Senior Research Fellowship in 2007 by MHRD, India.